Fall 2013

Instrumentation, Applications And Fundamentals Of Plasma Ionization Of Organic Molecules From Surfaces

Joshua Scott Wiley
Purdue University

Graduate School ETD Form 9
(Revised 12/07)

PURDUE UNIVERSITY
GRADUATE SCHOOL
Thesis/Dissertation Acceptance

This is to certify that the thesis/dissertation prepared

By Joshua S. Wiley

Entitled INSTRUMENTATION, APPLICATIONS AND FUNDAMENTALS OF PLASMA IONIZATION OF ORGANIC MOLECULES FROM SURFACES

For the degree of Doctor of Philosophy

Is approved by the final examining committee:

R. Graham Cooks
Chair

Mary J. Wirth

Chittaranjan Das

Peter T. Kissinger

To the best of my knowledge and as understood by the student in the *Research Integrity and Copyright Disclaimer (Graduate School Form 20)*, this thesis/dissertation adheres to the provisions of Purdue University's "Policy on Integrity in Research" and the use of copyrighted material.

Approved by Major Professor(s): R. Graham Cooks

Approved by: R. E. Wild 11/22/2013
Head of the Graduate Program Date

INSTRUMENTATION, APPLICATIONS AND FUNDAMENTALS OF PLASMA IONIZATION OF ORGANIC MOLECULES FROM SURFACES

A Dissertation

Submitted to the Faculty

of

Purdue University

by

Joshua S. Wiley

In partial Fulfillment of the

Requirements for the Degree

of

Doctor of Philosophy

December 2013

Purdue University

West Lafayette, Indiana

Dedicated to my parents and previous teachers for their continuous and loving support

ACKNOWLEDGMENTS

I would like to first acknowledge my parents, Dave and Linda Wiley, for support through each phase of my life and educational development. Without them, none of this would have been possible. I would like to thank my brother, David, for setting an example of how to live and enjoy life and for being someone I could always look up to. My extended family and friends has been an amazing network of support that has encouraged me to strive for the best. I have numerous teachers growing up to thank, all of which have played a role in my development. In particular, I would like to acknowledge Larry and Jeff Hauswald, Dennis Lopp, Karen York and Kevin Trobaugh as those teachers who have perhaps had the most impact in my educational development and career path. As an undergraduate at Indiana University, Prof. Gary Hieftje undoubtedly had a significant hand in introducing me to analytical chemistry and showing me how to both enjoy and succeed in the field. I would not be in analytical chemistry if not for him, and I am very grateful for what he has done for me. The graduate students in Prof. Hieftje's group were also instrumental in the development of my passion for analytical chemistry. In particular, Jake Shelley played a crucial role in teaching me to think, act and write as a successful scientist does. At Purdue, Prof. Cooks and the entire group have been amazing to work with. Prof. Cooks' passion for chemistry is truly contagious and his benevolence inspirational. Lastly, Achini Bandara has made the last 10 months

of graduate school enjoyable and exciting. She is always willing to lend an ear for discussion and her generosity has enriched my life. I cannot thank everyone who has played a major role in my life enough for helping me make it where I am today.

TABLE OF CONTENTS

Page

Page

Page

LIST OF TABLES

LIST OF FIGURES

Figure Page

Figure Page

Figure Page

Figure Page

ABSTRACT

Wiley, Joshua S., Ph.D., Purdue University, December 2013. Instrumentation, Applications and Fundamentals of Plasma Ionization of Organic Molecules from Surfaces. Major Professor: R. Graham Cooks.

Various aspects of the interaction of low-temperature plasma (LTP) ambient ionization with organic molecules and surfaces are discussed. As an application, LTP-MS has been used for the analysis of pesticides directly from fruits and vegetables revealing low parts per billion limits of detection (LODs). Due to low power and gas requirements, a battery-operated and handheld LTP probe was developed for the point-and-shoot MS analyses. Handheld LTP was compared with large-scale LTP on a benchtop and miniature MS revealing similar LODs for both. Long-distance ion transport up to one meter was also demonstrated with flexible tubing for non-proximate sample interrogation. Fundamentals of LTP-sample interaction were examined through spectroscopy and MS analysis. Spectroscopic studies have provided insights into reagent ion formation, with new evidence that He_2^+ acts as a charge carrier in the plasma. In addition, monochromatic and time-resolved 2D images of LTP emission from plasma bullet propagation to open air and various sample substrates were acquired. MS analyses

revealed chemical sputtering from alkyl halides and organic salts. Chemical sputtering that occurs in the LTP environment appears to be a reductive cleavage process and has resulted in two interesting reactions. More specifically, imidazolium-based ionic liquids have been found to selectively lose one of the two side chains as a function of the counter anion, and a partially fluorinated polymer was broken down into tetrafluoroethylene monomers which immediately polymerized to form perfluorinated alkyl chains.

CHAPTER 1

INTRODUCTION TO PLASMA-BASED AMBIENT IONIZATION MASS SPECTROMETRY

1.1 Background and Concepts

The ability to manipulate ions with electric and magnetic fields is fundamental to mass spectrometry. Molecular ionization processes can conveniently be grouped into four main types, electron ionization (EI), chemical ionization (CI), desorption ionization (DI) and spray ionization (SI). Traditionally, the key MS process of ionization has been implemented internally, under vacuum. Of the four main types of ionization methods, only SI in the form of electrospray ionization (ESI) is typically done at atmospheric pressure. Electrospray ionization (ESI)[1] is a solution-based ionization method which is almost always used with prior liquid chromatography separation. Most sample types are successfully ionized – and indeed give excellent analytical figures of merit - using one or other of the traditional ionization methods usually with the aid of prior chromatographic separation. The special case of rapid, direct ionization of complex mixtures is not handled well with the traditional methods although there are exceptions for selected chemical types of analytes, as in the case of alkaloids in plant materials[2] where soft ionization can be used to generate a set of intact ionized molecules followed by the use of tandem mass spectrometry to obtain structurally characteristic spectra.

Molecular ionization at atmospheric pressure was initiated with the study of vapors using a differentially pumped interface to the mass spectrometer[3] a method that proved to be very sensitive but one that was poor-suited to mixtures. This volume deals for the problem of how to analyze complex mixtures directly by mass spectrometry. This task requires that condensed phase samples be ionized and to do this quickly the experiment must necessarily be done in air. ESI itself is not suited to such tasks as it requires taking up the sample in solution and its performance is degraded by salts and competition effects in complex mixture samples. Desorption electrospray ionization (DESI)[4] is a method that was introduced to extend ESI in such a way as to allow direct analysis of samples in the solid state. Complex samples can be interrogated directly because DESI has a built-in sampling step based on solvent extraction. The successes of this technique encouraged a variety of other methods of generating ions from native samples in their ordinary environment, that is, ambient ionization mass spectrometry.[5] In all of these methods, the complex sample is interrogated to provide analyte ions which are transferred into the vacuum system. This selective transfer into vacuum of a portion of sample material is a further distinction between ambient ionization and electrospray ionization. So, even though ambient ionization methods are derived from and related to techniques based on ionization at atmospheric pressure, they are also distinct from them and form a class of methods that address the problem of rapid, direct mixture analysis.

One further comment on ambient ionization is made to note that the term ambient ionization refers to a particular class of methods used to create ions from samples in the ambient environment, as just noted. It could also be defined by the objective of the experiment which is the rapid analysis of ordinary objects in their native environment.

There are methods of ionization which allow ambient analysis but which might also be termed ambient ionization methods. For example, probe based methods in which a small sample is removed from an object and ionized by spray ionization might fall into this class. Such methods include the probes used by Hiraoka.[6] To take this point further, ionization of ordinary objects in their native environment can be performed in two ways: by direct methods or by sampling methods. The direct methods are by definition ambient ionization methods. Direct methods allow imaging and avoid the extra physical manipulations of the sampling methods. However, probe sampling may allow access to positions difficult to locate directly, relative to MS, although sampling using heated or unheated gas 'probes' can achieve sampling by passing over any object from which sample vapor may be transferred directly into the MS. The use of physical probes followed by ESI represents an important class of ambient analysis methods.

The ambient ionization experiments can be divided into categories in several ways: one method of categorization is based on the nature of the principal agency used: solvent sprays, electrical discharges and lasers. The topic of this dissertation, electrical discharges or plasma-based ambient ionization techniques, originated with the advent of direct analysis in real time (DART) in 2005.[7] This caused a platoon of other plasma-based methods to be developed ranging from flowing-atmospheric pressure afterglow (FAPA)[8] to plasma-assisted desorption ionization (PADI)[9] to low-temperature plasma (LTP)[10] and many more.[11] Each source offers its own uniqueness in geometry, materials, type of discharge, ac or dc voltages, temperature, etc. However, despite differences in how the discharges are formed or configured, each source yields similar reagent ions and their analytical performance is comparable.

Some of the advantages of ambient plasmas include excellent ionization efficiency (even nonpolar compounds), no solvents or waste generated, little dependence on sample placement and many are capable of portability for in-field analyses. However, the largest disadvantage, which limits their value as an ambient ionization source, is their inability to desorb/ionize large, non-volatile analytes due to heavily relying on thermal desorption. While some of the sources, like DART, employ heaters for increased desorption capabilities, the increased temperature still does not facilitate desorption for large peptides and proteins. Some of the plasma-based sources are self-heated (e.g. FAPA), while others are room temperature (e.g. LTP); however, heat can easily be implemented to yield similar performance for each of the sources.

The types of samples that are typically analyzed by plasma-based ambient ionization sources are smaller molecules with masses less than 500 Da, although this is not a hard mass cutoff. LTP (the topic of this dissertation) has been applied to the analysis of drugs of abuse,[12] fatty acids,[13-15] explosives[16] and pesticides.[17] One of the major advantages of LTP is its low power and helium consumption which allows it to be used as a portable ionization source for use with miniature mass spectrometers where it has been applied to melamine detection in milk,[18] explosives from surfaces[19] and the determination of organic vs. non-organic apples in supermarkets.[20] While LTP and all of the plasma-based ambient ionization sources have proven capable of providing good figures of merit for the chosen samples, they suffer a great deal by not being applicable to larger, non-volatile analytes.

If plasma-based ambient ionization is to compete with the desorption capabilities of spray-based and laser-based methods, a mechanism other than thermal desorption will

be necessary. One potential desorption mechanism is sputtering due to the presence of numerous reactive species with large amounts of internal energy in the plasma. Since it is known that ambient plasmas with excited helium, nitrogen, oxygen, and water species are incapable of inducing sputtering for many large molecules, it might be necessary to modify the gas or sample environment to facilitate sputtering. This is an experiment known as reactive desorption/ionization, and it will be the future of the field of plasma-based ambient ionization MS if the subfield is to compete with other ambient ionization techniques. If appropriate sample-plasma environments can be established to allow the desorption of larger molecules through reactive desorption/ionization, the advantages of portability, ease of use, and their solvent- and waste-free nature will go a long way in pushing plasma-based ambient ionization ahead of other ambient ionization methods.

This dissertation is aimed at taking a step toward advancing LTP ionization through the development of novel applications, instrumentation and fundamental studies. The next section is meant to be a guide discussing general LTP-MS procedures and practicalities. In chapter two results are shown for the direct analysis of pesticides from food items with LTP-MS as well as the development of a cordless, handheld and portable LTP probe for point-and-shoot analyses in chapter three. Portability is an area of plasma-based ionization that has not been emphasized much in the literature, but demanding applications suggest it will be important in the future with advanced miniature MS instrumentation. The final to chapters are focused on fundamentals of LTP, with Chapter four focusing on spectroscopic studies of the plume for the elucidation of reagent ion reactions and plasma-substrate interactions. The final chapter is the real cornerstone of this dissertation, focusing on non-thermal desorption mechanisms observed with LTP-

MS. It is this author's goal that the discovery of chemical sputtering with LTP and the investigation of the sputtering process leads to further improvement of plasma-based ionization through novel reactive desorption/ionization of non-volatile and potentially large biomolecular analytes.

1.2 Methods

1.2.1 LTP Setup

1.2.1.1 Safety Considerations

Exposed, ac high voltages were present at the LTP source and mass spectrometer inlet. Electrically insulating gloves and extreme care were used to prevent electrical shock. Material safety data sheets for all chemicals used were consulted prior to performing experiments.

1.2.1.2 LTP Dimensions and Geometries

A schematic of a typical LTP-MS experimental setup can be seen in Figure 1.1. In the original LTP configuration by Harper *et al*., the glass tube's outer diameter is 6.35 mm with an internal diameter of 3.75 mm.[10] Within the glass tube is a ground electrode made of stainless steel with an outer diameter of ~1.6 mm. A piece of copper tape is wrapped around the exterior of the glass tube as the high voltage electrode. Note that the width of the copper tape electrode will have an effect on the power that can be applied to

the plasma. Wider electrodes decrease the plasma density and allow for much higher powers to be supplied to the plasma without arcing, while having a less wide electrode will allow the plasma to operate at lower potentials. A similar effect can be observed with varying the diameter of the internal ground electrode. The typical potential range for this LTP configuration is 2.5 – 5 kV ac, and the frequency is not as crucial. The original LTP probe employed a voltage at 2.5 – 5 kHz, but this range has been extended to over 60 kHz and yields similar analytical sensitivity. Upon applying the ac potential in addition to the flow of a discharge gas (typically helium) at ~0.4 L/min through the glass tube, the plasma is formed and directed toward a sample.

The typical LTP-sample-MS orientation is similar to that in the visualization in Fig. 1.1. Neither angles nor distance have much effect on LTP-MS analyses. A standard LTP-MS distance from the probe to the sample is ~5 mm and the sample would be ~5 mm from the MS inlet. The angle labelled as "α" is typically 30° - 45°, but this is not critical as every angle from antiparallel (α = 0°) to 90° to 180° have been demonstrated and are effective. The particular angle at 180° is a geometry used in the coaxial LTP configuration, where the inlet capillary to the MS serves as the ground electrode inside the LTP probe. Excited species from LTP are pushed out of the glass tube to interact with sample and are then sucked into the MS inlet capillary/ground electrode. A coaxial LTP source has also been demonstrated that either uses an array of LTPs surrounding the MS inlet capillary or uses the MS inlet as the ground electrode within one LTP probe. LTP arrays offer another way of being able to increase the overall power that is supplied to the plasma without arcing.[21]

The LTP arrays utilized a smaller version of the LTP probe than the original LTP configuration. Despite the advantages of having an array of LTP probes, even having just one LTP probe of reduced geometry is advantageous. As will be discussed further in chapter three, an LTP probe with reduced dimensions is more suitable for portability. The required power to ignite the plasma is much less due to the thinner dielectric and more narrow electrode gap, which can be even further reduced if smaller electrodes are used. In addition, the smaller LTP probe handles lower discharge gas flow rates better than larger probes, since a constant gas flow rate will result in faster gas velocities and higher densities of the discharge gas with decreasing tubing diameter. Even though the exact reasoning is not clear, the smaller version of the LTP probe typically yields better analytical sensitivity than the larger probe. This point is also discussed further in chapter three.

1.2.1.3 Adjustable Parameters for an LTP Probe

For a constructed LTP source of any dimension/geometry, the major adjustable parameters that have an impact on desorption/ionization capabilities include choice and flow of discharge gas, positioning of the two electrodes, current/voltage applied and the application of heat. The latter two are intimately related, as increasing the applied power results in an increase in the plasma temperature via joule heating and leads to increased thermal desorption capabilities. However, as mentioned in the previous section, the use of either LTP arrays or larger/wider electrodes is needed to allow voltages high enough to induce heating without arcing. Adding an additional source of heat is possible and has been achieved with LTP by either directly heating the sample substrate or heating the

gas/plasma flow (which in turn heats the sample substrate). Both methods of heating yield similar results; however, direct heating of the sample substrate is generally used due to ease of implementation. Heating the gas/plasma requires a heating element around either the gas tube entering the LTP probe or directly on the glass tube in which the plasma is formed (somewhat similar to how heat is applied with DART[7]). Conversely, directly heating the sample substrate can be achieved simply with a heat gun placed under the sample. The effect of heat obviously depends on the temperature the sample substrate reaches, but as will be shown in chapter two, heating the sample substrate to ~150 °C leads to signal enhancement of approximately two orders of magnitude for many analytes as compared to analysis at room temperature. While increased sensitivity is usually a good thing, having to apply heat is not always practical (e.g. analysis of delicate samples like human skin or luggage). This is an advantage of LTP over heated sources like FAPA because LTP's room temperature nature makes it better suited for delicate samples, while also enabling it to be battery-operated for portability due to requiring less power.

Discharge gas composition also plays a large role in desorption/ionization capabilities. Note that the discharge gas flow rate is not crucial as long as it is high enough to push excited species out of the plasma to the sample but not so high that it causes unwanted turbulence. Helium is typically chosen as it yields the best sensitivity, but nitrogen, air, argon, carbon dioxide, and xenon have all been used with LTP-MS as well. It is not clear why helium is better than other discharge gases, but it is believed to be related to the fact that helium has much higher excited states (well above 20 eV) than each of the other gases and can form the necessary reagent ions more efficiently. Wright *et al*. have shown that adding 0.9% hydrogen to a helium DBD can result in even further

signal enhancement by a factor of 68 from helium alone.[22] The use of mixtures of discharge gases is an area of plasma-based ambient ionization that has not been heavily investigated but has the potential to positively impact both desorption and ionization capabilities. In particular, addition of low amounts of a gaseous reagent to enhance desorption/ionization with an air discharge gas would be beneficial for in field analyses. Air is an intriguing and greener option that is well-suited for portable instrumentation, but as will be discussed in chapter three, the sensitivity with an air-LTP with a majority of analytes is roughly two orders of magnitude worse than for He-LTP.

Electric field is another important parameter that can have an effect on analyte signal. Harper *et al.* have shown that increasing the gap between the ground and high voltage electrodes results in increased analyte fragmentation.[10] Adjustment of the high voltage amplitude and waveform also has a significant impact on both reagent ion formation as well as creating proper electric fields for ions of a given polarity reaching the MS inlet. Note that establishing a visible plasma with LTP should allow both negative and positive ions to be created; however, ions of both polarity do not always reach the MS inlet. This is believed to be due to positive or negative current/voltage spikes that vary as function of voltage and/or frequency and may create fields that are more favorable for ions of one polarity to reach the inlet. The dependence on frequency is difficult to characterize and will vary with every LTP source as inductance and capacitance changes. The role of voltage is complicated as well, but, in general, positive ions seem to reach the MS inlet more efficiently at lower potentials, whereas negative ions can be detected more efficiently at higher potentials with an overlap where both polarities reach the MS inlet at intermediate potentials. Various LTP configurations and

power supplies may behave differently though. As will be discussed in the next section, varying the potential has a definite impact on reagent ion formation, which can be advantageous for LTP-MS of some analytes.

1.2.2 Principles of LTP-MS Analyses

1.2.2.1 Reagent Ions

Plasma-based ambient ionization is generally believed to occur through thermal desorption of an analyte followed by typical atmospheric-pressure chemical ionization (APCI) reactions (cf. Figure 1.2). In this sense, plasma-based ambient ionization is only distinguished from APCI by the fact that ambient plasmas are capable of directly sampling an analyte from a surface, which is not achieved with a typical APCI setup. Furthermore, plasma-based ambient ionization and APCI can be further related to reduced pressure ionization techniques like EI and CI, in that all of the techniques involve thermal desorption of an analyte followed by ionization in the gas phase at either atmospheric or reduced pressure. There are three main types of reactions that occur during LTP ionization (cf. Fig. 1.2), which are proton transfer, electron transfer and adduct formation. In positive ion mode, protonated water clusters are responsible for the majority of analyte ionization through proton transfer. Species like N_2^+, O_2^+ and NO^+ are capable of ionizing an analyte via electron transfer, while NH_4^+ is capable of forming an analyte ion through the formation of an adduct. In negative ion mode, the various reagent ions include OH-, O_2^-, CO_3^-, CO_4^-, NO_2^- and NO_3^-, which combine to form ions through

each of the three mechanisms mentioned. As shown in Fig. 1.2, superoxide and nitrate are capable of electron transfer ionization and adduct formation.

Nitrate and other NO_x^- species are a good example of ions that are only formed at certain electric fields. Sekimoto *et al*. have shown that NO_x^- species are only formed at higher electric fields, versus CO_x^- species that are readily formed with lower electric fields. This has also been observed with LTP, where nitrates are only formed when larger ac voltages are applied. This is significant because, nitrate plays a large role in the ionization of various explosives (e.g. RDX) and other analytes through adduct formation. Some results are discussed in Chapter three, but many explosives will not ionize efficiently without the presence of nitrate anions. A similar dependence on voltage for reagent ion formation has not been observed to play a significant role in the positive ion mode, but variations in LTP background mass spectra can be observed.

1.2.2.2 Analysis of Gaseous, Liquid and Solid Samples

One advantage of plasma-based ambient ionization over spray- and laser-based methods is the ability to analyze samples from all three states of matter. Gases are the easiest sample to analyze with LTP-MS, but represent the least interesting samples as no desorption is required and they could be analyzed by any number of methods. Liquids can be analyzed with LTP-MS by analyzing either a small aliquot of the bulk solution on a surface or simply analyzing the bulk solution as shown by Harper *et al*.[10] However, analyzing small aliquots of the bulk solution will often yield better limits of detection, as many analytes give higher signal after the spot has dried. Note that drying actually

occurs at accelerated rates in a plasma environment at room temperature, which is believed to be due to electrolysis of the solvent. Solid samples represent a phase of matter that can be analyzed by LTP-MS and other plasma-based ambient MS methods, but they are also easily analyzed by spray- and laser-based MS methods. In general, the latter two methods will be a better choice for the analysis of solids, but lower molecular weight solids like pesticides and drugs of abuse can also analyzed efficiently with LTP-MS.

1.2.2.3 Necessity of Tandem MS

Any mass spectrum of ions produced under ambient conditions will be polluted with numerous peaks from contaminants in solvents, air or from surfaces. The number of peaks increases when performing an ambient MS experiment in which the unprocessed sample can be a complex mixture of molecules. In Figure 1.3A, is the full-scan LTP-MS spectrum in positive ion mode of 160 pg of terbuthylazine from a glass slide. Due to the overwhelming presence of chemical noise from background ions, there is no observable peak for terbuthylazine at *m/z* 230. Unless the relative abundance of the analyte of interest within the sample is unusually high, it is often necessary to use MS/MS to increase specificity and the signal-to-noise ratio to confirm the presence of an analyte peak. The MS/MS spectrum shown in Figure 1.3B was taken on the same terbuthylazine spot as in Fig. 1.3A; however, the peak at *m/z* 230 was isolated and fragmented revealing a characteristic fragment at *m/z* 174, which corresponds to loss of 2-methylpropene. Without tandem MS it would not have been possible to confirm the presence of terbuthylazine in the 160 pg sample and the LOD would be much worse.

1.2.2.4 Reactive LTP

Reactive ionization is a process by which an analyte is chemically derivatized to enhance ionization efficiency or to increase specificity. Reactive ionization has been achieved with spray-based techniques like DESI,[23] where secondary droplets emitted from a surface contain both analyte and a derivatizing agent and allow the reaction to occur in the solution phase. This type of reactive ionization is possible with LTP, but it is dependent on ion-molecule reactions as there is no solvent present to facilitate solution-phase chemistry. Unfortunately, ion-molecule reactions typically favor proton or electron transfer since these processes occur at further collision distances than the formation of a bound complex.[24] However, ion-molecule reactions are not impossible and have recently been demonstrated with LTP.[25] In the reactive LTP experiment, one of the reagents was introduced into the plasma before interacting with another reagent on the surface, which is preferred over having to place the derivatizing agent on top of the sample surface like a matrix. While no signal enhancement was claimed, their results prove that reactive ionization is possible with LTP.

If the ambient ionization process is broken down into two steps, desorption and ionization, both steps represent an opportunity to uses chemical reactions to enhance the process. Reactive ionization is commonly practiced with DESI and was also demonstrated with LTP, but there have been no reports of reactive desorption. As a spray-based technique, there is not as much need to enhance desorption; however, one potentially useful application would be if there were reagents that could be added to the spray to perform an immediate and online digestion of proteins or polymers, which are often difficult to desorb in a DESI-MS experiment. LTP and other plasma-based

ionization methods could also greatly benefit from reactive desorption if it allowed the detection of more nonvolatile analytes. Reactive desorption with LTP would require an alternative process to thermal desorption, as it seems impractical to add reagents into the plasma to increase the temperature at the sample surface. Instead, a type of sputtering process would need to be induced at a sample surface, like chemical sputtering, where reactions between excited reagents and a nonvolatile analyte result in the ejection of analyte fragments into the gas phase. This type of reactive desorption process through chemical sputtering has been discovered with LTP-MS and is the topic of chapter 5. It is through the further development of novel chemical sputtering processes that plasma-based ambient ionization must proceed if their desorption capabilities are to compete with other ambient ionization methods.

1.3 References

1. Fenn, J. B.; Mann, M.; Meng, C. K.; Wong, S. F.; Whitehouse, C. M. *Science* 1989, 246, 64.

2. Kondrat, R. W.; Cooks, R. G. *Anal. Chem.* 1978, 50, A81.

3. Horning, E. C.; Horning, M. G.; Carroll, D. I.; Dzidic, I.; Stillwel.Rn *Anal. Chem.* 1973, 45, 936.

4. Takats, Z.; Wiseman, J. M.; Gologan, B.; Cooks, R. G. *Science* 2004, 306, 471.

5. Monge, M. E.; Harris, G. A.; Dwivedi, P.; Fernández, F. M. *Chem. Rev.* 2013, 113, 2269.

6. Hiraoka, K.; Nishidate, K.; Mori, K.; Asakawa, D.; Suzuki, S. *Rapid Commun. Mass Spectrom.* 2007, 21, 3139.

7. Cody, R. B.; Laramee, J. A.; Durst, H. D. *Analytical Chemistry* 2005, 77, 2297.

8. Andrade, F. J.; Wetzel, W. C.; Chan, G. C. Y.; Webb, M. R.; Gamez, G.; Ray, S. J.; Hieftje, G. M. *Journal of Analytical Atomic Spectrometry* 2006, 21, 1175.

9. Ratcliffe, L. V.; Rutten, F. J. M.; Barrett, D. A.; Whitmore, T.; Seymour, D.; Greenwood, C.; Aranda-Gonzalvo, Y.; Robinson, S.; McCoustra, M. *Analytical Chemistry* 2007, 79, 6094.

10. Harper, J. D.; Charipar, N. A.; Mulligan, C. C.; Zhang, X. R.; Cooks, R. G.; Ouyang, Z. *Analytical Chemistry* 2008, 80, 9097.

11. Harris, G. A.; Galhena, A. S.; Fernandez, F. M. *Analytical Chemistry* 2011, *83*, 4508.

12. Jackson, A. U.; Garcia-Reyes, J. F.; Harper, J. D.; Wiley, J. S.; Molina-Diaz, A.; Ouyang, Z.; Cooks, R. G. *Analyst* 2010, 135, 927.

13. Garcia-Reyes, J. F.; Mazzoti, F.; Harper, J. D.; Charipar, N. A.; Oradu, S.; Ouyang, Z.; Sindona, G.; Cooks, R. G. *Rapid Communications in Mass Spectrometry* 2009, 23, 3057.

14. Zhang, J. I.; Costa, A. B.; Tao, W. A.; Cooks, R. G. *Analyst* 2011, 136, 3091.

15. Zhang, J. I.; Tao, W. A.; Cooks, R. G. *Analytical Chemistry* 2011, 83, 4738.

16. Garcia-Reyes, J. F.; Harper, J. D.; Salazar, G. A.; Charipar, N. A.; Ouyang, Z.; Cooks, R. G. *Analytical Chemistry* 2011, 83, 1084.

17. Wiley, J. S.; Garcia-Reyes, J. F.; Harper, J. D.; Charipar, N. A.; Ouyang, Z.; Cooks, R. G. *Analyst* 2010, 135, 971.

18. Huang, G. M.; Xu, W.; Visbal-Onufrak, M. A.; Ouyang, Z.; Cooks, R. G. *Analyst* 2010, 135, 705.

19. Dalgleish, J. K.; Hou, K.; Ouyang, Z.; Cooks, R. G. *Analytical Letters* 2012, 45, 1440.

20. Soparawalla, S.; Tadjimukhamedov, F. K.; Wiley, J. S.; Ouyang, Z.; Cooks, R. G. *Analyst* 2011, 136, 4392.

21. Dalgleish, J. K.; Wleklinski, M.; Shelley, J. T.; Mulligan, C. C.; Ouyang, Z.; Cooks, R. G. *Rapid Communications in Mass Spectrometry* 2013, 27, 135.

22. Wright, J. P.; Heywood, M. S.; Thurston, G. K.; Farnsworth, P. B. *Journal of the American Society for Mass Spectrometry* 2013, 24, 335.

23. Cotte-Rodriguez, I.; Takats, Z.; Talaty, N.; Chen, H. W.; Cooks, R. G. *Analytical Chemistry* 2005, 77, 6755.

24. Gunawardena, H. P.; He, M.; Chrisman, P. A.; Pitteri, S. J.; Hogan, J. M.; Hodges, B. D. M.; McLuckey, S. A. *Journal of the American Chemical Society* 2005, 127, 12627.

25. Benassi, M.; Garcia-Reyes, J. F.; Spengler, B. *Rapid Communications in Mass Spectrometry* 2013, 27, 795.

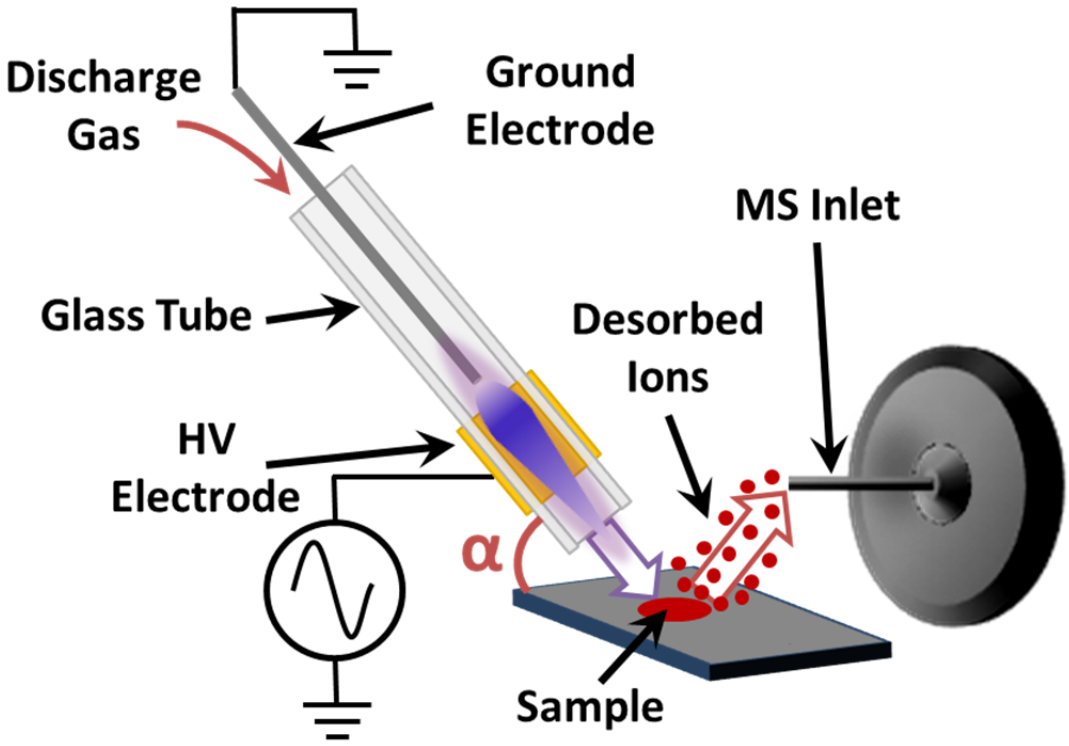

Figure 1.1 Diagram of a typical LTP-MS setup.

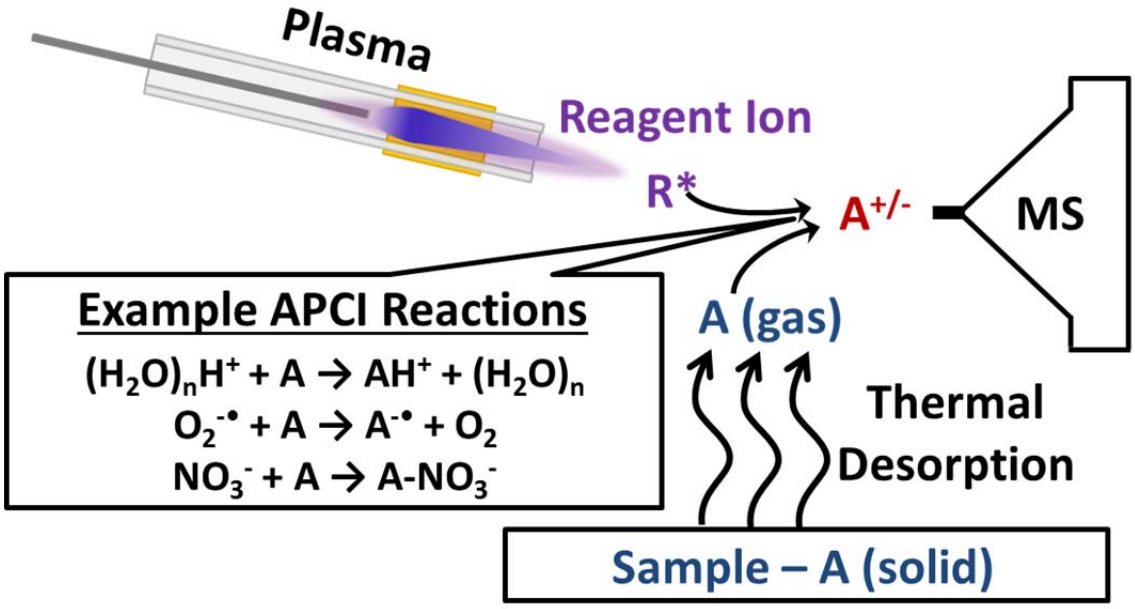

Figure 1.2 Diagram of LTP-MS experiment showing the overall desorption mechanism that is typically accepted. It involves thermal desorption of an analyte followed by common APCI reactions.

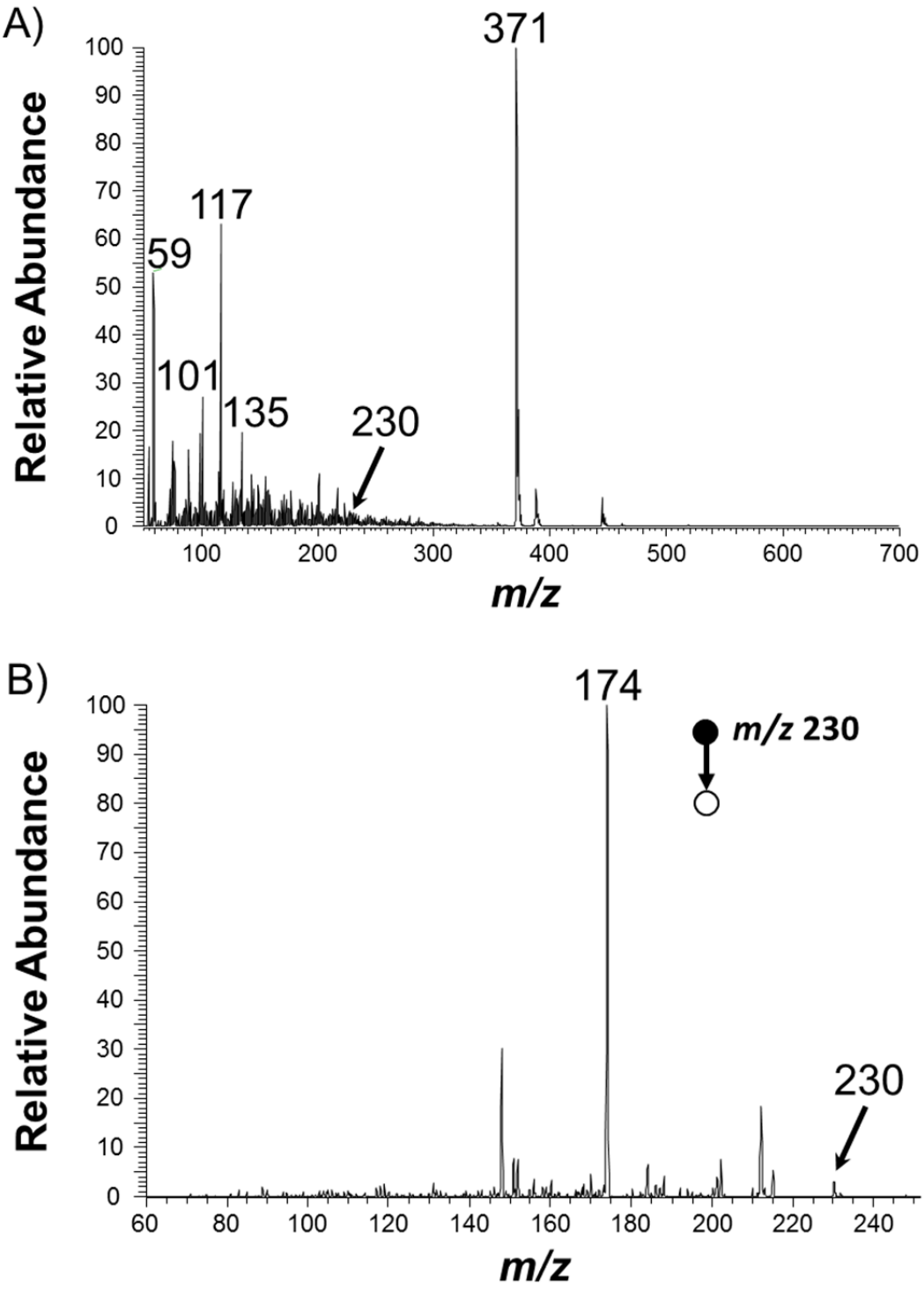

Figure 1.3 A) Full-scan LTP-MS and B) LTP-MS/MS of *m/z* 230 for 80 ppb terbuthylazine (2 µL spot) from a glass slide.

CHAPTER 2

SCREENING OF AGROCHEMICALS IN FOODSTUFFS USING LOW-TEMPERATURE PLASMA AMBIENT IONIZATION MASS SPECTROMETRY

2.1 Introduction

Pesticides are an integral part of the modern agricultural industry with over 1,000 different compounds in use as active pest exterminators.[1] Their use helps to ensure crop longevity which leads to greater food production. Pesticide consumption by humans and wildlife through residue presence in foodstuffs or in the water supply, however, has been shown to have adverse health effects.[2-5] Thus, it is important to detect and quantify trace levels of pesticides in relevant foodstuffs or water supplies.[6, 7] To help establish suitable constraints, maximum residue levels (MRLs) have been set by the European Union[8-11] and United States Environmental Protection Agency (US EPA)[12], providing limits for the amount of a given pesticide in consumables.

Targeted chemical analyses demand rapid, sensitive and specific techniques capable of detecting analytes in complex matrices. The methodology commonly used for sub-MRL verification involves either liquid chromatography (LC) or gas chromatography (GC) coupled with mass spectrometry (MS).[13, 14] Typically tandem MS experiments (LC-MS/MS or GC-MS/MS) are employed to increase structural identification and

decrease the chances of reporting false-positives.[15, 16] While these techniques have proven to be successful[14], the required sample preparation and chromatographic separation steps are time-consuming and may be cost-ineffective. Reducing or removing sample preparation will significantly decrease analysis time and assist in moving the analysis of complex samples out of the lab and towards automated, in situ protocols. Some of the most promising techniques for direct, real time analysis are based on new mass spectrometric methods in which samples are ionized in their native states and without prior preparation in the ambient environment.[17-20]

The advantages of ambient desorption ionization mass spectrometry[19, 20] have led to a plethora of diverse ambient desorption ionization sources with many different ionization and desorption techniques. These ambient desorption ionization sources have been categorized based upon their proposed desorption and ionization mechanisms.[19, 20] Some of the ambient ionization methods have already proven successful in pesticide residue detection as well as general food safety analysis. Chen *et. al*. used extractive electrospray ionization coupled with a hybrid quadrupole time-of-flight (QTOF) mass spectrometer to monitor fruit and vegetable maturity/quality in a non-invasive manner.[21] Jecklin *et al*. coupled the flowing atmospheric-pressure afterglow (FAPA; a plasma/thermal desorption ambient ionization method) with a QTOF mass spectrometer to analyze agrochemicals in juice, fruit peel, and salad leaf matrices achieving low ppb and sub-nanogram LODs without sample pretreatment.[22] Schurek *et al*. used direct analysis in real time (DART; combining thermal desorption with energetic species derived from an atmospheric pressure discharge) coupled with time-of-flight (TOF) MS as well as desorption electrospray ionization (DESI; droplet/liquid jet/gas impact)

coupled with a linear ion trap for the detection of strobilurin residues in wheat at limits of quantitation lower than or close to MRLs, ranging from 5-30 μg/Kg.[23] Most recently, Garcia-Reyes *et al*. used DESI-MS/MS with a quadrupole ion trap mass spectrometer for agrochemical detection from fruit peels and fruit extracts yielding results similar to those of Jecklin *et al*, both methods (FAPA and DESI) claiming detection limits as low as the 1-10μg/Kg range for selected multi-class pesticides in fruits and vegetables.[24]

Among the ambient ionization methods within the thermal desorption category, which rely on heat to increase signal response[19], several employ atmospheric pressure plasmas including, FAPA[25, 26], DART[27], desorption atmospheric pressure chemical ionization (DAPCI)[28], plasma-assisted desorption ionization (PADI)[29] and dielectric barrier discharge ionization (DBDI).[30] The recently introduced ambient plasma-based ionization technique, low-temperature plasma (LTP)[31], although somewhat similar to PADI has the key advantage that it permits the analysis of essentially any surface, regardless of shape or size, due to the probe configuration employed. Analysis of trace compounds on these solid surfaces as well as in complex matrices[32] is possible without the need for solvents or reagents except the carrier/discharge gas. The desorption mechanism for LTP is not yet elucidated, however, LTP can operate at room temperature (~30 °C) while providing sufficient signal, although in some cases signal enhancement is achieved upon heat.[32] An advantage of LTP over some of the other plasma-based techniques in that there is virtually no damage to the sample from excessive heat.

The current study reports on LTP-MS analysis of various agrochemicals in different foodstuffs, including LODs in different matrices and some semi-quantitative determinations. To evaluate the potential of LTP-MS for the proposed analyses, 13

compounds belonging to different pesticide categories were selected and spiked into or onto foodstuff samples such as fruits and vegetables. Analyses were performed via extracts taken from the sample and direct analysis of the peels. In addition, some of the pesticides were spiked into water to determine the efficacy of LTP-MS for agrochemical detection.

2.2 Experimental

2.2.1 Chemicals and Reagents

Pesticide analytical standards were purchased from Dr. Ehrenstorfer GmbH. (Ausburg, Germany) and from Riedel de Haën, Pestanal® quality (Seelze, Germany). Individual pesticide stock solutions (200 – 300 μg mL^{-1}) were prepared in methanol and stored at -20º C. Working solutions were prepared by appropriate dilution with acetonitrile. A Milli-Q-Plus ultra-pure water system from Millipore (Bedford, MA, USA) was used to obtain HPLC-grade water. HPLC-grade acetonitrile and methanol were obtained from Mallinckrodt Baker Inc. (Phillipsburg, NJ, USA). Formic acid was obtained from Fluka (Buchs, Switzerland). Primary-Secondary Amine (PSA) Bond Elut was purchased from Varian, Inc. (Palo Alto, CA, USA). Anhydrous magnesium sulfate, acetic acid and sodium acetate were purchased from Sigma-Aldrich.

2.2.2 Samples

Fruit and vegetable samples (oranges, lemons, apples, green peppers, persimmons, grapefruits tomatoes, pears and grapes samples) were purchased from different local markets. Two main experiments were performed: 1) Direct LTP-MS analysis on peels of fruits and vegetables were analyzed without any pre-treatment; and 2) LTP-MS analysis of acetonitrile extracts from a detailed extraction protocol which is usually used in pesticide testing and follows pesticide residue testing guidelines.

2.2.3 Method of Extraction from Fruits and Vegetables

A common procedure[33] (so-called "QuEChERS", from quick, easy, cheap, effective, rugged and safe) was used to obtain the acetonitrile extracts used for LTP-MS analyses. It comprises the following steps: a representative 15 g portion of previously homogenized sample was weighed in a 200 mL PTFE centrifuge tube. The sample (fruit/vegetable) was homogenized without any previous treatment or cleaning (i.e. removal of leaves or rinsing). The homogenization was carried out using a high speed blender (Ultraturrax). Then 15 mL of acetonitrile were added, and the tube was vigorously shaken for 1 min. After this time, 1.5 g of NaCl and 6g of $MgSO_4$ were added, and the shaking process was repeated for 1 min. The extract then was centrifuged (3700 rpm) for 1 min. 5 mL of the supernatant (acetonitrile phase) was then taken with a pipette and transferred to a 15 mL graduated centrifuge tube containing 250 mg of primary secondary amine (PSA) and 750 mg of $MgSO_4$, that was then energetically shaken for 20 s. The extract was then centrifuged again (3700 rpm) for 1 min. Finally,

an extract containing the equivalent of 1 g of sample per mL in 100% acetonitrile was obtained.

2.2.4 Low-Temperature Plasma Mass Spectrometry

Experiments were performed using a Thermo LTQ linear ion trap mass spectrometer (Thermo Finnigan San José, CA, USA) tuned for optimum detection of the precursor ion of interest via the Xcalibur software. LTP-MS analyses were performed in the positive and negative ion mode and spectra were collected in the automatic gain control mode with a maximum ion trap injection time of 200 ms and 2 microscans per spectrum. The main experimental parameters used were as follows: *m/z* range 150-600; capillary temperature: 200 ºC; tube lens (V): -65 V; capillary voltage: -15 V. Tandem mass spectrometry experiments (MS/MS) were performed using collision-induced dissociation (CID) experiments in order to confirm the presence of particular agrochemicals in the studied samples. These experiments were performed using an isolation window of 1.5 (*m/z* units) and 25-35 % collision energy (manufacturer's unit). The MS/MS spectral features of the studied agrochemicals are shown in Table 2.1; the data are consistent with previous literature on the same compounds using electrospray mass spectrometry.[34]

The LTP probe consists of a glass tube (O.D. 6.35 mm and I.D. 3.75 mm) with an internal grounded electrode (stainless steel, diameter: 1.57mm) centered axially, an outer electrode (copper tape) surrounding the outside of the tube, and the wall of the glass tube serving as a dielectric barrier.[31] An alternating high voltage, 5 – 10 kV at a frequency of

ca. 2.5 kHz, is applied to the outer electrode with the center electrode grounded to generate the dielectric barrier discharge. The AC voltage was provided by a custom built power supply with variable frequency and voltage, consuming less than 3 watts of total power. Helium (flow rate of 0.4 L/min) was used as a discharge gas and to push the reagent ions over the sample surface as well as transporting analyte ions to the mass spectrometer. The samples were placed on the sample holder, typically 0.5 cm away from the LTQ inlet and the LTP probe was placed with its end 4 mm away from the surface and with an angle of *ca.* 30° from the sample surface. In addition, each analysis (except for direct peel analysis) was done with the use of a heat gun (model HG-001VT, NTE Electronics, 44 Farrand St., Bloomfield, NJ 07003) directly under the sample holder to increase the temperature of the substrate (to ~150 °C), thereby increasing desorption capabilities and enhancing signal.

2.2.5 Direct LTP-MS Analyses of Fruit and Vegetable Skins

No sample treatment was required. A piece of *ca*. 2 cm^2 of peel was cut and exposed to the LTP probe. No heating was used in the direct examination of fruit skins.

2.2.6 LTP-MS Analyses of Fruit and Vegetable Extracts

Sample extracts from the QuEChERS method (3 μL of acetonitrile solution, no further pre-treatment) were deposited using a micropipette on a microscope glass slide (beveled micro slides, size 75 x 25 mm, thickness 1 mm, Gold Seal ®, Bencton and Dinckinson Company, Franklin Lakes, NJ USA) and analyzed by LTP-MS.

2.2.7 LTP-MS Analyses of Water Samples

No sample pre-treatment was required. Aliquots (3 μL of each solution) were deposited using a micropipette on a microscope glass slide and analyzed by LTP-MS.

2.3 Results and Discussion

There are four main analyses that were performed for the purposes of the study. The first is the analysis of standard solutions spiked with known amounts of agrochemical compounds to test the analytical performance for each agrochemical with LTP-MS. Secondly, QuEChERS extracts were spiked with agrochemicals for a proof of concept and rough comparison with typical LC-MS samples to ensure that LTP-MS is capable of identifying the compounds of interest in complex food matrices. The third analysis was performed on unspiked QuEChERS extracts to ensure similar qualitative performance as compared with LC-MS analyses. Note that concurrent LC-MS analyses of these same extracts were performed as a reference method but the data was not displayed. Lastly, and most emphatically, the direct analysis of real unspiked fruits/vegetables was performed to examine the capability of LTP-MS to perform rapid analyses with no sample preparation as a possible pre-screening methodology. This last analysis takes advantage of the key features of LTP-MS and is seen as the most probable application for *in situ* measurements.

2.3.1 LTP-MS Screening of Agrochemicals in Standard Solutions

Representative product ion MS/MS spectra of the agrochemicals used in this study can be found in the Supporting Information. (For more information on tandem mass spectrometry scans see Schwartz *et. al*.[35]) They were obtained by spotting 3 μL of the sample dissolved in methanol onto a glass slide. As is typical of ambient ionization sources, soft ionization occurs with the protonated molecule typically being observed as the unique ion in the positive ion mode. No fragmentation was observed in these compounds. Table 2.1 shows the structure, molecular weight, most abundant ion in the full mass scan, and the molecular ion and characteristic fragments (obtained from MS/MS) for each agrochemical in the study. Improved LODs were obtained using MS/MS, which is a common situation for complex mixtures. The product ion MS/MS data also help confirm the presence of particular agrochemicals in the spectrum. Thus, no full MS spectra are displayed.

Application of heat to the glass substrate bearing the sample was found to increase signal, due to an increase in vapor pressure of the analyte at higher temperatures which increases the number of analyte molecules in the gas phase so that they can be ionized by chemical ionization processes. The signal enhancement due to the use of a heated substrate has been discussed for LTP by Huang *et. al*.[32] In the current study, signal was found to be enhanced 10-100 times depending on the compound at a temperature of 150 °C. Figure 2.1 shows the signal enhancement for the characteristic fragment at m/z 174 in the MS/MS product ion spectrum of the $[M+H]^+$ for atrazine (m/z 216) which accompanies heating. This thermal enhancement is approximately two orders of magnitude, from ~11 (a.u.) with no heat to ~1100 (a.u.) with heat.

A summary of the basic LTP-MS performance for agrochemical detection coming from dried standard solution spots along with LODs (determined by S/N = 3) for different matrices is displayed in Table 2.2. When performing MS/MS experiments, the LODs of the studied agrochemicals were appropriately low. For example, in the case of the herbicides ametryn and terbuthylazine, the LOD was 0.1 μg L^{-1} (0.3 pg absolute), which is well below the typical MRL of 5 μg L^{-1} for many pesticides in water (typical MRLs in food range from 10-500 μg/kg).[8] The range of LODs for analyte standards (in pure solvents) was 0.1- 15 μg L^{-1} (0.3-45 pg absolute). Most of the compounds tested showed remarkable sensitivity in LTP-MS approaching that attainable with conventional direct infusion electrospray MS.

Table 2.2 also displays the results of calibration curves plotted for each of the agrochemicals. The curves were generated by recording three spectra for each concentration of a given compound and taking an average of a three second interval of the most abundant characteristic fragment ions to obtain each data point (each plot included four data points). Relative standard deviations (RSD) values, not shown, ranged from 10-30%. However, over 18 months of experience with LTP has shown that this estimate of 10-30% RSD is likely overly cautious, as the typical range is *ca*. 10-15%, and even as low as 8-10% with the use of a three to ten second average. Even with the large RSD, adequate correlation coefficients (r^2) were achieved for each compound, showing promise for the use of LTP-MS as a semi-quantitative tool. Note the term 'semi'-quantitative is employed because LTP-MS is not intended to be a true quantitative method replacing the standard LC-MS approach. Instead, LTP-MS is applicable to pre-screening and should be complementary to LC-MS. Thus, the calibration curves were

performed to show that the true sensitivity is adequate for pre-screening and that a general trend of linearity is exhibited. The concentrations used in the calibration plots varied with the analyte and were likely limited by the dynamic range of the ion trap mass analyzer, which tends to be $10^3 - 10^4$. Another widely varying parameter was the true sensitivity (slope of the calibration curve), with the smallest values being ~0.03 counts.ng/mL for compounds like ethoxyquin and imazalil, and the largest being ~30 counts.ng/mL for compounds like ametryn, terbuthylazine and DEET. The data suggest that the calibration curves are adequate for screening purposes, with a concentration range over two orders of magnitude and r^2 values better than 0.98 in most cases.

2.3.2 LTP-MS Screening of Agrochemicals in Food Extracts

To evaluate the performance of LTP-MS for semi-quantitative screening of agrochemicals in foodstuffs, different experiments were performed using fruit and vegetable extracts spiked with known amounts of the studied analytes at concentrations in the range 0.1 to 100 ppb. Three representative fruits and vegetables in with different types of matrices were selected for study: tomato (high water content), orange (high acid content (organic)) and pepper. Interestingly, the LODs in fruit and vegetable extracts were not much worse than those obtained for standard solutions (see Figure 2.2 for example MS/MS spectra). LODs of the studied agrochemicals were as low as 0.2 μg kg^{-1} sample (0.6 pg) for ametryn and terbuthylazine in tomato and ranged from 0.2 - 20 μg kg^{-1} sample (0.3-60 pg) for this set of compounds in the presence of the matrices. The matrix results are slightly higher than those obtained in neat solvent (depending upon the complexity of the matrix and the MS/MS transition examined). In spite of the large

amount of matrix material (including sugar, dyes, etc.), the results for most of the studied compounds are once again satisfactory for screening purposes. The original acetonitrile extract contained 1 g/mL of fruit/vegetable. Three μL of extract was spotted onto the glass slide, which is equivalent to 3 mg of fruit/vegetable sample.

The LOD results are suffice considering they are below MRL regulatory levels for the studied compounds in fruit and vegetables. The regulations established in each country vary depending on the pesticide and the agricultural commodity. For instance, the MRL allowed for fungicides such as thiabendazole, imazalil, prochloraz, and bitertanol in fruits typically ranges from 1-10 mg kg^{-1} in Japan, the United States, and Europe. Other commodity/pesticide combinations of regulated chemicals are typically in the range of 0.05-1 mg kg^{-1} per compound.[8-11] Bearing this in mind, the proposed approach fulfills the sensitivity requirements for pesticide testing of authorized agrochemicals in fruits and vegetables.

2.3.3 Direct LTP-MS Screening of Agrochemicals on Fruit Samples

In addition to extract analysis, direct analysis of fruit peels, without agrochemical spiking was performed. The detection of imazalil directly from lemon and orange peels is shown in Figure 2.3 along with its detection in traditional QuEChERS extracts of an apple and a grapefruit (Figure 2.4). Note that LC-MS analysis of the fruits was performed for comparison and confirmed that imazalil is the only agrochemical present in the QuEChERS extracts. This is likely true because, as a fungicide, imazalil is typically applied to the fruit/vegetable in the final stage of their production. Thus, LTP-MS is an

ideal methodology for the direct screening of many fungicides on foodstuffs due to their presence mainly at the surface, which may easily and directly be analyzed via LTP-MS. The LTP-MS methodology being explored proves advantageous due to the absence of sample preparation, no solvent requirements, and no sample destruction. The ionization process occurred directly on the surface of the peel without having to use any solvent treatment. LTP-MS could prove to be a useful tool for any industry handling large quantities of fruit, such as the soft drink or food-packaging companies.

2.3.4 LTP-MS Screening of Agrochemicals in Water

Samples from various lakes, ditches, and bottled water were analyzed via LTP-MS for the presence of common agrochemicals (atrazine, DEET, and terbuthylazine). Fortunately for consumers and local residents, samples did not contain detectable amounts of any of the common agrochemicals. However, to determine if LTP-MS is capable of detecting the agrochemicals (atrazine, DEET, and terbuthylazine) present at low-levels, water samples were spiked with the three analytes. A sample MS/MS spectrum was recorded and displayed in Figure 2.5 for atrazine (1 ppb) and terbuthylazine (10 ppb). LODs were estimated to be 6 pg (2 ppb) for atrazine and terbuthylazine and 36 pg (12 ppb) for DEET, using a 3 μL sample of solutions of these three agrochemicals and taking a total time of less than 30 seconds for the measurement. In the case of atrazine, the LOD is below the maximum contaminant level for drinking water, established by US EPA.[12] Terbuthylazine is considered an organic contaminant by US EPA although the tolerated concentration has yet to be declared. The present results

reveal the potential of LTP-MS for trace detection of agrochemicals in environmental water samples.

2.4 Conclusions

The current study suggests that LTP-MS could be a significant tool in the field of agrochemical detection. A large number of agrochemicals can be detected with LODs below MRL regulations, regardless of the sample being in a solvent or a more complex matrix. Advantages of LTP-MS over typically-used chromatographic techniques include a decrease in overall analysis time due to minimal to no sample preparation, as well as the lack of a need for solvents in which direct analysis of a fruit's surface may be analyzed with no destruction. It is not suggested that this or any other ambient ionization method replace chromatography/mass spectrometry methods as reference methods; simply that primary field analysis should be possible using the new methods. In terms of quantitative analyses, the proposed LTP-MS method does not match the performance of reference chromatography-based methods. However, despite the overall analytical performance in terms of precision (RSD %), the speed, chemical specificity, detection limits and satisfactory linear response do suggest its immediate use for trace agrochemical detection.

2.5 References

1. Tomlin, C. *The Pesticide Manual-A World Compendium*, 13th edn., British Crop Protection Council (BCPC), Hampshire, UK, 2003.

2. Andreotti, G.; Freeman, L. E. B.; Hou, L. F.; Coble, J.; Rusiecki, J.; Hoppin, J. A.; Silverman, D. T.; Alavanja, M. C. R. *Int. J. Cancer*, 2009, 124, 2495-2500.

3. Fieten, K. B.; Kromhout, H.; Heederik, D.; de Joode, B. V. *Am. J. Epidemiol.*, 2009, 169, 1500-1506.

4. Hirsch-Ernst, K.; Marx-Stolting, P.; Moeller, T.; Pfeil, R.; Banasiak, U. 46th Congress of the European-Societies-of-Toxicology, Dreden, GERMANY, 2009.

5. Saldana, T. M.; Basso, O. Hoppin, J. A.; Baird, D. D.; Knott, C.; Blair, A.; Alavanja, M. C. R.; Sandler, D. P. *Diabetes Care*, 2007, 30, 529-534.

6. Richardson, S. D. *Anal. Chem.*, 2008, 80, 4373-4402.

7. Richardson, S. D. *Anal. Chem.*, 2007, 79, 4295-4323.

8. *Available at: http://www.codexalimentarius.net/mrls/pestdes/jsp/pest_q-e.jsp (accessed March 2009).*

9. *Available at: http://ec.europa.eu/food/plant/protection/pesticides/regulation_ec_396_2005_en.htm (accessed March 2009)*

10. *Council Directive of 15 July 1991 (91/414/EEC) concerning the placing ofplant protection products on the market (OJ L 230 19.8.1991).p1.*

11. *Available at: www.europa.eu.int/comm/food/index_en.htm (accessed March 2009)*

12. *Available at: www.epa.gov/safewater/contaminants/index.html (accessed March 2009).*

13. Fernandez-Alba, A. R. *Chromatographic-Mass Spectrometric Food Analysis for Trace Determination of Pesticide Residues*, Comprehensive Analytical Chemistry, Vol. XLII; Elsevier, Amsterdam, The Netherlands, 2005.

14... Alder, L.; Greulich, K.; Kempe, G.; Vieth, B. *Mass Spectrom. Rev.*, 2006, 25, 838-865.

15. Soler, C.; Pico, Y. *Trends in Analytical Chemistry*, 2007, 26, 103-115.

16. Pico, Y.; Blasco, C.; Font, G. *Mass Spectrom. Rev.*, 2004, 23, 45-85.

17. Cooks, R. G.; Ouyang, Z.; Takats, Z.; Wiseman, J. M. *Science*, 2006, 311, 1566-1570.

18. Harris, G. A.; Nyadong, L.; Fernandez, F. M. *Analyst*, 2008, 133, 1297-1301.

19. Van Berkel, G. J.; Pasilis, S. P.; Ovchinnikova, O. *J. Mass Spectrom.*, 2008, 43, 1161-1180.

20. Venter, A.; Nefliu, M.; Cooks, R. G. *Trac-Trends Anal. Chem.*, 2008, 27, 284-290.

21. Chen, H. W.; Sun, Y. P.; Wortmann, A.; Gu, H. W.; Zenobi, R. *Anal. Chem.*, 2007, 79, 1447-1455.

22. Jecklin, M. C.; Gamez, G.; Touboul, D.; Zenobi, R. *Rapid Commun. Mass Spectrom.*, 2008, 22, 2791-2798.

23. Schurek, J.; Vaclavik, L.; Hooijerink, H.; Lacina, O.; Poustka, J.; Sharman, M.; Caldow, M.; Nielen, M. W. F.; Hajslova, J. *Anal. Chem.*, 2008, 80, 9567-9575.

24. Garcia-Reyes, J. F.; Jackson, A. U.; Molina-Diaz, A.; Cooks, R. G. *Anal. Chem.*, 2009, 81, 820-829.

25. Andrade, F. J.; Shelley, J. T.; Wetzel, W. C.; Webb, M. R.; Gamez, G.; Ray, S. J.; Hieftje, G. M. *Anal. Chem.*, 2008, 80, 2646-2653.

26. Andrade, F. J.; Wetzel, W. C.; Webb, M. R.; Gamez, G.; Ray, S. J.; Hieftje, G. M. *Anal. Chem.*, 2008, 80, 2654-2663.

27. Cody, R. B.; Laramee, J. A.; Durst, H. D. *Anal. Chem.*, 2005, 77, 2297-2302.

28. Takats, Z.; Cotte-Rodriguez, I.; Talaty, N.; Chen, H. W.; Cooks, R. G. *Chem. Commun.*, 2005, 1950-1952.

29. Ratcliffe, L. V.; Rutten, F. J. M.; Barrett, D. A.; Whitemore, T.; Seymour, D.; Greenwood, C.; Aranda-Gonzalvo, Y.; Robinson, S.; McCoustra, M. *Anal. Chem.*, 2007, 79, 6094-6101.

30. Na, N.; Zhao, M.; Zhang, S.; Yang, C.; Zhang, X. *J. Am. Soc. Mass Spectrom.*, 2007, 18, 1859-1862.

31. Harper, J. D.; Charipar, N. A.; Mulligan, C. C.; Zhang, X. R.; Cooks, R. G.; Ouyang, Z. *Anal. Chem.*, 2008, 80, 9097-9104.

32. Huang, G. M.; Ouyang, Z.; Cooks, R. G. *Chem. Commun.*, 2009, 556-558.

33. .Anastassiades, M.; Lehotay, S. J.; Stajnbaher, D.; Schenck, F. J. *J. AOAC Int.*, 2003, 86, 412-431.

34. Garcia-Reyes, J. F.; Hernando, M. D.; Ferrer, C.; Molina-Diaz, A.; Fernandez-Alba, A. R. *Anal. Chem.*, 2007, 79, 7308-7323.

35. Schwartz, J. C.; Wade, A. P.; Enke, C. G.; Cooks, R. G. *Anal. Chem.*, 1990, 62, 1809-1818.

Table. 2.1 LTP-MS for Trace Analysis of 14 Multi-Class Agrochemicals

Compound	Structure	Nominal Monoisotopic Mass	Species detected (+/-)	MS/MS
Ametryn	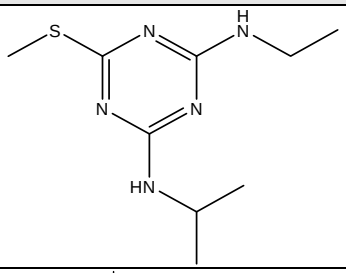	227	$[M+H]^+$	228 → 186
Amitraz	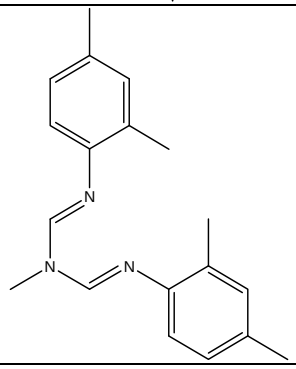	293	$[M+H]^+$	294 → 163
Atrazine	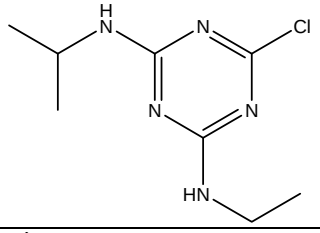	215	$[M+H]^+$	216 → 174
Buprofezin	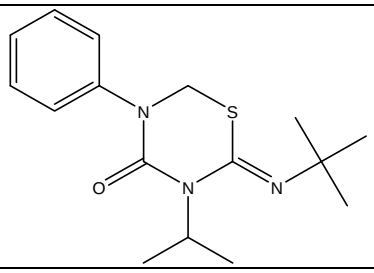	305	$[M+H]^+$	306 → 201; 116
DEET	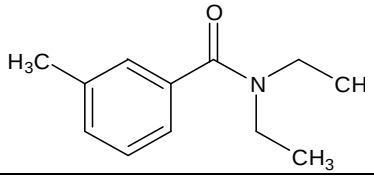	191	$[M+H]^+$	192 → 119 →91
Diphenylamine	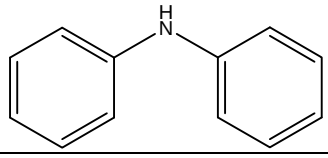	169	$[M+H]^+$	170 → 92

Table 2.1, continued

Compound	Structure	Nominal Monoisotopic Mass	Species detected (+/-)	MS/MS
Ethoxyquin	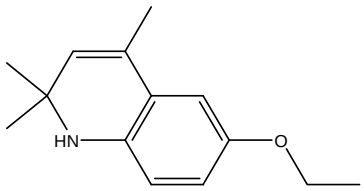	217	$[M+H]^+$	218 → 190; 176
Imazalil	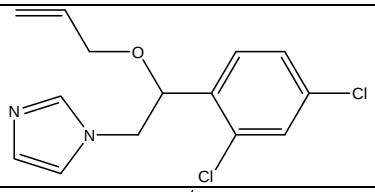	296	$[M+H]^+$	297 → 255; 201; 159
Isofenphos-methyl	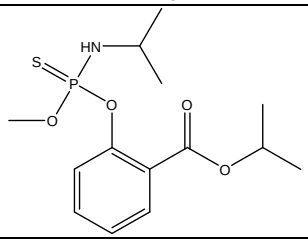	331	$[M+H]^+$	332→ 290; 271; 231
Isoproturon	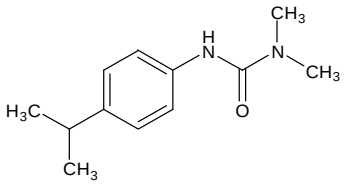	206	$[M+H]^+$	207 → 165;72
Malathion	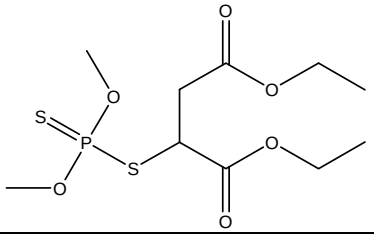	330	$[M+H]^+$	331 → 285; 127
Parathion-ethyl	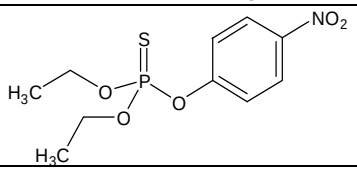	291	$[M+H]^+$	292 → 264; 236
Terbuthylazine	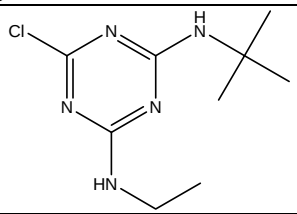	229	$[M+H]^+$	230→ 174

Table 2.2 Analytical Performance of Low-Temperature Plasma Mass Spectrometry (LTP-MS/MS) for the Analysis of Agrochemicals in Fruits and Vegetables

Compound	Conc. Range Tested ($ng\ g^{-1}$)	Calibration Equation [y (a.u.), x ($ng\ ml^{-1}$)]	Correl. Coeff. r^2	Limit of detection (LOD)[a]* LOD Solvent	LOD pepper	LOD orange	LOD tomato
Ametryn	8 – 400	y = 38.1x + 299	0.9797	0.1 ng g^{-1} (0.3 pg)	0.4 ng g^{-1} (1.2 pg)	0.4 ng g^{-1} (1.2 pg)	0.2 ng g^{-1} (0.6 pg)
Amitraz	1 - 1000	y = 0.335x + 18.2	0.9948	2 ng g^{-1} (6 pg)	200 ng g^{-1} 600 pg	6.6 ng g^{-1} (20 pg)	20 ng g^{-1} (60 pg)
Atrazine	8 - 2000	y = 24.4x - 816	0.9992	0.2 ng g^{-1} (0.6 pg)	1 ng g^{-1} (3 pg)	1.5 ng g^{-1} (4.5 pg)	0.4 ng g^{-1} (1.2 pg)
Buprofezin	8 – 400	y = 0.425x - 2.56	0.9996	2 ng g^{-1} (6 pg)	2 ng g^{-1} (6 pg)	6.6 ng g^{-1} (20 pg)	2 ng g^{-1} (6 pg)
DEET	8 – 10^4	y = 52.4x - 914	0.9988	3 ng g^{-1} (9 pg)	6.6 ng g^{-1} (20 pg)	15 ng g^{-1} (45 pg)	15 ng g^{-1} (45 pg)
Diphenylamine	8 - 2000	y = 0.647x - 9.66	0.9914	8 ng g^{-1} (24 pg)	6.6 ng g^{-1} (20 pg)	10 ng g^{-1} (30 pg)	15 ng g^{-1} (45 pg)
Ethoxyquin	400 - 2000	y = 0.0345x - 20.7	0.9971	15 ng g^{-1} (45 pg)	20 ng g^{-1} (60 pg)	20 ng g^{-1} (60 pg)	20 ng g^{-1} (60 pg)
Imazalil	10 – 500	y = 0.0316x + 9.27	1	5 ng g^{-1} (15 pg)	10 ng g^{-1} (30 pg)	10 ng g^{-1} (30 pg)	10 ng g^{-1} (30 pg)
Isofenphos-methyl	1 – 100	y = 0.899x + 8.47	0.9992	1 ng g^{-1} (3 pg)	10 ng g^{-1} (30 pg)	13.3 ng g^{-1} (40 pg)	20 ng g^{-1} (60 pg)
Isoproturon	8 – 400	y = 0.729x + 6.73	0.9969	8 ng g^{-1} (24 pg)	10 ng g^{-1} (30 pg)	20 ng g^{-1} (60 pg)	10 ng g^{-1} (30 pg)
Malathion	80 - 2000	y = 0.0414x + 4.54	0.984	2 ng g^{-1} (6 pg)	6.6 ng g^{-1} (20 pg)	20 ng g^{-1} (60 pg)	5 ng g^{-1} (15 pg)
Parathion-ethyl	8 - 2000	y = 9.18x + 837	1	0.6 ng g^{-1} (2 pg)	3 ng g^{-1} (9 pg)	13.3 ng g^{-1} (40 pg)	10 ng g^{-1} (30 pg)
Terbuthylazine	8 - 2000	y = 30.5x - 570	0.9976	0.1 ng g^{-1} (0.3 pg)	0.66 ng g^{-1} (2 pg)	0.66 ng g^{-1} (2 pg)	0.2 ng g^{-1} (0.6 pg)

[a] LODs were calculated in MS/MS mode -calculated as S/N = 3- with matrix-matched standards and neat solvent standards. Acetonitrile-based fruit and vegetable extracts from QuEChERS procedure containing 1 g of matrix/mL were analyzed without further treatment. LOD (expressed as ng g^{-1}) were calculated with matrix-matched standards prepared with pepper, orange and tomato using the QuEChERS procedure. 3µL of each matrix-matched standard were deposited on a glass slide and analyzed by LTP-MS/MS

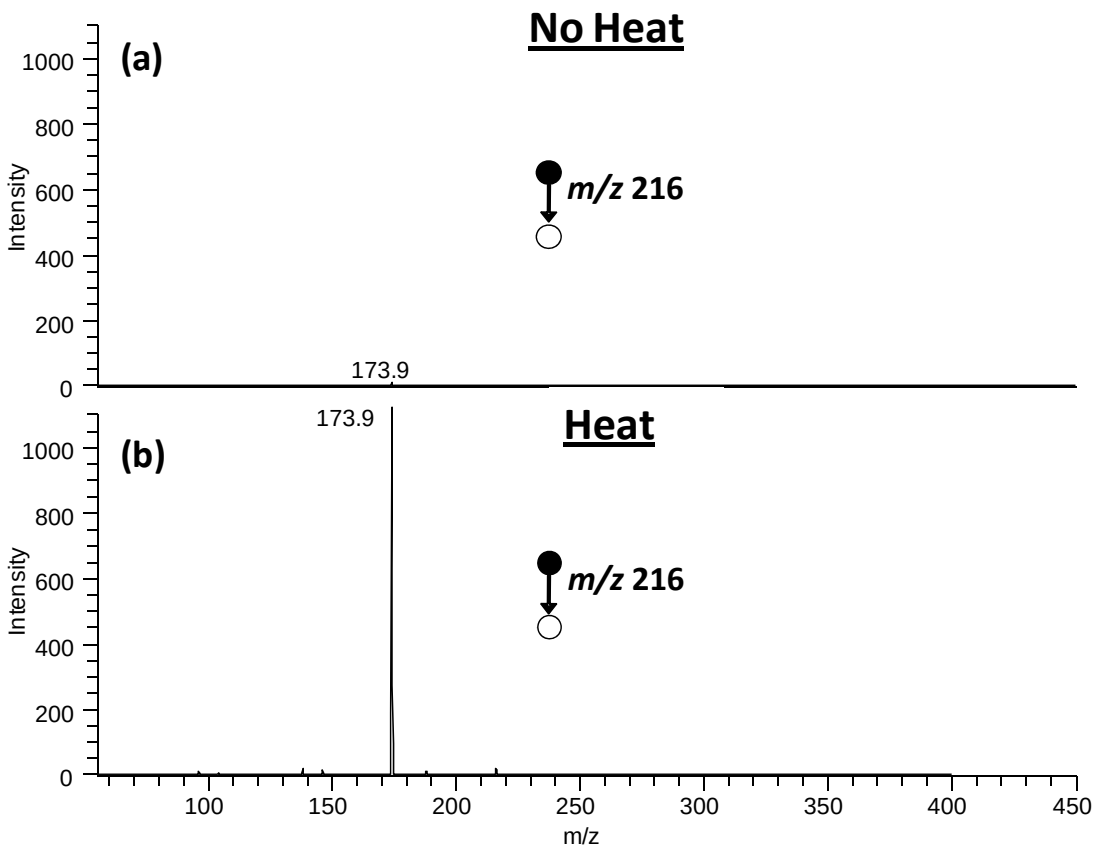

Figure 2.1 Comparison of signal for a (a) non-heated substrate versus a (b) heated substrate for the MS/MS spectrum $[M+H]^+$ (*m/z* 216) of atrazine.

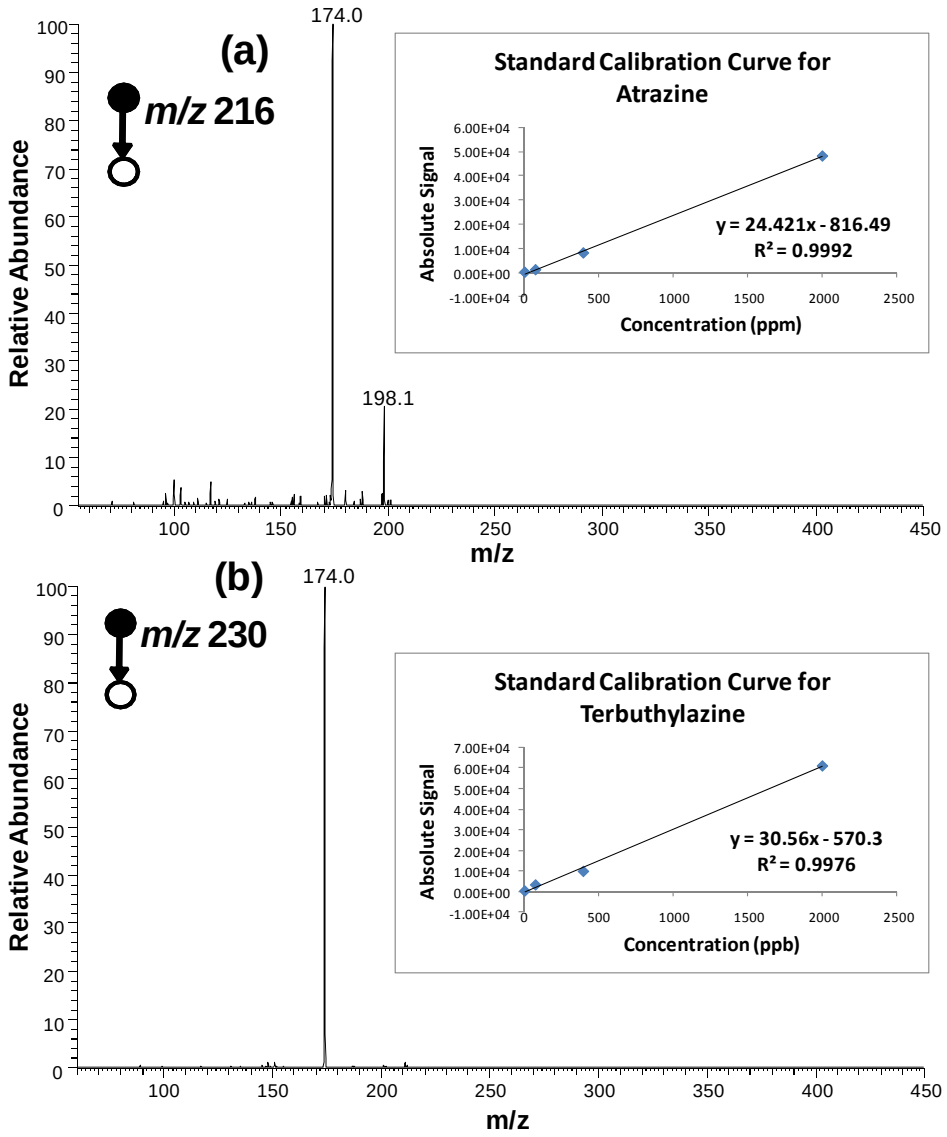

Figure 2.2 (a) LTP-MS/MS analysis of atrazine in an orange (QuEChERS) extract spiked with 10 µg Kg^{-1} (MS/MS: *m/z* 306 → 201); b) LTP-MS/MS analysis of terbuthylazine in a tomato (QuEChERS) extract spiked with 15 µg Kg^{-1} (MS/MS: *m/z* 228 →186). The LTP-MS experiments were performed using 3 µL of sample extracts spotted onto the glass substrate heated at 150 °C, with examination by tandem mass spectrometry. Example calibration curves for both analytes are overlaid onto the corresponding spectrum.

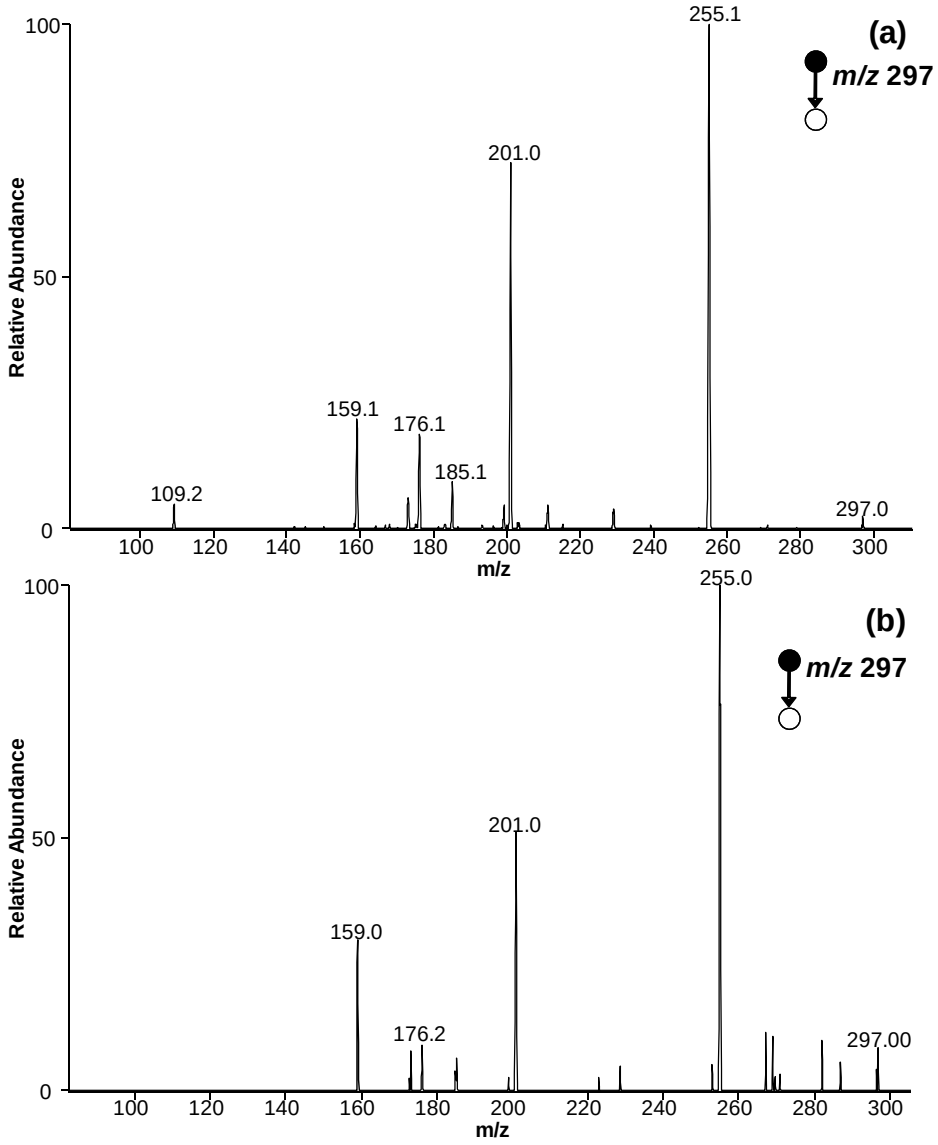

Figure 2.3 Identification of the fungicide imazalil in unspiked market purchased citrus fruits samples by LTP-MS/MS, (a) orange; (b) lemon. The main characteristic fragment ions of imazalil are: *m/z* 255, 201, 159, 176 and 109. The analyses were performed directly on the peel of the fruits without the use of heat using standard LTP-MS without substrate.

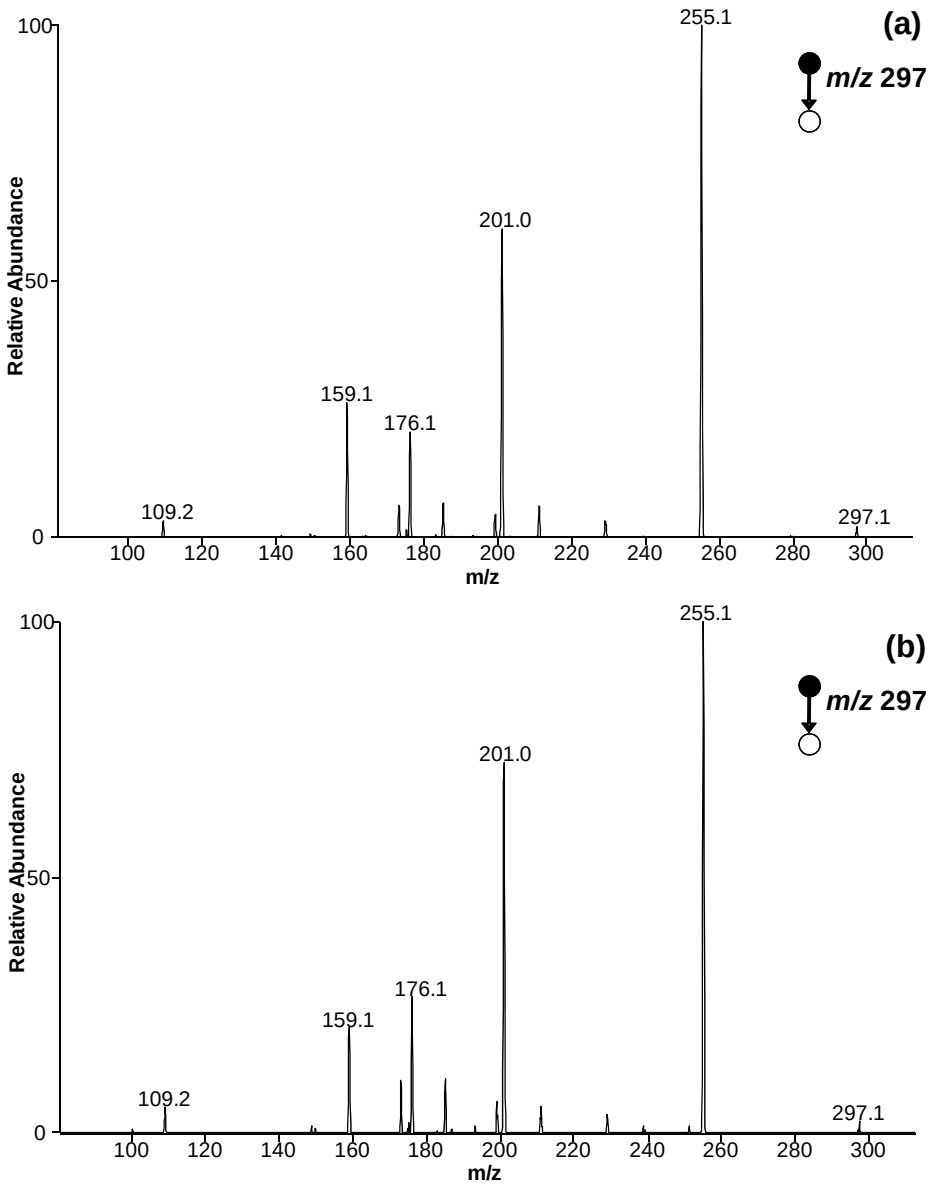

Figure 2.4 Analysis of real unspiked fruit samples by LTP-MS/MS (after sample extraction with QuEChERS protocol); (a) LTP-MS/MS analysis of an apple extract where imazalil was detected (0.28 mg Kg^{-1} by LC-MS analysis); (b) LTP-MS/MS analysis of a grapefruit extract where imazalil was detected (0.12 mg Kg^{-1} by LC-MS analysis). The LTP-MS experiments were performed using 3 µL of sample extracts spotted onto the glass substrate heated at 150 °C, with examination by tandem mass spectrometry.

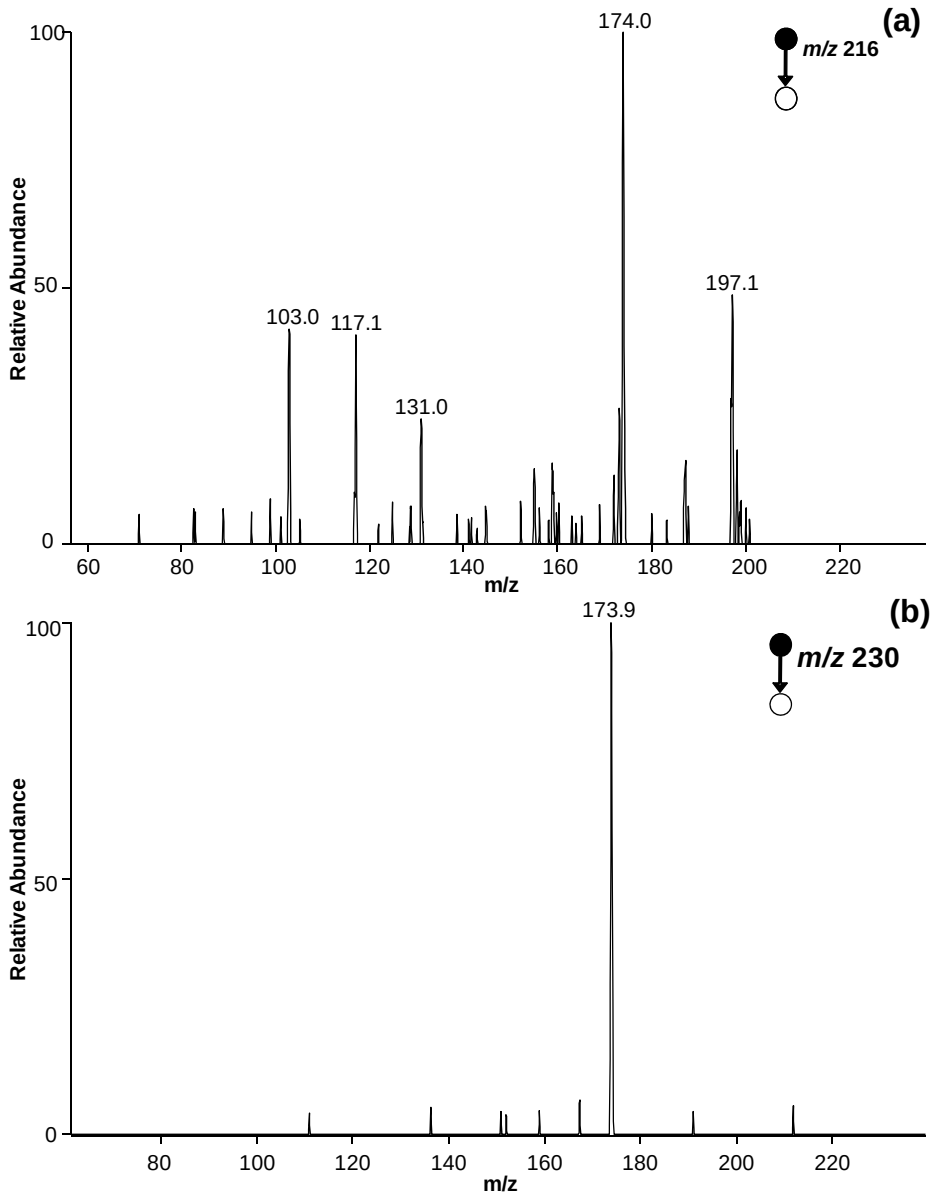

Figure 2.5 Detection of selected herbicides spiked into environmental water samples by LTP-MS/MS. (a) Detection of atrazine (spiking level: 1 μg L^{-1}) in an aqueous solution (MS/MS: *m/z* 216 → 174); (b) Detection of terbuthylazine (spiking level: 10 μg L^{-1}) in aqueous solution (MS/MS: *m/z* 230 → 174). The LTP-MS experiments were performed using 3 μL of the water sample (without any sample preparation) spotted onto the glass substrate heated at 150 °C, with examination by tandem mass spectrometry.

CHAPTER 3

HANDHELD LOW-TEMPERATURE PLASMA PROBE FOR PORTABLE "POINT-AND-SHOOT" AMBIENT MASS SPECTROMETRY

3.1 Introduction

Miniaturization of analytical instrumentation for portability and field-applicability has been an area of interest in many areas of science. A common hurdle for the development of portable instrumentation is the ability to maintain adequate analytical performance with a more compact and potentially less sophisticated device. Techniques such as Raman spectroscopy[1] and X-Ray fluorescence (XRF)[2] have been shown to overcome many of the hurdles of portability and are commonly used in the field. One aspect of maintaining appropriate analytical performance with any technique pertains to the ability to present the sample to the instrument so it can be efficiently and effectively probed. Methods such as attenuated total reflectance for IR absorption spectroscopy[3] and laser-induced breakdown spectroscopy (LIBS)[4] for atomic emission spectroscopy have substantially simplified the sampling process and proven useful for portable instrumentation.

Of the many portable analytical instrumentations available, none possess the ability to provide a measurement as specific, sensitive and broadly applicable as mass spectrometry (MS), which can be accentuated with tandem MS to expand capabilities for

complex-mixture analysis. An intriguing approach to sample collection and introduction is through ambient MS, which incorporates direct sampling and desorption/ionization from a sample in its native environment in one step. While initially a difficult task, miniature MS instruments now have the ability to introduce ions formed in the ambient environment into the reduced-pressure mass analyzer by limiting ion introduction to a short period of time via a discontinuous atmospheric-pressure interface (DAPI).[5] Using DAPI, the coupling of ambient ionization methods with a miniature mass spectrometer enables rapid, *in situ* analysis of complex mixtures without sample pretreatment;[6,7] however, this coupling has mostly been achieved in the laboratory setting due to the lack of true source portability. While many of the ambient ionization methods have shown impressive performance and simplification of procedure, they are often bulky when considering the gases, solvents, electrical power and/or solvent pumps that are needed for operation. This limits the possibility of size reduction as well as increasing setup time. For example, desorption electrospray ionization (DESI)[8] requires a syringe pump for solvent flow as well as gas flow rates of approximately 1 L/min,. There also exist ambient ionization sources based on lasers,[9-11] which currently are not portable but have been demonstrated to desorb viruses, bacteria and blood cells for MS analysis[12] and can be combined with electrospray ionization (ESI) for increased ionization efficiency.[13] Consequently, there is still a need for a handheld and portable device with the ability to easily interrogate surfaces.

Of the many ambient ionization sources,[14] only a few exhibit the properties necessary for complete portability. One technique that is easily made portable is paper-spray ionization,[15] which requires triangular pieces of paper to deposit each sample on,

solvent, and a power supply providing ~3.5 kV. A similar technique to paper spray has utilized wooden toothpicks instead of paper, making it easier to sample from some surfaces, and is a promising technique for forensic investigations.[16] A modified version of DESI, Venturi easy ambient sonic-spray ionization (V-EASI),[17] can also be made portable because a syringe pump is not required and canned air can be used to supply the nebulizing gas.[18]

Plasma-based ambient ionization techniques are an intriguing approach for portability due to their inherent lack of solvent and generated waste, as well as the ability to change the discharge gas composition for increased desorption/ionization capabilities.[19,20] Plasma assisted desorption/ionization (PADI)[21] is a technique that has been demonstrated as a potentially portable ambient ionization source without the need of a pressurized gas.[22] Another plasma-based approach that meets all of the requirements for portability is low-temperature plasma (LTP) ambient ionization, based on a room-temperature dielectric barrier discharge.[23] The ability of LTP to operate at gas flow rates below 100 mL/min with powers less than one Watt, allows the plasma to be powered by small batteries along with a miniature helium tank. No solvents or liquid/gas pumps are necessary. In addition, the ability to directly analyze solid, liquid and gaseous samples with LTP-MS allows for a wide variety of applications.[23-25]

Here, we present the development and application of the first handheld and wireless LTP source for point-and-shoot analyses on both bench-top and miniature mass spectrometers. A major benefit of the handheld LTP source pertains to the reduced setup time and its ease of use. The entire source, including consumables such as helium and power, is enclosed in a handheld device weighing ~0.9 kg. Various samples have been

analyzed to compare the analytical performance of the handheld source to the LTP source described by Harper *et al*.[23] as well as the effects of helium versus air as the discharge gas. A long-distance ion transport interface from the sampling region to the MS inlet has demonstrated the ability to analyze samples at locations that are non-proximate to the mass spectrometer.

3.2 Experimental

3.2.1 Chemicals and Reagents

Pesticide analytical standards were purchased from Dr. Ehrenstorfer GmbH. (Ausburg, Germany) and from Riedel de Haën, Pestanal® quality (Seelze, Germany). Analytical standards of explosives were purchased from Cerilliant Corporation (Round Rock, Texas). Individual pesticide and explosive stock solutions (200 – 300 μg mL^{-1}) were prepared in methanol and stored at -20 °C. Working solutions were prepared by appropriate dilution with acetonitrile. A Milli-Q-Plus ultra-pure water system from Millipore (Bedford, MA, USA) was used to obtain HPLC-grade water. HPLC-grade acetonitrile and methanol were obtained from Mallinckrodt Baker Inc. (Phillipsburg, NJ, USA).

3.2.2 Handheld Low-Temperature Plasma Ion Source

The handheld LTP source consisted of a battery-powered circuit, a glass tube for plasma formation, a miniature helium cylinder with a regulator (49615HeK, Leland Limited Inc., South Plainfield, NJ, USA), and a plastic housing (A9056208, OKW

Enclosures, Inc., Bridgeville, PA, USA). The circuit, converting a low, DC potential to a high, AC potential, is discussed in greater detail in the 'Results and Discussion' section. Parts used for the circuit consisted of an N-channel MOSFET (497-2758-5-ND, Digi-key, Thief River Falls, MN, USA), 555 timer (497-1963-5-ND, Digi-key, Thief River Falls, MN, USA), 6-volt regulator (497-1444-5-ND, Digi-key, Thief River Falls, MN, USA), step-up transformer (28K077, Information Unlimited, Amherst, NJ, USA) and a 7.4-volt, 900 mAh lithium polymer battery (Tenergy Corp., Fremont, CA, USA). The entire source cost less than $290 USD in parts, which included $198 USD for the gas regulator.

The actual LTP probe used was a smaller version of the one reported previously.[23] A 1/16" Swagelok® tee was used to connect a 1.6-mm o.d. PEEK® gas line, a borosilicate capillary (1.6 mm o.d., 0.86 mm i.d.) and a grounded stainless-steel wire (32 AWG) that is coaxially positioned inside the glass capillary. The gas line contains an additional 1-cm long piece of PEEK® capillary (100 μm i.d., 1.6 mm o.d.) to restrict He flow to the plasma to extend the lifetime of the miniature He cylinder; the flow rate could be controlled by adjusting the outlet pressure on the helium regulator. The high-voltage electrode on the outside of the glass tube consisted of a coiled and soldered wire (approximately 2 mm in width) and was positioned such that the internal grounded wire terminated in the center of the external electrode. The external electrode was connected to the high-voltage output from the secondary winding of the transformer. A mechanical trigger connected to the positive terminal of the battery completed the circuit and, along with the flow of either He or air as the discharge gas, enabled plasma formation. It is important to note that when air was used as the discharge gas in these studies, it was typically supplied by a large cylinder of compressed air. However, a small diaphragm

pump (NMP015M, KNF Neuberger, Inc., Trenton, NJ, USA) can also be used to supply flowing air to the plasma region by supplying 6 volts (regulated) from the battery, but the pump greatly increased power consumption and was not used in these studies to conserve battery power. This small pump adds minimal weight (65 g) and size to the device while providing sufficient air flow to sustain the discharge.

3.2.3 Benchtop Mass Spectrometer

Initial experiments were performed using a benchtop Thermo LTQ linear ion trap mass spectrometer (Thermo Finnigan San José, CA) tuned for optimum detection of the precursor ion of interest via the Xcalibur software. LTP-MS analyses were performed in the positive- and negative-ionization mode, making no changes to the source including the applied voltage, and spectra were collected with automatic gain control enabled, a maximum ion-trap injection time of 200 ms, and 2 microscans per spectrum. The main experimental parameters used were as follows: capillary temperature: 200 ºC; tube lens: -65 V; capillary voltage: -15 V. Tandem mass spectrometry experiments (MS/MS) were performed via collision-induced dissociation (CID) in order to confirm the presence of particular agrochemicals in the studied samples. These experiments were performed using an isolation window of 1.5 Th and 25 - 35% collision energy (manufacturer's scale). Long-distance ion transport was achieved with a direct connection of a one-meter-long Tygon® tube (1/8" o.d. and 1/16" i.d.) to the LTQ inlet capillary, which pulled ions to the LTQ from a Tygon® and Teflon® sampling vessel that enclosed the LTP sampling region when placed flush with a sample.

3.2.4 Miniature Mass Spectrometer

Experiments on a miniature mass spectrometer were performed using a Mini 10.5 mass spectrometer as described by Gao *et. al.*[5] Key features include the use of a rectilinear ion trap (RIT), TPD011 hybrid turbomolecular pump (Pfeiffer Vacuum Inc., Nashua, NH), a two-stage diaphragm roughing pump (KNF Neuberger Inc., Trenton, NJ), and a discontinuous atmospheric pressure interface (DAPI) all combined as a compact device weighing ~10 kg and consuming less than 75 W. The DAPI consisted of a pinch valve (390NC24330, ASCO Valve Inc., Florham Park, NJ) surrounding conductive tubing (i.d. of 1.6 mm., an o.d. of 3.2 mm., and a length of 5.0 cm), which was connected to two capillaries. A transfer capillary (i.d. 1 mm, o.d. 1.6 mm, 5 cm length) was connected via Swagelok® fittings to allow direct injection of ions into the RIT while the sampling capillary (i.d. 250 μm, o.d. 1.6 mm, 10 cm length) was filed to a point and exposed to atmosphere. Upon application of a variable 5 V pulse from the Mini 10.5, the pinch valve would open for a short period of time, which allowed packets of air/ions from atmosphere to enter the ion trap. Mini 10.5 operating conditions include: 15 ms DAPI open time, *m/z* 50 – 500 mass range, grounded and non-heated inlet capillary. MS/MS was performed via notch broadband isolation and resonant excitation of the selected ion.

3.3 Results and Discussion

3.3.1 Specifications of Handheld LTP

A diagram of the handheld LTP probe is shown in Figure 3.1a with a photograph shown in Figure 3.1c. The overall weight of the handheld source is 910 g, which reduces to ~280 g when air is used as the discharge gas due to the replacement of the helium cylinder and regulator by a diaphragm pump. The cost of parts for the entire source is quite inexpensive, with most of the cost due to the regulator, and easy to assemble. The incorporation of a PEEK® flow restrictor reduced helium flow rates to 100 mL/min or less, depending on the back pressure supplied by the regulator. With this configuration and a back pressure of ~70 kPa, there was sufficient helium in the cylinder to sustain the plasma for over 8 hours. In addition, the simple, battery-operated power supply, (shown in Figure 3.1b) was able to power the plasma with ~2 kV_{p-p} at 100 kHz for over two hours continuously. It should be noted that the total time of operation of the source in the field is much longer, considering the power supply is only triggered on when needed; the helium supply may be turned off while not in use for a prolonged lifetime as well, typically lasting 8 – 10 hours before requiring a battery recharge or new helium cylinder. The circuit utilized a 7.4-V, 900 mAh Li-polymer battery, which was down-regulated to 6 V for circuit stability by a voltage regulator. The constant 6-V output was applied to one lead of the primary winding of a transformer as well as a 555 timer. The output of the 555 timer, which was wired in an astable configuration with a repetition rate of ~100 kHz with 50% duty cycle, was connected to the gate of an N-channel MOSFET. The drain of the MOSFET was connected to the other lead on the primary winding of the transformer,

while the source of the transistor was held at ground. One end of the secondary winding provided the high-voltage AC waveform for the LTP, while the other was grounded. Even though the input to the transformer was a square wave, the circuit behaves as resonant LC circuit, so the output closely resembles a sine wave.

3.3.2 Handheld LTP Testing on Benchtop MS

3.3.2.1 Tablet Analysis

The performance of the handheld LTP probe was characterized through various applications on a conventional benchtop ion-trap instrument. Pharmaceutical tablet analysis has been a targeted application for ambient MS analysis since the onset of the field,[22,26-29] acting as a demonstration of direct sample analysis with no preparation. Figure 3.2 shows mass spectra recorded for the direct analysis of a headache relief tablet with handheld LTP-MS (acquired with a Thermo LTQ). The spectra reveal the three active ingredients: caffeine, acetaminophen and aspirin. In the positive-ion mode (c.f. Figure 3.2a), the ion $[M+H]^+$, where M indicates an intact molecule, was detected for all three compounds at 195 Th for caffeine, 152 Th for acetaminophen and 181 Th for aspirin (not labeled). Numerous adduct and fragment peaks were also evident, especially for aspirin. The same experiment was also done in the negative-ionization mode, without changing any of the ion-source settings. Analysis of the tablet in the negative-ion mode revealed a small peak for the proton-abstraction ion, $[M-H]^-$, of aspirin at *m/z* 179 as well

as a fragment ion at *m/z* 137, $[M\text{-}H\text{-}C_2H_2O]^-$, as the most abundant peak (c.f. Figure 3.2b). No negative ions were detected for acetaminophen or caffeine because of their high gas-phase basicities. The assignments of each of the detected species were verified with MS/MS.

3.3.2.2 Large-Scale vs. Handheld LTP

One important metric of the handheld, portable version of the LTP probe is how well it compares with the large-scale LTP probe. The conditions used for the handheld and large-scale probes are listed in Table 3.1. Note that the conditions for the large-scale LTP probe were the same as those used in the original optimization experiments.[23] The large-scale LTP source was operated with a lower-frequency voltage waveform, increased voltage/power, increased helium flow rates and within a larger diameter glass tube in comparison to the handheld LTP probe. Figure 3.3 displays MS/MS data recorded for a common agrochemical, atrazine (24 pg, absolute on SURFACE) using the large-scale (Figure 3.3a) and handheld (Figure 3.3b) LTP with a Thermo LTQ. The fragmentation observed is due to propene loss from $[M+H]^+$.

Using optimized conditions for each probe on the same MS instruments, the absolute signal was slightly larger with the handheld LTP probe as was the S/N which was ~22 for the handheld probe and ~16 for the large-scale probe. This trend was also true for most other analytes when comparing the two sources. Of the eleven

agrochemicals analyzed, LODs ranged from essentially identical to about an order of magnitude better with the handheld LTP source (c.f. Table 3.2). While the small discrepancies in LODs between the large-scale and handheld LTP source could be attributed to various instrumental and operating parameters, including gas-flow profile, source-to-sample orientation, detector efficiency, it is clear that reducing the power and helium flow for the handheld LTP setup did not negatively affect the analytical performance.

3.3.2.3 Effect of Discharge Gas: Air vs. Helium

Another capability of the handheld LTP probe includes the use of either helium or simply air as discharge gas. To remain consistent in comparing the use of an air and a helium discharge, similar voltages were used for each gas, which included the use of the same PEEK® flow restrictor and a large cylinder with a back pressure of 140 kPa. It should be noted that while the voltage was held constant for the helium and air plasmas, the current was not, resulting in different currents/powers for the two discharges. Figures 3.4a and 3.4b show tandem mass spectra using a handheld LTP with a Thermo LTQ for the detection of 1.2 ng of the agrochemical isoproturon obtained with helium and air, respectively, as the discharge gas, revealing fragments at 72 and 165 Th. Interestingly, the signal was between one and two times higher with helium as compared to air. The LODs obtained for the analysis of other agrochemicals that readily undergo proton transfer (c.f. Table 3.2), were typically 1 – 2 orders of magnitude better with a helium

LTP. Trinitrotoluene (TNT) was a unique example where no analyte ions were detected with air LTP, despite being able to readily detect analyte ions with helium LTP. This phenomenon is attributed to the fact that TNT ionizes by a different mechanism, either deprotonation or electron attachment, than the eleven pesticides that favor protonation. The use of air establishes a difference in the LTP sampling region, so that neither ionization mechanism can take place for TNT. This point is further evidenced in Figures 3.4c and 3.4d, where there is much less chemical noise in the negative ion mode when using air-based LTP. It has been seen in other studies that the use of helium as a discharge gas for LTP often produces an abundance of background ions as compared to a nitrogen- or air-based LTP,[23] likely due to excited states of helium exceeding 19 eV capable of ionizing a greater range of species.

Examples of cases where the analytical performance was similar when either air or helium was used as the discharge gas includes the analysis of explosives that readily undergo nitrate adduction, as with RDX, PETN and tetryl. In Figure 3.4, the analysis of 200 pg of RDX with both plasma gases in the handheld LTP revealed the $[M+NO_3]^-$ adduct at *m/z* 284 (cf. Figures 3.4c and 3.4d) using a Thermo LTQ. The signal for RDX was higher when helium was used, but the ratio of the signal to the surrounding chemical noise was much poorer. Overall, the detection limits (c.f. Table 3.2) are roughly the same for air and helium discharges for explosives which undergo nitrate addition. In general, helium is the appropriate choice for achieving better LODs for most samples, unless

nitrate addition is expected. The ability of both helium and air plasmas to generate NO_3^- and higher-order nitrate clusters in large abundance in the ambient air from N_2 and O_2 allows sufficient adduct formation with appropriate analytes. However, the reason for reduced sensitivity with air versus helium for proton transfer ionization is unclear, but is likely due to a difference in reagent ion formation with the different discharge gas compositions.

3.3.3 Handheld LTP on Mini 10.5 MS

The coupling of handheld LTP with a miniature mass spectrometer results in a completely field-portable instrument, capable of analyzing gaseous, liquid and solid samples in their native, ambient environment. The process of minimizing helium and power consumption in comparison to large-scale LTP has led to other benefits. The decreased voltage for operation of the source reduced the radiated AC noise which has adverse effects on the MS instrumentation as observed with previous versions of the LTP. In addition, lower helium flow rates also helped when coupling the source to a Mini MS which has limited pumping capacity because the performance of the small turbomolecular pumps degrades when helium is being pumped. This phenomenon has required the use of supplemental pumping in the past,[30] which was not needed for coupling of the handheld LTP with the Mini 10.5 MS.

An MS/MS spectrum for 1.2 ng of malathion on the Mini 10.5 (c.f. Figure 3.5) reveals the expected loss of ethanol. Tandem mass spectra for malathion and other pesticides were used in determining LODs for handheld LTP on the miniature instrument. Absolute quantities within an order of magnitude of a few nanograms could confidently be detected for all of the agrochemicals and produced adequate signal for the qualitative assessments often desired for *in situ* experiments. The Mini 10.5 instrument did not have the ability to detect negative ions, so explosives were not analyzed.

Another potential compound class of interest for detection by a portable instrument is drugs of abuse. The detection of illicit drugs with the large-scale LTP on a benchtop instrument has been demonstrated,[24] with LODs in the range of picograms to nanograms, absolute. In the current study, the ability to detect a drug directly from an individual's finger after a few hours after exposure was tested. A small amount, 1 μg, of methamphetamine was deposited onto a human finger and analyzed two hours after application with handheld LTP-Mini 10.5 MS/MS. The subject was allowed to perform daily tasks with his hands as usual for the two hours. It should be noted that, the subject did not wash his hands between the time of spotting the drug and analysis. The spectrum in Figure 3.6 was obtained by direct analysis of the finger with the handheld LTP probe, revealing the presence of methamphetamine with the $[M+H]^+$ and characteristic fragment ions present at 150 and 119 Th respectively. The non-destructive and room-temperature nature of the handheld LTP allows analysis of delicate samples, such as human skin, without damage or discomfort.

3.3.4 Long-Distance Ion Transfer

To demonstrate the most likely way a handheld ambient ionization source would be used in the field, a long-distance ion transfer system was implemented to help transport ions from non-proximate sampling regions to the MS inlet. Similar designs have been reported by Cotte-Rodriguez *et al*. for non-proximate detection with DESI[31] and by Garimella *et al*., where simulations and experimental results demonstrated that plastic tubing allows effective transfer of ions produced by DESI and LTP for distances over one meter.[32] This simple system, diagrammatically shown in Figure 3.7a, consisted of a large Tygon® and Teflon® vessel, which can be placed flush with a sample surface, allowing interaction of excited species from the LTP with the sample in a fixed geometry. The ions/neutral species were then transferred to the MS inlet via a flexible one-meter-long Tygon® tube. Laminar flow is established 1 cm into the tube, so any reasonable bends in the tube had little effect on signal. The vacuum within the Thermo LTQ created the suction necessary to pull the ions/neutrals to the MS inlet. This setup was tested on the commercial bench-top Thermo LTQ. Cocaine, highly prevalent on United States banknotes,[33] was detected on an untreated U.S. one dollar bill using tandem MS (Figure 3.7b). The expected loss of benzoic acid yields the base peak at 182 Th from the parent $[M+H]^+$ ion at 304 Th. Figure 3.7c is the resulting mass spectrum from the analysis of 10 µg of RDX on a glass microscope slide. Again, the $[M+NO_3]^-$ ion was present at *m/z* 284. With the current setup, around two orders of magnitude of signal loss was

experienced and remains an area of future work as well as the implementation of long-distance ion transport on miniature MS instruments.

3.4 Conclusions

A handheld low-temperature plasma probe has been developed for both miniature and bench-top MS applications. Despite using lower power and helium flow rates in comparison to a conventional, large-scale LTP, there was no loss in analytical performance with the handheld LTP-MS setup. While helium was typically used as the discharge gas, due to typically obtaining better LODs, air was also effective for many analytes. When using air, the weight of the handheld source was ~280 g, with electrical current from a 7.4 Li-polymer battery being the only consumable. When coupled with a Mini 10.5 MS, LODs at the nanogram level were achieved for various agrochemicals as well as the ability to directly detect methamphetamine from skin; however, the desorption capabilities of plasma sources inherently limit the methodologies to lower molecular weight analytes. The demonstration of long-distance ion transfer with the handheld LTP and a flexible transfer line has shown the potential for point-and-shoot analysis with a free range of motion about the MS instrument.

3.5 References

1. Sutherland, W. S.; Alarie, J. P.; Stokes, D. L.; Vodinh, T. *Instrum. Sci. Technol.* 1994, 22, 231.

2. Karttunen, J. O.; Evans, H. B.; Niemann, R. L.; Henderson, D. J.; Markovic.Pj *Anal. Chem.* 1964, 36, 1277.

3. Harrick, N. J. *J. Phys. Chem.* 1960, 64, 1110.

4. Debrasguedon, J.; Liodec, N. *C.R. Hebd. Acad. Sci.* 1963, 257, 3336.

5. Gao, L.; Cooks, R. G.; Ouyang, Z. *Anal. Chem.* 2008, 80, 4026.

6. Sanders, N. L.; Kothari, S.; Huang, G.; Salazar, G.; Cooks, R. G. *Anal. Chem.* 2010, 82, 5313.

7. Sokol, E.; Noll, R. J.; Cooks, R. G.; Beegle, L. W.; Kim, H. I.; Kanik, I. *Int. J. Mass Spetrom.* 2011, 306, 187.

8. Takats, Z.; Wiseman, J. M.; Gologan, B.; Cooks, R. G. *Science* 2004, 306, 471.

9. Brady, J. J.; Judge, E. J.; Levis, R. J. *Rapid Commun. Mass Spectrom.* 2009, 23, 3151.

10. Nemes, P.; Vertes, A. *Anal. Chem.* 2007, 79, 8098.

11. Shelley, J. T.; Ray, S. J.; Hieftje, G. M. *Anal. Chem.* 2008, 80, 8308.

12. Peng, W. P.; Yang, Y. C.; Kang, M. W.; Tzeng, Y. K.; Nie, Z. X.; Chang, H. C.; Chang, W.; Chen, C. H. *Angew. Chem. Int. Ed.* 2006, 45, 1423.

13. Rezenom, Y. H.; Dong, J.; Murray, K. K. *Analyst* 2008, 133, 226.

14. Monge, M. E.; Harris, G. A.; Dwivedi, P.; Fernández, F. M. *Chemical Reviews* 2013, 113, 2269.

15. Wang, H.; Liu, J.; Cooks, R. G.; Ouyang, Z. *Angew. Chem.-Int. Edit.* 2010, 49, 877.

16. Hu, B.; So, P. K.; Chen, H. W.; Yao, Z. P. *Anal. Chem.* 2011, 83, 8201.

17. Santos, V. G.; Regiani, T.; Dias, F. F. G.; Romao, W.; Jara, J. L. P.; Klitzke, C. F.; Coelho, F.; Eberlins, M. N. *Anal. Chem.* 2011, 83, 1375.

18. Schwab, N. V.; Porcari, A. M.; Coelho, M. B.; Schmidt, E. M.; Jara, J. L.; Visentainer, J. V.; Eberlin, M. N. *Analyst* 2012, 137, 2537.

19. Heywood, M. S.; Taylor, N.; Farnsworth, P. B. *Anal. Chem.* 2011, 83, 6493.

20. Wright, J. P.; Heywood, M. S.; Thurston, G. K.; Farnsworth, P. B. *J. Am. Soc. Mass. Spectrom.* 2013, 24, 335.

21. Ratcliffe, L. V.; Rutten, F. J. M.; Barrett, D. A.; Whitmore, T.; Seymour, D.; Greenwood, C.; Aranda-Gonzalvo, Y.; Robinson, S.; McCoustra, M. *Anal. Chem.* 2007, 79, 6094.

22. Bowfield, A.; Barrett, D. A.; Alexander, M. R.; Ortori, C. A.; Rutten, F. M.; Salter, T. L.; Gilmore, I. S.; Bradley, J. W. *Rev. Sci. Instrum.* 2012, 83, 063503.

23. Harper, J. D.; Charipar, N. A.; Mulligan, C. C.; Zhang, X. R.; Cooks, R. G.; Ouyang, Z. *Anal. Chem.* 2008, 80, 9097.

24. Jackson, A. U.; Garcia-Reyes, J. F.; Harper, J. D.; Wiley, J. S.; Molina-Diaz, A.; Ouyang, Z.; Cooks, R. G. *Analyst* 2010, 135, 927.

25. Zhang, Y.; Ma, X.; Zhang, S.; Yang, C.; Ouyang, Z.; Zhang, X. *Analyst* 2009, 134, 176.

26. Chen, H. W.; Talaty, N. N.; Takats, Z.; Cooks, R. G. *Anal. Chem.* 2005, 77, 6915.

27. Green, F. M.; Salter, T. L.; Stokes, P.; Gilmore, I. S.; O'Connor, G. *Surf. Interface Anal.* 2010, 42, 347.

28. Steeb, J.; Galhena, A. S.; Nyadong, L.; Facundo, J. J.; Fernandez, M. *Chem. Commun.* 2009, 4699.

29. Williams, J. P.; Scrivens, J. H. *Rapid Commun. Mass Spectrom.* 2005, 19, 3643.

30. Huang, G.; Xu, W.; Visbal-Onufrak, M. A.; Ouyang, Z.; Cooks, R. G. *Analyst* 2010, 135, 705.

31. Cotte-Rodriguez, I.; Mulligan, C. C.; Cooks, G. *Anal. Chem.* 2007, 79, 7069.

32. Garimella, S.; Xu, W.; Huang, G.; Harper, J. D.; Cooks, R. G.; Ouyang, Z. *J. Mass Spectrom.* 2012, 47, 201.

33. Armenta, S.; de la Guardia, M. *Trac-Trend Anal. Chem.* 2008, 27, 344.

Table 3.1 Specifications of handheld LTP versus large-scale LTP.

	Handheld LTP	Large-Scale LTP
Frequency	100 kHz	2.8 kHz
Voltage	~2 kV	5 – 15 kV
Gas Flow	<100 mL/min	~400 mL/min
Weight	0.910 kg	*~67 kg
Probe O. D.	1.5 mm	6.35 mm
Probe I. D.	0.86 mm	3.75 mm

*Weight includes LTP source, function generator, DC power supply, gas regulator and a 6.9 kL helium gas cylinder

Table 3.2 Limits of detection for various analytes with handheld and large-scale LTP-MS/MS with air and helium discharge gases.

Analyte Category	Analyte	LODs* (ng) Air Handheld LTP	He Handheld LTP	He Large-Scale LTP	He Handheld LTP/Mini MS
Pesticides	Amitraz	0.3	0.05	0.8	50
	Atrazine	0.01	0.003	0.005	0.1
	Buprofezin	0.2	0.004	0.04	0.2
	DEET	0.2	0.04	0.003	0.6
	Diphenylamine	0.6	0.04	0.07	0.2
	Ethoxyquin	300	0.9	8	30
	Isofenphos-methyl	6	0.09	1	10
	Isoproturon	0.7	0.04	0.2	6
	Malathion	5	0.2	0.7	1
	Paration-ethyl	0.2	0.05	0.01	200
	Terbuthylazine	0.004	0.001	0.006	0.3
Explosives	RDX	0.02	0.02	n.m.	n.m.
	TNT	n.d.	0.02	n.m.	n.m.
	PETN	0.2	0.05	n.m.	n.m.
	Tetryl	2	2	n.m.	n.m.

*LODs were calculated based on S/N = 3 from a calibration curve of at least 3 points using at least 3 repetitions for each point. The linear equation from the calibration curve was used to calculate the LOD between the lowest concentration detected and the highest concentration not detected (varying each concentration by ~one order of magnitude).

n.d. – not detected; n.m. – not measured

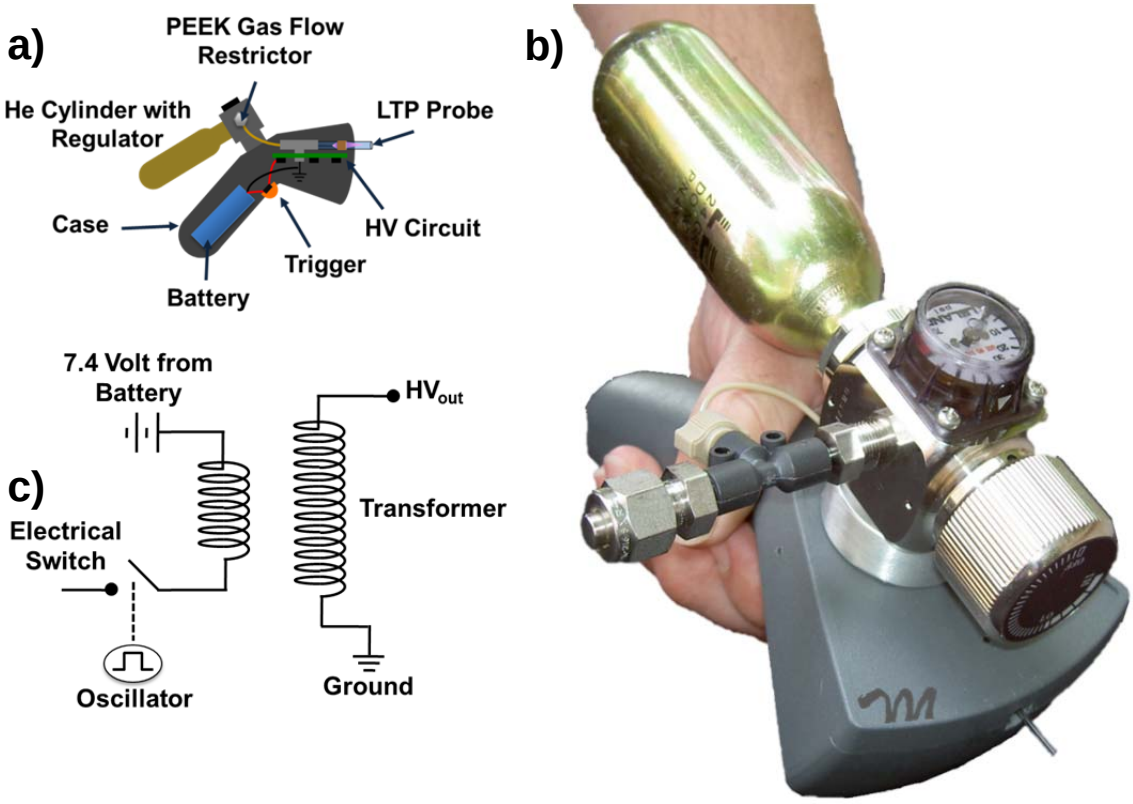

Figure 3.1 (a) Schematic and (b) photograph of the handheld LTP ionization source. (c) Schematic of the circuit used for the handheld LTP probe.

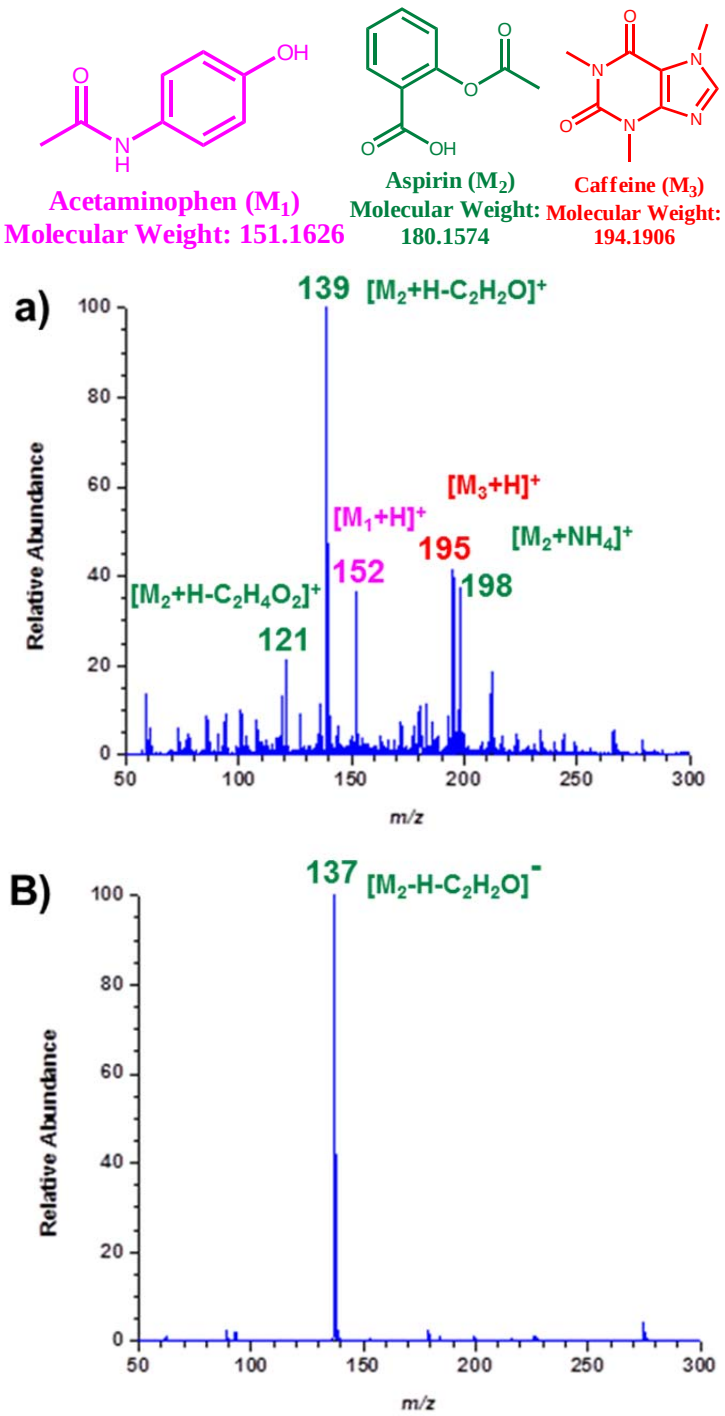

Figure 3.2 Direct handheld LTP-MS analysis of a headache relief tablet on the Thermo LTQ in (a) positive ion and (b) negative ion mode. Peaks labeled in magenta, green and red are related to acetaminophen, aspirin and caffeine respectively. Both spectra were acquired with a Thermo LTQ.

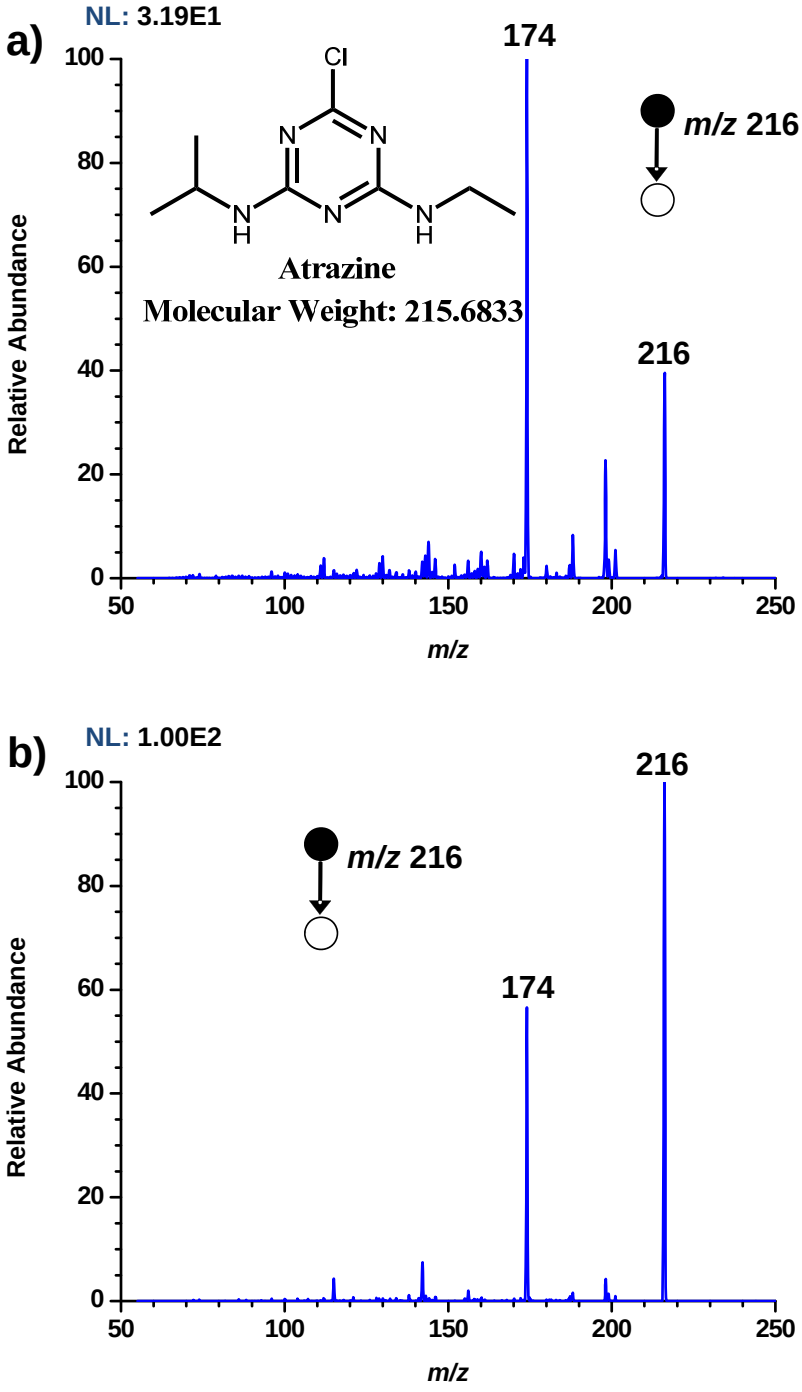

Figure 3.3 Analysis of 24 pg atrazine with (a) large-scale and (b) handheld LTP-MS/MS. Both spectra were acquired with a Thermo LTQ using the optimized conditions for each LTP probe.

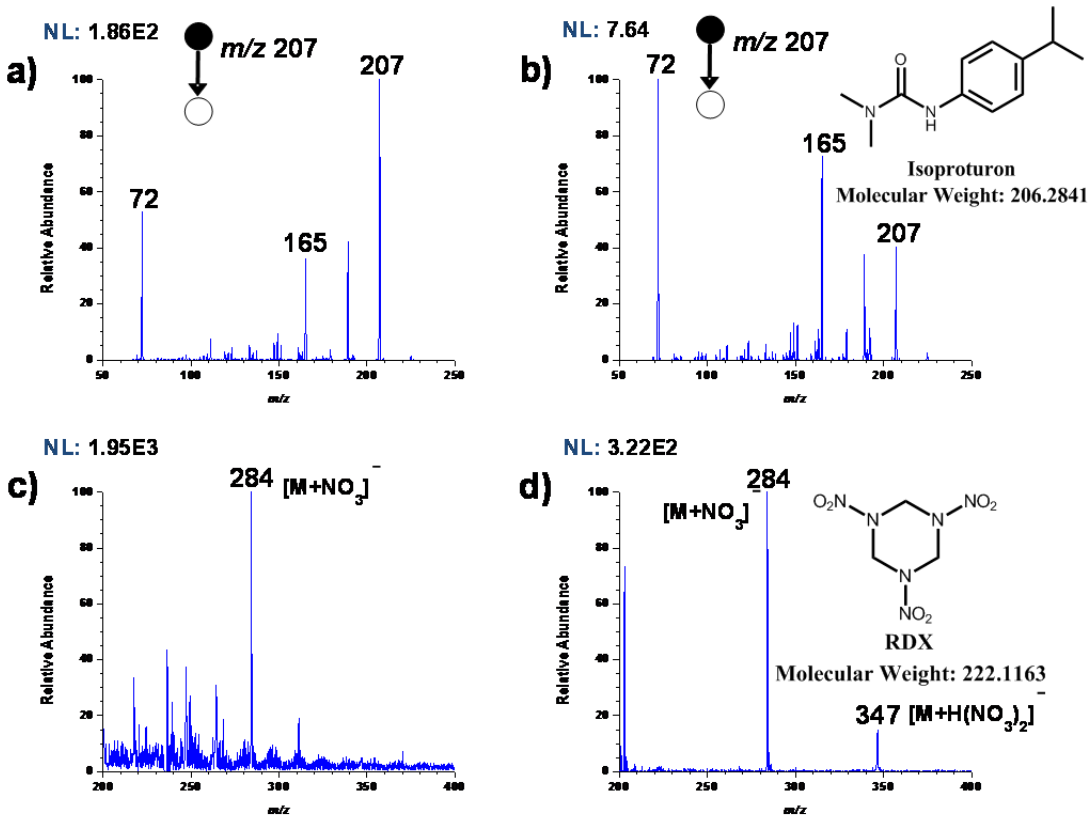

Figure 3.4 Positive ion tandem mass spectrum of 1.2 ng isoproturon with (a) helium- and (b) air-based handheld LTP. Negative-ion full-scan mass spectrum of 200-pg RDX with (c) helium and (d) air used as the discharge gas. All four spectra acquired with a Thermo LTQ. Air was supplied by a large compressed air cylinder for air-based handheld LTP.

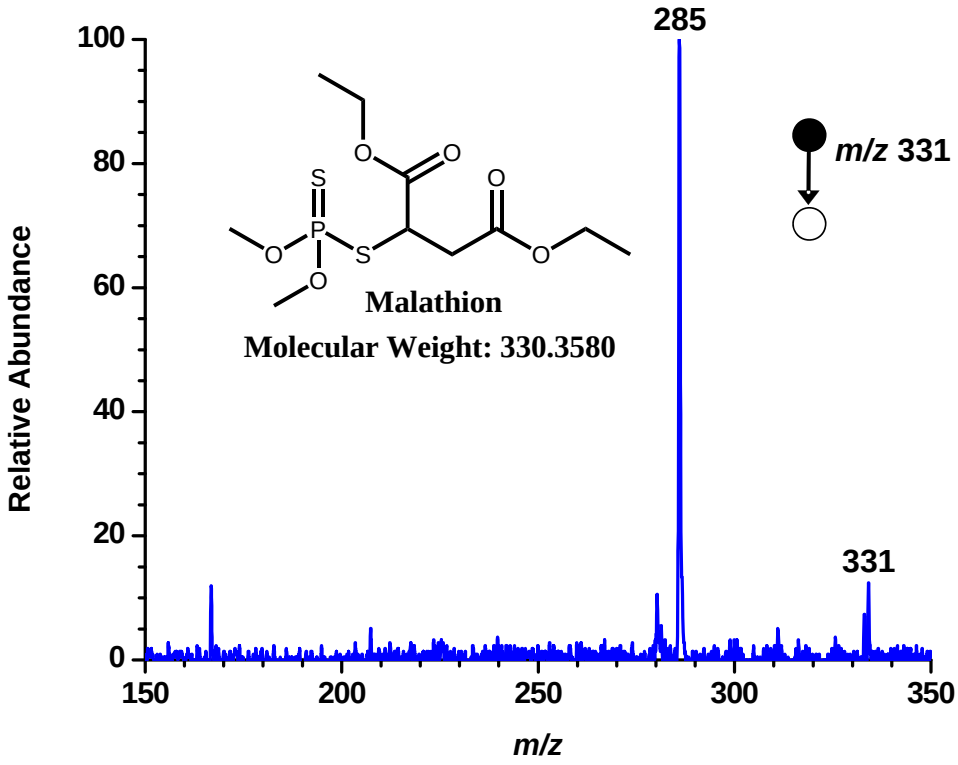

Figure 3.5 Handheld LTP MS/MS spectrum of 1.2 ng malathion using the Mini 10.5 MS.

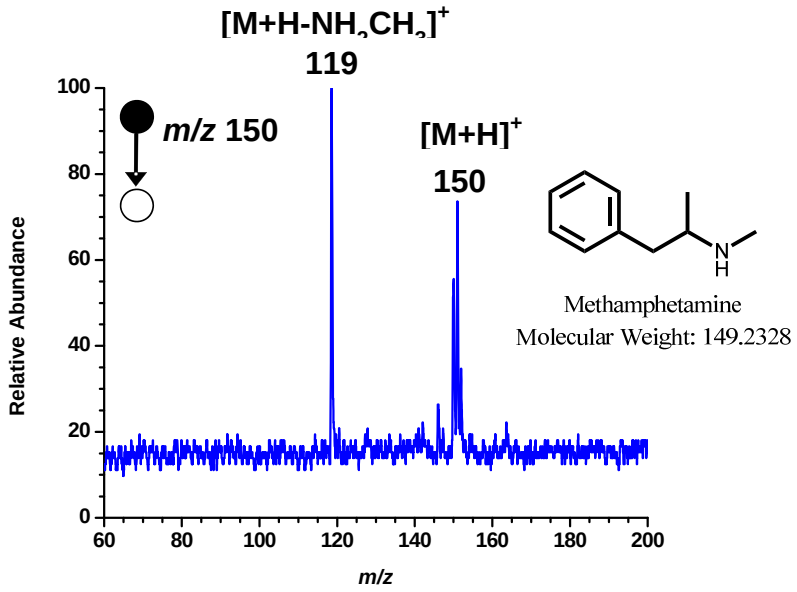

Figure 3.6 Analysis of 1 µg methamphetamine on an individual's finger two hours after being deposited with handheld LTP-MS/MS with a Mini 10.5 MS.

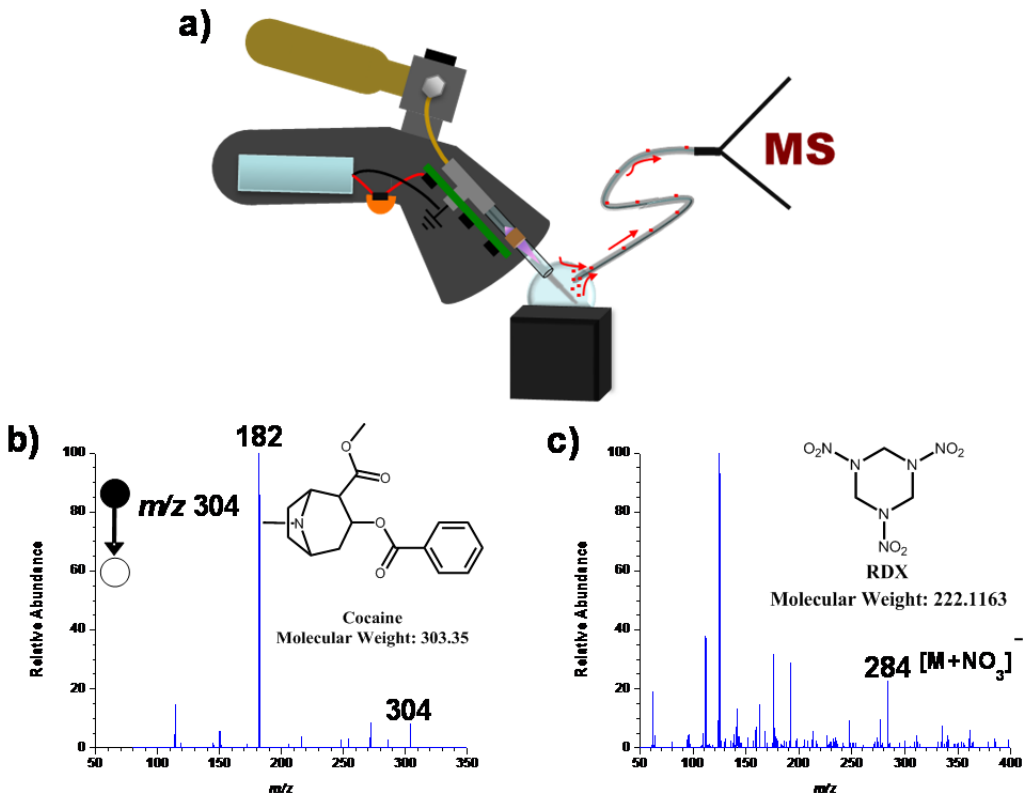

Figure 3.7 (a) Schematic of the handheld LTP with an interface used for long-distance ion transport to a Thermo LTQ. (b) The analysis of a U.S. one dollar bill with this configuration as well as (c) 10 µg of RDX from a glass slide.

CHAPTER 4

FUNDAMENTALS OF LTP: EMISSION SPECTROSCOPY

4.1 Introduction

A wide range of analytical techniques are readily used to characterize atmospheric- and reduced-pressure plasmas. One technique and focus of this dissertation is mass spectrometry, which is useful in identifying both positive and negative ions in the plasma. Electrical measurements, such as current and voltage, can help in the classification of discharge type (i.e. corona, glow, arc, etc.). In addition, a Langmuir probe allows one to obtain information such as electron temperature, electron density, and electric potential of a plasma. Plasma temperature, which is proportional to the power of a discharge, can easily be measured with various thermometric devices like thermocouples; however, IR thermography cameras are better suited for two- and three-dimensional temperature plots, as has previously been used to characterize LTP temperature profiles.[1]

While the various techniques are effective for their intended measurements, one technique that provides many of these metrics and more is emission spectroscopy. Hence, to better understand LTP on a fundamental level, various emission studies of the plasma plume were performed. From spectroscopic studies, several fundamental features of the plasma can be identified. Where mass spectrometry is used to determine the

composition of ions in the plasma, with emission spectroscopy it is possible to identify both ions and neutrals based on distinct emission wavelengths. In addition, extraction of the total energy balance or distributions among the various excited species in the plasma, as well as determination of electron density and electron and rotational temperatures (kinetics) is also permitted by emission spectroscopy.[2-4] Knowledge of the species responsible for atomic and molecular emission may also assist in the elucidation of desorption and ionization processes.[5-7] In the literature, He-based low frequency plasmas typically yield emission from OH, O, He, N_2 and $N_2^{+\bullet}$ species.[8]

The focus of this chapter is on the characterization of LTP through various emission spectroscopy studies. Full emission spectra over the visible light range help to determine which excited atomic and diatomic species are present in the discharge. For diatomic species, rotational temperatures were calculated by fitting with a Boltzmann distribution. The electron number density was calculated from H_β emission.[3] A monochromatic imaging spectrometer (MIS) was used to visualize 2D images of various emitting species under different plasma conditions. By using very short exposure times, it was possible to obtain time-resolved images of emission corresponding to plasma bullet propagation.[9,10] Positioning a fluorophore-coated glass-slide into the path of the LTP as well as on the focal plane of the MIS also provided some perspective into plasma-surface interactions.

4.2 Experimental

4.2.1 Atomic Emission Spectrometer

A series of UV-Vis spectroscopic studies were completed using an ACTIVA inductively coupled plasma atomic emission spectrometer (Horiba-Jobin Yvon, Longjumeau, France) spectrometer (c.f. Figure 4.1) equipped with a two-dimensional charge coupled device (CCD) detector. The ICP torch was removed and an LTP probe was fixed to a three-dimensional translation stage in the ICP compartment vertically to be aligned with the ICP torch axis and focused onto the entrance 20 μm slit of the spectrometer. The combination of the 2D CCD detector with a Czerny-Turner grating configuration allowed simultaneous measurement of the entire vertical emission profile of the plasma. Spectra were collected over a range of 200 – 780 nm as well as 1D spatial profiles for defined spectral ranges. Using a demagnification ratio of 3.12 : 1, a measurement height of 21.5 mm was possible. An exposure time of ~1 minute was necessary to obtain adequate signal-to-noise due to the relatively low emission intensities of LTP.

4.2.2 Monochromatic Imaging Spectrometer

A monochromatic imaging spectrometer (MIS) was used to obtain two-dimensional images of LTP emission (c.f. Figure 4.2). The instrument consisted of a collimating lens (plano-convex, fused silica, 48 mm dia.), a Heath monochromator (model EU 700, Heath Co., Benton Harbor, MI, USA), a focusing lens (plano-convex, fused silica, 48 mm dia.), and an intensified charge coupled device (iCCD, PI-MAX, 512 x 512 pixels, Princeton Instuments Inc., Trenton, NJ, USA). An LTP source was placed at a distance approximately equal to the focal length from the first collimating lens. This detection system enabled time-averaged (steady-state) and time-resolved images of single transitions of emitting species in the LTP plume. Time-averaged emission profiles were acquired with 10 second exposure times under various plasma conditions.

Nanosecond time-resolved images were acquired by gating the detector with the input LTP waveform. In each of the time-resolved 2D images, the gate delay refers to the time difference between the rising edge of the 5-volt square wave used for LTP and the beginning of the 100-200 ns time window at which emission was detected by the iCCD (c.f Figure 4.3). Each image was the summation of exposure for 35,000 gates with gate widths of either 100 or 200 ns. In two of the experiments, interaction of the plasma with a surface was studied by placing the surface in the focal plane of the MIS and aiming LTP emission at the surface, while recording time-resolved emission profiles. In one study, the surface was a sharp needle and emission at 391.2 nm (from N_2^+) was monitored. In a second study, the surface was a glass microscope slide coated with yellow highlighter and emission at 507 nm (near the λ_{max} of a fluorophore in the highlighter) was monitored.

4.2.3 LTP Probe for Spectroscopic Studies

The LTP probe was the same as the one used in chapter 2 for the analysis of agrochemicals. In short, the probe was the same configuration as the larger version used by Harper *et al*.[11] It consisted of the larger diameter glass tubing (in comparison to the handheld LTP probe) along with an applied voltage of 5 – 10 kV at 2.8 kHz. Spectra shown in this chapter were collected using a He carrier gas, but Ar was used as well and revealed emission only from excited Ar species.

4.3 Results and Discussion

4.3.1 Identification of LTP Emission Species

An advantage of emission spectroscopy over MS for the characterization of plasma species lies with the ability to identify both neutral and charged species. In plasma-based MS, the only species that can be identified are long-lived ions that survive transmission from ambient air to vacuum for separation and detection. It is possible to study much shorter-lived and potentially higher energetic species in emission spectroscopy. However, a major advantage of MS is that larger, polyatomic ions are detected which is only possible in emission spectroscopy if the polyatomic species fluoresce, and even then the sensitivity is much greater with MS. Instead, with emission spectroscopy, smaller atomic and diatomic species can be identified and characterized, providing insight into the initial plasma reactions that lead to reagent ion formation. The emission spectrum of the LTP probe at a carrier gas flow of 1.6 L/min is depicted in

Figure 4.4. The atomic emission species that can be identified in the spectrum include He (706.5 nm), $O^{\bullet}$ (777 nm) and $H^{\bullet}$ (H_{α} – 656.3 nm; H_{β} – 486.2 nm), while the molecular species observed include N_2 (337.1 nm), $^{\bullet}OH$ (306.5 nm) and N_2^+ (391.2 nm). He-LTP emission is similar to other He plasmas in the literature; however, the emission profile of the LTP probe is unique, with differences most likely occurring because of the unique electrical characteristics (i.e. voltage/current) and geometrical configurations of each plasma. The most intense emission detected is from the $N_2^{+\bullet}$ at 391.2 nm ion followed by N_2 (337.1) and He (I, 706.5 nm). Both $N_2^{+\bullet}$ (15.6 eV)[12] and He(I) (~22.7 eV; 3^3S_1 triplet state)[12] are expected to play a large role in LTP ionization through charge transfer and penning ionization reactions, respectively. One such reaction is depicted in reaction Scheme 4.1 for the formation of water clusters,[12-14] which are thought to be the major reagent ions responsible for analyte protonation. Note that He^* is an excited metastable, and is the species that results from the loss of a photon from the 3^3S_1 triplet state (i.e. emission of 706.5 nm photon).

$$He^* + N_2 \rightarrow He + N_2^+ + e^-$$
$$N_2^+ + 2N_2 \rightarrow N_4^+ + N_2$$
$$N_4^+ + H_2O \rightarrow H_2O^+ + 2N_2$$
$$H_2O^+ + H_2O \rightarrow H_3O^+ + OH$$
$$H_3O^+ + (n-1)H_2O \rightarrow (H_2O)_n H^+$$

Scheme 4.1 Commonly accepted APCI mechanism for water cluster formation from He*

4.3.2 Calculation of Electron Density

Electron density is an important metric for plasmas as it describes the degree of ionization of species in the plasma. Due to charge balancing, there must be a positive ion for every electron in the plasma, so the positive ion density also must be on the order of the electron density. In addition, the electron density can also be an important metric for the formation of negative reagent ions in the plasma, which are essential for forming negative analyte ions. The electron density was approximated using the Stark broadening of the H_β line at 486.2 nm.[6] Further details about how the electron number density was calculated can be found in the publication by Chan *et al*.[15] In essence, Stark broadening was estimated as the difference between the measured Lorentzian linewidth of H_β (53.6 pm) and van der Waals broadening (44.6 pm), which is 9.0 pm. The use of an equation given by Gigosos *et al*.[16] provided an estimation of an electron density of 9.9×10^{12} cm^{-3}. This is in close approximation to other ambient He-based discharges.[17] When considering the number of molecules in the same volume (as calculated from the ideal gas law) is 10^{19}, assuming the electron density is in close proximity to the ion density suggests an ionization efficiency on the order of $10^{-6} - 10^{-7}$. While seemingly low, the ionization efficiency is on par with atmospheric-pressure plasmas and is often higher for reduced pressure plasmas. In addition, the electron density was calculated from emission in the LTP afterglow, where the electron density is expected to be less than in the space between the two electrodes where primary plasma reactions occur.

4.3.3 2D Images of Steady-State LTP Emission

In Figure 4.5, steady-state images of the LTP plume with a He flow rate of 0.6 L/min can be observed for N_2^+ (391.2 nm), He* (706.5 nm) and N_2 (337.1 nm) emission. The intensity scale, displayed above each image, was varied so that population distributions of the respective emitting species could be compared. For all three emitting species, the most intense emission occurred near the end of the plume (disregarding intense emission occurring inside the probe for He* in Figure 4.5b). Interestingly, the distance from the LTP probe to the center of the most intense emission was further for N_2 (~2.8 mm) when compared with N_2^+ and He* which both had local maxima in emission intensity at ~2.0 mm from the end of the probe. It is possible that the difference in maxima for N_2^+ and N_2 is due to the recombination of N_2^+ with an electron to form N_2 which then emits a photon further downstream. Another possibility is that the discrepancy in emission profiles is due to regions of varying energy in the plasma. The more energetic species would be expected to be in closer proximity to the LTP probe (where the initial discharge began) with less energetic species at further distances from the probe. This is in fact the case as N_2^+ and He* with energies of 18.8 and ~22.7 eV respectively have emission maxima at ~2.0 mm versus ~2.8 mm for N_2 with ~3.7 eV of energy.

In a typical LTP-MS experiment involving proton transfer, it is better to have the sample placed outside the visible and more energetic afterglow region of the plasma. Proton transfer tends to occur with lower efficiency when samples are placed in the more energetic, visible portion of the LTP afterglow. This could either be due to not having sufficient proton transfer reagent ions in the high-energy afterglow or potentially due to

neutralization of the analyte with high-energy species that have opposite polarity (e.g. positive ions capturing electrons). On the contrary, it is possible that the visible afterglow region of the plasma is better suited for higher energy desorption processes, such as chemical sputtering, due to the presence of species with over 22 eV in this region; although this has yet to be demonstrated.

Figure 4.6 displays steady-state images of emission at 706.5 nm at various helium flow rates. As previously mentioned, this corresponds to a transition from one excited state of He* to a metastable state (He^m). Thus, these profiles give an estimate of the relative distribution of He^m in the plasma plume. The role of He^m can be understood from the reactions shown earlier in Scheme 4.1, which reveals a commonly accepted APCI mechanism for the production of water clusters starting with He^m. Water clusters are of immense importance in LTP-MS analysis due to their role in proton transfer ionization. In particular H_3O^+ likely plays the largest role due to its low proton affinity (PA) at ~690 kJ/mol which enables it to transfer a proton to many different compounds, much more so than two proton-bound waters [$(H_2O)_2H^+$] which has a PA of ~808 kJ/mol due to solvation effects.[18] However, even $(H_2O)_2H^+$ is capable of transferring a proton to many species, such as amines which tend to have a PA greater than 900 kJ/mol. It follows then, that increased emission at 706.5 nm and consequent production of He^m should lead to increased water cluster formation which ultimately leads to increased ionization capabilities.

Figure 4.7 shows mass spectra recorded at 1.0 L/min and 0.4 L/min He flow rates. The higher flow rate, which reveals increased He* emission as depicted in Fig. 4.6, also yields increased water cluster production (*m/z* 37 corresponds to $(H_2O)_2H^+$). Note that

other flow rates were attempted as well and revealed the same trend. It should also be noted that this trend does not necessarily suggest that higher flow rates will yield more analyte signal from proton transfer. With the large-scale LTP geometry, 0.4 l/min of helium usually provides sufficient reagent ion formation that the analyte typically seems to be the limiting reagent. This is further evidenced by the handheld LTP probe discussed in the previous chapter, which utilizes flow rates below 100 mL/min and still provides similar or even better sensitivity than the large-scale probe with its larger He flow rates. In fact, increasing the flow rate to over 1 l/min with the large-scale LTP actually decreases analyte signal for typical probe to sample distances. This could be due to changes in the gas flow profiles or potentially because of elongation of the visible afterglow to the sample surface, which can result in less formation of proton transfer products as previously discussed.

Unlike adjusting the helium flow, varying the LTP power by changing the voltage supplied to the probe does not reveal a simple trend of increased emission with increased power (c.f. Figure 4.8). Instead, there appears to be a local maximum of emission within the afterglow at about 2.1 W, even though the intensity of emission from within the tube appears to increase with increased power. The explanation of this phenomenon is not fully understood. However, it would appear that 2.1 W is the optimal power to operate at over this power range, as it should allow the highest abundance of He^m to be formed outside of the LTP tube where more nitrogen and water are accessible for the formation of protonated water clusters via reaction Scheme 4.1. This claim is further substantiated by the fact that when performing analyses with LTP-MS at different powers, there is typically a point at which increasing the power decreases signal for proton transfer

products. However, the actual optimum power setting is likely to change with different configurations of the LTP probe as well as different He flow rates. It would have been interesting to determine whether the intense emission in the afterglow at 2.1 W was a local or global maximum, but this was not possible due to discharge instability and arcing at higher potentials.

4.3.4 Rotational Temperatures and Reactions for LTP Reagent Ion Formation

Rotational temperatures of diatomic species in a plasma can be determined by fitting one of its branches of emission (R or P) with a Boltzman distribution.[15] Typically, rotational temperatures are a good indicator of gas-kinetic temperature due to the rapid equilibrium of rotational levels with translational energy of the molecule. A good example of this can be observed in Figure 4.9, which shows rotational temperatures for two different species at various positions within and outside the LTP probe. In the case of OH, there was no deviation within experimental error between the typical measured gas kinetic temperature and the rotational temperature of OH (290 – 300 K). However, the rotational temperature for N_2^+, calculated from the distribution of N_2^+ rotational levels for 12 emission lines in the R branch, did not display the same trend.

Interestingly, the N_2^+ rotational temperatures are significantly higher than the gas kinetic temperature. Within the LTP probe, the rotational temperature of N_2^+ is around 350 K and actually rises to ~550 K at the furthest edge of the afterglow. Note that when changing helium flow rates, there was no effect on the maximum rotational temperature; only the distance at which the maximum occurred from the LTP probe changed.

Discovering the N_2^+ rotational temperatures were above 350 K has actually led to a better understanding of how N_2^+ is being formed in the various regions of the plasma by considering the various pathways in which N_2^+ can be formed. A more detailed explanation of how the rotational temperatures were obtained as well as how the elucidation of the reaction mechanisms can be found in the manuscript by Chan *et al*.[15] The first mechanism that was ruled out is direct electron ionization (EI) of nitrogen, due to the lack of spatial correlation between the emission from N_2 and N_2^+ (c.f. 2D emission profiles in Fig. 4.5 or 1D emission profiles in Figure 4.10). The spatial emission distributions of these two species should overlap if EI were the dominant mechanism. Instead, either charge transfer or Penning ionization from a higher energy species must be taking place.

It makes the most since that one of the highly excited forms of helium would be responsible for the ionization of N_2 due to being the only likely species in the plasma with the necessary ~14.5 eV to ionize nitrogen. Below are three potential reactions of helium species with nitrogen that could play a role. The first two are charge transfer (CT) reactions and have been reported to yield N_2^+ rotational temperatures near 900 K.[19,20] Reaction 3 is the Penning ionization (PI) of N_2 from He^m and results in N_2^+ rotational temperatures of ~360 K.[20]

(1) CT from He_2^+: $He_2^+ + N_2 \rightarrow 2\ He + N_2^+$

(2) CT from He^+: $He^+ + N_2 \rightarrow He + N_2^+$

(3) PI from He^m: $He^m + N_2 \rightarrow He + N_2^+ + e^-$

The rotational temperatures within the LTP probe and in the initial parts of the plume are in strong agreement with those that arise from PI in reaction 3. However, the increase in rotational temperature in Figure 4.9 to 550 K suggests that a charge transfer mechanism is also taking place (either reaction 1 or 2). Furthermore, it has been found that reaction 1 is the more likely of the two reactions for two main reasons. It has been reported in the past that He_2^+ is in much greater abundance than He^+ for DBDs at atmospheric pressure.[21] (2) The vibrational states of N_2^+ found for the He-LTP more closely resemble those that result for a CT from He_2^+ than for a CT from He^+.[22] Thus, He_2^+ must be responsible for the formation of N_2^+ and acts as an energy carrier in the He-LTP plume.

Furthermore, the relative emission intensities of various species in the LTP plume as well as the information that has been obtained from rotational temperature measurements has been compiled in Figure 4.10. There are a few interesting findings when looking at the overlay of the 1D emission profiles of N_2, N_2^+ and He*. As previously mentioned, there is a discrepancy between the emission profiles of N_2 and N_2^+. Also of interest is the profile of He* emission in Fig. 4.10, which reveals a global maximum within the tube, a decrease, and then a local maximum at the same distance from the probe as the N_2^+ emission maximum. Note that the same trend was also discovered in the 2D monochromatic images in Fig. 4.5. This overlap in emission profiles suggests that both He* and N_2^+ are being formed by the same reagent (i.e. He_2^+). The different reactions occurring in the various regions of the LTP plume are displayed in Fig. 4.10. In the first region, within and just outside of the discharge tube, is the region where He_2^+ is being formed by the three different reactions shown. Note this is also the

region where N_2^+ is being formed by PI from He^m. In the next region, He_2^+ reacts with nitrogen to form N_2^+ and also recombines with an electron and dissociates to form He* and He. The final region is the least energetic, where either recombination of N_2^+ with an electron or the excitation of N_2 by lower energy species occurs.

4.3.5 Time-Resolved and 2D LTP Emission

Time-resolved images of 2D LTP emission were acquired by gating the iCCD with the input frequency to the LTP and adjusting the gate delay to obtain images at different time points. In Figure 4.11, 2D and time-resolved images were acquired for emission from He* (706.5 nm), N_2^+ (391.2 nm) and N_2 (337.1 nm) and are displayed such that each column corresponds to the same gate delay for each 2D emission profile. The gate width was 200 ns for each image with 35,000 gates per exposure. The images of He* emission revealed that a propagating energy wave, or plasma bullet,[13] travels between gate delays of 16.0 and 18.4 μs at ~3,000 m/s (much faster than the He gas velocity which is at ~0.4 m/s). Plasma bullets were also observed for $N_2^{+\bullet}$ and N_2, although their emission over the same 200 ns exposure times was much more spatially dispersed than that of He* emission. Comparing the timing and positioning of plasma bullets for each of the three species has allowed further insights into the mechanisms discussed in the previous section.

He* emission stops after a gate delay of 18.4 μs, but continues for N_2^+ and N_2 until 19.6 μs. The fact that N_2^+ and He* seem to propagate at similar times with similar spatial correlation up until a gate delay of 18.4 μs suggests they are being formed via a

similar mechanism. As introduced in the previous section, it is believed that He_2^+ is responsible for the formation and consequent emission of He* and N_2^+ in this initial time of bullet propagation between gate delays of 16 – 18.4 μs. However, the fact that He* emission stops, while N_2^+ emission continues after a gate delay of 18.4 μs, suggests that another mechanism is responsible for the formation of N_2^+ during gate delays of 18.4 and 19.6 μs. The most probable candidate is He^m, which is formed as a result of He* emission; so even though He* emission stops at 18.4 s, He^m is still around for the next 1.2 μs to ionize nitrogen. Other interpretations of the relationship between the time-resolved images of N_2^+ and He* exist; however, the idea of two or more mechanisms being responsible for nitrogen ionization is supported by rotational temperatures of N_2^+, the comparison of steady state emission profiles and the 2D time-resolved images.

Emission at 337.1 nm (N_2) follows a similar time correlation with N_2^+ and He* emission, but the distribution is shifted further from the LTP probe. This could be attributed to the plasma bullet acting as a travelling energy wave, where emission from N_2 would be expected to occur first as the lower tail of the energy wave propagates and is followed by the higher energy part which is capable of exciting He to over 22.7 eV. The formation of N_2* is believed to occur as a result of the excitation of ground state N_2 up until a gate delay of 18.4 μs. After this time, N_2 emission starts again and closely correlates with N_2^+ in time and space. Hence, for gate delays of 18.4 – 19.6 μs, it is believed that N_2* is formed via recombination with an electron. Note that the recombination of N_2^+ with an electron may also contribute at earlier gate delays, but due to the lack of spatial correlation with N_2^+ and He*, excitation of ground state N_2 is likely the larger contributor.

4.3.6 LTP Interactions with Sample Substrates

Emission from the LTP probe has provided some insight into the reactions responsible for reagent ion formation, but unfortunately this does not reveal anything about the interaction of LTP species with a sample substrate. Emission spectroscopy is not well suited for studying this type of plasma interaction as most molecular samples do not emit light in the visible region. However, two interesting plasma-sample substrate interactions were monitored with emission spectroscopy: 1) plasma focusing to a grounded needle and 2) fluorescence from a highlighter-coated glass slide.

The first interaction studied was based on a finding by Huang *et al*. (unpublished data) that increased signal was observed when a sample was analyzed by LTP from a grounded and sharpened metal needle. The time-resolved emission of N_2^+ to an electrically grounded needle is shown in Figure 4.12. The image acquired at a gate delay of 21 μs shows the LTP plume beginning to anchor to the needle. In contrast to the images shown in section 4.3.5, no plasma bullet was shown propagating towards the needle. Instead there was steady emission between the LTP probe and the needle that intensified until gate delays of 26 – 27 μs and slowly decreased until a gate delay of 33 μs. Interestingly, emission decreased in intensity just before reaching the needle, yet was very intense at the point of the needle. In comparison with the plasma bullets not interacting with a surface/substrate from Fig. 4.11, which had a lifetime of ~3 μs, the emission between the probe and the needle alone lasts about four times longer. The intense emission from the needle continues on until a gate delay of ~80 μs, as what is believed to be a corona discharge caused by charging of the needle by LTP. In all, emission from N_2^+ lasts about 60 μs, which is nearly 20 times longer than the plasma

bullets in the typical LTP configuration. It is possible that the either the increase in emission duty cycle for N_2^+ (from ~1% to ~18%) or the increased emission intensity at the needle tip could be responsible for the increased sensitivity observed for the LTP-MS analysis of a sample from a needle.

Figure 4.13a shows the MIS setup used to investigate the interaction between LTP with a mock sample on a glass slide. A glass slide coated with highlighter ink was placed perpendicular to the light path and the LTP probe was placed 45° from the glass slide such that the plasma plume was allowed to directly interact with the flourophore sample. The wavelength monitored was near the λ_{max} of the flourophore in the highlighter at 507 nm. Unfortunately, the fluorophore in the highlighter could not be detected by LTP-MS as LTP typically has difficulties with the desorption/ionization of dyes.

Figure 4.13b displays time-resolved images of the plasma-induced highlighter emission. The plasma reaches the substrate at a gate delay of ~22.9 μs as determined by the increased emission at 507 nm. The intense emission then lingers for ~0.5 μs until it starts to disperse in a V-pattern at ~23.4 μs. The spreading/fading slowly continues in this V-pattern until it surpasses the focal area of the lensing system at 24.7 μs. It is of interest which plasma species is causing excitation of the highlighter flourophore and whether it is electronic or photonic. The initial low-intensity spike of emission that occurs at a gate delay of 22.0 μs, is thought to be through photonic excitation from either N_2^+ or N_2 due the time gap between emission at 22 μs and the intense emission at 22.9 μs (when plasma species actually reach the glass slide). The low intensity could be attributed to the distance between photon emission from within the LTP at early gate delays, resulting in a low intensity of photons reaching the surface.

If the intense emission at later gate delays is caused by an excited helium species, it must be through electronic excitation because full emission spectra indicate that He lacks abundant emission of photons capable of exciting and inducing fluorescence at 507 nm (most emission of He is ~700 nm). N_2^+ is likely capable of exciting the flourophore via an electronic or a photonic mechanism because it emits light at 391.2 nm and also has an energy greater than 15 eV. It is believed that the intense excitation for 0.5 μs is due to electronic excitation from He* or He^m because the duration is similar to the lifetime of He* emission at the same respective distance from LTP probe which is also ~0.5 μs, whereas emission from N_2 and N_2^+ lasts for ~1.5 μs (c.f Fig. 4.11). The lower extent of excitation/emission at later gate delays could come from other species that endure longer excited lifetimes than He through either electronic or photonic processes. It should be noted that plasma bullets were not measured for all emitting species in the LTP plume, so the role of these other species cannot be ruled out. However, the emission intensities suggest He*, N_2 and N_2^+ are the most abundant and perhaps more likely to cause the observed excitation at the highlighter surface.

Another parameter worth noting is the spot size of the plasma for chemical imaging. The goal in most MS imaging experiments is to obtain the smallest spot size or highest resolving power. The 2D images of emission from a sample substrate have helped provide some indication of what the spot size of excitation is for LTP-MS. In mimicking a typical LTP-MS experiment, the interaction of the plasma with highlighter on a glass slide suggests a spot size with a 3 – 4 mm diameter. This is quite large and could explain why LTP is not considered to be well-suited for MS imaging, despite an attempt by Liu *et al*.[23] The images in Fig. 4.12 for the LTP-needle interaction suggest a

much smaller spot size with a diameter of 0.4 – 0.5 mm at the tip of the needle. If this was the actual spot size for LTP-MS imaging, it would be acceptable; however, without performing the MS imaging experiment it cannot be certain that desorption/ionization occurs within the same confined spot. In practice, it was difficult to obtain spot sizes less than 1 mm due to the fact that most samples that can be analyzed with LTP-MS have a fairly high vapor pressure.

4.3.7 Implications of Emission Data on LTP Desorption/Ionization Mechanism

There has been evidence suggesting that non-thermal desorption/ionization mechanisms are capable of taking place with LTP. Experiments conducted with LTP on a Teflon substrate have revealed clusters of peaks separated by 50 *m/z* units, which correspond to different lengths of the fluorocarbon chain. The only way these ions can form is if LTP is able to break the C-C bond in the polymer (with a bond energy greater than 3.8 eV). The momentum of the species in the plasma at ambient thermal energies alone is clearly incapable of breaking this bond. There are two main possibilities that should be considered for why LTP is capable of breaking a C-C bond in Teflon (although all possible desorption mechanisms are considered in the following chapter): 1) spikes of increased temperature occur during plasma bullet propagation or 2) a chemical sputtering-type process.

The possibility of local spikes of intense heat during plasma bullet propagation can be ruled out due to the rotational temperature data discussed previously. While the rotational temperatures of N_2^+ clearly had not reached equilibrium with translational

energy, the OH rotational temperature should serve as a better indicator. Figure 4.9 revealed that the OH rotational temperatures were approximately room temperature at ~300 K. The OH rotational temperatures were calculated by fitting the distribution of different OH lines with a Boltzmann distribution. Combining this with the fact that there is no OH emission when the plasma bullet is not present indicates that the rotational temperatures reported in Figure 4.9 are representative of the temperatures during the plasma bullet propagation. This is because the distribution of OH peaks that occurred during the time interval of plasma bullet propagation will not be distorted by the absence of OH emission during the rest of the time interval. Thus, the 300 K rotational temperatures calculated for OH indicate that there is not a spike in temperature during plasma bullet propagation, and another mechanism must be responsible for breaking the C-C bond in Teflon.

One potential mechanism is chemical sputtering through vertical electronic transitions within surface-bound molecules. There are two possibilities by which this electronic transition can take place. The first is by a high energy electron bombarding the surface. However, the energy of the electrons propagating at the speed of the plasma bullet (~3,000 m/s) would be merely 25.6 micro-eV, which is clearly not enough energy to desorb a surface analyte (10^6 m/s electron would be needed for eV energies). In addition, C-C bond breaking from Teflon can occur even when the visible part of the plasma is not in contact with the polymer, which is significant because free electrons are quickly solvated or form anions once out of the high-energy and visible part of the plasma where they are formed. Another method of electron transfer that can occur is via interaction of an ion or electronically excited atom/molecule donating its energy to the

surface analyte. This is more plausible for several reasons, with the first being that there are many highly excited species above 20 eV in a He plasma that are clearly capable of breaking chemical bonds as well as various radicals and ions that can also provide energy for chemical reactivity. Also, the fact that He-LTP was capable of exciting a fluorophore in highlighter ink through electronic excitation from He* suggests this type of energy transfer is possible from excited gas-phase species to a surface-bound analyte.

The desorption/ionization model, while attempting to explain some of the observed examples of non-thermal desorption with LTP-MS, has little supporting evidence and does not explain the inability to detect certain compounds with mass spectrometry. It does not explain the failure to observe pre-charged molecules and certain organic ions. Specifically, the failure to desorb/ionize dyes like rhodamine 6G and organic lipids are not yet explained. In the next chapter, this non-thermal desorption mechanism will be investigated in much further detail.

4.4 References

1. Dalgleish, J. K.; Wleklinski, M.; Shelley, J. T.; Mulligan, C. C.; Ouyang, Z.; Cooks, R. G. Rapid Communications in Mass Spectrometry 2013, 27, 135.

2. Andrade, F. J.; Wetzel, W. C.; Chan, G. C. Y.; Webb, M. R.; Gamez, G.; Ray, S. J.; Hieftje, G. M. Journal of Analytical Atomic Spectrometry 2006, 21, 1175.

3. Ionascut-Nedelcescu, A.; Carlone, C.; Kogelschatz, U.; Gravelle, D. V.; Boulos, M. I. Journal of Applied Physics 2008, 103.

4. Ochkin, V. N. Spectroscopy of Low Temperature Plasma; Wiley-VCH Verlag GmbH & Co. KGaA: Weinheim, 2009.

5. Eliasson, B.; Egli, W.; Kogelschatz, U. Pure and Applied Chemistry 1994, 66, U1766.

6. Kong, M. G.; Deng, X. T. Ieee Transactions on Plasma Science 2003, 31, 7.

7. Korzec, D.; Finantu-Dinu, E. G.; Teschke, M.; Engemann, J.; Miclea, M.; Kunze, K.; Franzke, J.; Niemax, K. Plasma Sources Science & Technology 2006, 15, 345.

8. Kim, S. J.; Chung, T. H.; Bae, S. H. Thin Solid Films 2009, 517, 4251.

9. Lu, X.; Laroussi, M. Journal of Applied Physics 2006, 100.

10. Vogel, N. I.; Kochan, N. Physical Review Letters 2001, 86, 232.

11. Harper, J. D.; Charipar, N. A.; Mulligan, C. C.; Zhang, X. R.; Cooks, R. G.; Ouyang, Z. Anal. Chem. 2008, 80, 9097.

12. Dzidic, I.; Carroll, D. I.; Stillwell, R. N.; Horning, E. C. Anal. Chem. 1976, 48, 1763.

13. Horning, E. C.; Carroll, D. I.; Dzidic, I.; Haegele, K. D.; Horning, M. G.; Stillwel.Rn Journal of Chromatographic Science 1974, 12, 725.

14. Kambara, H.; Mitsui, Y.; Kanomata, I. Anal. Chem. 1979, 51, 1447.

15. Chan, G. C. Y.; Shelley, J. T.; Jackson, A. U.; Wiley, J. S.; Engelhard, C.; Cooks, R. G.; Hieftje, G. M. Journal of Analytical Atomic Spectrometry 2011, 26, 1434.

16. Gigosos, M. A.; Gonzalez, M. A.; Cardenoso, V. Spectrochimica Acta Part B-Atomic Spectroscopy 2003, 58, 1489.

17. Martens, T.; Bogaerts, A.; Brok, W. J. M.; van der Mullen, J. J. A. M. Journal of Analytical Atomic Spectrometry 2007, 22, 1033.

18. Goebbert, D. J.; Wenthold, P. G. European Journal of Mass Spectrometry 2004, 10, 837.

19. Endoh, M.; Tsuji, M.; Nishimura, Y. Journal of Chemical Physics 1983, 79, 5368.

20. Belikov, A. E. Chemical Physics 1997, 215, 97.

21. Deloche, R.; Monchicourt, P.; Cheret, M.; Lambert, F. Physical Review A 1976, 13, 1140.

22. Leventhal, J. J.; Earl, J. D.; Harris, H. H. Physical Review Letters 1975, 35, 719.

23. Liu, Y.; Ma, X.; Lin, Z.; He, M.; Han, G.; Yang, C.; Xing, Z.; Zhang, S.; Zhang, X. Angewandte Chemie-International Edition 2010, 49, 4435.

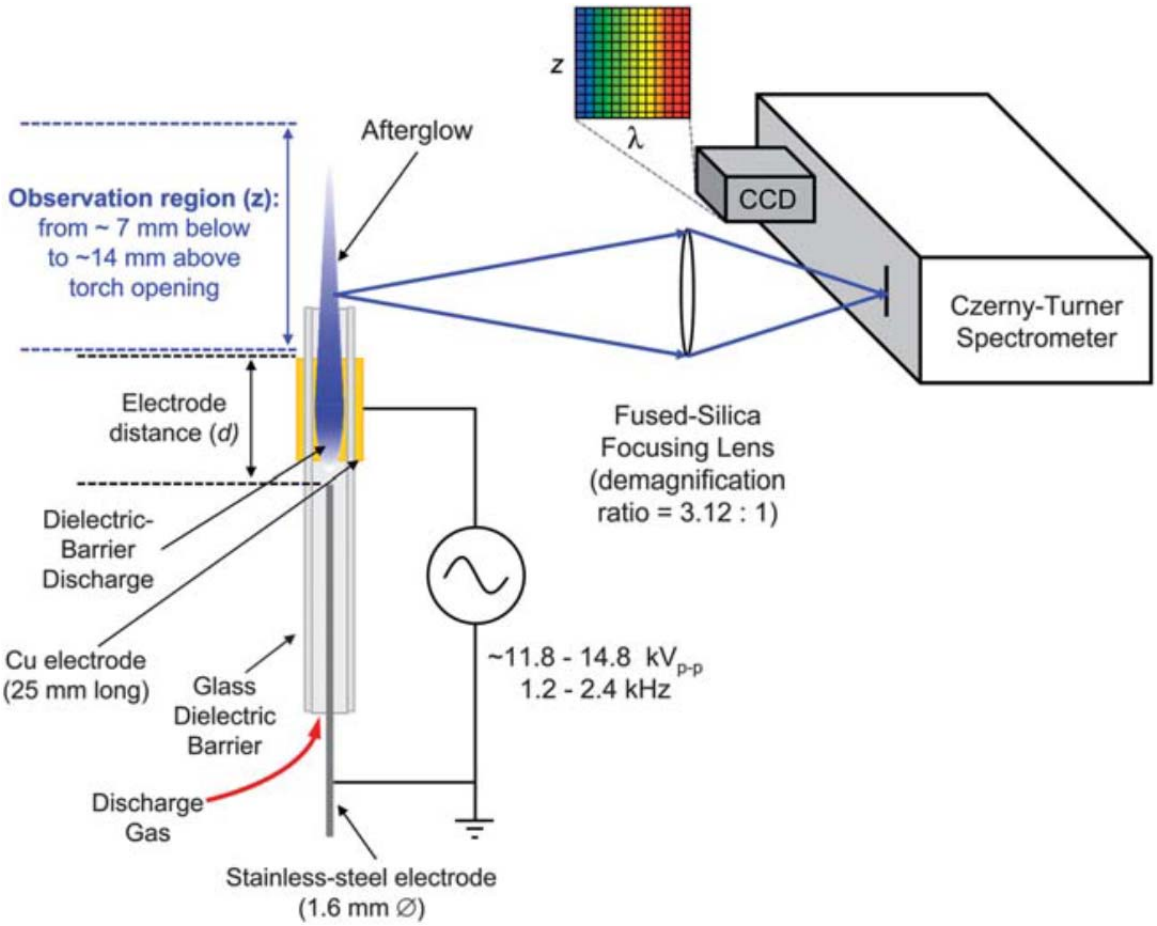

Figure 4.1 Schematic of the instrumental setup used to obtain 1D LTP emission profiles. This configuration allows full emission spectra to be recorded over a 7 mm observation region, which is where the LTP plume was carefully positioned.

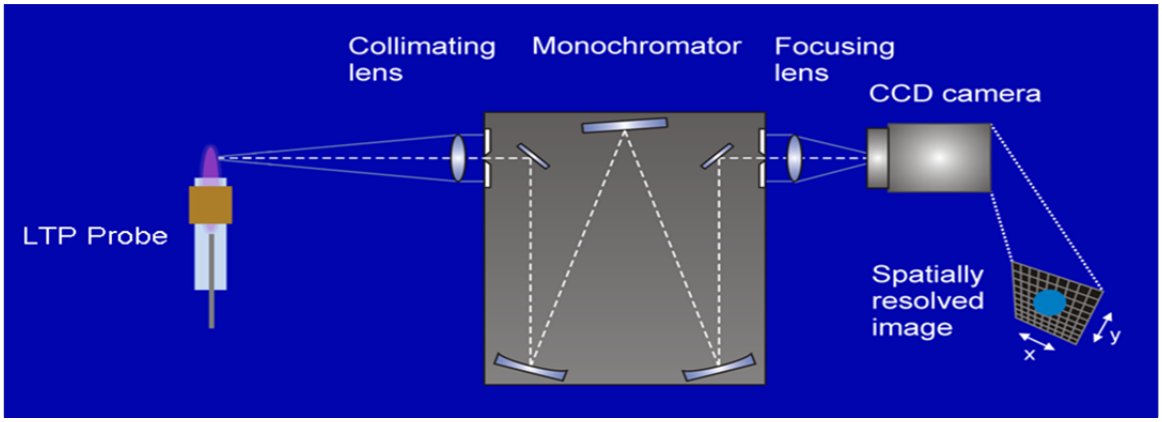

Figure 4.2 Diagram of the monochromatic imaging spectrometer (MIS) used for steady-state and time-resolved 2D emission images for LTP optical characterization.

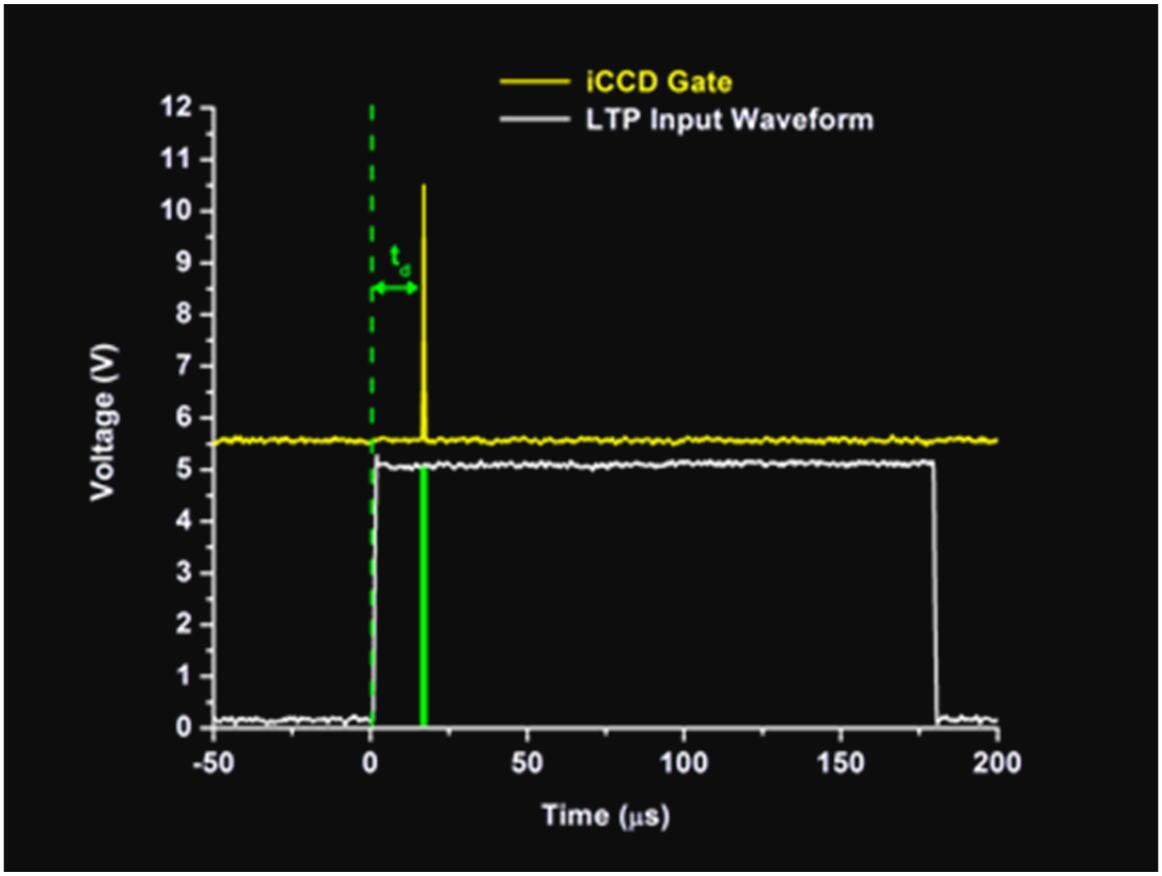

Figure 4.3 Gate sequence diagram for the LTP time-resolved emission profiles, where the LTP input square wave was used as a trigger and a delay was varied to provide images at various time points in the overall waveform.

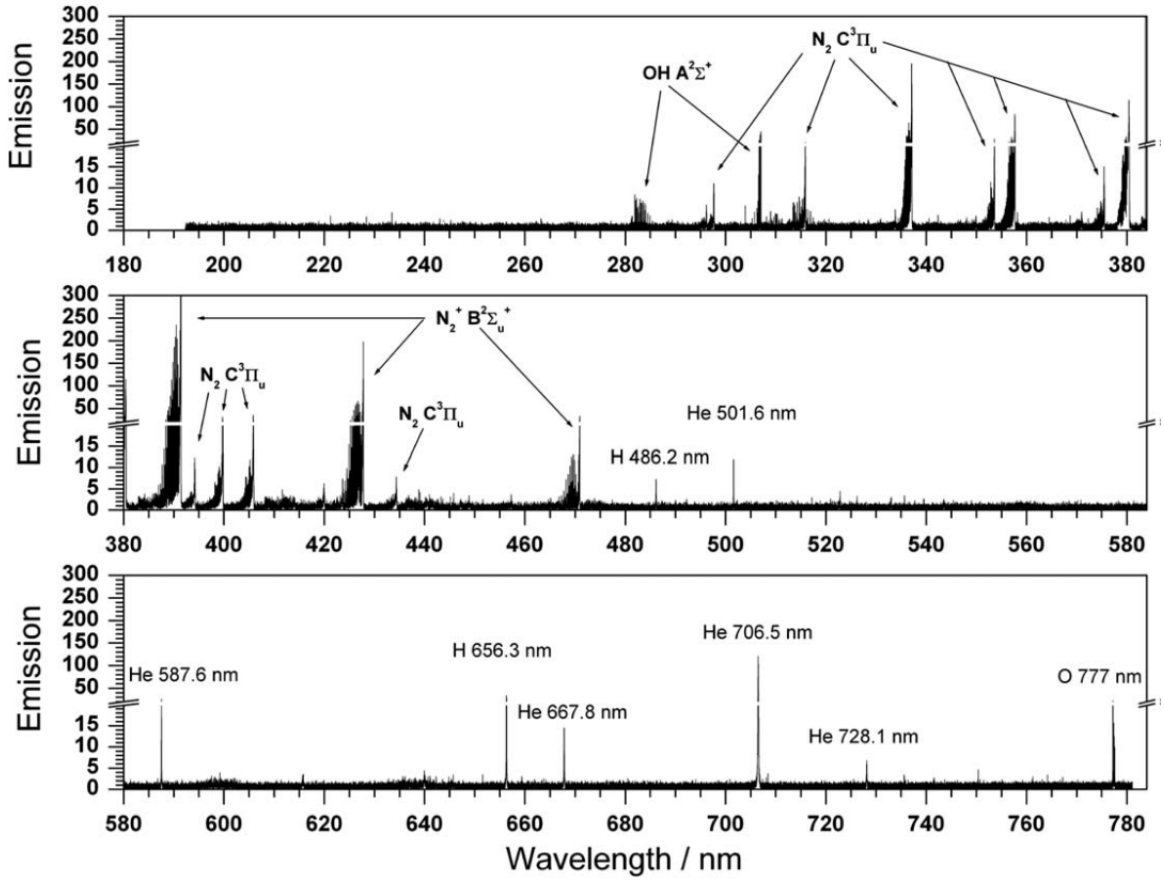

Figure 4.4 1-D Emission profile of a helium LTP (exposure time of 1 minute).

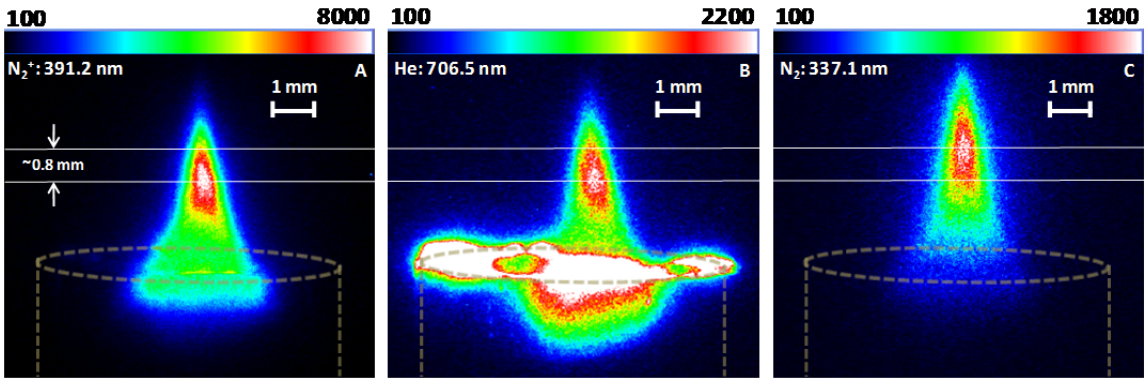

Figure 4.5 Steady-state, monochromatic emission profiles of A.) $N_2^{+\bullet}$ (391.2 nm), B.) He (706.5 nm) and C.) N_2 (337.1 nm) from the LTP probe (brown dashed line). (LTP: 0.6 L/min He, 2.8 kHz) (iCCD: 10 s exposure, gain 180)

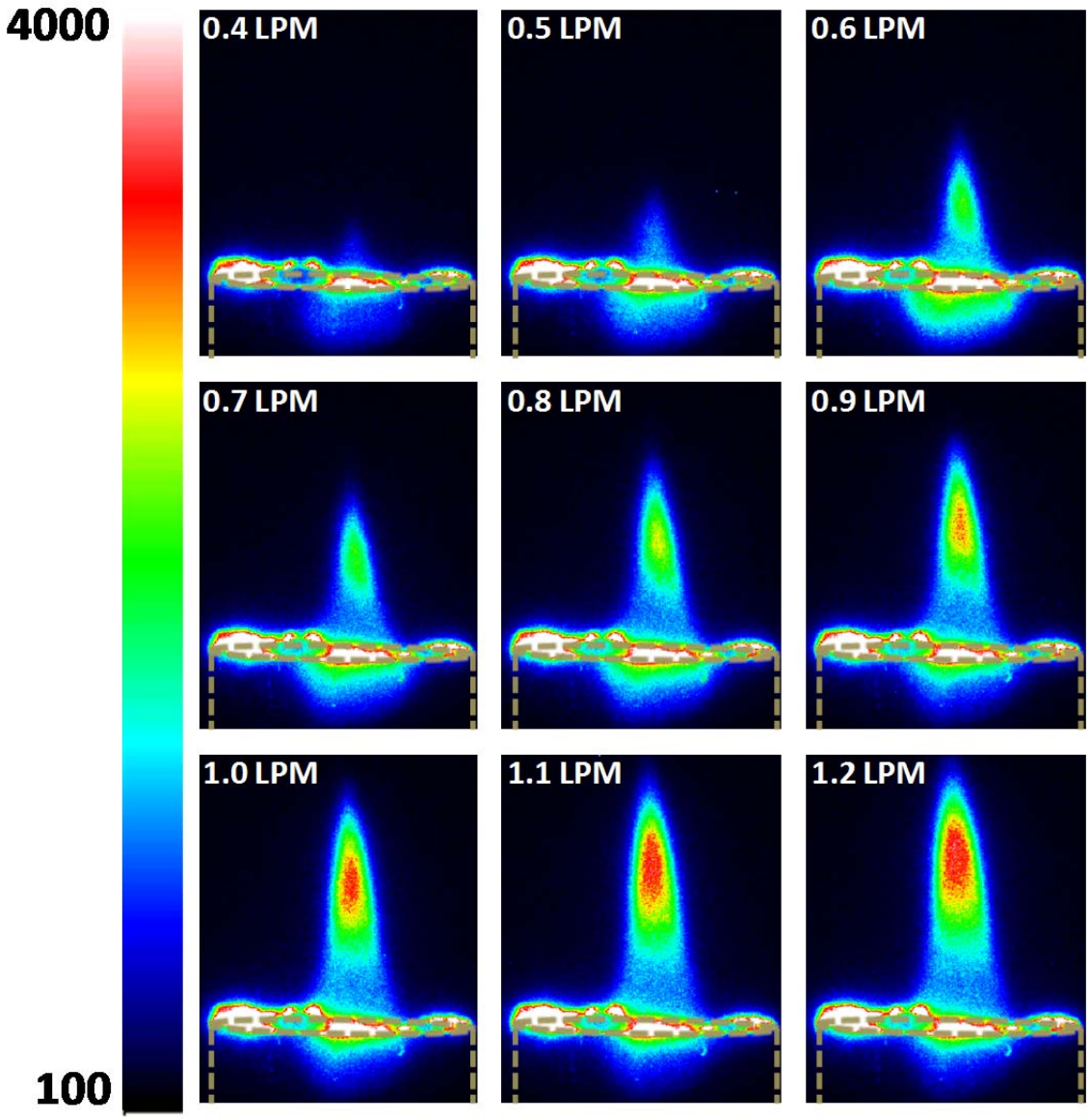

Figure 4.6 Steady-state LTP emission from He* (706.5 nm) at various He flow rates. Brown dashed line corresponds to location of the LTP probe.

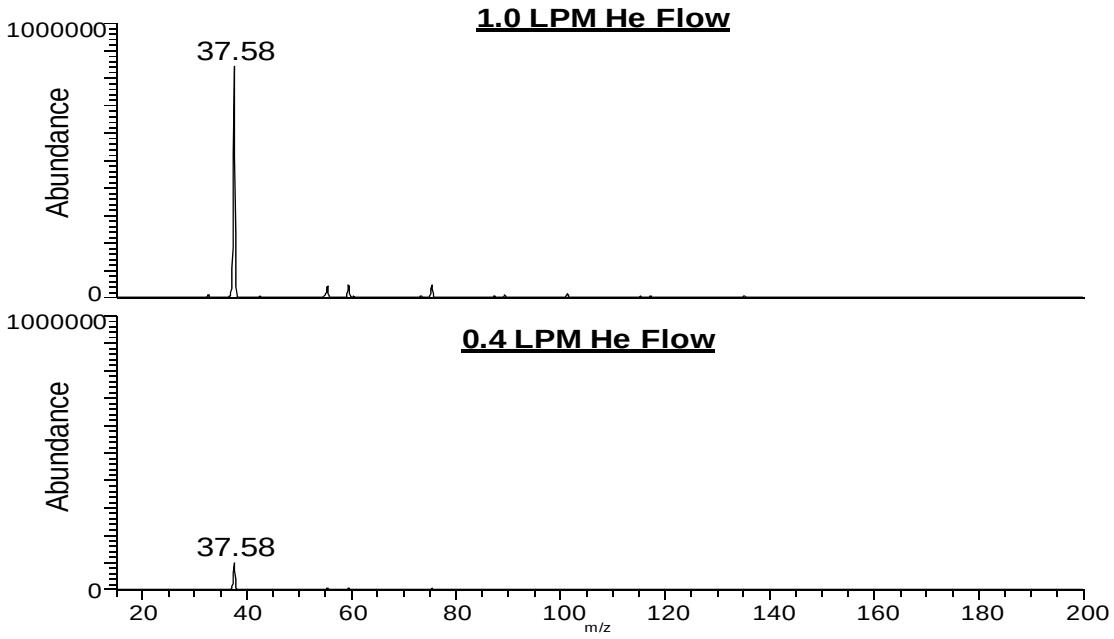

Figure 4.7 Background mass spectra recorded from LTP at two different He flow rates.

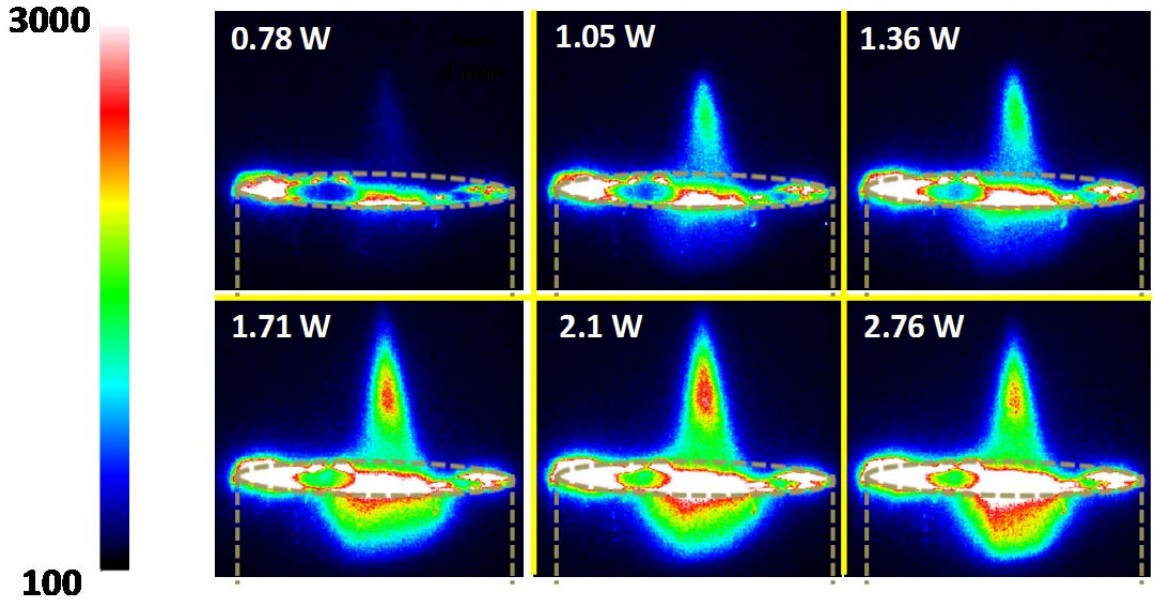

Figure 4.8 Steady-state LTP emission from He* (706.5 nm) as a function of power consumption. Brown dashed line corresponds to location of the LTP probe.

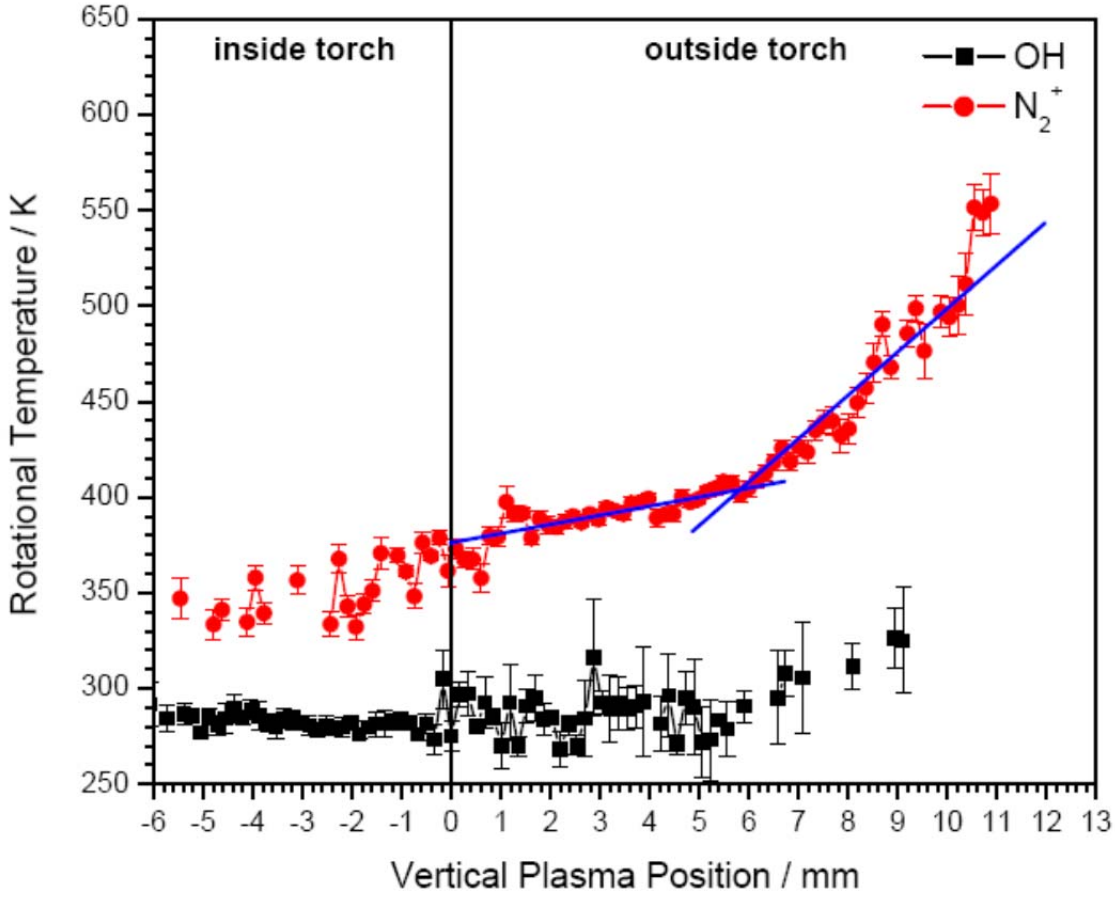

Figure 4.9 Vertical profile of measured OH and N_2^+ rotational temperatures of He-LTP. Note the monotonically increasing trend for the N_2^+ rotational temperature. The two straight lines for the N_2^+ rotational temperature are included for visualization purposes. The error bars represent only the error of the slope in the linear regression. Helium flow - 1.60 L/min

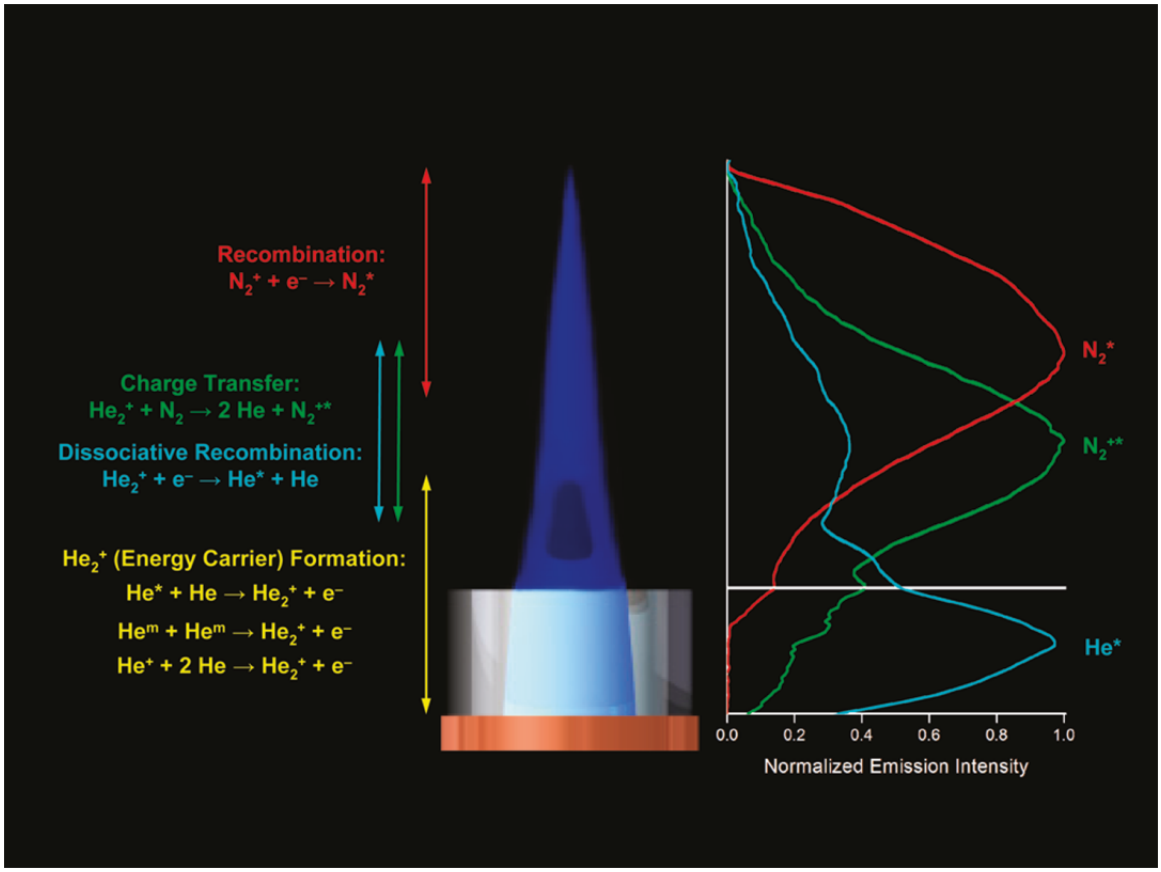

Figure 4.10 Schematic diagram showing the identified spatially dependent reactions for the afterglow and reagent-ion formation in the LTP probe ambient ionization source. The spectra on the right correspond to N_2, N_2^+ and He emission as a function of distance (scaled such that it aligns with the picture of the LTP probe to the left).

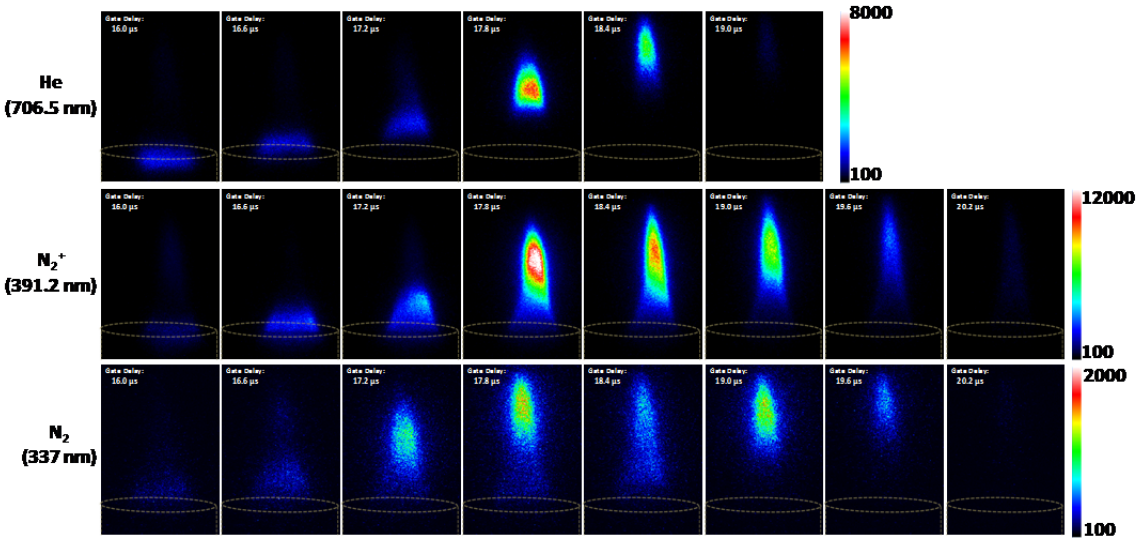

Figure 4.11 Time-resolved emission at 706.5, 391.2 and 337 nm, revealing plasma bullet propagation for He, N_2^+ and N_2 emission respectively. The gate width was 200 ns with an overall exposure of 35,000 gates for each image. Brown dashed line corresponds to location of the LTP probe.

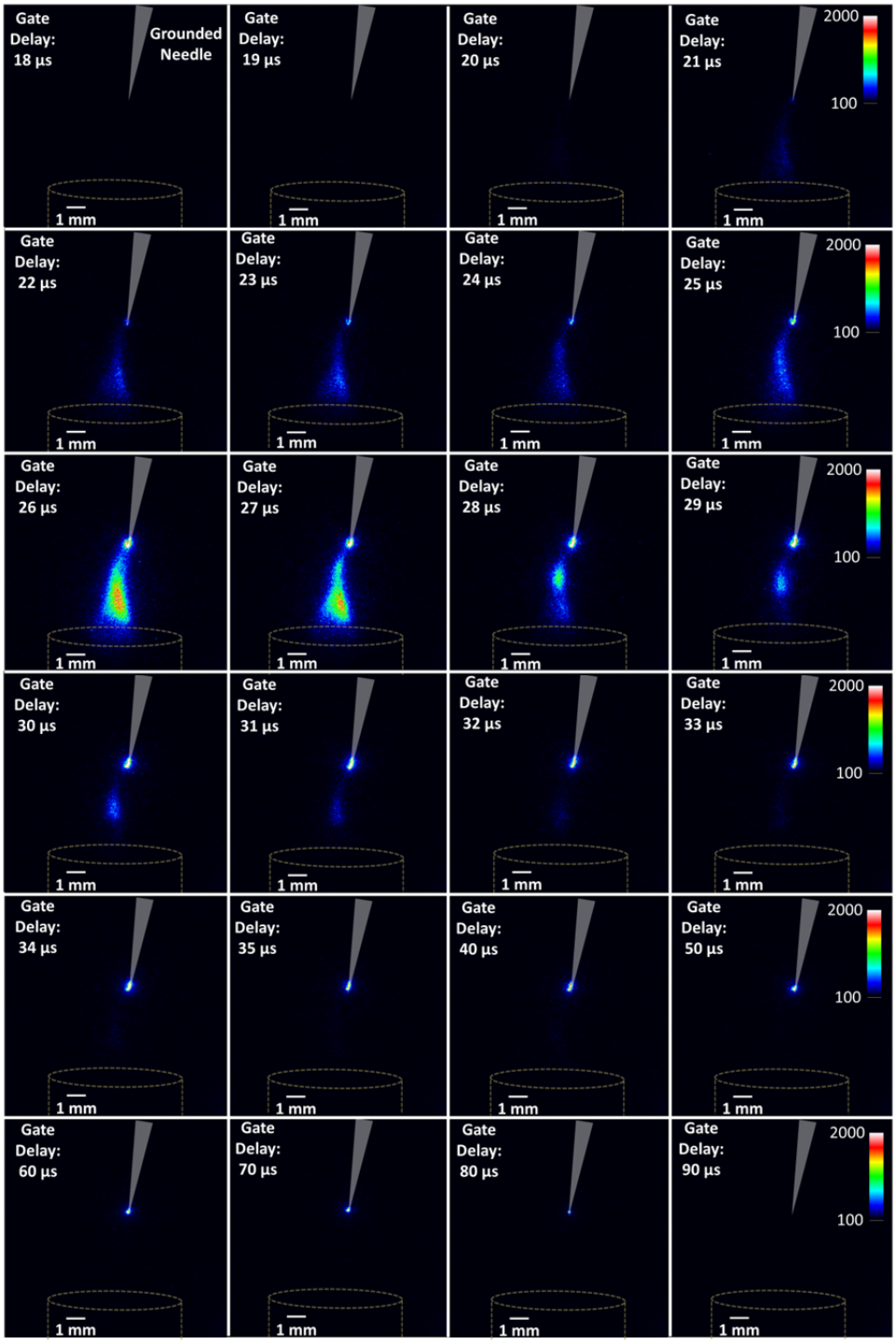

Figure 4.12 Time-resolved, 2D emission of $N_2^{+\bullet}$ at 391.2 nm for the interaction of LTP with an electrically grounded needle (for gate delays between 18 and 90 µs after the rising edge of the square wave used for the LTP source). The gate width was 200 ns with an overall exposure of 35,000 gates for each image. Brown dashed line corresponds to location of the LTP probe.

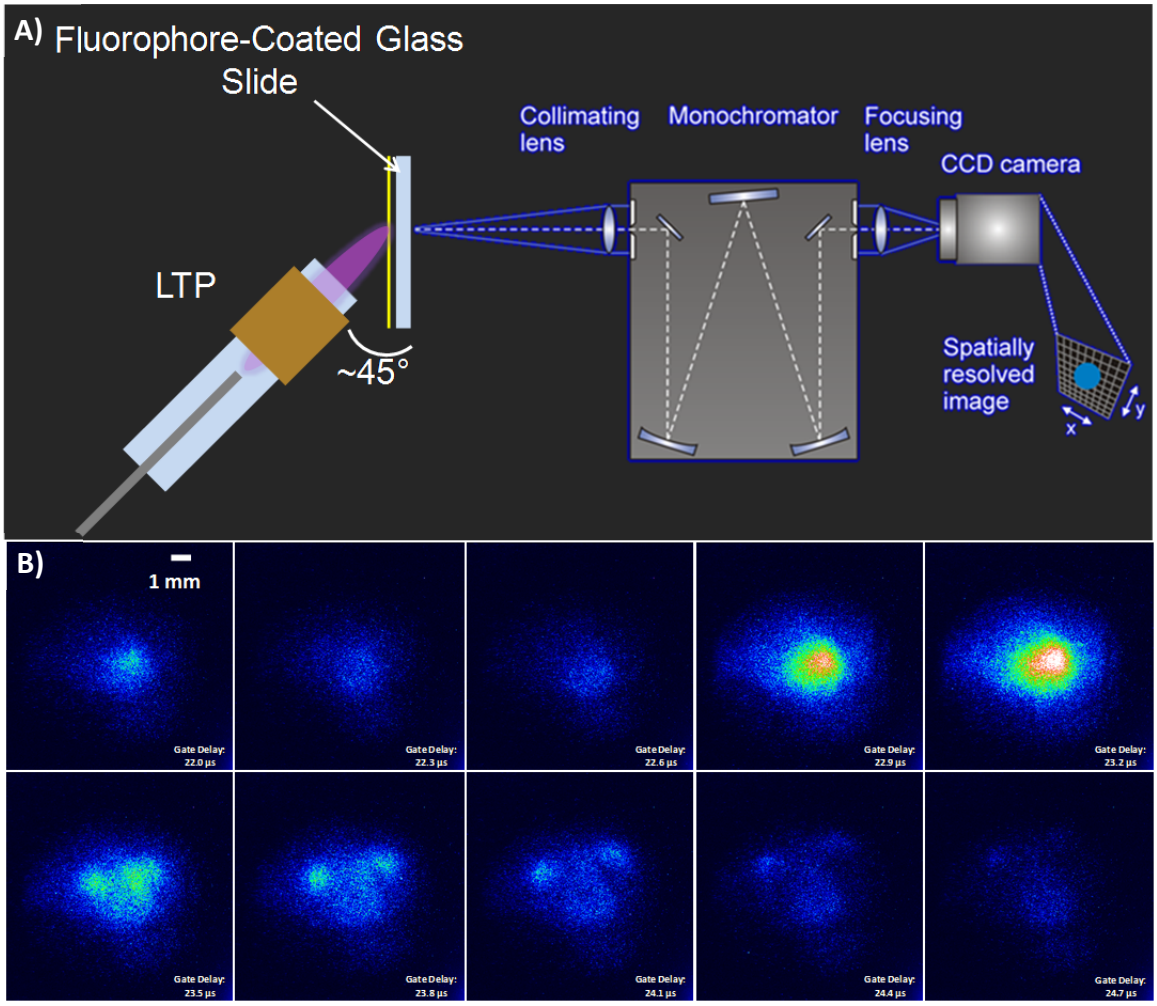

Figure 4.13 A) MIS configuration used to monitor plasma-sample interactions. B) Time-resolved images of low-temperature plasma-highlighter (λ_{max} near 507 nm) interactions at various gate delays. The gate width was 100 ns with an overall exposure of 35,000 gates for each image.

CHAPTER 5

FUNDAMENTALS OF LTP: NON-THERMAL DESORPTION VIA CHEMICAL SPUTTERING

5.1 Introduction

Sputtering is a process in which particles are removed from a surface as a result of interaction with an incident particle. There are two main types of sputtering: chemical and physical. Physical sputtering occurs when kinetic energy of an impinging particle leads to removal of a surface particle. In contrast, chemical sputtering is not based on momentum of the impinging particle, but instead relies on chemical reactivity to liberate a surface-bound particle into the gas phase. Both of these sputtering phenomenon are traditionally observed at reduced pressure, as is the case in secondary ion mass spectrometry (SIMS) where larger ions (i.e. Ar^+, Cs^+, C_{60}^+, etc.) are accelerated toward a surface. Reduced pressures are important for physical sputtering so that the projectile ion/particle can gain enough momentum to remove material from a surface. However, the fact that chemical sputtering is dependent on reactivity and not momentum suggests it does not necessarily have to occur at reduced pressure.

Not too surprisingly, there have been many reports of chemical sputtering at atmospheric pressure with the use of plasmas, first demonstrated by Rossmann *et al*. where emission spectra of vapor phase metals were recorded as a result of RF plasma

exposure to a solid substrate.[1] This general process has proven useful for the semi-conductor industry in the growth of metal oxide films, which is a process that also occurs during the sputtering of the metals as a result of reactive oxygen species in the plasma. Another industry that has benefited from ambient sputtering induced by plasma is in the polymer industry for the manipulation of polymer properties. It was originally shown that a Tesla coil could introduce polar oxygen groups on a polyolefin surface.[2] Later it was shown that in addition to functionalizing polymers with oxygen, exposure of a polymer to a corona discharge in an oxygen environment at 1 atm. caused the mass of the polymer to decrease through the release of CO_2 and H_2O.[3] As a biomedical application, it has been proposed through simulation of an ambient DBD interacting with a lipid-like surface (mimicking a cell membrane), that sputtering yields of ten or more percent should be possible as a result of various reactive oxygen species in the plasma;[4] however, there was no experimental proof. Note that one common theme of all of the sputtering that has occurred under ambient environments is the role of excited oxygen species, which have been found to not only functionalize the surface, but have also been present in the gas-phase sputter products.

Despite numerous accounts of ambient sputtering in other fields, mass spectrometry, which has a long history of physical and chemical sputtering at reduced pressure, seems somewhat antiquated with regards to its lack of evolution to atmospheric-pressure sputtering. A major hurdle for mass spectrometry is that it has traditionally been performed entirely at reduced pressure, from ionization to ion detection. Hence, it is not surprising that sputtering phenomenon have not been reported under ambient conditions in a mass spectrometric experiment. Despite having the capability of producing ions at

atmospheric pressure and introducing them to reduced pressure mass analyzers since the early 1970s,[5] it was only recently in 2004 that methods were developed to directly interrogate surfaces with spray-based[6] and plasma-based[7] ambient ionization methods. It is this overlap of the use of plasmas for various sputtering applications in polymer and semi-conductor industries as well as their recent development for ambient ionization mass spectrometry that has led to the current investigation of the role of chemical sputtering as a desorption/ionization process for mass spectrometry.

Desorption processes for plasma-based ambient ionization sources for mass spectrometry (MS) have mainly been attributed to thermal energy; however, there have been hints of non-thermal desorption with ambient plasmas with no mechanistic explanation.[8,9] In the report by Xing *et al*., metals were the sample of choice and it was found that a DBD could remove metals from the surface, but the use of an inductively coupled plasma (ICP) to ionize the metals after DBD exposure suggests the metals leaving the surface were not ions.[9] In the other study, plasma assisted desorption ionization (PADI) was used to interrogate various polymers and small molecules, and the authors suggested a non-thermal mechanism must be taking place but did not offer an explanation.[8] In order to develop plasma-based ambient ionization for broader applications, a better explanation of non-thermal desorption processes is needed. The range of molecules that can be analyzed via thermal desorption, followed by ionization, is limited to smaller, more volatile samples. Applying more heat by various methods will increase the range of molecules that thermally desorb, but bulkier molecules such as proteins and polymers are still inaccessible. Only through a higher energy process like chemical sputtering will the analysis of such low-volatility molecules be possible. The

focus of this chapter is to better understand if and how non-thermal desorption processes occur during an LTP-MS experiment.

5.2 Experimental

5.2.1 LTP-MS Analysis

The handheld LTP probe discussed in Chapter 3 was used for all analyses in the chapter. Helium was used as the discharge gas. All reagents and solvents were purchased from Sigma-Aldrich (St. Louis, MO). Analysis of pure analyte solids and liquids were performed by dipping the closed end of a melting point tube into the pure analyte and holding in the sampling region of the LTP in front of the MS inlet. Diluted analyte solutions were analyzed by pipetting a small aliquot (2 – 3 μL) onto a glass slide. In cases where heat was applied, a small heating element with controller was used to heat up a metal block and the glass slide (with sample) was placed on top.

5.2.2 Solution-Phase Electrochemistry

Solution-phase electrochemistry was achieved using a configuration shown in Figure 5.10A. Graphite electrodes (~1 mm dia.) were spaced ~1 mm apart. 20 μL of 1 ppTh acetylcholine in water was spotted such that both graphite electrodes were in contact with the droplet and voltage/current was supplied via a 30V dc power supply (AX503, AEMC Instruments, Dover, MA, USA). Three μL of pre- and post-electrochemistry treated acetylcholine solution was placed onto filter paper (Whatman

Grade 1) and analyzed via paper spray mass spectrometry, which required cutting the paper into a sharp triangle followed by application of 20 – 30 μL of methanol and 3.5 kV to the paper to generate an electrospray-type process.

5.2.3 Self-Assembled Monolayer (SAM) Surface

Self-assembled monolayers (SAMs) of 3,3,4,4,5,5,6,6,7,7,8,8,9,9,10,10,10-Heptadecafluoro-1-decanethiol (F-SAM) on Au substrate were prepared by a reported method by Chidsey *et al*.[10] 10 x 10 mm Au coated (200 nm thickness) silicon wafers (International Wafer Service, Inc. Cofax, CA) were cleaned with a piranha solution (3:1 sulfuric acid to hydrogen peroxide) to remove any contaminants and washed with distilled water and ethanol respectively. The cleaned substrates were immersed in 1 mM solution of thiol in ethanol for 24 h (enough time for SAM to form via gold-sulfur covalent bond). After the SAM had formed it was thoroughly washed with ethanol several times and dried under nitrogen atmosphere to ensure no unreacted thiol remained on the surface.

5.3 Results

5.3.1 LTP-MS Analysis of Non-Volatile Halogenated Analytes

A self-assembled monolayer (SAM) is produced by spontaneous covalent bonding of a long-chain thiol to a gold surface through a Au-S bond. An advantage of SAMs is that they are an excellent sample substrate to study chemical sputtering due to their thermal stability, ensuring that the chemical moiety for which the chemical sputtering is to occur with is not prematurely in the gas phase. The heavily fluorinated SAM, referred to as F-SAM (cf. Figure 5.1A), was prepared and exposed to excited species from LTP. The resulting mass spectrum (cf. Figure 5.1B) reveals ions which were produced by the cleavage of C-C bonds at multiple locations. Figure 5.1C shows structures of the most abundant ions detected and were confirmed using accurate mass measurements on an LTQ Orbitrap as well as tandem MS.

The ions at *m/z* 319, 369 and 419 correspond to straight perfluorinated alkyl anions with six through eight carbons respectively. Ions at *m/z* 313, 363, 413 and 463 are perfluorinated alkyl chains, with five through eight carbons respectively, which have been functionalized with a carboxylate on the end where the C-C bond cleavage occurred. This was confirmed by accurate mass data which revealed two oxygens were present as well as by MS/MS data that revealed the loss of 44 Da (CO_2). Note that the once CO_2, was lost, for example from the ion at m/z 463, the fragment at m/z 419 is identical to the one in the full mass spectrum and their tandem MS is the same. The peaks at *m/z* 426, 476 and 526 correspond to HNO_3 adducts of the perfluorinated alkyl carboxylates at m/z

363, 413 and 463 respectively. Nitric acid is formed in large abundance with LTP and adducts to certain negative ions. It is easy to identify an ion that contains a nitric acid adduct because large isolation windows are needed to efficiently isolate the parent peak and very low CID energies (less than 15% manufacturer's units) result in complete fragmentation to a daughter ion that is 63 Da lower than the parent.

Figure 5.2 shows the analysis of another halogenated and non-volatile analyte, thyroxine. Note that, with a molecular weight above 776 Da, the ambient vapor pressure of thyroxine has not been measured but was calculated to be 1.24×10^{-17} Torr in the Syracuse Research Corporation (SRC) physprop database (SRC, Inc., http://esc.syrres.com/fatepointer/search.asp). The vapor pressure is too low to allow the molecule to be thermally desorbed by LTP. Hence, the LTP mass spectrum of thyroxine in Fig. 5.2 does not show an intact molecular ion. Instead, it predominantly shows I_2^- and I_3^- at *m/z* 254 and 381 respectively, which are formed as a result of cleavage of the carbon-iodide bond.

5.3.2 LTP-MS Analysis of Fluorinated Polymers

Various polymers were interrogated via LTP-MS by simply placing the pure and intact polymer in the LTP sampling region. Figure 5.3A shows the LTP-MS analysis of polytetrafluoroethylene (PTFE or Teflon®) in negative ion mode on a Thermo Exactive Orbitrap. In the spectrum is a wide distribution of peaks spaced by 50 Da, corresponding to a difference of one CF_2 unit. The spectrum shown in Figure 5.3B is zoomed in over a region slightly greater than 100 *m/z* units to better show the various peaks that are present

in the spectrum. Since the spectrum was acquired on an Orbitrap, it was possible to obtain the chemical formula for each of the peaks. Note that the peaks from the LTP-MS analysis of PTFE have anywhere from 1 – 5 oxygens added to the chain and this distribution changes as a function of the potential applied and the discharge gas used (both nitrogen and argon plasmas also give ions from PTFE with different distribution). In addition, some of the peaks (e.g. *m/z* ~538/588) have a hydrogen, which is likely present at the terminal carbon (i.e. $–CF_2CHF_2$) as one possible termination of PTFE polymerization. Other possible termination pathways include the formation of a double bond (i.e. $–CFCF_2$) or $-CF_2CF_3$ at the terminus. Each of these types of ions are present in the mass spectrum, suggesting the method could be useful for fast and direct Teflon® characterization, but more work is needed to elucidate ion structures, reduce the variability in mass spectra and reduce the amount of oxidation which complicates the spectra. Further insight as to how the oxygens are adding to the perfluoroalkyl chains is also of interest in determining the desorption/ionization mechanism.

Figure 5.4A shows the LTP-MS analysis of poly(chlorotrifluoroethylene) (PCTFE) in negative ion mode. Note that the mass spectrum shows peaks separated a repetitive cycle of 50 and then 66 Da, which correspond to cleavage after every CF_2 and CFCl group respectively. Similar to the F-SAM ions, the major series of PCTFE ions in the spectrum are terminated with a carboxylate and are nitric acid adducts. However, the other end of the PCTFE ions terminated with a double bond, so the formula for the ion at *m/z* 320 would be $CFCl=CF\text{-}CFCl\text{-}CF_2\text{-}CO_2^-\bullet HNO_3$. Interestingly, there is a bimodal distribution with PCTFE, where ions that were cleaved such that CFCl was adjacent to the carboxylate on the end (i.e. *m/z* 386, 502, 620, 736, etc.) were lower in abundance

than ions cleaved where CF_2 preceded the carboxylate (i.e. *m/z* 320, 436, 552, 670, 786, etc.).

The LTP-MS analysis of poly(vinylidene fluoride) (PVDF) was not as straight forward (c.f. Figure 5.4B). Despite having a structure that continuously alternates between CH_2 and CF_2 units, there was not a corresponding mass spectrum that showed peaks separated by 14 and then 50 Da. Instead, there was a cluster of peaks from *m/z* 238 – 414 that were separated by about 14 Da and there was a separate distribution of peaks at higher masses separated by 100 Da. Performing MS^4 (c.f. Figure 5.5A) confirmed that *m/z* 526 was the nitric acid adduct of a straight perfluorinated alkyl chain with a carboxylate terminal (the same as the ion detected from F-SAM in Fig. 5.1B).

5.3.3 LTP-MS Analysis of Organic Salts

Organic salts represent another class of compounds that are typically very non-volatile. Even when heated to 200 °C, no ions were detected by MS for the organic salts studied in this section despite their pre-charged nature, which should automatically yield gas-phase ions upon thermal desorption. When exposed to excited LTP species at room temperature, there were still no intact parent cations observed. Instead, only fragments of the organic salts were detected as shown in Table 5.1. As seen in the table, a wide variety of organic salts were observed to exhibit a similar type of reactivity by undergoing cleavage directly adjacent to the charged cite in the cation. Figure 5.6A shows the analysis of tetraoctylammonium bromide, where one of the octyl groups connected to the cationic, quaternary ammonium was displaced with a proton. In Figure

5.6B, the LTP-MS analysis of benzylhexadecyldimethyl ammonium chloride revealed displacement of the benzyl group again with a proton. Note that both of the organic salts in Fig. 5.6 contained a quaternary ammonium involved in only sigma bonding, and one of the four sigma bonds was broken.

Similar reactions can be observed for quaternary ammoniums involved in pi-bonding as well as for compounds containing tertiary oxygen. Shown in Figure 5.7A is the mass spectrum obtained for the LTP interrogation of ethylpyridinium bromide, which contains a quaternary ammonium involved in pi-bonding. Similar to, the examples in Fig. 5.6, the LTP-MS analysis of ethylpyridinium reveals the displacement of the ethyl group with a proton. Figure 5.7B displays the LTP-MS spectrum of an organic salt containing tertiary oxygen, 2-(2,5-Dioxopyrrolidin-1-yl)-1,1,3,3-tetramethyluronium tetrafluoroborate. Again, no peaks for the parent uronium cation at *m/z* 214 exist, but similar to the quaternary ammoniums, cleavage of the nitrogen-oxygen bond resulted in protonated tetramethylurea at *m/z* 117. It is also worth noting that the proton-bound dimer of tetramethylurea at *m/z* 233 is present, suggesting that neutral tetramethylurea is formed during the fragmentation of the uronium salt.

5.3.4 LTP-MS Analysis of Imidazolium Ionic Liquids

Many of the imidazolium salts are unique in that they are liquid at room temperature, hence the name ionic liquids, yet have very low volatility and are difficult to volatilize. Although, there have been reports of thermally desorbing some ionic liquids at higher temperatures.[11] Given their related structure, imidazolium ionic liquids react in a

similar manner as the quaternary ammoniums from the previous section. This can be seen in Table 5.1 where diisopropylimidazolium and 1-butyl-2,3-dimethylimidazolium chloride react via the replacement of an isopropyl and butyl group respectively and with a proton. However, it should be noted that the imidazolium salts are resonantly stabilized such that both nitrogens in the ring share the positive charge. While the symmetric diisopropylimidazolium can only lose an isopropyl group, 1-butyl-2,3-dimethylimidazolium and many other imidazoliums can lose either a methyl or a butyl group. The ability to react at either partially cationic nitrogen was examined further by analyzing 1-ethyl-3-methylimidazolium (1E3MI), 1-methyl-3-propylimidazolium (1M3PI) and 1-butyl-3-methylimidazolium (1B3MI) with various counter anions. The analysis of 1E3MI chloride and 1E3MI methyl carbonate can be found in Figures 5.8A and 5.8B. The data for the analysis of all three imidazoliums with various anions can be found in Table 5.2 with attention paid to the preference of losing methyl or the larger alkyl group.

5.4 Discussion

5.4.1 Examining Potential Desorption Pathways

The most prominent desorption process for plasma-based ambient ionization MS is undoubtedly thermal, even with LTP which is a room temperature plasma. This is possible because most of the analytes that are "desorbed" and ionized with LTP have an appreciable vapor pressure at room temperature (typically 10^{-7} Torr or higher) such that

there is a sufficient abundance of the analyte in the gas-phase (due to the excellent sensitivity of MS) even without applying heat. The samples discussed in this chapter are unique in that they have little to no vapor pressure in the room temperature LTP reaction region. It should be further noted that the LTP reaction region is ~5 cm downstream from the highly energetic and visible part of the plasma (where plasma bullet propagation occurs). Thus, any temperature spikes which may have been possible in the highly energetic plasma bullets would have cooled/equilibrated by the time the sample is reached, 5 cm past the termination of the plasma bullet. Hence, the mass spectrum in Fig. 5.1 revealing excessive C-C bond cleavage from F-SAM, which is covalently bound to a gold substrate, can be dismissed as being due to a thermal process.

Similarly, thermal desorption has been ruled for the analysis of organic salts. A major indication that thermal desorption is not occurring is that simply heating the organic salts, which are pre-charged, up to 200 °C in front of the MS inlet revealed no signal. Although, the analysis of ionic liquids with atmospheric pressure thermal desorption ionization (APTDI) MS has been reported and yields the intact cation/anion as well as clusters of the anion/cation pairs at 250 °C.[11] In a typical plasma-based ambient ionization experiment, where thermal desorption is the major desorption pathway, increasing the temperature of the analyte substrate will increase the volatility of the analyte and, hence, result in a higher MS signal. However, if no thermal desorption is occurring, increasing the temperature of the analyte substrate should not have a significant effect on MS signal. To examine the role of temperature on the LTP-MS analysis of organic salts, LTP-MS/MS spectra were acquired by analyzing acetylcholine chloride from a glass microscope slide heated to various temperatures.

The expected product from the reductive cleavage of acetylcholine in the LTP environment is 2-dimethylaminoethyl acetate (as shown in Table 5.1), with an *m/z* of 132 after being protonated. The MS/MS of protonated 2-dimethylaminoethyl acetate results in ions at *m/z* 87 and 72, which correspond to the loss of dimethylamine and acetic acid, respectively. For Figures 5.9a and 5.9b, the temperature of the glass slide was held at 25 and 100 °C, respectively, and the signal of the fragment at *m/z* 87 was monitored with respect to time (i.e. the selected ion chronogram) and plotted on a log rhythmic scale on the y-axis. The chronograms show an interesting trend where there is no signal in the bulk solution, but in a minimally-solvated state there is a large signal enhancement before decreasing again after the spot dries. The decrease in signal from the minimally-solvated state to the dry spot has been attributed to the formation of ionic bonds that are more energy-consuming to break, whereas the minimally-solvated state provides both a high concentration of acetylcholine as well as weakened ionic interactions through solvation that permit significant reactivity. Nevertheless, the chronograms show no significant difference in absolute signal for analysis of the dried salt from 25 °C to 100 °C. However, the signal increases over two orders of magnitude when the organic salt is heated to 200 °C (Figure 5.9C). Note that the signal actually begins to increase once the glass slide is heated to 150 °C. This is a due to thermal degradation of acetylcholine, which has been shown to occur with similar quaternary ammoniums in the range of 140 to 180 °C.[12]

After ruling out thermal desorption, the remaining desorption methods to be considered include solvent-assisted, acoustic, field, laser, physical sputtering, high-energy electron sputtering and chemical sputtering. Both solvent-assisted and acoustic

desorption can be quickly ruled out because there is no solvent or acoustic wave present in LTP. Field desorption also is not possible because the electric field is not nearly high enough in the LTP reaction region which is at least 5 cm from the high voltage electrodes. As for a laser-based mechanism, LTP does produce visible and UV photons, but given that the sample substrate is placed 5 cm away from the visible plasma, the photons would quickly be quenched such that the intensity would not be high enough to allow significant desorption. In addition, the LTP source has not exhibited similar desorption abilities as lasers for other non-volatile analytes.

The three desorption processes yet to be ruled out all involve some type of sputtering. Physical sputtering might be possible in ambient conditions if the electric field is high enough to accelerate reagent ions to the sample substrate, but as previously mentioned, the electric field is too low and the pressure is too high in the reaction region of the LTP such that ions could not have enough kinetic energy to induce sputtering. As was briefly discussed in the last chapter, it is also very unlikely that bare electrons would exist over a distance of 5 cm in ambient air, from their formation in the initial DBD to the LTP reaction region, because they are quickly converted to anions or become solvated in an ambient environment. There certainly would not be a high enough flux of high-energy electrons in the LTP reaction region to allot for significant desorption. Hence, the only remaining desorption mechanism that cannot be ruled out is chemical sputtering.

Chemical sputtering is considered a reactive process. This fits well with the fact that each product of the LTP interaction with non-volatile alkyl halides and organic salts involved breaking of chemical bonds, which is the basis of chemical reactions. Furthermore, chemical sputtering requires a reactive species in the gas phase that can

break bonds within surface-bound molecules. A plasma is well-suited at providing numerous reactive and gas-phase species in the form of ions, radicals, excited metastables and even reactive neutrals like ozone. Each of these species exist over long distances/times in air allowing them to interact with and ionize samples in the LTP reaction region. In addition to ionization through proton transfer, electron transfer and adduct formation, reactive oxygen species like ozone have been used for the ozonolysis and ionization of fatty acids with LTP.[13,14] Taking everything into consideration, including the fact that sputtering phenomenon have been observed with ambient plasmas in the literature,[1-3] chemical sputtering is considered as the major desorption pathway of the samples in this chapter.

What is novel in the present work is that chemical sputtering can not only occur with LTP at atmospheric pressure, but that the ambient sputtering process can produce ions for MS detection and can consequently be an important mechanism for plasma-based desorption/ionization. Previous literature has revealed that ambient plasmas are capable of producing CO_2 and H_2O from hydrocarbon chains (similar to combustion)[3] as well as gas-phase, neutral metals from solid, metal-containing substrates through a sputtering process.[1,9] However, the LTP-MS analysis of non-volatile alkyl halides and organic salts reveals that large multi-atom species can be produced by an ambient sputtering process, in contrast to the atomic and triatomic sputtering products shown in previous work. Better understanding the mechanism by which chemical sputtering occurs may lead to increased desorption/ionization capabilities of non-volatile analytes with plasma-based ionization techniques.

5.4.2 Evidence for Chemical Sputtering through Reductive Cleavage

5.4.2.1 Similarities with Solution-Phase Reductive Cleavage and Gas-Phase ETD

An advantage of chemical sputtering over other desorption methods is that it is based on reactivity. If the reactions responsible for the observed chemical sputtering of non-volatile halogenated compounds and organic salts can be elucidated, it might be possible to change the reaction environment to enable or enhance reactivity toward specific samples (i.e. reactive ionization) or to pursue new reactions altogether. One of the first pieces in better understanding the chemical sputtering reaction is found in Figures 5.7B, 5.8A and 5.8B. The presence of the proton-bound dimer of the reaction products in each of the three mass spectra indicates that a neutral fragment is released during the LTP-induced chemical sputtering of organic cations. Hence, in the case of the uronium salt in Fig. 5.7A, neutral tetramethyl urea was necessarily produced to allow formation of the dimer with protonated tetramethyl urea. This suggests neutral tetramethyl urea was an intermediate prior to becoming a protonated ion. This means that a two-step process where neutral tetramethylurea is formed via chemical sputtering in the first step and released into the gas phase and ionized via proton transfer by reagent ions in the plasma (i.e. protonated water clusters) in the second step. Note that, similar to organic salts which are reduced from a cation to a neutral in the chemical sputtering process, F-SAM was also reduced, except from a neutral to an anion.

This type of cleavage closely resembles electron transfer reactions that have been observed in solution-phase chemistry. Similar electron transfer reactions have been

shown in the gas phase as well and will be briefly discussed below. The solution-phase reaction is typically done as an electrochemical reaction known as reductive cleavage with a variety of reagents which include organic salts and alkyl halides. Ross *et al*. demonstrated that quaternary ammoniums will get reduced and break apart to a neutral tertiary amine and an alkyl radical (or carbanion in the two-electron process) during reductive cleavage (c.f. Scheme 5.1).[15]

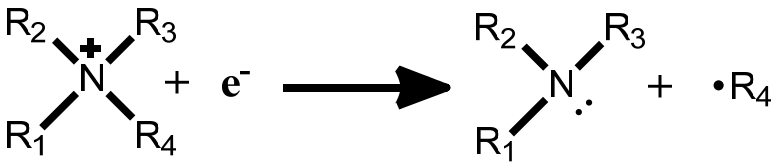

Scheme 5.1 Reductive cleavage of a quaternary ammonium

Note that if the site of electron transfer, the quaternary ammonium in this case, is only involved in sigma bonds, the incoming electron will occupy an antibonding σ-orbital that causes the observed α-cleavage of an alkyl group in a concerted mechanism.[16] In the case where the site of the incoming electron is involved in π–bonding (as with pyridiniums, imidazoliums and uroniums), the reduced radical may exist as an intermediate (as observed with cyclic voltammetry) but eventually α-cleavage of a σ-bond is observed.[16] These phenomena correspond well with LTP-MS spectra, which have revealed the production of neutral tertiary amines for quaternary ammoniums involved in both σ- and π–bonding. However, after their production, the neutral amines are rapidly protonated in the plasma due to their high basicity and the abundance of acidic water clusters.

Despite a fair amount of literature on the solution-phase electrochemical reaction, the correlation of the reactivity of the proposed chemical sputtering via reductive cleavage with solution-phase reductive cleavage was examined using one of the organic salt reagents. Figure 5.10A shows an image of the crude electrochemical setup on a glass slide with two graphite electrodes but no reference electrode. Electrochemistry was carried out for ~2 minutes by placing a 20 μL drop of 1 ppTh acetylcholine chloride to cover both electrodes and applying 1.5 volts to one electrode and grounding the other. Figure 5.10B shows a paper spray[17] mass spectrum of normal acetylcholine chloride. The spectrum in Figure 5.10C was acquired after electrochemistry in the methanol-acetylcholine chloride solution for two minutes. It is clear that the protonated 2-dimethylaminoethyl acetate product (*m/z* 132) is not observed before electrochemistry, but it appears afterwards, just as in the LTP-MS analysis of acetylcholine. Hence, the reactivity of acetylcholine in the LTP environment is similar to that of the solution-phase electrochemical reaction.

In contrast to cationic species which yield two neutral fragments upon reductive cleavage, alkyl halides tend to yield a negatively charged halide and an alkyl radical (c.f. Scheme 5.1B).

Scheme 5.2 Reductive cleavage of an alkyl halide

Note that the reduction step results in a product with one less charge, so while cations form two neutral fragments, neutrals like alkyl halides yield an anion and a neutral. In

solution phase, reductive cleavage rates vary from molecule to molecule; for example, alkyl iodides have been observed to have much higher cleavage rates than alkyl fluorides, due to having weaker carbon-halogen bonds. If reductive cleavage is responsible for the observed chemical sputtering with LTP-MS, this could explain why carbon-iodide bonds were readily cleaved in non-volatile samples like thyroxine, while heavily fluorinated alkyl chains showed a propensity for C-C cleavage. The bond dissociation energy (BDE) for C-C (~3.6 eV) is weaker than the C-F bond (~5 eV), whereas the BDEs for C-I (~2.5 eV) and C-Cl (~3.4 eV) are lower than the C-C BDE.[18]

These BDEs can also help explain the LTP-MS spectrum of PCTFE in Fig. 5.4A in terms of reductive cleavage. Assuming a reductive cleavage process was responsible for the LTP mass spectrum of PCTFE, ions at *m/z* 502, 620, 736, etc. are a result of electron transfer to the CClF carbon. This is because these ions contain one more CClF (66 Da) than the ions at *m/z* 436, 554 and 670, and since the other, neutral terminus of the ion remains constant, CClF is the site where reductive cleavage was initiated for ions at *m/z* 502, 620, 736, etc. There are two possible reasons for why the proposed reductive cleavage at a CClF site occurs at a lower rate than at a CF_2 site: 1) the presence of the chlorine induces less of a partial positive on the carbon which makes it slightly less likely to take part in electron transfer than a carbon with two fluorines or 2) the C-Cl bond cleavage competes with the C-C cleavage due to being slightly lower in energy. Either explanation favors reductive cleavage as the responsible chemical sputtering mechanism.

If chemical sputtering is occurring in the LTP environment through a reductive cleavage process, a question arises of which species in the plasma causes the reduction. One obvious candidate would be excited oxygen species due to their role in sputtering

processes in previous experiments with ambient plasmas.[1-4] Marotta *et al*. have more thoroughly investigated the role of excited oxygen anions (O_2^-, $O_2(H_2O)^-$ and O_3^-) by using APCI to create the ions at atmospheric pressure and then selecting one in the first quadrupole of a triple quad MS.[19] In the second quadrupole they introduced halothane ($CHBrCl\text{-}CF_3$) vapor, allowing its interaction with their selected oxygen anions. The resulting mass spectra revealed that each of the three species were able to undergo either dissociative electron transfer or nucleophilic substitution with halothane, suggesting these reactive oxygen species are capable of causing the reductive cleavage proposed herein with structurally similar non-volatile samples. Interestingly, similar studies using NO_2^-, $N_2O_2^-$ and NO_3^-, which are readily formed in ambient plasmas like LTP, revealed no electron transfer reactions at all. Hence, excited oxygen anions are most likely responsible for the reactions at hand; however, other possibilities exist including other anions and reactive neutrals like ozone.

As Marotta *et al*. also pointed out, the dissociation reactions can occur through either electron transfer or nucleophilic substitution. LTP-MS data also suggests that both of these reactions could be taking place. The LTP-MS analysis of F-SAM, fluoropolymers, and some of the quaternary ammoniums revealed products that could arise from direct electron transfer as well as products with oxygens covalently attached which could have been a result of nucleophilic substitution. Unfortunately, it is not possible to know whether oxygen addition occurred during or after the sputtering process, so its role as a chemical sputtering reaction is still unclear. However, considering gas-phase processes in vacuum, two reacting species must first come into a bound orbit before becoming close enough for electron transfer to occur.[20] If the species continue to

attract during the collision, they can form a long-lived complex that can lead to covalent modification. Hence, it is possible that a species like O_2^- is responsible for the observed chemical sputtering with LTP via multiple reaction pathways; in some cases the collision results in electron transfer but in others they become close enough to form a complex which allows nucleophilic substation.

5.4.2.2 Signal Enhancement with Common Electrochemical Mediator

For many electrochemical processes, the use of electrochemical mediators, such as tetracyanohydroquinone (TCNQ), has become common to increase the rate of electron transfer to a target molecule. One important property of an electrochemical mediator is the formal potential, which should be within a few hundred millivolts to that of the target molecule (cf. Fultz *et al*. for a table of common mediators and their formal potentials).[21] To further examine if reductive cleavage is taking place, the mediated reductive cleavage of acetylcholine chloride was attempted using TCNQ as an electrochemical mediator. TCNQ was mixed with acetylcholine, with each concentration at 10 ppTh. Two µLs of TCNQ/acetylcholine solution were spotted on one area of a glass slide and two µLs of 10 ppTh of pure acetylcholine in methanol were spotted two cm away. Each spot was allowed to dry and then exposed to LTP-MS/MS, yielding the chronogram in Figure 5.11 for the MS/MS fragment of *m/z* 132 at *m/z* 87. The spot with the TCNQ/acetylcholine mixture was analyzed three times, resulting in a ~20-fold enhancement. The enhancement in signal further suggests a reductive cleavage process, in which the rate can be increased with the right selection of an electrochemical mediator.

Due to the significant enhancement in MS signal observed, mediated electrochemistry is a promising reactive experiment to increase the sensitivity for plasma-based ambient ionization MS. As has been done extensively with DESI-MS through general reactive ionization,[22] the process of mediated electrochemistry could provide a means of not only increasing sensitivity, but also extending the range of non-volatile analytes that can be analyzed with plasma-based ambient ionization. It should be noted that reactive ionization through mediated electrochemistry with LTP is different from the general reactive chemistry demonstrated with DESI-MS. Mediated electrochemistry with LTP is primarily enhancing the desorption process, as this is the part of desorption/ionization that often limits LTP-MS analyses; whereas with DESI-MS, reactions are often used to increase ionization efficiency. Carefully choosing gaseous, liquid or solid mediators to facilitate novel chemical sputtering reactions will be necessary if plasma-based techniques are going to be able to compete with the desorption capabilities of ambient ionization sources that rely on solvent-assisted desorption for the analysis of peptides, proteins, and other heavy molecules.

5.4.3 Novel Reactions with LTP-MS

5.4.3.1 Synthesizing Carboxylate-Terminated Perfluoroalkyl Polymers Directly from Polyvinylidene Fluoride in One Step with an Ambient Plasma

Plasma polymerization has been a common process for the formation of polymer films since its introduction in the 1960s[23] and was later shown to also be successful with ambient plasmas.[24] In forming a polymeric film, one important property is the ability to

adhere to a surface. Polytetrafluoroethylene (PTFE), for example, does not adhere well to many surfaces. However, oxidation of the polymer has been shown to increase adhesion capabilities,[25] which is a process that can be done with an atmospheric-pressure plasma.[26] Besides functionalization capabilities, another advantage of plasma polymerization is the solvent-free nature of the method, only requiring gases and an electrical discharge. While the lack of solvents makes for a potentially greener process, the gaseous monomers used for polymerization can be hazardous and are not ideal to work with. If possible, a solid reagent could prove to be useful as a precursor for polymerization.

As previously discussed, ambient plasmas have proven capable of chemically sputtering species from various non-volatile materials (including polymers). Hence, in the right environment, plasmas have the ability to both build and break polymers. If the sputtering process from a solid material can yield typical monomeric units, it would then be possible to build polymers from a solid precursor in a plasma. Previous reports of obtaining triatomic sputtering products with ambient plasmas suggest it may be possible to yield small monomers from large molecular precursors.[3] While the solid precursor could be any type of molecule, it could even be another polymer which gets converted into a different polymer based on the monomeric units that are formed. In the present work, a partially fluorinated polymer is converted into a pure perfluorinated polymer with a carboxylate terminus upon mere exposure to an ambient plasma environment.

The LTP-MS analyses of two different fluoropolymers are shown in Fig. 5.4. Both analyses reveal chemical sputtering products as most fluoropolymers do under LTP interrogation. As discussed previously, PTCFE shows an expected distribution of peaks

separated by a repeating sequence of 66 and 50 Da for mass differences of CClF and CF_2 units respectively. However, the mass spectrum in Figure 5.4B reveals a peculiar distribution of ions. Despite having a structure of alternating CH_2 and CF_2 units, the mass spectrum does not reveal this type of spacing (i.e. peaks alternating in spacing by 14 and 50 Da). Instead, there is a distribution of peaks spaced out by 100 Da at higher masses (*m/z* 526 – 726) as well as a distribution spaced out by 14 – 16 Da at lower masses (*m/z* 238 – 414). Performing tandem MS on one of the peaks in the distribution spaced by 100 Da, *m/z* 526, (cf. Fig. 5.5A and 5.5B for MS^4 spectrum and corresponding structures of ions at each stage of CID) revealed that the ion was a nitric acid adduct of a perfluorinated alkyl chain of eight carbons with a carboxylate terminus ($C_9F_{17}O_2^-\bullet HNO_3$). This is the same ion that was detected in the LTP-MS analysis of F-SAM at *m/z* 526.

The question arises of how $-(CH_2CF_2)_n-$ becomes $CF_3(CF_2)_nCO_2^-$ (n = 8, 10, 12) upon mere exposure to an ambient plasma? The most plausible explanation is that these perfluorinated alkyl chains exist already in the polymer and are merely being chemically sputtered by LTP. However, there are two reasons why this is unlikely. First, PVDF is formed by the polymerization of a vinylidene difluoride ($H_2C=CF_2$), which is unable to form a straight perfluorinated chain via traditional polymerization techniques. Secondly, the spacing of the perfluorinated peaks are spaced 100 Da apart, versus the perfluorinated ion peaks in the LTP-MS spectrum of F-SAM which were only 50 Da apart. Hence, the chemical sputtering process should be indiscriminate and cleave at every C-C bond in a perfluorinated alkyl chain, resulting in peaks separated by 50 Da. The fact that the peaks are spaced apart by 100 Da indicates that the ions must be created through a

polymerization process, which necessarily occurs by sequential addition of monomeric units (100 Da in the case of tetrafluoroethylene, TFE).

This means that the plasma must be breaking PVDF down into single CF_2 units that then recombine with another CF_2 unit to form TFE ($F_2C=CF_2$). Once TFE is formed, it can then rapidly polymerize in the plasma via a typical plasma polymerization process. It is not known when the carboxylate is added to the polymeric chain, as it could be at the beginning of polymerization or after the perfluorinated polymer has been formed. However, the fact that the peaks remained spaced by 100 Da suggests that the carboxylate may have been present during or even before polymerization occurred, because if the neutral fluoropolymer was formed without the carboxylate present it should rapidly fragment via electron transfer dissociation to yield spacing by 50 Da (as commonly observed with perfluorinated species).

Building a carboxylate-terminated perfluorinated polymer from a partially fluorinated precursor with an atmospheric and room-temperature plasma is a novel process with potential applications in materials chemistry. The lack of solvents and gases (other than a discharge gas which can even be air) make it a green process for potential applications of preparing polymer films. The example shown is particularly suited for polymeric films due to the incorporation of the carboxylate terminus on PTFE, leading to increased adhesion abilities. While the conversion of one polymer to a structurally different polymer was demonstrated, it should also be possible to form similar polymers from any molecule with an appropriate abundance of CF_2 groups. A potential application is for the plasma-induced recycling of environmental waste, where it could be useful for converting partially fluorinated or perfluorinated polymer waste to PTFE films. Such a

scale-up could have a significant impact and could even be extended to other non-fluorinated materials if the right plasma conditions are chosen.

5.4.3.2 Selective Cleavage of Imidazolium Side Chains as a Function of the Anion

As shown in Fig. 5.8, an imidazolium cation can react to lose either side-chain attached to the nitrogens as a function of the anion. For example, 1E3M will lose an ethyl group upon LTP exposure when chloride is the counteranion (cf. Fig. 5.8A) but preferentially loses methyl with a methyl carbonate anion (cf. Fig. 5.8B). Table 5.2 shows data for the LTP-MS analysis of 1E3MI, 1M3PI and 1B3MI with various anions. Included in the table is the ratio of the methyl loss to the larger R-group loss, where R is ethyl, propyl and butyl for 1E3MI, 1M3PI and 1B3MI respectively. When harder, monoatomic anions were the counteranion (Cl^-, Br^- and I^-) the reaction always favored loss of the larger R-group. In contrast, the use of softer, polyatomic anions (phosphate, methyl carbonate and acetate) preferentially yielded loss of the methyl group for all three cations. The one potential outlier is thiocyanate, which when analyzed as a salt with 1B3MI, preferentially favored methyl loss.

While thiocyanate is a polyatomic anion, it is very small, lying somewhere between acetate and iodide in size. It could be suggested that size or hardness of the anion plays a role and somehow causes different stacking that leads to the selective reaction; however, the extent of polarity of the reaction products is quite striking when looking at the ratios of the side-chain losses. If size/hardness was responsible for the difference in reactivity, it would be expected that varying the size of the anion would

vary the ratio of the side-chain losses such that at some point there is a transition where the ratio is ~1:1. This does not seem to be the case, as the 1B3M salt with one of the seemingly transitional anions, thiocyanate, favors the R-loss ~4 orders of magnitude greater than the methyl loss. There also is no trend towards favoring the methyl loss more when varying the counteranion from chloride to iodide. Nevertheless, neither size/hardness nor the stacking of the ionic liquid can be ruled out as contributing to the selective reactivity. It is worth noting that each of the salts with anions that preferentially experience R-group loss are all ogygen-containing. It is possible that in the presence of these oxygen-containing anions, the methyl ester is being formed as opposed to loss of the R-group. However, there is little evidence to support this claim. While the reason for the reactivity has yet to be discerned, the fact that these imidazolium salts exhibit very selective reactivity based on the nature of the anion is novel in and of itself.

5.5 Conclusions

Of the three main parts of this chapter (fluoropolymer analysis, organic salt analysis and understanding the mechanism of chemical sputtering), there are a few holes that still need further explanation. In particular, the LTP-MS spectrum of Teflon has not been fully interpreted as to how the ions are formed and how oxygens are being added to the perfluoroalkyl chains. In fact, the addition of oxygen to any of the samples is not fully understood. This is partially due to the fact that the gas-phase reagent that initiates chemical sputtering is not known. The likely reagent is some sort of reactive oxygen species (O, O_2^-, O_3^-, O_3, etc.) and, depending on the collision, the reaction is either electron transfer or oxygen addition if a reaction complex is formed. Another possibility

for oxygen addition for the cases of F-SAM and Teflon analysis is the reaction of negatively charged perfluorinated alkyl ions with carbon dioxide to form the carboxylate-terminated ion. In the case of the organic salts, in addition to not knowing the gas-phase reagent, the biggest question is concerning the analysis of imidazolium salts. It is clear that the cleavage of the R-group is a selective process, but the reason for the selectivity is not clear. It is possibly due to the hardness of the counteranion, and the ion-ion stacking in the ionic liquid, but further reasoning or even modelling is needed to confirm.

Despite not fully understanding each of the desorption/ionization processes in this chapter, there have been many significant findings from this work. For the first time, non-thermal desorption via chemical sputtering with an ambient plasma has been demonstrated to yield large fragment ions as a significant desorption mechanism for plasma-based ambient ionization MS. The type of chemical sputtering seems to follow a reductive cleavage process for many of the samples. This has led to reactive desorption for the LTP-MS analysis of acetylcholine by addition of a common electrochemical mediator (TCNQ) with a signal enhancement of ~20. Chemical sputtering with LTP has also lead to novel reactions via breaking a partially fluorinated polymer into smaller components and subsequently building a perfluorinated polymer with a carboxylate terminus as well as the selective side-chain cleavage of ionic liquids based on the counteranion. It is through the investigation of novel chemical sputtering reactions with plasma-based ambient ionization sources that the field might one day advance to a different tier and be able to compete with spray- and laser-based methods by enabling the desorption/ionization of new non-volatile materials like proteins/peptides.

5.6 References

1. Stephens, R. Journal of Analytical Atomic Spectrometry 1988, 3, 1137.

2. Rossmann, K. Journal of Polymer Science 1956, 19, 141.

3. Cooper, G. D.; Prober, M. Journal of Polymer Science 1960, 44, 397.

4. Babaeva, N. Y.; Ning, N.; Graves, D. B.; Kushner, M. J. Journal of Physics D-Applied Physics 2012, 45.

5. Horning, E. C.; Horning, M. G.; Carroll, D. I.; Dzidic, I.; Stillwel.Rn Anal. Chem. 1973, 45, 936.

6. Takats, Z.; Wiseman, J. M.; Gologan, B.; Cooks, R. G. Science 2004, 306, 471.

7. Cody, R. B.; Laramee, J. A.; Durst, H. D. Anal. Chem. 2005, 77, 2297.

8. Salter, T. L.; Gilmore, I. S.; Bowfield, A.; Olabanji, O. T.; Bradley, J. W. Anal. Chem. 2013, 85, 1675.

9. Xing, Z.; Wang, J. A.; Han, G. J.; Kuermaiti, B.; Zhang, S. C.; Zhang, X. R. Anal. Chem. 2010, 82, 5872.

10. Chidsey, C. E. D.; Liu, G. Y.; Rowntree, P.; Scoles, G. Journal of Chemical Physics 1989, 91, 4421.

11. Neto, B. A. D.; Meurer, E. C.; Galaverna, R.; Bythell, B. J.; Dupont, J.; Cooks, R. G.; Eberlin, M. N. Journal of Physical Chemistry Letters 2012, 3, 3435.

12. Xie, W.; Gao, Z.; Pan, W.-P.; Hunter, D.; Singh, A.; Vaia, R. Chemistry of Materials 2001, 13, 2979.

13. Zhang, J. I.; Costa, A. B.; Tao, W. A.; Cooks, R. G. Analyst 2011, 136, 3091.

14. Zhang, J. I.; Tao, W. A.; Cooks, R. G. Anal. Chem. 2011, 83, 4738.

15. Finkelstein, M.; Petersen, R. C.; Ross, S. D. Journal of the American Chemical Society 1959, 81, 2361.

16. Grimshaw, J. In Electrochemical Reactions and Mechanisms in Organic Chemistry; Elsevier B.V.: 2000, p 89.

17. Wang, H.; Liu, J.; Cooks, R. G.; Ouyang, Z. Angewandte Chemie-International Edition 2010, 49, 877.

18. Blanksby, S. J.; Ellison, G. B. Accounts of Chemical Research 2003, 36, 255.

19. Marotta, E.; Bosa, E.; Scorrano, G.; Paradisi, C. Rapid Communications in Mass Spectrometry 2005, 19, 391.

20. Gunawardena, H. P.; He, M.; Chrisman, P. A.; Pitteri, S. J.; Hogan, J. M.; Hodges, B. D. M.; McLuckey, S. A. Journal of the American Chemical Society 2005, 127, 12627.

21. Fultz, M. L.; Durst, R. A. Analytica Chimica Acta 1982, 140, 1.

22. Cotte-Rodriguez, I.; Takats, Z.; Talaty, N.; Chen, H. W.; Cooks, R. G. Anal. Chem. 2005, 77, 6755.

23. Goodman, J. Journal of Polymer Science 1960, 44, 551.

24. Donohoe, K. G.; Wydeven, T. Journal of Applied Polymer Science 1979, 23, 2591.

25. Klupfel, B.; Lehmann, D. Journal of Applied Polymer Science 2006, 101, 2819.

26. Okubo, M.; Tahara, M.; Saeki, N.; Yamamoto, T. Thin Solid Films 2008, 516, 6592.

Table 5.1 Structures and mass of parent cations and the respective ions that were detected as a result of LTP-MS analysis.

Starting Material	MW	Structure of Starting Material	Predominant LTP-MS Ion Detected	Major Ion(s) *m/z*
Tetrahexyl ammonium bromide	354.41	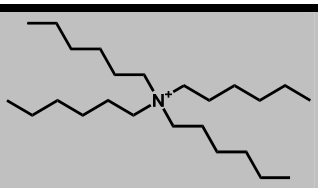	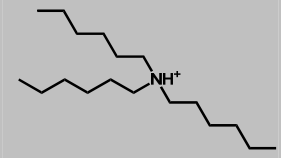	270
Tetraoctyl ammonium bromide	466.53	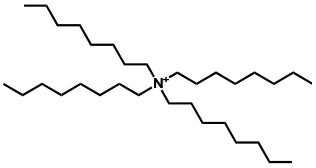	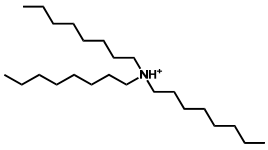	354
1-Methylpyridin-1-ium chloride	94.06	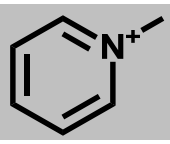	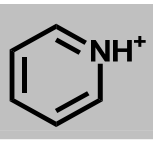	80
1-Ethylpyridin-1-ium chloride	108.08	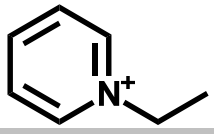	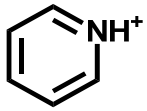	80
Benzylhexadecyl-dimethyl ammonium chloride	360.36	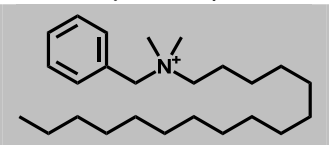	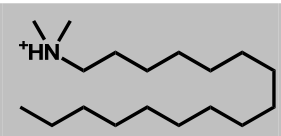	270
Acetylcholine chloride	146.12	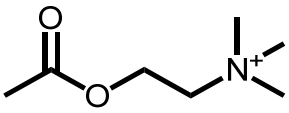	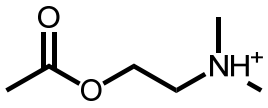	132
2-Amino-N,N,N-trimethylethan-aminium bromide	103.12	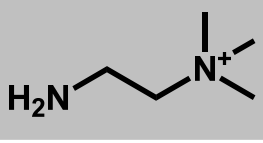	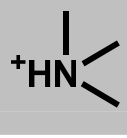	60
3-Bromo-N,N,N-trimethylpropan-1-aminium bromide	180.04	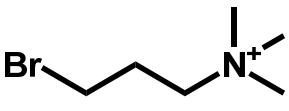	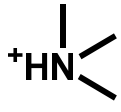	60

Table 5.1, continued

Starting Material	MW	Structure of Starting Material	Predominant LTP-MS Ion Detected	Major Ion(s) *m/z*
1,3-Diisopropyl-imidazolium Chloride	153.24	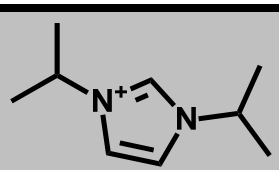	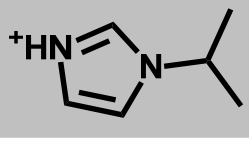	111
1-Butyl-2,3-dimethyl-imidazolium	153.24	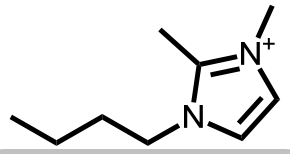	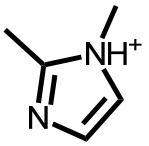	97
2-(2,5-Dioxopyrrolidin-1-yl)-1,1,3,3-tetramethyluronium tetrafluoroborate	214.12	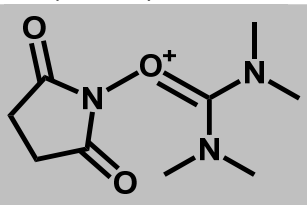	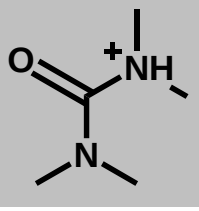	117
FC-135 N,N,N-Trimethyl-3-(perfluorooctylsulfonamido)propan-1-aminium iodide	599.07	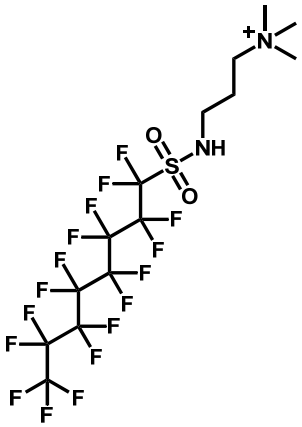	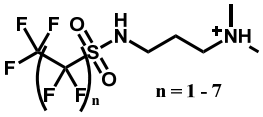 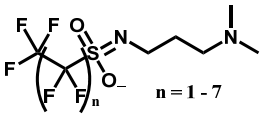	**Positive** 185 + 50n (n = 2 – 8) 199 + 50n (n = 2 – 8) **Negative** 183 + 50n (n = 2 – 8)
Thyroxine	776.69	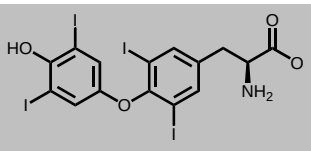	I_2^-	254

Table 5.2 Data for the LTP-MS analysis of 1-ethyl-3-methylimidazolium, 1-methyl-3-propylimidazolium and 1-butyl-3-methylimidazolium as pure samples with various counter-anions. Attention is given to which alkyl side group is lost more preferentially.

Cation	Anion	Major Ion Detected with LTP-MS	Methyl- to R-Loss Ratio*
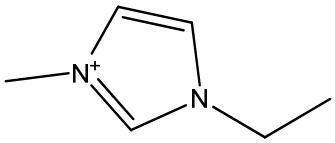 1-ethyl-3-methylimidazolium	Cl^-	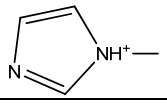	0.0024
	Br^-	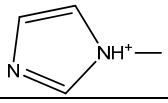	0.052
	I^-	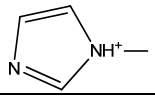	0.00032
	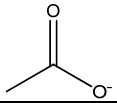	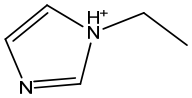	18
	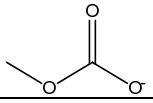	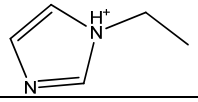	170
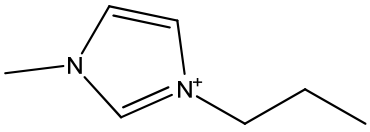 1-Methyl-3-propylimidazolium	I^-	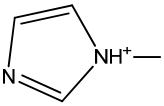	0.00032
	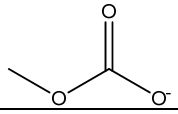	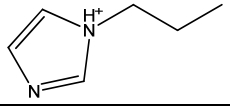	83,000
	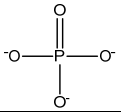	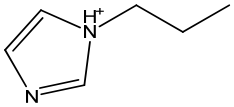	14
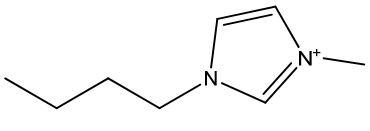 1-butyl-3-methylimidazolium	Cl^-	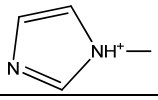	0.00022
	I^-	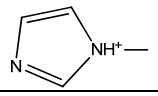	0.033
	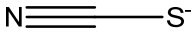	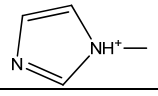	0.00013
	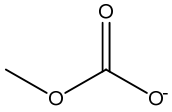	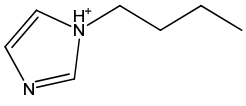	250

*R represents either the ethyl, propyl or butyl side chain for the respective imidazolium

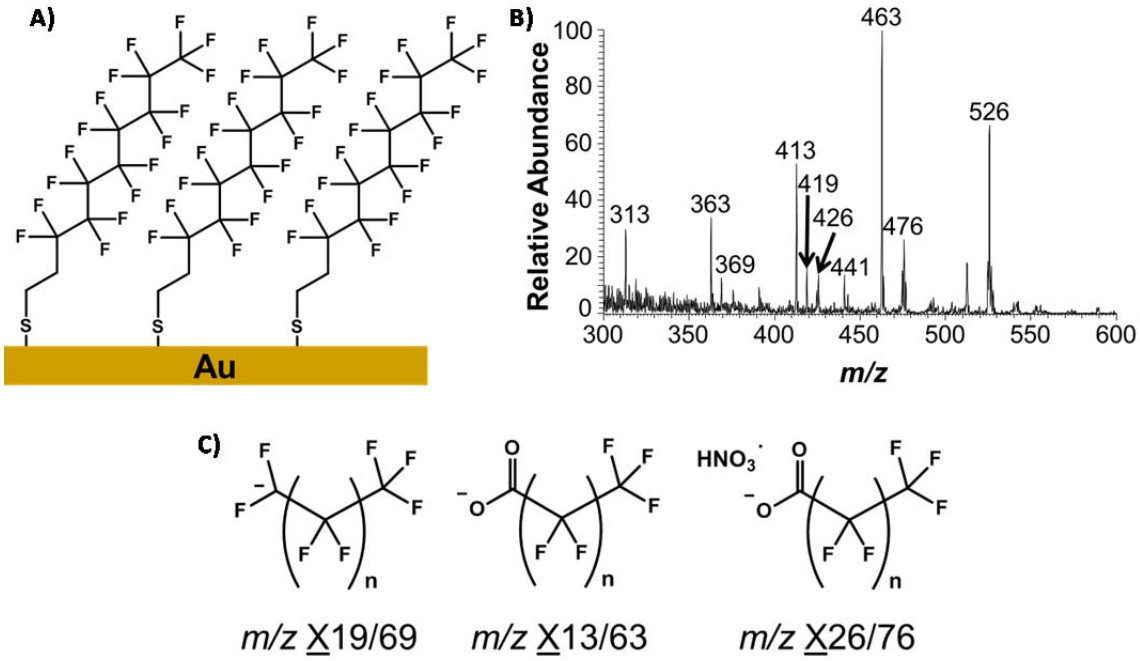

Figure 5.1 A) Diagram of an F-SAM. B) Negative ion LTP mass spectrum of F-SAM at room temperature. C) Structures of three types of ions detected from the LTP-MS analysis of F-SAM (structures were confirmed with accurate and tandem MS).

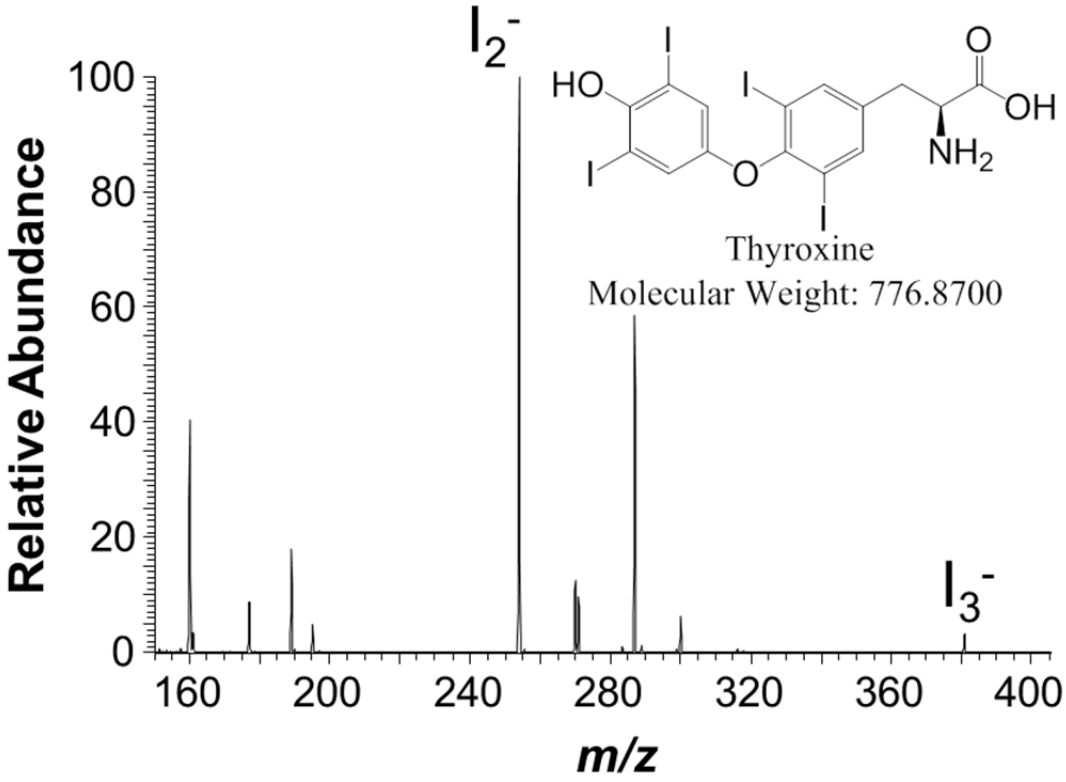

Figure 5.2 LTP-MS analysis of 100 ng of thyroxine from a glass surface in negative ion mode at room temperature.

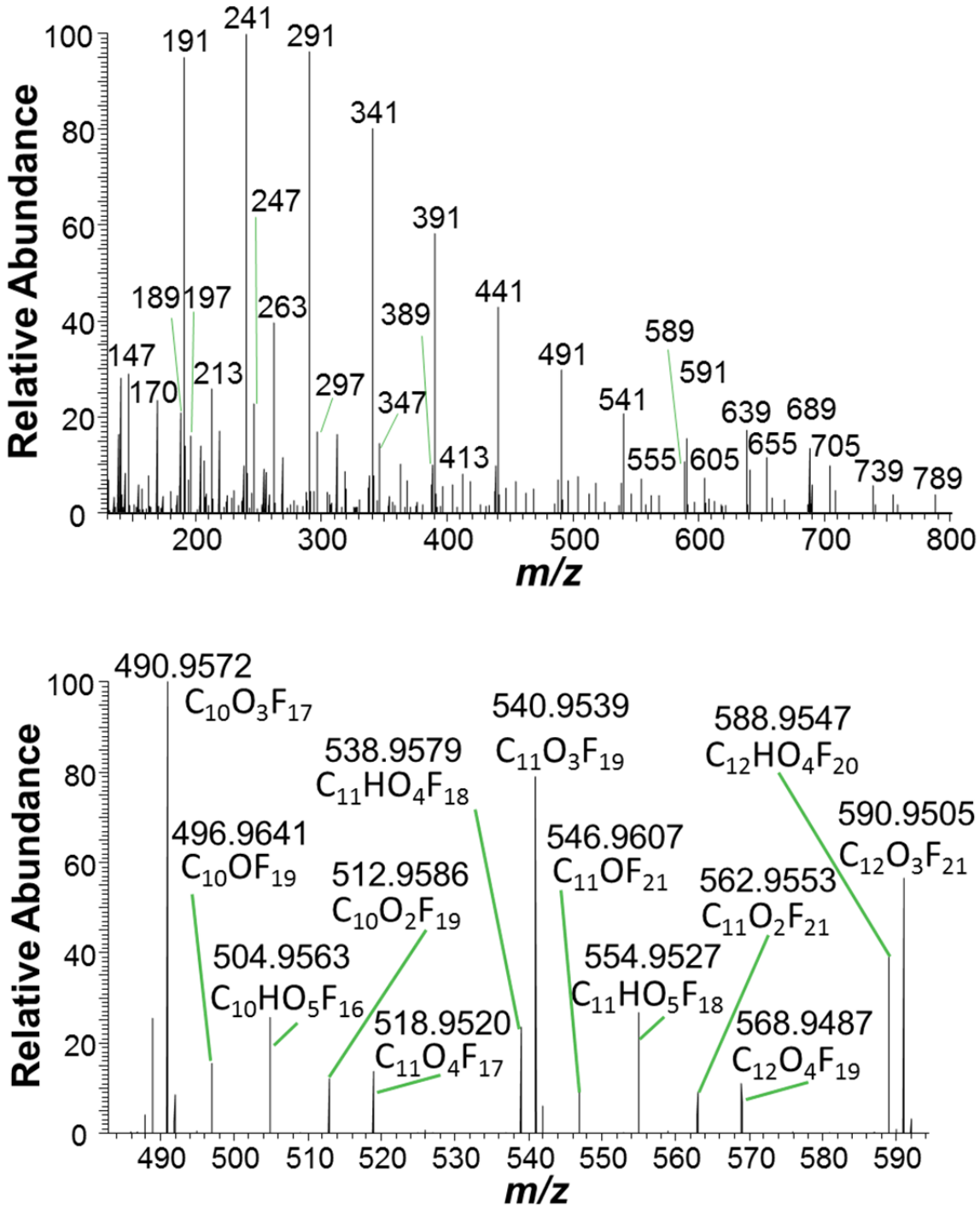

Figure 5.3 LTP-MS analysis of polytetrafluoroethylene (PTFE) in negative ion mode on a Thermo Exactive Orbitrap over A) a wide mass range and B) a more narrow range with different peaks labelled by their chemical formula.

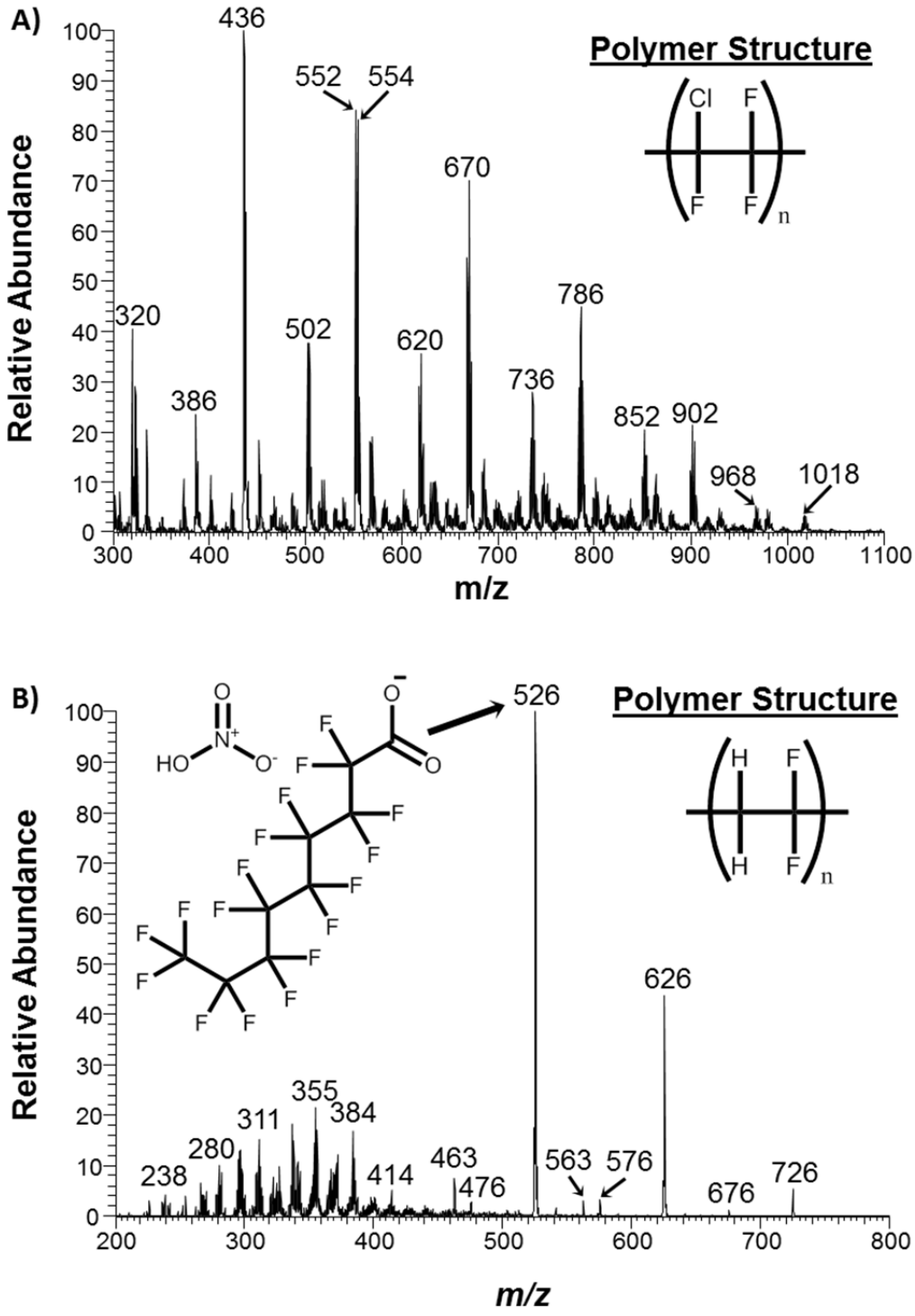

Figure 5.4 LTP-MS analysis of A) poly(chlorotrifluoroethylene) and B) poly(vinylidene fluoride) in negative ion mode at room temperature.

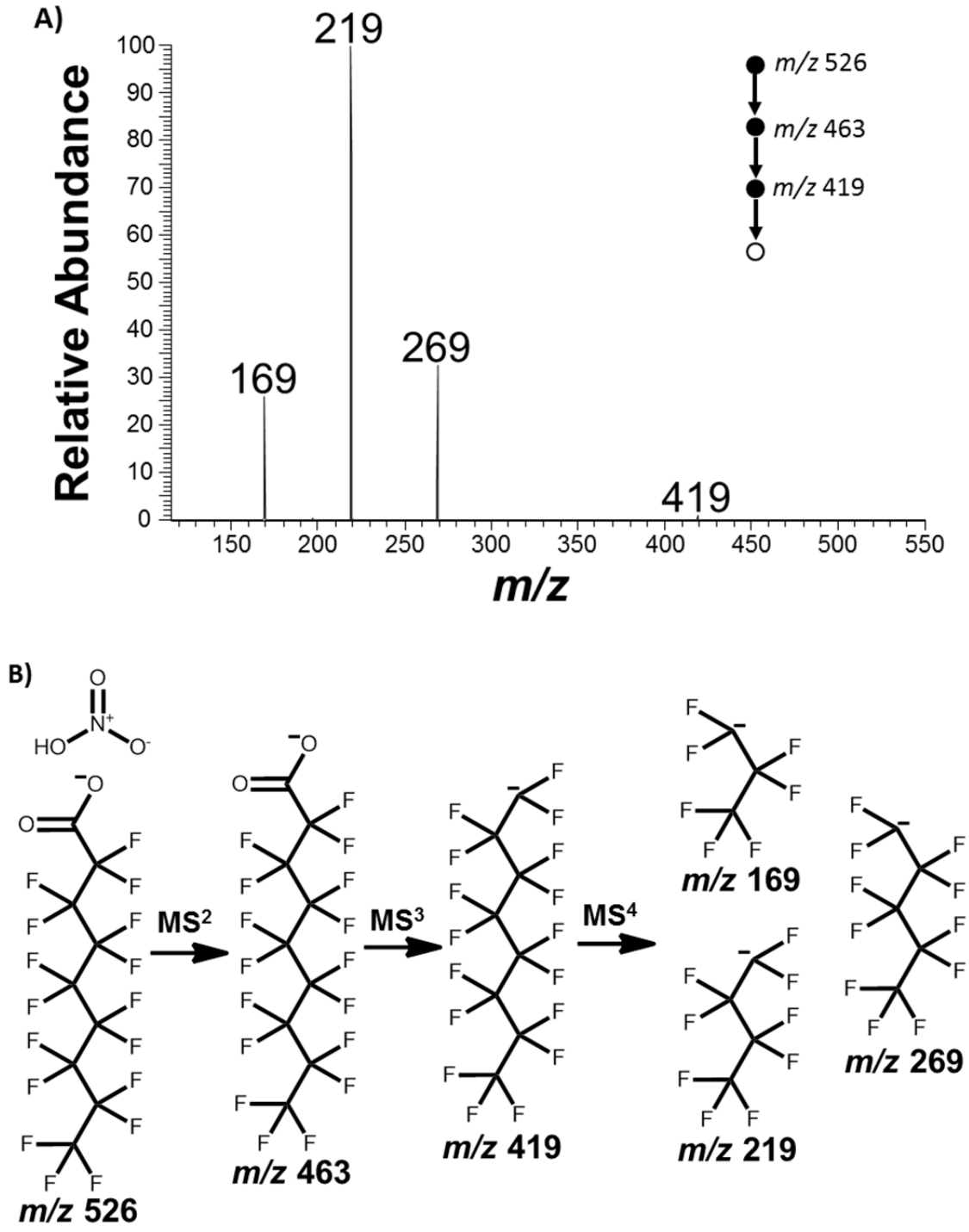

Figure 5.5 A) LTP-MS^4 analysis of poly(vinylidene fluoride) in negative ion mode and B) the corresponding ion structures at each stage of the MS^4 analysis.

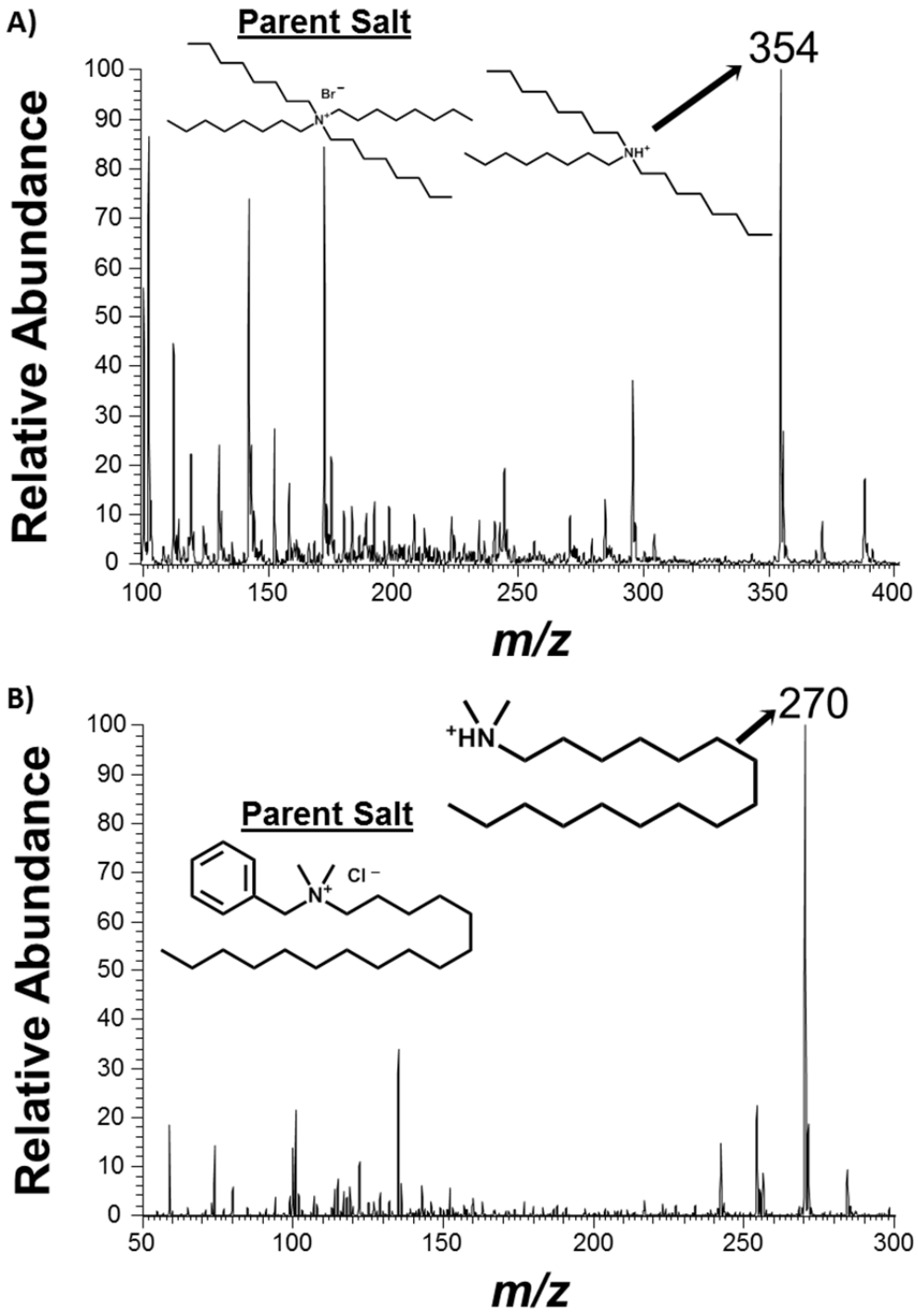

Figure 5.6 LTP-MS analysis of A) tetraoctylammonium bromide and B) benzylhexadecyldimethyl ammonium chloride dry from a glass substrate at room temperature in positive ion mode.

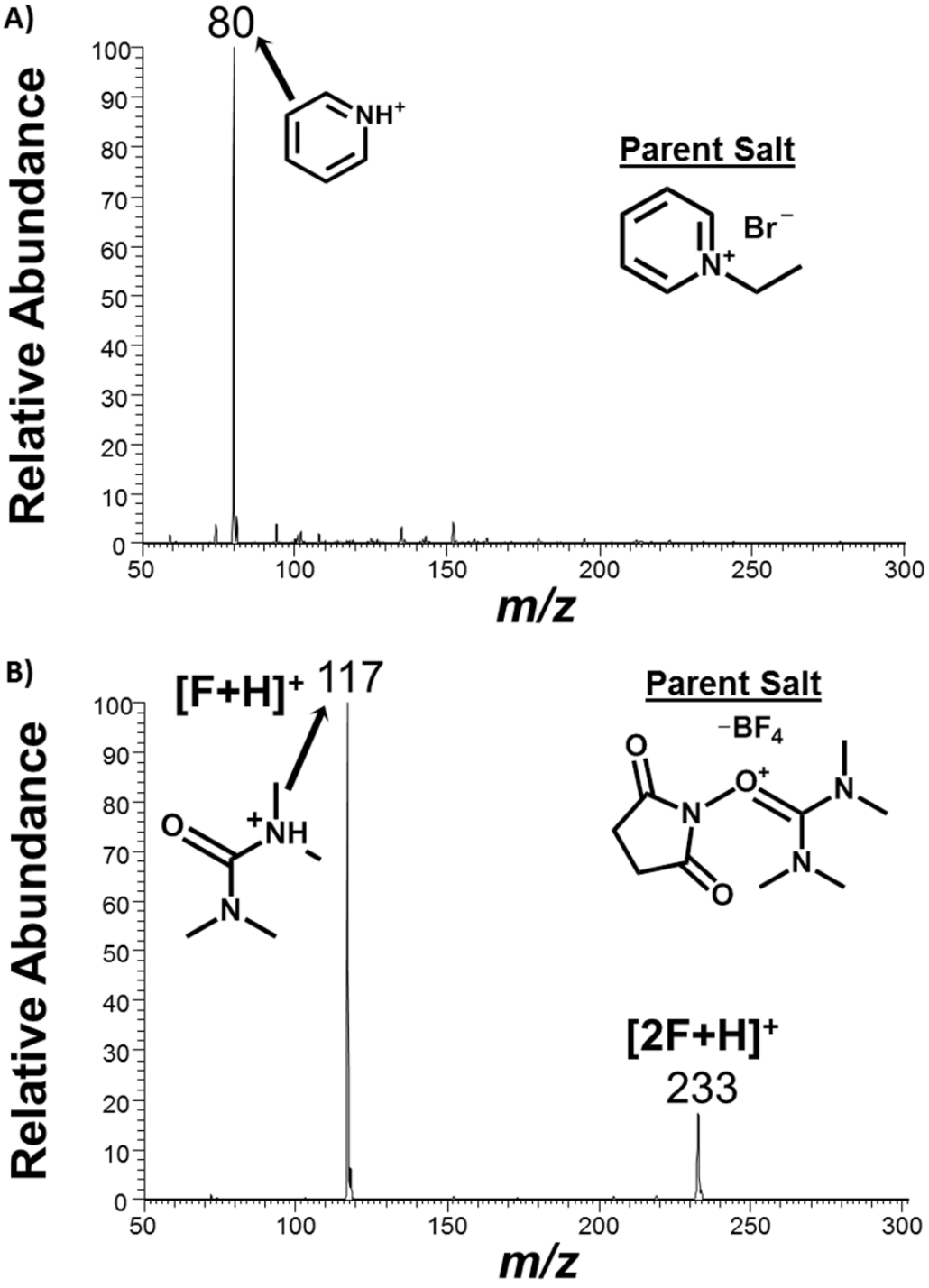

Figure 5.7 LTP-MS analysis of A) ethylpyridinium bromide and B) 2-(2,5-Dioxopyrrolidin-1-yl)-1,1,3,3-tetramethyluronium tetrafluoroborate dry from a glass substrate at room temperature in positive ion mode.

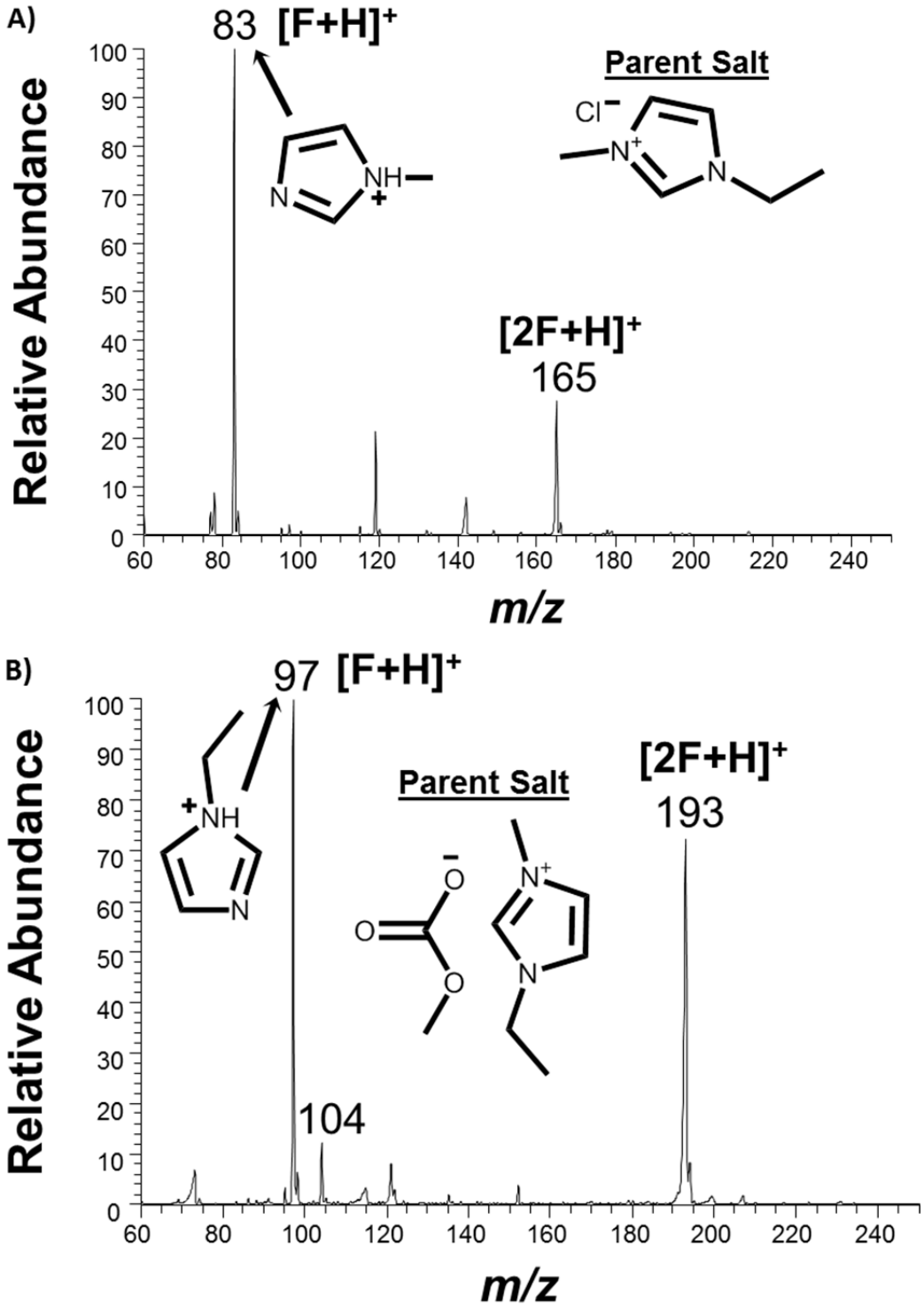

Figure 5.8 LTP-MS analysis of A) 1-ethyl-3-methylimidazolium chloride and B) 1-ethyl-3-methylimidazolium methyl carbonate pure from a glass substrate at room temperature in positive ion mode.

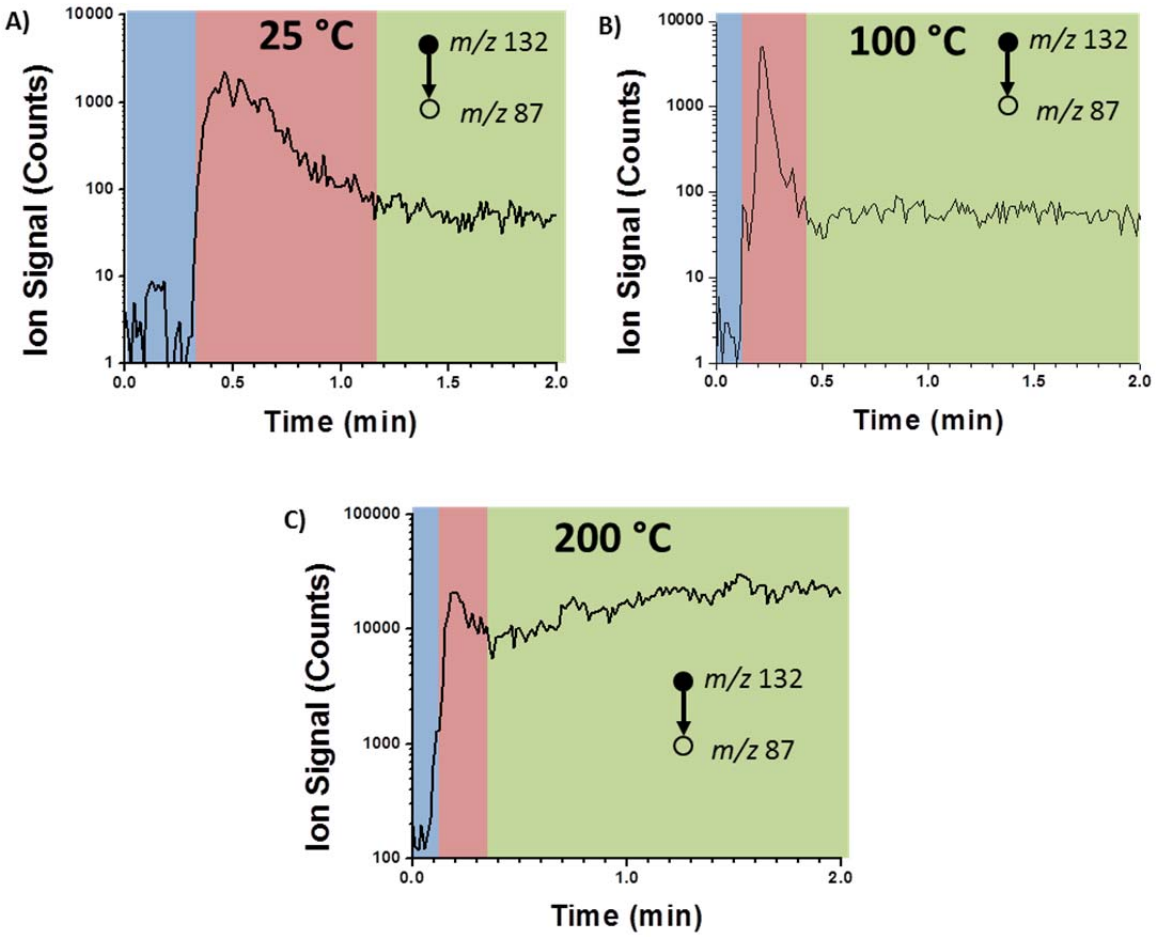

Figure 5.9 Selected ion chronogram of *m/z* 87 from the MS/MS of *m/z* 132 for the LTP-MS/MS analysis in positive ion mode of acetylcholine from a two µl droplet on a glass substrate at A) ~25 °C, B) ~100 °C and C) 200 °C. Areas of the chronograms are color coated for regions where bulk solvent was still present in a large sample-containing droplet (blue), sample is minimally solvated with very small film of solvent remaining (red), and the sample is dry on the surface (green).

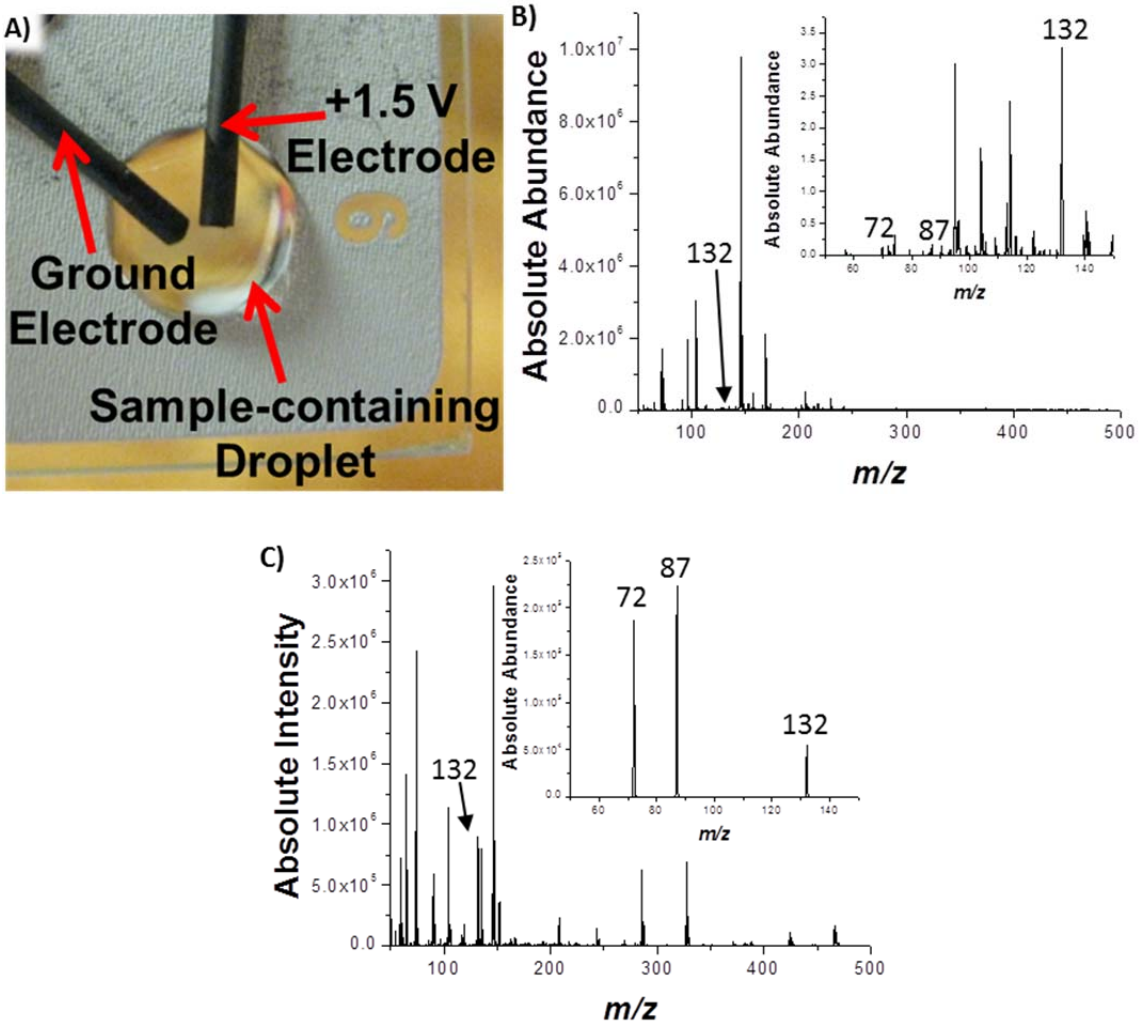

Figure 5.10 A) Photo of a crude electrochemical cell used for solution-phase electrochemistry in droplets without a reference electrode. Paper spray mass spectrum in positive ion mode of an acetylcholine chloride solution in water (MS/MS of *m/z* 132 inset) using methanol as the spray solvent B) before and C) after performing electrochemistry on the acetylcholine chloride solution.

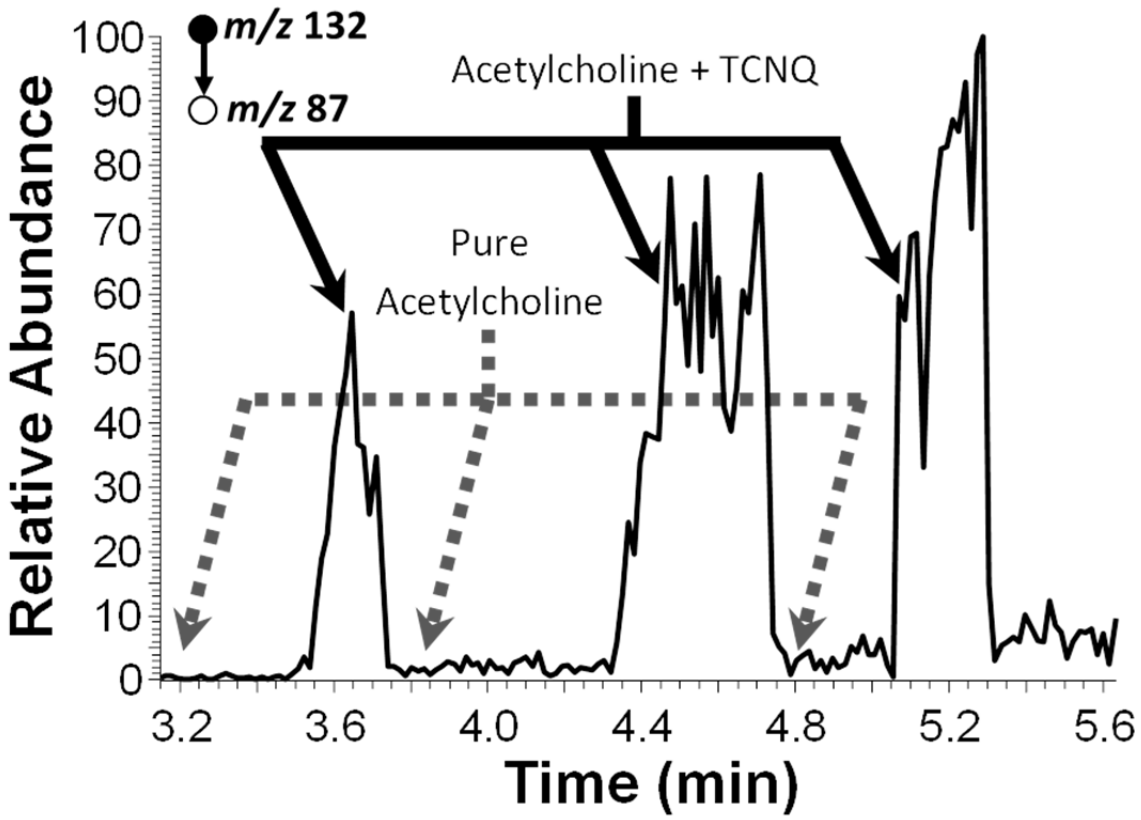

Figure 5.11 Selected ion chronogram of *m/z* 87 from the MS/MS of *m/z* 132 for switching between the LTP-MS/MS analysis in positive ion mode of two separate dried spots on a glass slide at room temperature. One spot contained pure acetylcholine while the other contained acetylcholine and tetracyanoquinodimethane (TCNQ).

VITA

VITA

Joshua Scott Wiley was born and raised in Corydon, Indiana, a small town in the southern part of the state. He graduated from Corydon Central High School as valedictorian in May 2004. After high school, he went to Indiana University to pursue a degree in chemistry. During his sophomore year he was introduced to Prof. Gary Hieftje and started doing research in his lab the summer between his sophomore and junior years. It was then that his passion for analytical chemistry began while studying fundamentals of plasma-based ambient ionization sources, and he won various awards from Indiana University as well as an American Chemical Society Analytical Chemistry Award in 2007. He also began presenting at technical conferences where he gave his first talk at Pittcon in 2008 and his first poster at FACSS in 2008 where he won a FACSS student poster award. In 2008, he continued his pursuit of knowledge in analytical chemistry in the PhD program at Purdue University as a Ross Fellow working for Prof. R. Graham Cooks. Working in the Cooks group, he continued studying fundamentals of plasma-based ambient ionization while working with the low-temperature plasma (LTP) probe. In fall 2010, he was an awarded a Department of Energy (DOE) Fellowship that was focused on studying plasma-surface interactions with LTP-MS. Thanks to DOE funding, he was able to develop a battery-powered, handheld LTP probe for "point-and-shoot" MS analyses and also began investigating chemical sputtering processes with LTP-MS over a

three-year span. His combined work at Purdue and Indiana Universities has resulted in eight publications with more on the way, and he has given four invited lectures, four non-invited lectures and a three posters at various conferences internationally. In 2013, he was selected by Purdue faculty to receive the Thomas W. Keough award for an accomplished student in mass spectrometry. After graduate school he would like to pursue a career in either academia or at a national lab.

PUBLICATIONS

PUBLICATIONS

1. **Wiley, J. S.**; Shelley, J. T.; Cooks, R. G., Handheld Low-Temperature Plasma Probe for Portable "Point-and-Shoot" Ambient Ionization Mass Spectrometry. *Anal. Chem*. **2013**, 85 (14), 6545-52.

2. Soparawalla, S.; Tadjimukhamedov, F. K.; **Wiley, J. S.**; Ouyang, Z.; Cooks, R. G., In-Situ Analysis of Agrochemical Residues on Fruit using Ambient Ionization on a Handheld Mass Spectrometer. *Analyst* **2011**, 136 (21), 4392-6.

3. Shelley, J. T.; **Wiley, J. S.**; Hieftje, G. M., Ultrasensitive Ambient Mass Spectrometric Analysis with a Pin-to-Capillary Flowing Atmospheric-Pressure Afterglow Source. *Analytical Chemistry* **2011**, 83 (14), 5741-8.

4. Chan, G. C.; Shelley, J. T.; Jackson, A. U.; **Wiley, J. S.**; Engelhard, C.; Cooks, R. G.; and Hieftje, G. M., Spectroscopic Plasma Diagnostics on a Low-Temperature Plasma Probe for Ambient Mass Spectrometry. *Journal of Analytical Atomic Spectrometry* **2011**, 26 (7), 1434-44.

5. Chan, G. C.; Shelley, J. T.; **Wiley, J. S.**; Engelhard, C.; Jackson, A. U.; Cooks, R. G.; Hieftje, G. M., Elucidation of Reaction Mechanisms Responsible for Afterglow and Reagent-Ion Formation in the Low-Temperature Plasma Probe Ambient Ionization Source. *Analytical Chemistry* **2011**, 83 (10), 3675-86.

6. Jackson, A. U.; Garcia-Reyes, J. F.; Harper, J. D.; **Wiley, J. S.**; Molina-Diaz, A.; Ouyang, Z.; Cooks, R. G., Analysis of drugs of abuse in biofluids by low temperature plasma (LTP) ionization mass spectrometry. *Analyst* **2010**, 135 (5), 927-33.

7. **Wiley, J. S.**; Garcia-Reyes, J. F.; Harper, J. D.; Charipar, N. A.; Ouyang, Z.; Cooks, R. G., Screening of agrochemicals in foodstuffs using low-temperature plasma (LTP) ambient ionization mass spectrometry. *Analyst* **2010**, 135 (5), 971-9.

8. Shelley, J. T.; **Wiley, J. S.**; Chan, G. C. Y.; Schilling, G. D.; Ray, S. J.; Hieftje, G. M., Characterization of Direct-Current Atmospheric-Pressure Discharges Useful for Ambient Desorption/Ionization Mass Spectrometry. *Journal of the American Society for Mass Spectrometry* **2009**, 20 (5), 837-44.

To be submitted for publication by the Royal Society of Chemistry as a chapter in the book entitled Ambient Ionization Mass Spectrometry

Chapter 12: Desorption Electrospray Mass Spectrometry

Joshua S. Wiley[1], Zoltan Takats[2], Zheng Ouyang[3,4] and R. Graham Cooks[1,4]

[1] Purdue University, Dept. of Chemistry, West Lafayette, IN 47907 USA
[2] University of London Imperial College of Science and Technology and Medicine, Faculty of Medicine, Department of Surgery & Cancer, London SW7 2AZ, England
[3] Purdue University, Weldon School of Biomedical Engineering, West Lafayette, IN 47907 USA
[4] Purdue University, Center of Analytical Instrumentattion Development, West Lafayette, IN 47907 USA

ABSTRACT

This chapter encompasses applications, fundamentals, instrumentation and future perspectives of desorption electrospray ionization (DESI) mass spectrometry (MS). Since it was first reported in 2004, DESI has paved the way for the development of ambient ionization MS with a wide variety of applications ranging from the analysis of pharmaceutical and illicit drugs to biological lipids and fatty acids. DESI-MS imaging has proven to be one of the most important applications of DESI, yielding comparable data to non-ambient MS imaging techniques for tumor classification, virtual fingerprint chemical mapping and many other imaging applications. The development of DESI-MS for such a wide variety of applications has been aided by fundamental studies, which have established a mechanism in which primary DESI droplets first cause analyte dissolution followed by splashing from the surface to produce secondary, sample-containing droplets. A major area that has evolved directly from increased mechanistic understanding is the development of reactive DESI-MS, where reagents are added so as to react with analyte in the secondary droplets to yield better specificity and/or ionization efficiency. In addition to enhancing analytical performance, reactivity in these small secondary droplets often occurs at rates many orders of magnitude faster than bulk-phase reactions. Another developing area of DESI-MS application is its use as an intrasurgical tool to obtain tissue diagnosis including tumor margin assessment. The implementation of DESI-MS for novel applications like these as well as its use in conjunction with a portable mass spectrometer is covered.

12.1 Background and Concepts

The ability to manipulate ions with electric and magnetic fields is fundamental to mass spectrometry. Molecular ionization processes can conveniently be grouped into four main types, electron ionization (EI), chemical ionization (CI), desorption ionization (DI) and spray ionization (SI). Traditionally, the key MS process of ionization has been implemented internally, under vacuum. Of the four main types of ionization methods, only SI in the form of electrospray ionization (ESI) is typically done at atmospheric pressure. Electrospray ionization (ESI)[1] is a solution-based ionization method which is almost always used with prior liquid chromatography separation. Most sample types are successfully ionized – and indeed give excellent analytical figures of merit - using one or other of the traditional ionization methods usually with the aid of prior chromatographic separation. The special case of rapid, direct ionization of complex mixtures is not handled well with the traditional methods although there are exceptions for selected chemical types of analytes, as in the case of alkaloids in plant materials[2] where soft ionization can be used to generate a set of intact ionized molecules followed by the use of tandem mass spectrometry to obtain structurally characteristic spectra.

Molecular ionization at atmospheric pressure was initiated with the study of vapors using a differentially pumped interface to the mass spectrometer[3] a method that proved to be very sensitive but one that was poor-suited to mixtures. This volume deals for the problem of how to analyze complex mixtures directly by mass spectrometry. This task requires that condensed phase samples be ionized and to do this quickly the experiment must necessarily be done in air. ESI itself is not suited to such tasks as it requires taking up the sample in solution and its performance is degraded by salts and

competition effects in complex mixture samples. Desorption electrospray ionization (DESI),[4] the subject of this chapter, is a method that extends ESI in such a way as to allow direct analysis of samples in the solid state. Complex samples can be interrogated directly because DESI has a built-in sampling step based on solvent extraction. The successes of this technique encouraged a variety of other methods of generating ions from native samples in their ordinary environment, that is, ambient ionization mass spectrometry.[5] In all of these methods, the complex sample is interrogated to provide analyte ions which are transferred into the vacuum system. This selective transfer into vacuum of a portion of sample material is a further distinction between ambient ionization and electrospray ionization. So, even though DESI is derived from and related to electrospray ionization, it is also distinct from it and with the other ambient ionization methods forms a class of methods that address the problem of rapid, direct mixture analysis.

The ambient ionization experiments can be divided into categories in several ways: one method of categorization is based the nature of the principal agency used: solvent sprays, electrical discharges and lasers. DESI uses a single agency, charged droplets, to perform the desorption (extraction) step and also the ionization process. In other cases two separate agents are used as in electrospray laser desorption ionization (ELDI),[6] where the desorption step is performed by a UV-laser and ionization of the resulting vapor phase neutrals by charged droplets. DESI, as depicted in the schematic in Figure 12.1, belongs to the spray-based, single agency category.

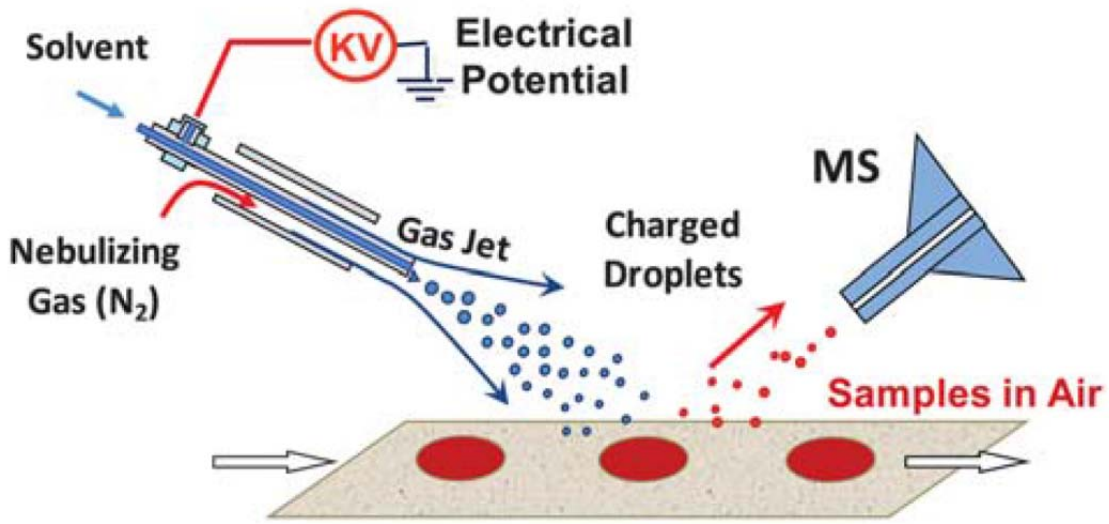

Figure 12.1 Schematic of the DESI-MS experiment

One further comment on ambient ionization is made to note that the term ambient ionization refers to a particular class of methods used to create ions from samples in the ambient environment, as just noted. It could also be defined by the objective of the experiment which is the rapid analysis of ordinary objects in their native environment. There are methods of ionization which allow ambient analysis but which might also be termed ambient ionization methods. For example, probe based methods in which a small sample is removed from an object and ionized by spray ionization might fall into this class. Such methods include the probes used by Hiraoka.[7] To take this point further, ionization of ordinary objects in their native environment can be performed in two ways: by direct methods or by sampling methods. The direct methods are by definition ambient ionization methods. Direct methods allow imaging and avoid the extra physical manipulations of the sampling methods. However, probe sampling may allow access to positions difficult to locate directly, relative to MS, although sampling using heated or

unheated gas 'probes' can achieve sampling by passing over any object from which sample vapor may be transferred directly into the MS. The use of physical probes followed by ESI represents an important class of ambient analysis methods.

12.2 Implementation

A DESI source utilizes a solvent flow at 0.5 – 5 μl/min., a nebulizing gas at linear velocities in the 100 – 250 m/s range and a DC potential in the range of 2 – 5 kV. The initial charged droplets impact the sample surface and form, by a simple splash, secondary droplets which contain dissolved analyte and are also electrically changed. The electric charge leads to coulomb explosion to create smaller droplets and assists in the formation of dry ions, either by the ion evaporation or by the charge residue model, both of which are familiar as processes that occur in the standard ESI experiment. Note that the DESI experiment can be done without applying a voltage and in special cases the nature of the sample might demand this. This version of the experiment is termed easy ambient sonic-spray ionization (EASI);[8] however, applying voltage increases the droplets' charge accumulation and allows for more efficient ionization.

An aspect of DESI that is relatively critical is the angle of the spray emitter with respect to the surface and MS inlet capillary. The angle between DESI source and sample surface is typically in the range of 40-70°, but a geometry-independent DESI has been developed in which the spray moves perpendicularly onto the sample plane and the sampling inlet is antiparallel to this.[9] This is readily implemented using coaxial capillary to primary and secondary droplets. In addition to direct impact onto the surface by the charged droplet stream, a transmission mode DESI may be employed, where the DESI emitter is positioned directly in front of and antiparallel to the MS inlet capillary and the

sample placed on a mesh in between the DESI source and the inlet capillary.[10] Further important parameters include the spray tip-to-surface and spray tip-to-MS inlet distances.

12.3 Mechanism

The DESI experiment can be broken down into two main steps: surface wetting followed by splashing of secondary microdroplets and their transfer to the mass spectrometer (the DESI phenomenon has been observed to take place also on hot surfaces, presumably following an alternative mechanism, see below). The first step requires that the solvent dissolve the analyte from the sample surface. Hence, changing the solvent will greatly affect the overall ionization efficiency, based on the solubility and dissolution kinetics of an analyte in the spray solvent. Once the analyte is in solution on the wetted surface, new droplets impact the surface and cause a splash event in which secondary analyte-containing microdroplets are ejected. Given that the surface is either electrically insulated or kept at a non-zero potential relative to the MS inlet, the departing droplets still carry electric charge, which makes them amenable to the generation of free gas-phase ions by electrospray-like ionization mechanisms.

The combination of simulations and phase Doppler particle analysis has helped to confirm the main proposed mechanism. As seen in the histogram of droplet sizes in Figure 12.2a,[11] the average size of the droplets in a typical experiment is 3 μm and the histogram in Figure 12.2b[11] reveals an average velocity of 150 m/s. In addition, the DESI-MS analysis of thermometer ions has suggested a median internal energy distribution centered at ~2 eV (cf. Figure 12.2c),[12] which is low and similar to ESI and corresponds well with the soft ionization that is observed with both techniques. In a less common alternative to the described mechanism, ion formation may occur following

neutral molecule desorption into the gas phase, which helps account for DESI observed on hot and electrically conductive (and grounded) surfaces.

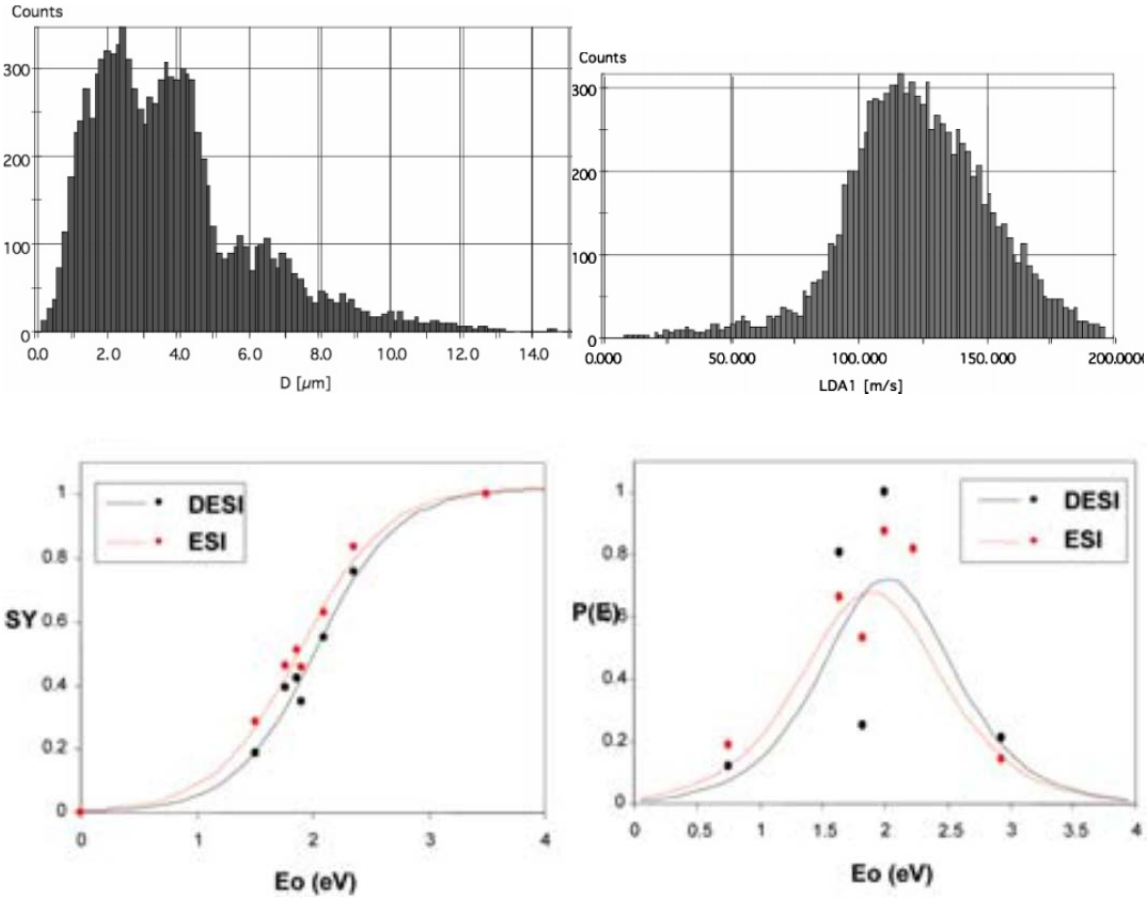

Figure 12.2 A) Histogram of A) diameters of droplets at 5 mm from the sprayer tip with a 2 μL/min solvent flow rate and B) velocities of droplets at 2 mm from the sprayer tip with a 5 μL/min solvent flow rate. Both histograms were obtained using phase Doppler particle analysis with 50% methanol/water solution and a gas pressure of 1130 kPa. C) Calculated breakdown (left) and internal energy (right) curves for DESI and ESI sources using the survival yield method.

12.4 Analytical Performance with Small and Large Molecules in Food, Energy and Forensics

12.4.1 Wide Applicability

As a spray-based technique, DESI is able to desorb/ionize samples ranging from small molecules to salts[13] to proteins.[14,15] Furthermore, DESI is able to analyze raw biofluids deposited onto solid carrier surfaces including blood and urine with little matrix effects. A major advantage of DESI and other spray-based ambient ionization methods is the ability to derivatize an analyte in the course of ionization to increase sensitivity or specificity, as discussed in greater detail in the next section. These reactions occur in small droplets and increase sensitivity and/or specificity, as discussed in greater detail in the next section. Reactive DESI has allowed the analysis of many analytes that are difficult to ionize, including steroids,[16] triacylglycerol species[17,18] and saturated hydrocarbons.[19] Only requiring solvents, voltage and gas flow, DESI is capable of being coupled with a miniature mass spectrometer and used for in-field analyses. A fieldable derivative of DESI called Venturi (very easy ambient sonic-spray) has also been developed; it uses no voltage, no syringe pump and an air canister to supply gas flow.[20]

Spray-based ambient ionization methods are arguably the most versatile of the three categories, combining field-portability with wide applicability. Techniques based on laser desorption/ionization tend to have an excellent mass range, but are less suitable for in-field analyses. Techniques based on laser desorption/ionization tend to have an excellent performance for heavier compounds, but are not well-suited to in-field analysis. Plasma-based techniques rely heavily on thermal desorption as the primary desorption mechanism, and, consequently, are often limited to lower molecular weight (typically less

than m/z 500) and more volatile analytes. However, plasma-based ambient ionization sources are well-suited for field applicability and various associated small-molecule applications. One area where both laser- and plasma-based ambient ionization excel over spray-based methods is for the analysis of non-polar analytes, which is difficult with DESI-MS but can be achieved as is discussed later in the section on reactive DESI.

12.4.2 Positive/Negative Ions

As is the case with ESI-MS, the ability to produce both negative and positive ions is easily achieved with DESI by applying a potential the same polarity as that of the intended ion. In the negative ion mode, the $[M-H]^-$ is predominantly detected but electron transfer and adduct formation can also be observed yielding for example, $M^{-\bullet}$ and $[M+Cl]^-$ ions. Analogously, proton transfer is most common in the positive ion mode, $[M+H]^+$ ions usually predominating, however, sodium and potassium adducts are also common and $M^{+\bullet}$ formation occurs for particular analytes.

12.4.3 Trace/Bulk Analysis

A common problem with ESI and especially nanospray ionization deals with the spray emitter clogging when a large amount of floating material is present in unprepared native samples. In a DESI-MS experiment, the sample is directly desorbed from a surface and therefore clogging of the spray emitter is not a factor. This allows the analysis of bulk samples and raw matrices, especially samples consisting of high salt content, that are not easily analyzed with ESI or nanospray MS. While the sensitivity of

DESI is generally inferior to ESI methods by a small factor, the method features sufficiently low LOD values (typically sub-nanogram absolute) for most practical applications.

12.4.4 Necessity of Tandem MS

Any mass spectrum of ions produced under ambient conditions will be polluted with numerous peaks from contaminants in solvents, air or from surfaces. The number of peaks increases when performing an ambient MS experiment in which the unprocessed sample can be a complex mixture of molecules. In Figure 12.3A, is the full-scan DESI-MS spectrum in negative ion mode of diluted and dried human plasma, containing a mixture of micronutrients (including folic acid at 50 ppb). While there is a small peak for the $[M-H]^-$ of folic acid at *m/z* 440, it is hard to discern from chemical noise. Unless the relative abundance of the analyte of interest within the sample is unusually high, it is often necessary to use MS/MS to increase specificity and the signal-to-noise ratio to confirm the presence of an analyte peak. The MS/MS spectrum shown in Figure 12.3B was taken on the same human plasma sample as in Figure 12.3A; however, the peak at *m/z* 440 was isolated and fragmented to unique fragments at *m/z* 311, 422 and 396, which correspond to losses of $C_5H_5O_4$, H_2O and CO_2 respectively. Tandem MS not only helps confirm that the analyte of interest is present but also significantly increases the signal-to-noise ratio.

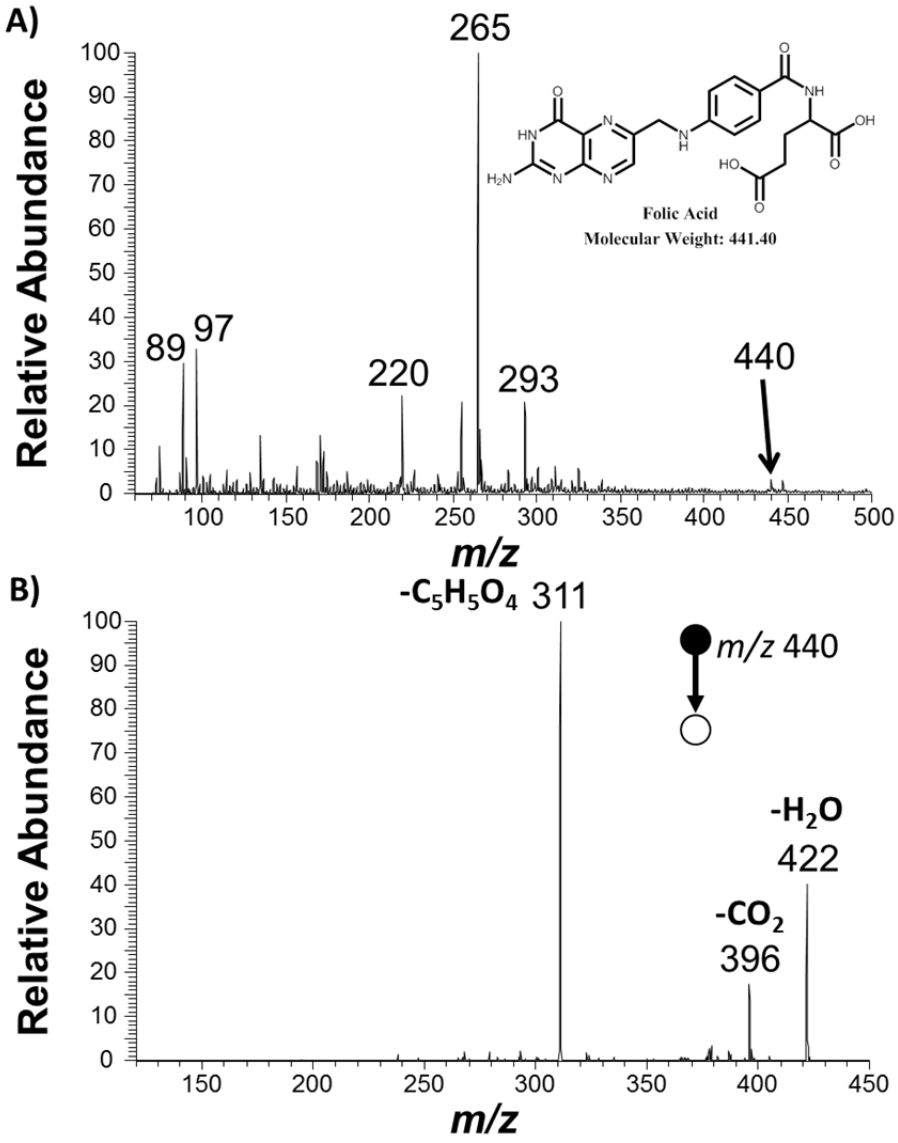

Figure 12.3 A) Full DESI mass spectrum of some drug in blood (should not see large peak for drug). C) DESI-MS/MS spectrum for drug in blood.

12.4.5 Solvents, Surfaces and Mass Range

As a spray-based ionization technique, DESI is capable of desorbing/ionizing analytes with a wide range of masses. Desorption of an analyte is dependent on solubility, so it is common to adapt the solvent mixture to capably dissolve the analyte.

Besides analyte solubility, the solvent system has to be electrically conductive and volatile (i.e. it should evaporate without leaving a solid residue) under given experimental conditions. Mixtures of methanol and water are most commonly used; however, combinations of acetonitrile, ethanol and dimethylformamide are also used as well as the addition of a weak acid (i.e. formic or trifluoroacetic acid) to facilitate proton transfer. Selecting the appropriate solvent mixture is not always sufficient to ensure desorption of an analyte, due to unfavorable surface tension or dissolution kinetics. While the successful DESI-MS analysis of proteins has been reported from liquid samples,[14,15] attempting DESI-MS from biological tissue yields no protein signal when using typical DESI spray solvents. The non-covalent interaction of an analyte with the substrate on which it resides can decrease the probability of desorption, even when working with surfaces more inert than biological tissue. For example, many analytes yield higher signal from a Teflon® surface as compared with a glass surface.[16]

12.5 Applications

As the first ambient ionization method developed, DESI has been used for a wide variety of applications. In this section, each of the major categories of DESI-MS applications will be discussed; however, given the extensive use of DESI-MS over the past near-decade, it will not be possible to cover each and every application.

12.5.1 Analysis of Formulated Pharmaceuticals

One application of DESI-MS is for the direct, rapid analysis of pharmaceutical drug tablets. The ability to sample from a tablet directly, without requiring destruction of the tablet, makes DESI-MS a practical technique for quality control on pharmaceutical products. Figure 12.4 (from Chen *et al*.) shows the DESI-MS spectrum of an Excedrin tablet (Figure 12.4a), where all three active ingredients (aspirin, acetaminophen and caffeine) were detected, and a Centrum vitamin tablet (Figure 12.4b) in which thirteen vitamins were successfully detected (only seven are labeled in the full MS spectrum).[21] In addition to the $[M+H]^+$ peaks for acetaminophen and caffeine, the two most abundant ions in the spectrum are the sodium adducts of acetaminophen and aspirin at *m/z* 174 and 203 respectively. Chen *et al*. also reported the ability to measure 2.67 Claritin tablets per second by having the tablets on a moving belt setup, demonstrating the potential of DESI-MS for high throughput quality control of pharmaceutical tablets.[21] While pharmaceutical tablets have been heavily targeted with DESI-MS, tablets of illicit drugs have also been examined as a potential forensics application.[22,23]

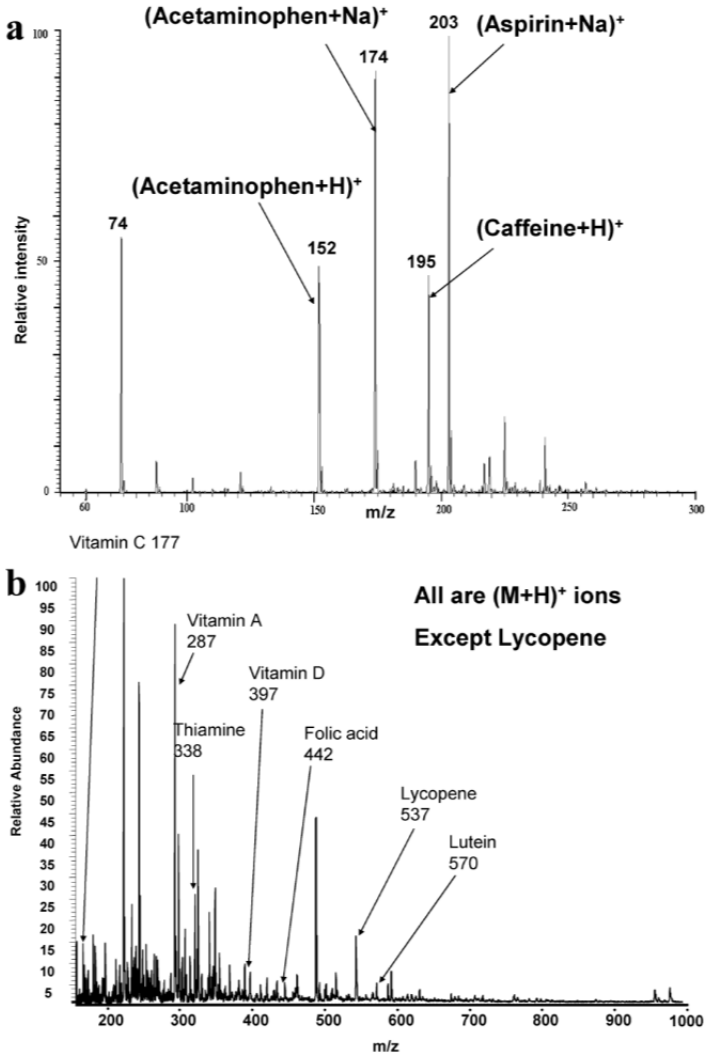

Figure 12.4 DESI-MS of an A) Excedrin and B) Centrum vitamin tablet with methanol:water (1:1) in positive ion mode.[21]

12.5.2 Analysis of Biofluids

While the analysis of tablets is an example of detecting a mixture of analytes at higher abundances near the % level, the analysis of biofluids containing these drugs or other metabolites within often requires greater sensitivity. Much effort has been directed towards the analysis of biomatrices with DESI-MS for a wide variety of applications.

Since biological fluids represent mostly liquid phase samples, their DESI-MS analysis generally requires a simple preparation step, which results in a solid phase sample. Sample preparation may comprise deposition of fluids onto solid surface followed by drying or the absorption of biofluid by porous medium (e.g. filter paper). The latter can also be used to selectively bind interfering matrix components, for instance inorganic salts by the porous medium. The DESI-MS analysis of urine has been applied to lung cancer biomarker screening in mice,[24] diagnosis of patients with inborn errors in metabolism,[25] screening for anabolic steroids (discussed further in the reactive DESI section)[16] and drugs of abuse.[26] Thanks to the non-destructive nature of DESI, skin has also been analyzed by DESI-MS for the analysis of explosives,[27] gunshot residues,[28] personal care products[29] as well as other areas of forensics and clinical chemistry.[30] The analysis of human plasma with DESI-MS has also been demonstrated for various purposes.[31-33] However, separating blood plasma from whole blood is not always a necessary step for DESI-MS analyses. The analysis of dried blood spots (DBSs) plays an important role in the medical community for applications ranging from neonatal screening to pharmaco-/toxicokinetic studies to therapeutic drug monitoring. DESI-MS has successfully been applied to the direct analysis of DBSs for model compounds (sitamaquine, terfenadine, and prazosin), achieving linearity from 10 – 10,000 ng mL^{-1}.[34] However, an ambient ionization method which is perhaps more suitable and has been heavily tested for DBS analysis is paper spray ionization.[35]

12.5.3 Food Safety

A nice review for the DESI-MS analysis of chemical food contaminants has been prepared by Nielen *et al*.[36] Applications of DESI-MS to food safety include: the analysis of strobilurin fungicides in wheat,[37] agrochemicals on fruits and vegetables,[38] arsenic speciation on animal feeds and plant foods,[39] Sudan dyes in food,[40] dithiocarbamate fungicides in fruit,[41] lipid profiling of bacteria,[42] triglycerides in foods[18] and melamine in milk.[43] The number of applications extend beyond these listed and should only continue to grow as demanded. As mentioned by Nielen et al., the ability for DESI-MS to be performed on site to provide qualitative or semi-quantitative information makes it an intriguing approach for sample pre-screening in the field, limiting the number of samples that get sent back to the lab.

12.5.4 Forensic and Public Safety

As with food safety, DESI-MS has also been heavily applied to forensics, and a recent review detailing the areas of forensics that have been targeted has been written by Morelato *et al*.[44] Again, the ability for *in situ* analyses has warranted the wide application of DESI-MS to forensic studies, which demands rapid, direct and efficient methodologies for in-field analyses. Some of the forensic applications that have been targeted by DESI-MS include: the analysis of illicit drugs, gunshot residues, explosives, inks and counterfeited documents, fingerprints, and chemical warfare agents. Explosives have also been analyzed by DESI on a miniature MS.[45] Currently, many in-field forensic investigations are performed with ion mobility or Raman spectrometers, which lack the

overall combination of sensitivity, specificity and broad applicability of MS. As miniature MS instruments continue to develop and become smaller,[46] they should eventually replace these techniques, with ambient ionization as the means of directly sampling from crime scene materials, luggage at airport security, etc.

12.5.5 Microorganisms (bacteria, algae, embryos)

In close relation to public and food safety, microorganisms have been another targeted area for DESI-MS analysis. As mentioned previously, various types of bacteria have been analyzed and distinguished based on their distinct lipid profiles.[42] Also relying on lipid signatures, a recent effort has been made to chemically study oocytes, blastocysts and embryos.[17,47,48] In a study where pre-implanted embryos were obtained at various stages and directly analyzed with DESI-MS, two- and four-cell embryos were seemingly more synthetically active than unfertilized oocytes with a wider range of phospholipids detected as well as higher fatty acid signals.[49] While phospholipids and fatty acids have been an excellent target analyte for the characterization of various microorganisms due to their ability to readily form anions, sometimes it is necessary to choose a target analyte which might not form an ion of either polarity very well. In a study where DESI-MS was performed directly on marine algal tissue, various anions (e.g. Cl- and Br-) were added to the spray solvent to increase the sensitivity for the detection of bromophycolide (an antimicrobial chemical defense agent) in a reactive DESI experiment.[50]

12.6 Reactive DESI

12.6.1 Concept/Overview

Reactive ionization is an emerging area of ambient mass spectrometry and is based on adding reagents which can derivatize an analyte in order to enhance desorption or ionization abilities. This is typically done by converting an analyte to a charged product or one that can be efficiently ionized. In a DESI-MS experiment, this is typically done by putting the derivatizing reagent in the spray solvent while the analyte is on a surface. After impact with primary reagent-containing droplets, secondary droplets are emitted from the surface, which contain a distribution of both compounds, allowing reactions to occur. Despite the small reaction times between dissolution of the analyte and drying of the droplets in the inlet capillary, a wide variety of reactions have been demonstrated with DESI-MS. In fact, results have indicated that reactions often occur at accelerated rates in the confined droplets. One likely reason is the large change in pH that occurs as a result of the voltage applied and the decreasing droplet size which promote acid/base-catalyzed chemistry. Two reactions that have been demonstrated are shown in Schemes 12.1 and 12.2 below. The first utilized phenylboronic acid to recognize cis-diol functionalities at a surface due to the selective ability to form the cyclic boronate (cf. Scheme 12.1).[51] In Scheme 12.2 is the reaction of boric acid with phosphonate esters, commonly used as chemical warfare agents, to form the hydrolysis product.[52] The various types of reactions that have been demonstrated with DESI-MS are discussed in this section.

Scheme 12.1

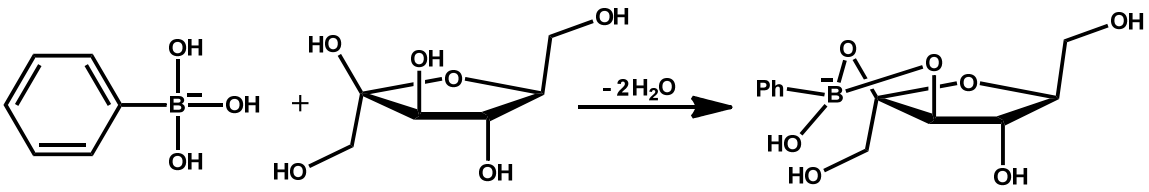

Scheme 12.2

12.6.2 Steroids

Two closely related reactions have been demonstrated for the DESI-MS analysis of ketosteroids, which represent an intriguing target for analytical methods due to the use of illegal anabolic steroids and testosterone in sports. The first DESI-MS reaction with ketosteroids involved the addition of hydroxylamine in the spray solvent, which becomes protonated during the electrospray process and can attack the carbonyl of the steroid.[16] As observed in Scheme 12.3, the oxime is the final product; however, the intermediate shown in the scheme just after hydroxylamine addition has been detected at a higher abundance than the oxime. Figure 12.5a shows the reactive DESI mass spectrum of 20 ng of epitestosterone where hydroxylamine was doped into the spray solvent. Note that while the oxime (m/z 304) was detected with higher abundance than the intermediate (m/z 322), this was not observed for all ketosteroids and DESI conditions.[16]

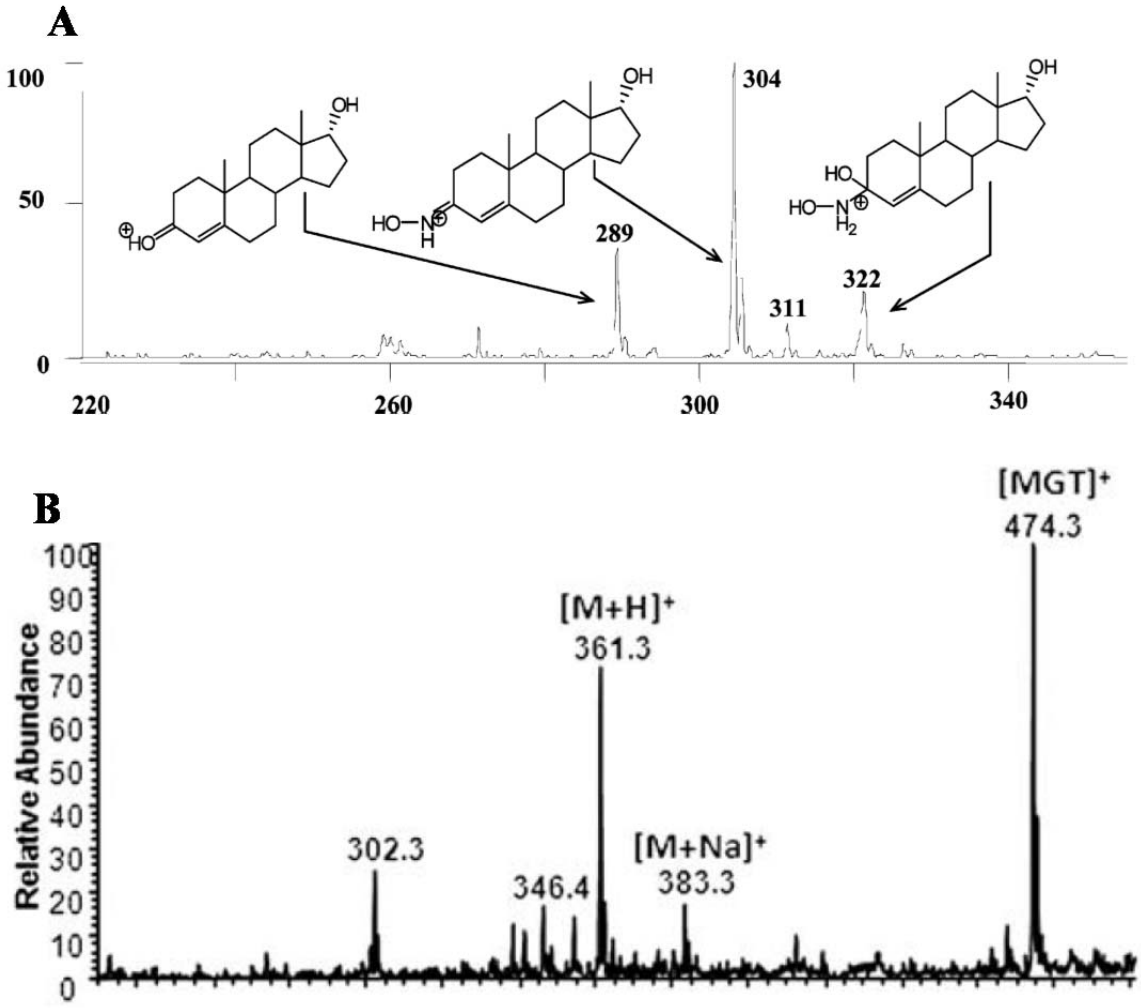

Figure 12.5 Reactive DESI-MS of A) 20 ng of epitestosterone with hydroxylamine[16] and B) 200 ng of cortisone with Girard's Reagent T.[53]

Scheme 12.3

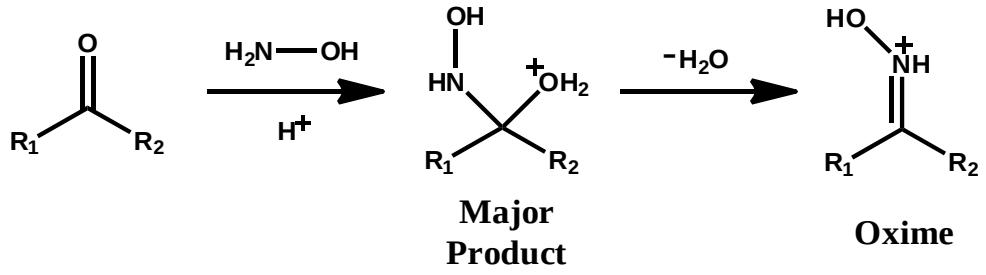

Another reaction that has been demonstrated with ketosteroids is shown in Scheme 12.4, and is similar to the hydroxylamine reaction except that a hydrazine, Girard's reagent T (GT), was used to attack the carbonyl.[53] The advantage of using GT is that it has a permanent charge, which remains with the product after formation, ultimately increasing sensitivity as a result of not having to ionize the product. Figure 12.5b shows a reactive DESI mass spectrum of 200 ng of cortisone where GT was doped into the spray solvent. The major product was the hydrazone as shown in Scheme 12.4, labeled as $[MGT]^+$ in the mass spectrum at *m/z* 474.3.

Scheme 12.4

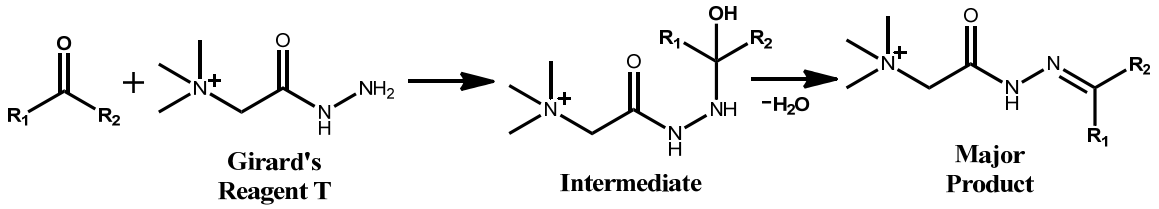

12.6.3 Oxidation Reactions

While a reaction involving covalent bond formation between a reagent in the spray solvent and a surface-bound analyte is typical for reactive DESI, there are other routes of reactive ionization with DESI-MS. One such alternative is based on electrochemistry and can be done with or without the addition of reagents into the spray solvent. For this to occur, special DESI spray conditions (namely higher voltages) are required. In this experiment, which has been used to oxidize carboxylic acids[54] as well as saturated hydrocarbons,[19] a discharge is formed as a result of the higher-than-normal

electric field and results in the formation of oxygen radicals which are very strong oxidizing agents. In a case where reagents, such as iodine and potassium bichromate, were added to the spray solvent, signal enhancement over two orders of magnitude was achieved for the oxidation of dibutyl dithiocarbamate to form $M^{+\bullet}$.[55] Interestingly, this enhancement was only observed during the short timescale of mixing during DESI-MS; whereas, allowing the reagents to be mixed together longer during an electrosonicspray ionization (ESSI) MS experiment allowed other reactions to occur and much less enhancement of $M^{+\bullet}$ signal was observed.

12.6.4 Metal Attachment

As with electrochemistry, another reactive DESI approach that does not require covalent bond formation is through metal adduction, which is a non-covalent association between a metal ion and a neutral analyte molecule. For some analytes, the ability to bind to a charged metal ion is highly favorable and results in increased specificity/sensitivity. This has recently been achieved by the addition of silver to the spray solvent, which is able to readily form stable adducts with olefins.[56] In this study, $AgNO_3$ was doped into the spray solvent and used for the analysis of various unsaturated lipids and fatty acids, providing greater specificity and up to 50 times signal enhancement. Further application of Ag^+ cationization has been demonstrated for the analysis of bovine oocytes, in which adduction with Ag^+ allowed detection of triacylglycerol.[17] Silver cations are also intriguing for other applications, such as chelation with aromatic compounds through pi-stacking;[57] although this has not been demonstrated with DESI-MS. While other metals may also result in adduct formation

with analytes, there have been no such reports for DESI-MS besides Na^+ and K^+ adducts which often occur without doping their salts into the spray solvent. However, other adducting reagents have been doped into the DESI spray for various applications including chloride and trifluoroacetate for explosives[27,58] and bromophycolides[50] as well as ammonium for triglycerides.[18]

12.6.5 Cholesterol/Betaine Aldehyde

As a marker for monitoring heart disease such as triglycerides, cholesterol is another analyte that is difficult to ionize but has also been detected with reactive DESI-MS. The reaction involved the use of betaine aldehyde, which is susceptible to nucleophilic attack by the alcohol functional group in cholesterol (ca. Scheme 12.5 for general reaction scheme).[59] The hemiacetal was detected at *m/z* 488.6 for the reactive DESI-MS analysis of cholesterol. The ability to detect cholesterol by reactive DESI was further demonstrated directly from rat brain tissue while keeping track of the spatial distribution of cholesterol along with phospholipids, an experiment known as mass spectral imaging.

Scheme 12.5

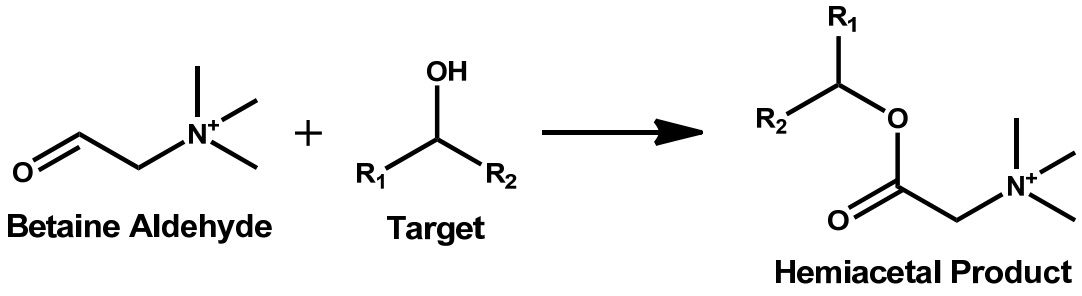

12.7 DESI-MS Imaging

12.7.1 Introduction

Perhaps one of the most intriguing applications of DESI-MS is for the 2-D mapping of chemical entities from a surface in an experiment known as MS imaging. Historically, secondary ion mass spectrometry (SIMS) and matrix-assisted laser desorption ionization (MALDI) have been used extensively for MS imaging and are capable of resolving chemical features on a surface at less than ~100 nm with SIMS[60] and at just a few microns with MALDI-MS. While both of these techniques offer better spatial resolution than DESI-MS, which can be as low as 30 μm, the advantage of imaging with DESI-MS stems from the ability to analyze a surface with no pretreatment at atmospheric pressure. Hence, there are no interferences from matrix ions as observed with MALDI-MS and the possibility of sample contamination is greatly reduced. Another advantage of imaging with DESI-MS is due to its nondestructive nature. With no morphological damage to the sample during DESI interrogation, it can then be used for other studies without concern of any information loss.[61] Applications of DESI-MS imaging have ranged from plant, animal and human tissues to human fingerprints for forensics; each of which will be discussed further.

12.7.2 Tissue

Analysis of lipids in human/animal tissue is perhaps the most explored and fascinating application of DESI-MS imaging. The unique distribution of lipids in different types and/or disease states of tissue allows appropriate classification when

relative abundances of the ionized lipids are compared in the mass spectra. Fortunately, many lipids have high ionization efficiencies and are easily detected with DESI-MS. As a result, many types of tissue have been analyzed from a wide variety of animals with DESI-MS, including brain,[62-64] bladder,[65,66] spinal cord,[67] prostate,[68] kidney,[69] eye lens[70] and adrenal glands.[71] As an example of distinguishing different types of tissue, Figures 12.6a and 12.6b reveal DESI mass spectra of gray and white matter (respectively) from a mouse brain. It is clear that the lipid profiles are very different between the gray and white matter, with *m/z* 834.4 (a phosphatidylserine, PS 18:0/22:6) as the base peak in the gray matter and *m/z* 888.8 (a sulfatide, ST 24:1) the base peak in white matter. Two-dimensional images of the relative abundances of these peaks are plotted in Figures 12.6c and 6d. When the two ion images are overlaid, there is a clear distinction between the gray and white matter regions (Figure 12.6e). If the mouse brain is sliced throughout its entirety, 2D images can be acquired and stacked for each tissue section, resulting in a three-dimensional image as in Figure 12.7.

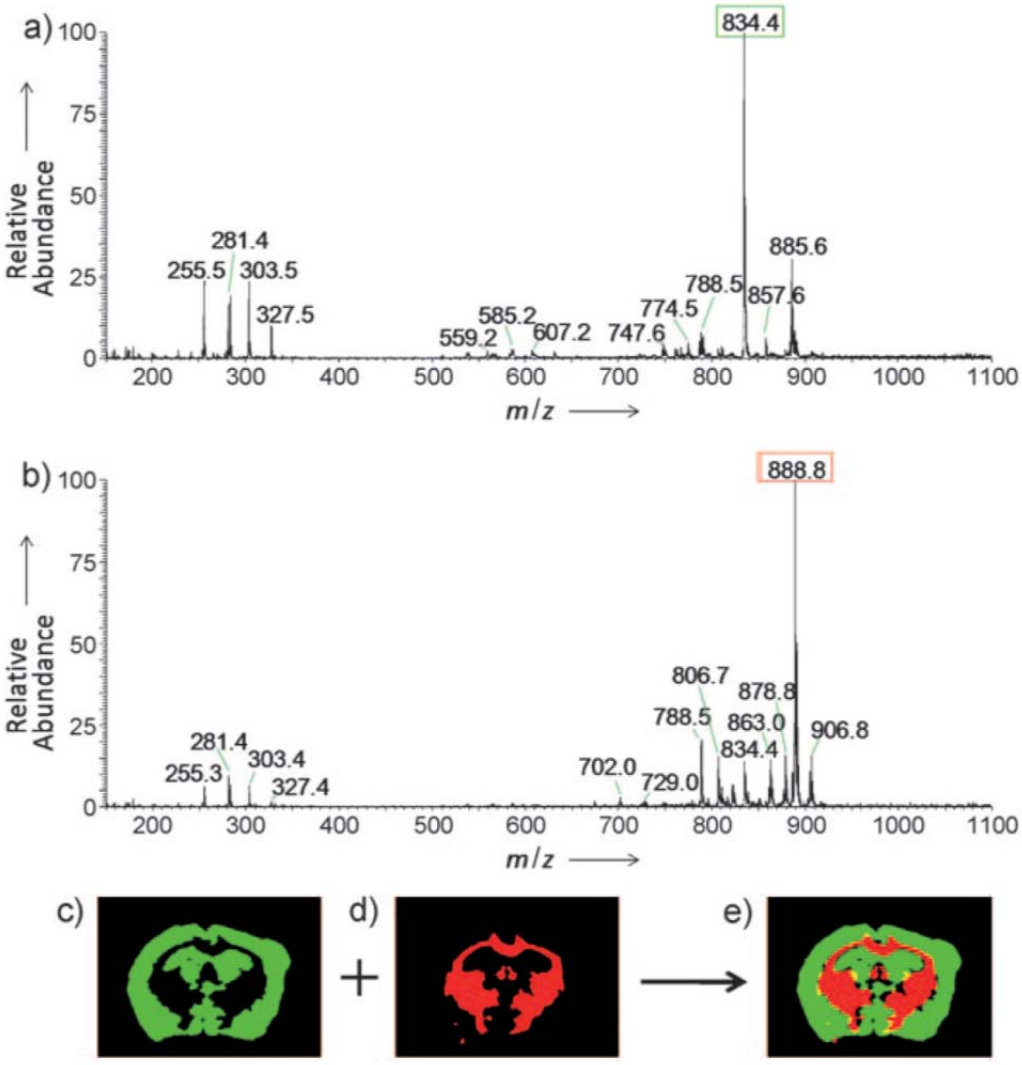

Figure 12.6 Negative ion mode mass spectrum of A) gray and B) white matter of a mouse brain. The 2D plot (or ion image) of C) *m/z* 834.4 and D) m/z 888.8 as well as E) the overlaid ion images of *m/z* 834.4 and 888.8.

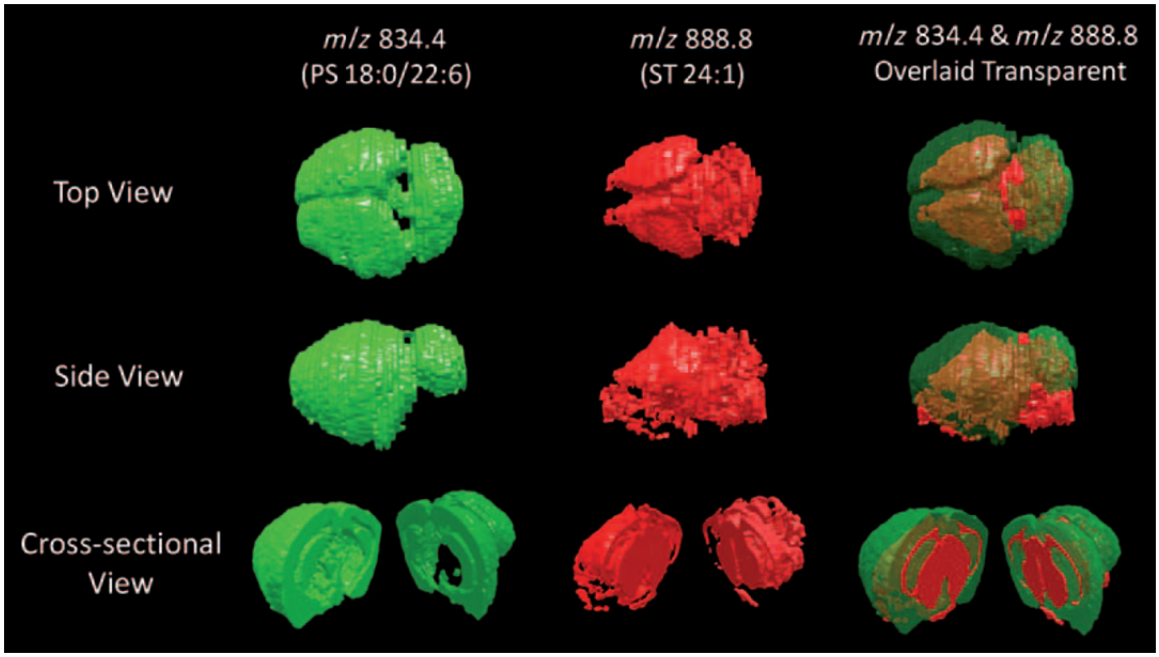

Figure 12.7 3D models of the mouse brain by DESI-MS. Top, side, and cross-sectional views are shown for the 3D construction of the distribution of a) PS 18:0/22:6 in green b) ST 24:1 in red, and c) the transparent overlaid distributions of PS 18:0/22:6 and ST 24:1.

Not all DESI-MS imaging applications are this clear-cut in terms of being able to distinguish between different types of tissue. A prime example, and major application of DESI-MS imaging, is in the identification and classification of the disease state of tissue, especially cancerous versus noncancerous tissue. This has been pushed even further in some studies which have been able to determine the stage of diseased tissue, such as distinguishing astrocytoma grades,[62] using DESI-MS imaging. Classification of the disease state of tissue is often achieved by monitoring relative distributions of lipids and/or fatty acids and analyzing with a statistical classification method such as principle component analysis (PCA). Mass spectral data is then correlated with H&E stains read by a pathologist. For many samples the distribution of fatty acids and lipids is enough to allow the classification of cancerous versus noncancerous tissue with the aid of PCA, as

observed in the DESI-MS imaging of dog and human bladders.[65,66] In the case of human prostate, classification of tissue by lipid and fatty acid profiles was difficult; however, cholesterol sulfate was found to be a cancer biomarker and allowed for accurate correlation of 64 of 68 tissue samples.[68]

12.7.3 Natural Products

Imaging of natural products is an intriguing application of DESI-MS due to the real possibility of imaging live organisms since no matrices are required and the ionization process is non-destructive and can be done with biologically-friendly solvents. The use of reactive DESI-MS to allow the detection of fungal inhibitors on tropical seaweed, as discussed previously, was also performed as an imaging experiment by Lane *et al*., revealing patches of the bromophycolides on the surface at sufficient concentrations for fungal inhibition.[72] One problem with directly imaging an organism without first cutting it into sections with smooth surfaces is due to large deviations in signal that can occur as a result of spraying to/from a rough surface. One method of overcoming this has been to make an imprint of the sample to be imaged and then acquire the DESI-MS image from the smooth imprinted surface. The use of imprints for DESI-MS imaging has been applied to characterization of bacterial culture products[73] as well as various tissues including barley leaves,[74] St John's wort and Jimson weed,[75] Lam seed and mouse brain,[76] and various plant leaves for measuring nonfluorescent chlorophyll catabolites.[77] Many of these experiments were also performed directly on the sample as well, but imprints were used due to yielding better performance.

12.7.4 DESI Imaging in Forensics

One of the first applications of DESI-MS imaging was for the analysis of inks, with a forensics focus on identifying counterfeited documents by distinguishing which dyes were used on which regions of the document.[78] Another application which has gained a large amount of public interest is the DESI-MS imaging of latent fingerprints.[79] For a typical crime scene investigation, the ability to merely match a fingerprint's pattern with that of a suspect is a powerful route of incrimination. However, the ability to combine chemical information with visualization of the pattern can be very useful. One such example is when multiple fingerprints overlap on a surface. The ability to correlate certain chemicals with each fingerprint can allow the distinction and visualization of each fingerprint, which otherwise would not have been possible. In addition, searching for various drugs or their metabolites within the fingerprint could provide insight into the mental state of the suspect.

12.7.5 Spatial Resolution

Spatial resolution is defined as the shortest distance at which two distinct features may be resolved in an MS image. Since the onset of the field of MS imaging, there has been a great amount of interest in increasing spatial resolution (i.e. decreasing the distance at which features can be resolved). While some analyses require very high spatial resolutions, as with MS imaging of single cells, the time required must be taken into consideration. For every decrease in the pixel size for an imaging experiment, the number of pixels and, consequently, time of acquisition increases quadratically for a

constant overall image area. Initial attempts to measure the spatial resolution of DESI-MS were done by Ifa *et al.* by scanning over ink lines, suggesting a spatial resolution less than 200 μm.[80] In general, a standard DESI-MS imaging experiment provides a spatial resolution of about 180 μm; however, there has been a push to go even lower with reports by Kertesz *et al.* suggesting ~40 μm resolution for printed patterns on paper,[81] while Campbell *et al*. reported ~35 μm resolution for DESI-MS imaging of mouse brain.[82] For each of these studies, various parameters including gas back pressure, capillary sizes, solvent selection and solvent flow rate were carefully tuned to achieve a spatial resolution below 50 μm. Further improvements in spatial resolution are possible, but will likely require added engineering in the design of the DESI source.

12.7.6 Data Analysis Strategies

Data analysis is generally aimed either at the determination of the concentration of certain species on the surface or the classification of the mass spectra obtained from spatially well-defined areas of the sample. A typical example for the former case is the quantification of drug molecules and drug metabolites in tissue sections, while pixel-by-pixel histological classification of mass spectrometric images represents a good instance for the latter case. Nevertheless, in both cases the DESI imaging data requires data pre-processing, comprising mass spectrometric calibration, normalization of the signal and optional co-registration of mass spectrometric data with any other – usually optical – image of the sample. Mass spectrometric recalibration is critical in case of high-resolution time-of-flight (TOF) analyzers, since these the mass accuracy drift of these instruments can be significant within the timeframe of an imaging experiment (up to a

few tens of hours). Normalization of signal is expected to compensate for the overall instrumental fluctuation of signal intensity. Various normalization strategies have been described including normalization to TIC, median intensity or certain, arbitrarily chosen peaks in the spectra, which are expected to show uniform concentration within the sample. Since DESI-MS imaging is non-destructive, the analysis is usually followed by morphological imaging, comprising histological staining and optical imaging (scanning). In order to establish correlation between the two types of data, co-registration is necessary with accuracy better than half of the MS pixel diameter. Co-registration algorithms allow translation, rotation and two dimensional stretching of images, in order to maximize the overlap.

Coarse quantification of certain detected species is easily achievable by visualizing the normalized intensity distribution of the corresponding molecular ion, however this approach provides only relative values and also does not take into account the different matrix effects taking place in different tissue types. More accurate quantification requires the determination of histology-dependent response factors by the parallel analysis of the corresponding tissue types by DESI-MS and LC-MS at different concentration levels.

DESI-MS imaging datasets can also be interpreted as a set of MS profiles associated with the biochemical/clinical status of the tissues. Since the individual spectra are treated as spectroscopic fingerprints, no identification or quantification of detected species is required. In these cases at first an authentic ‘training’ or ‘learning’ dataset is acquired, which serves as a basis to create a multivariate statistical model. This model is used for the identification of unknown spectra in the test datasets. As an example, DESI-

MS imaging data was collected from a colon adenocarcinoma set and spectra were analyzed using a combination of principal component analysis and linear discriminant analysis. Statistical models were created to separate DESI-MS fingerprints of different histological tissue types (mucosa, adenocarcinoma, smooth muscle) and also patients with different predictive tumor marker statuses and the models were validated for test sets. Although the multivariate approach has tremendous value regarding the identification of tissue types, the training sets are expected to represent population-level variance of the spectral fingerprints which may require the analysis of several hundreds of samples for a single pathology. Further problems are associated with the experimental variance of DESI-MS data, which may exceed the biological/histological variance, making proper identifications difficult. Further standardization of DESI imaging parameters and development of more robust hardware (especially regarding spray emitters) is expected to lift these constraints and allow the construction of global, histologically-specific DESI-MS spectral libraries available for all users worldwide.

12.8 Future Perspectives

12.8.1 Miniature Mass Spectrometers and in situ Analysis

Miniature mass spectrometers have been in development for quite some time, but until the recent develop of discontinuous atmospheric pressure interface (DAPI),[83] miniature MS had been based on reduced pressure ionization. The advent of DAPI, which affords the limited pumping ability of a miniature instrument by pulsing gas/ion

introduction to just 10-20 ms of a ~1 second duty cycle, has allowed the use of various ionization sources which operate at atmospheric pressure. Most importantly, the coupling of ambient ionization with miniature MS is possible, which is ideal for rapid, *in situ* analyses. As previously discussed, the ability to perform MS/MS is essential for these types of analyses, so a geometrically-simplified version of the linear ion trap has been employed which uses planar electrodes, the rectilinear ion trap (RIT).[84] The other advantage of using an ion trap mass analyzer is due its ability to operate at higher pressure in comparison to most other mass analyzers.

12.8.2 Synchronized and Inductive DESI

While DESI has been coupled to miniature MS in the laboratory setting,[45,83,85,86] sampling efficiency and the need for high gas flow rates have made actual *in situ* analyses rather impractical. A method of mitigating both of these issues is by ion source and MS sampling synchronization. Many mass analyzers are pulsed, only introducing ion packets over small time windows, while the majority of the time is used for ion transfer and mass analysis. To better optimize sampling, a synchronized DESI-MS experiment has been demonstrated in which voltage is applied inductively and both gas and solvent flows are pulsed in synchronization with ion introduction into the MS.[87] This has resulted in an overall reduction of N_2 flow from 2 L min^{-1} to 0.2 L min^{-1}, solvent flow from 5 μL min^{-1} to 0.5 μL min^{-1} as well as 100-fold increases in sensitivity and sampling efficiency. Figure 12.8a shows a schematic of this setup on a miniature MS instrument, with the overall pulse sequence of potentials used in the synchronized experiment in Figure 12.8b. Figures 12.8c and 12.8d show the synchronized DESI-MS of 10 ng

cocaine on a glass substrate and standard DESI-MS of 1 µg cocaine on a glass substrate, respectively. Despite analyzing 100 times less sample in with synchronized DESI-MS, the signal for cocaine at *m/z* 304 is still higher.

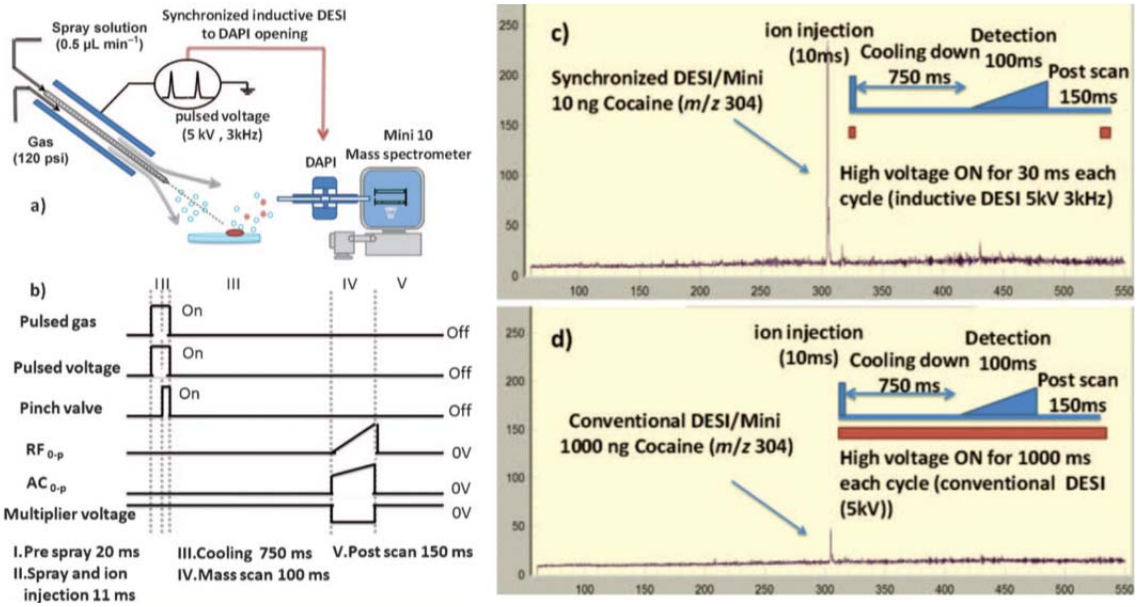

Figure 12.8 Synchronized DESI-MS A) schematic and B) pulse sequence. C) Synchronized DESI-MS cocaine (10 ng) and D) standard DESI-MS of cocaine (1 µg), both from a glass slide.

12.8.3 Endoscopic Diagnostics using DESI

DESI sampling/ionization using charged droplets allows direct analysis of endogenous compounds from biological tissues.[64,88] The characteristic lipid profiles assist in the diagnosis of pathology. To extend the method further, we are exploring the use of DESI and related methods for intra-surgical and endoscopic procedures, where in-vivo chemical analysis would provide molecular information potentially of value for decision-making. A MS system with a sampling probe that can be fitted into an

endoscope would enable this capability. Analytes on the tissue are ionized and transferred to the MS for analysis. However, to apply the DESI method in-vivo, the conditions of the ambient ionization need to be biocompatible. The high voltage (4-5 kV) and organic solvents typically applied for DESI cannot be used. The damage to the tissue surface also needs to be minimal and previously introduced histologically compatible solvents like N,N-dimethylformamide (DMF) / ethanol[61] cannot be used.

An MS sampling probe designed for endoscopic chemical analysis uses charged droplets for sampling but with a number of signification modifications to minimize physical damage to biological tissues. [89] As shown in Figure 12.9, the sampling probe consists of a capillary sprayer and a coaxial transmission tube. The fronts of the capillary sprayer and transmission tube are bundled together to form an endoscopic probe. The capillary sprayer is made of two silica capillaries, one inside another. The inner capillary is used to deliver solvent (4-8 μL/min) while the outer capillary is used for deliver auxiliary nitrogen gas (1.5 - 5.2 L/min). When the open end of the endoscopic probe is placed at the sampling spot, the spray plume generated from the capillary sprayer bounces back carrying chemicals extracted from the sampling tissue through the transmission tube. Transport of droplets through the transmission tube and into MS inlet allows spectra to be recorded. As a demonstration, a rat brain tissue section was analyzed with the sampling probe and the spectra recorded from white matter and grey matter agree with previous DESI results.

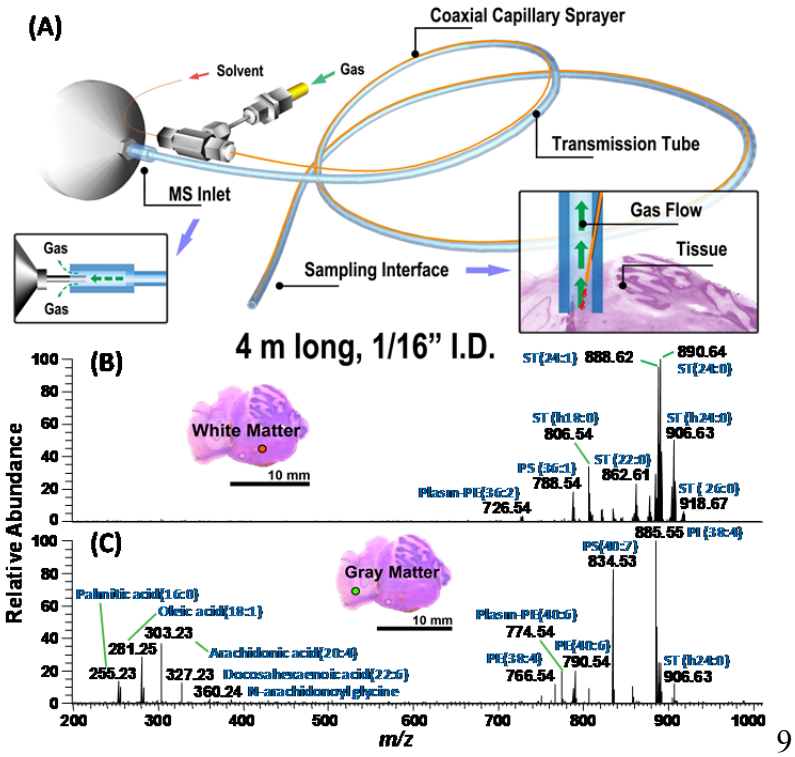

Figure 12.9 (a) Schematic setup of endoscopic sampling ionization probe. The probe is used to collect spectra from a rat brain tissue on the (b) white matter and (c) grey matter, respectively.

This long distance ion transport tubing allows ions to be transported over 4 m,[90] which is adequate for endoscopic applications. The use of pure water as the DESI solvent provides higher single intensity after the transportation, presumably due to the slower but more efficient desolvation of water droplets in the tubing. The high voltage used in DESI was also abandoned just as is done in sonic-spray ionization, since the high velocity gas flow provides enough signal intensity (Figure 12.9b). Typically, a tissue section would be damaged by the high velocity gas flow, but this can be simply solved by introducing a pulling force to drag the gas backward into the MS inlet with an additional diaphragm pump (Figure 12.9c). With all these features, the endoscopic sampling probe is suitable for in-situ and non-invasive biological analysis. The endoscopic sampling

probe can be coupled with a portable Mini 12 mass spectrometer, [91] which provides real time MS measurement at the point-of-care. This system could provide specific chemical information about biological tissues for biomedical studies and clinical diagnostics in the doctor's offices or the surgery.

12.9 Acknowledgements

The authors acknowledge support of their work by National Science Foundation (CHE 13-07264) and the National Institutes of Health (EB015722-01). J.S.W. acknowledges fellowship support from the US Department of Energy.

12.10 References

(1) Fenn, J. B.; Mann, M.; Meng, C. K.; Wong, S. F.; Whitehouse, C. M. *Science* **1989**, *246*, 64.

(2) Kondrat, R. W.; Cooks, R. G. *Anal. Chem.* **1978**, *50*, A81.

(3) Horning, E. C.; Horning, M. G.; Carroll, D. I.; Dzidic, I.; Stillwel.Rn *Anal. Chem.* **1973**, *45*, 936.

(4) Takats, Z.; Wiseman, J. M.; Gologan, B.; Cooks, R. G. *Science* **2004**, *306*, 471.

(5) Monge, M. E.; Harris, G. A.; Dwivedi, P.; Fernández, F. M. *Chemical Reviews* **2013**, *113*, 2269.

(6) Shiea, J.; Huang, M. Z.; Hsu, H. J.; Lee, C. Y.; Yuan, C. H.; Beech, I.; Sunner, J. *Rapid Commun. Mass Spectrom.* **2005**, *19*, 3701.

(7) Hiraoka, K.; Nishidate, K.; Mori, K.; Asakawa, D.; Suzuki, S. *Rapid Commun. Mass Spectrom.* **2007**, *21*, 3139.

(8) Haddad, R.; Sparrapan, R.; Eberlin, M. N. *Rapid Commun. Mass Spectrom.* **2006**, *20*, 2901.

(9) Venter, A.; Cooks, R. G. *Anal. Chem.* **2007**, *79*, 6398.

(10) Chipuk, J. E.; Brodbelt, J. S. *J. Am. Soc. Mass Spectrom.* **2008**, *19*, 1612.

(11) Venter, A.; Sojka, P. E.; Cooks, R. G. *Anal. Chem.* **2006**, *78*, 8549.

(12) Nefliu, M.; Smith, J. N.; Venter, A.; Cooks, R. G. *J. Am. Soc. Mass Spectrom.* **2008**, *19*, 420.

(13) Sokol, E.; Jackson, A. U.; Cooks, R. G. *Central European Journal of Chemistry* **2011**, *9*, 790.

(14) Ferguson, C. N.; Benchaar, S. A.; Miao, Z.; Loo, J. A.; Chen, H. *Anal. Chem.* **2011**, *83*, 6468.

(15) Miao, Z.; Wu, S.; Chen, H. *J. Am. Soc. Mass Spectrom.* **2010**, *21*, 1730.

(16) Huang, G.; Chen, H.; Zhang, X.; Cooks, R. G.; Ouyang, Z. *Anal. Chem.* **2007**, *79*, 8327.

(17) Gonzalez-Serrano, A. F.; Ferreira, C. R.; Pirro, V.; Eberlin, L. S.; Heinzmann, J.; Lucas-Hahn, A.; Niemann, H.; Cooks, R. G. *Reproduction Fertility and Development* **2013**, *25*, 262.

(18) Gerbig, S.; Takats, Z. *Rapid Commun. Mass Spectrom.* **2010**, *24*, 2186.

(19) Wu, C.; Qian, K.; Nefliu, M.; Cooks, R. G. *J. Am. Soc. Mass Spectrom.* **2010**, *21*, 261.

(20) Santos, V. G.; Regiani, T.; Dias, F. F. G.; Romao, W.; Jara, J. L. P.; Klitzke, C. F.; Coelho, F.; Eberlins, M. N. *Anal. Chem.* **2011**, *83*, 1375.

(21) Chen, H. W.; Talaty, N. N.; Takats, Z.; Cooks, R. G. *Anal. Chem.* **2005**, *77*, 6915.

(22) Leuthold, L. A.; Mandscheff, J. F.; Fathi, M.; Giroud, C.; Augsburger, M.; Varesio, E.; Hopfgartner, G. *Rapid Commun. Mass Spectrom.* **2006**, *20*, 103.

(23) Rodriguez-Cruz, S. E. *Rapid Commun. Mass Spectrom.* **2006**, *20*, 53.

(24) Chen, H. W.; Pan, Z. Z.; Talaty, N.; Raftery, D.; Cooks, R. G. *Rapid Commun. Mass Spectrom.* **2006**, *20*, 1577.

(25) Pan, Z. Z.; Gu, H. W.; Talaty, N.; Chen, H. W.; Shanaiah, N.; Hainline, B. E.; Cooks, R. G.; Raftery, D. *Anal. Bioanal. Chem.* **2007**, *387*, 539.

(26) Kauppila, T. J.; Talaty, N.; Kuuranne, T.; Kotiaho, T.; Kostiainen, R.; Cooks, R. G. *Analyst* **2007**, *132*, 868.

(27) Justes, D. R.; Talaty, N.; Cotte-Rodriguez, I.; Cooks, R. G. *Chemical Communications* **2007**, 2142.

(28) Zhao, M.; Zhang, S.; Yang, C.; Xu, Y.; Wen, Y.; Sun, L.; Zhang, X. *Journal of Forensic Sciences* **2008**, *53*, 807.

(29) Salter, T. L.; Green, F. M.; Faruqui, N.; Gilmore, I. S. *Analyst* **2011**, *136*, 3274.

(30) Katona, M.; Denes, J.; Skoumal, R.; Toth, M.; Takats, Z. *Analyst* **2011**, *136*, 835.

(31) Chipuk, J. E.; Gelb, M. H.; Brodbelt, J. S. *Anal. Chem.* **2010**, *82*, 4130.

(32) Kennedy, J. H.; Wiseman, J. M. *Rapid Commun. Mass Spectrom.* **2010**, *24*, 309.

(33) Xu, G.; Chen, B.; Liu, G.; Yao, S. *Analyst* **2010**, *135*, 2415.

(34) Wiseman, J. M.; Evans, C. A.; Bowen, C. L.; Kennedy, J. H. *Analyst* **2010**, *135*, 720.

(35) Wang, H.; Liu, J.; Cooks, R. G.; Ouyang, Z. *Angew. Chem.-Int. Edit.* **2010**, *49*, 877.

(36) Nielen, M. W. F.; Hooijerink, H.; Zomer, P.; Mol, J. G. J. *Trac-Trends Anal. Chem.* **2011**, *30*, 165.

(37) Schurek, J.; Vaclavik, L.; Hooijerink, H.; Lacina, O.; Poustka, J.; Sharman, M.; Caldow, M.; Nielen, M. W. F.; Hajslova, J. *Anal. Chem.* **2008**, *80*, 9567.

(38) Garcia-Reyes, J. F.; Jackson, A. U.; Molina-Diaz, A.; Cooks, R. G. *Anal. Chem.* **2009**, *81*, 820.

(39) Ziqing, L.; Mengxia, Z.; Sichun, Z.; Chengdui, Y.; Xinrong, Z. *Analyst* **2010**, *135*, 1268.

(40) Chen, H. W.; Zhang, X.; Luo, M. B. *Chinese Journal of Analytical Chemistry* **2006**, *34*, 464.

(41) Cajka, T.; Riddellova, K.; Zomer, P.; Mol, H.; Hajslova, J. *Food Additives and Contaminants Part a-Chemistry Analysis Control Exposure & Risk Assessment* **2011**, *28*, 1372.

(42) Zhang, J. I.; Talaty, N.; Costa, A. B.; Yu, X.; Tao, W. A.; Bell, R.; Callahan, J. H.; Cooks, R. G. *Int. J. Mass Spectrom.* **2011**, *301*, 37.

(43) Shuiping, Y.; Jianhua, D.; Jian, Z.; Bin, H.; Jianqiang, L.; Huanwen, C.; Zhiquan, Z.; Xiaolin, Q. *Anal. Chem.* **2009**, *81*, 2426.

(44) Morelato, M.; Beavis, A.; Kirkbride, P.; Roux, C. *Forensic Science International* **2013**, *226*, 10.

(45) Sanders, N. L.; Kothari, S.; Huang, G.; Salazar, G.; Cooks, R. G. *Anal. Chem.* **2010**, *82*, 5313.

(46) Xu, W.; Manicke, N. E.; Cooks, G. R.; Ouyang, Z. *Jala* **2010**, *15*, 433.

(47) Ferreira, C. R.; Eberlin, L. S.; Hallett, J. E.; Cooks, R. G. *Reproduction Fertility and Development* **2012**, *24*, 132.

(48) Hallett, J. E.; Ferreira, C. R.; Eberlin, L. S.; Cooks, R. G. *Reproduction Fertility and Development* **2012**, *24*, 163.

(49) Ferreira, C. R.; Pirro, V.; Eberlin, L. S.; Hallett, J. E.; Cooks, R. G. *Anal. Bioanal. Chem.* **2012**, *404*, 2915.

(50) Nyadong, L.; Hohenstein, E. G.; Galhena, A.; Lane, A. L.; Kubanek, J.; Sherrill, C. D.; Fernandez, F. M. *Anal. Bioanal. Chem.* **2009**, *394*, 245.

(51) Chen, H.; Cotte-Rodriguez, I.; Cooks, R. G. *Chemical Communications* **2006**, 597.

(52) Song, Y.; Cooks, R. G. *Journal of Mass Spectrometry* **2007**, *42*, 1086.

(53) Girod, M.; Moyano, E.; Campbell, D. I.; Cooks, R. G. *Chem. Sci.* **2011**, *2*, 501.

(54) Benassi, M.; Wu, C. P.; Nefliu, M.; Ifa, D. R.; Volny, M.; Cooks, R. G. *Int. J. Mass Spectrom.* **2009**, *280*, 235.

(55) Nefliu, M.; Cooks, R. G.; Moore, C. *J. Am. Soc. Mass Spectrom.* **2006**, *17*, 1091.

(56) Jackson, A. U.; Shum, T.; Sokol, E.; Dill, A.; Cooks, R. G. *Anal. Bioanal. Chem.* **2011**, *399*, 367.

(57) Nikolova-Damyanova, B. *Journal of Chromatography A* **2009**, *1216*, 1815.

(58) Cotte-Rodriguez, I.; Takats, Z.; Talaty, N.; Chen, H. W.; Cooks, R. G. *Anal. Chem.* **2005**, *77*, 6755.

(59) Wu, C. P.; Ifa, D. R.; Manicke, N. E.; Cooks, R. G. *Anal. Chem.* **2009**, *81*, 7618.

(60) Benninghoven, A. *Surf. Sci.* **1994**, *299*, 246.

(61) Eberlin, L. S.; Ferreira, C. R.; Dill, A. L.; Ifa, D. R.; Cheng, L.; Cooks, R. G. *Chembiochem* **2011**, *12*, 2129.

(62) Eberlin, L. S.; Dill, A. L.; Golby, A. J.; Ligon, K. L.; Wiseman, J. M.; Cooks, R. G.; Agar, N. Y. R. *Angew. Chem.-Int. Edit.* **2010**, *49*, 5953.

(63) Eberlin, L. S.; Ifa, D. R.; Wu, C.; Cooks, R. G. *Angew. Chem.-Int. Edit.* **2010**, *49*, 873.

(64) Wiseman, J. M.; Ifa, D. R.; Song, Q.; Cooks, R. G. *Angew. Chem.-Int. Edit.* **2006**, *45*, 7188.

(65) Dill, A. L.; Eberlin, L. S.; Costa, A. B.; Zheng, C.; Ifa, D. R.; Cheng, L.; Masterson, T. A.; Koch, M. O.; Vitek, O.; Cooks, R. G. *Chemistry-a European Journal* **2011**, *17*, 2897.

(66) Dill, A. L.; Ifa, D. R.; Manicke, N. E.; Costa, A. B.; Ramos-Vara, J. A.; Knapp, D. W.; Cooks, R. G. *Anal. Chem.* **2009**, *81*, 8758.

(67) Girod, M.; Shi, Y.; Cheng, J.-X.; Cooks, R. G. *Anal. Chem.* **2011**, *83*, 207.

(68) Eberlin, L. S.; Dill, A. L.; Costa, A. B.; Ifa, D. R.; Cheng, L.; Masterson, T.; Koch, M.; Ratliff, T. L.; Cooks, R. G. *Anal. Chem.* **2010**, *82*, 3430.

(69) Dill, A. L.; Eberlin, L. S.; Zheng, C.; Costa, A. B.; Ifa, D. R.; Cheng, L.; Masterson, T. A.; Koch, M. O.; Vitek, O.; Cooks, R. G. *Anal. Bioanal. Chem.* **2010**, *398*, 2969.

(70) Ellis, S. R.; Wu, C.; Deeley, J. M.; Zhu, X.; Truscott, R. J. W.; Panhuis, M. I. H.; Cooks, R. G.; Mitchell, T. W.; Blanksby, S. J. *J. Am. Soc. Mass Spectrom.* **2010**, *21*, 2095.

(71) Wu, C.; Ifa, D. R.; Manicke, N. E.; Cooks, R. G. *Analyst* **2010**, *135*, 28.

(72) Lane, A. L.; Nyadong, L.; Galhena, A. S.; Shearer, T. L.; Stout, E. P.; Parry, R. M.; Kwasnik, M.; Wang, M. D.; Hay, M. E.; Fernandez, F. M.; Kubanek, J. *Proc. Natl. Acad. Sci. U. S. A.* **2009**, *106*, 7314.

(73) Watrous, J.; Hendricks, N.; Meehan, M.; Dorrestein, P. C. *Anal. Chem.* **2010**, *82*, 1598.

(74) Li, B.; Bjarnholt, N.; Hansen, S. H.; Janfelt, C. *Journal of Mass Spectrometry* **2011**, *46*, 1241.

(75) Thunig, J.; Hansen, S. H.; Janfelt, C. *Anal. Chem.* **2011**, *83*, 3256.

(76) Ifa, D. R.; Srimany, A.; Eberlin, L. S.; Naik, H. R.; Bhat, V.; Cooks, R. G.; Pradeep, T. *Anal. Methods* **2011**, *3*, 1910.

(77) Muller, T.; Oradu, S.; Ifa, D. R.; Cooks, R. G.; Krautler, B. *Anal. Chem.* **2011**, *83*, 5754.

(78) Ifa, D. R.; Gumaelius, L. M.; Eberlin, L. S.; Manicke, N. E.; Cooks, R. G. *Analyst* **2007**, *132*, 461.

(79) Ifa, D. R.; Manicke, N. E.; Dill, A. L.; Cooks, G. *Science* **2008**, *321*, 805.

(80) Ifa, D. R.; Wiseman, J. M.; Song, Q.; Cooks, R. G. *Int. J. Mass Spectrom.* **2007**, *259*, 8.

(81) Kertesz, V.; Van Berkel, G. J. *Rapid Commun. Mass Spectrom.* **2008**, *22*, 2639.

(82) Campbell, D. I.; Ferreira, C. R.; Eberlin, L. S.; Cooks, R. G. *Anal. Bioanal. Chem.* **2012**, *404*, 389.

(83) Gao, L.; Cooks, R. G.; Ouyang, Z. *Anal. Chem.* **2008**, *80*, 4026.

(84) Ouyang, Z.; Wu, G. X.; Song, Y. S.; Li, H. Y.; Plass, W. R.; Cooks, R. G. *Anal. Chem.* **2004**, *76*, 4595.

(85) Keil, A.; Talaty, N.; Janfelt, C.; Noll, R. J.; Gao, L.; Ouyang, Z.; Cooks, R. G. *Anal. Chem.* **2007**, *79*, 7734.

(86) Sokol, E.; Noll, R. J.; Cooks, R. G.; Beegle, L. W.; Kim, H. I.; Kanik, I. *Int. J. Mass Spectrom.* **2011**, *306*, 187.

(87) Huang, G. M.; Li, G. T.; Ducan, J.; Ouyang, Z.; Cooks, R. G. *Angew. Chem.-Int. Edit.* **2011**, *50*, 2503.

(88) Wu, C.; Dill, A. L.; Eberlin, L. S.; Cooks, R. G.; Ifa, D. R. *Mass Spectrometry Reviews* **2013**, *32*, 218.

(89) Chen, C.-H.; Lin, Z.; Garimella, S.; Zheng, L.; Shi, R.; Cooks, R. G.; Ouyang, Z. *Analytical chemistry* **2013**, *Under Review*.

(90) Garimella, S.; Xu, W.; Huang, G. M.; Harper, J. D.; Cooks, R. G.; Ouyang, Z. *Journal of Mass Spectrometry* **2012**, *47*, 201.

(91) Li, L.; Chen, T.-C.; Ren, Y.; Hendricks, P. I.; Cooks, R. G.; Ouyang, Z. *Analytical chemistry* **2013**, *Under Review*.

analytical chemistry

Editors' Highlight

pubs.acs.org/ac

Handheld Low-Temperature Plasma Probe for Portable "Point-and-Shoot" Ambient Ionization Mass Spectrometry

Joshua S. Wiley, Jacob T. Shelley,[†] and R. Graham Cooks*

Department of Chemistry and Center for Analytical Instrumentation Development (CAID), Purdue University, 560 Oval Drive, West Lafayette, Indiana 47907, United States

Supporting Information

ABSTRACT: We describe a handheld, wireless low-temperature plasma (LTP) ambient ionization source and its performance on a benchtop and a miniature mass spectrometer. The source, which is inexpensive to build and operate, is battery-powered and utilizes miniature helium cylinders or air as the discharge gas. Comparison of a conventional, large-scale LTP source against the handheld LTP source, which uses less helium and power than the large-scale version, revealed that the handheld source had similar or slightly better analytical performance. Another advantage of the handheld LTP source is the ability to quickly interrogate a gaseous, liquid, or solid sample without requiring any setup time. A small, 7.4-V Li-polymer battery is able to sustain plasma for 2 h continuously, while the miniature helium cylinder supplies gas flow for approximately 8 continuous hours. Long-distance ion transfer was achieved for distances up to 1 m.

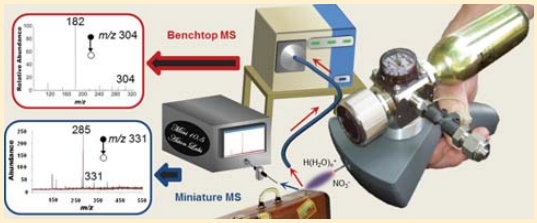

Miniaturization of analytical instrumentation for portability and field-applicability has been of interest in many areas of science. A common hurdle in development of portable instruments is maintenance of adequate analytical performance in a more compact and potentially less sophisticated device. Raman spectroscopy[1] and X-ray fluorescence (XRF)[2] have overcome the hurdles to portability and are commonly used in the field. Maintaining appropriate analytical performance with any technique requires presentation of the sample to the instrument so it can be efficiently and effectively probed. Methods such as attenuated total reflectance for IR absorption spectroscopy[3] and laser-induced breakdown spectroscopy (LIBS)[4] for atomic emission spectroscopy have substantially simplified the sampling process and have been proven useful for portable instrumentation.

Among analytical instruments, none possess the ability to provide a measurement as specific, sensitive, and broadly applicable as mass spectrometry (MS), capabilities that can be accentuated by using tandem MS to enable complex-mixture analysis. An intriguing approach to sample collection and introduction is through ambient ionization MS, which incorporates direct sampling and desorption ionization from a sample in its native environment in one step. While initially a difficult task, miniature MS instruments now have the ability to introduce ions formed in the ambient environment into the reduced-pressure mass analyzer by limiting ion introduction to a short period of time via a discontinuous atmospheric-pressure interface (DAPI).[5] Using DAPI, the coupling of ambient ionization sources with miniature mass spectrometers enables rapid, in situ analysis of complex mixtures without sample pretreatment;[6,7] however, this coupling has mostly been achieved in the laboratory setting due to the lack of true source portability. While many of the ambient ionization methods have shown impressive performance and simplified procedures, they are often bulky when considering the gases, solvents, electrical power, and/or solvent pumps that are needed for operation. This limits the size reduction as well as increases setup time. For example, desorption electrospray ionization (DESI)[8] requires a syringe pump for solvent flow as well as gas flow rates of approximately 1 L/min. There also exists ambient ionization sources based on lasers,[9−11] which are currently not portable but have been demonstrated to desorb viruses, bacteria, and blood cells for MS analysis[12] and can be combined with electrospray ionization (ESI) for increased ionization efficiency.[13] Consequently, there is still a need for a handheld and portable device with the ability to easily interrogate surfaces.

Of the many ambient ionization sources,[14] only a few exhibit the properties necessary for complete portability. One such technique is paper-spray ionization,[15] which requires triangular pieces of paper to deposit the sample, solvent, and a power supply providing ∼4 kV. A related technique has utilized wooden toothpicks instead of paper, making it easier to sample from some surfaces.[16] A modified version of DESI, Venturi easy ambient sonic-spray ionization (V-EASI),[17] can also be made portable because a syringe pump is not required and canned air can be used to supply the nebulizing gas.[18]

Plasma-based ambient ionization techniques are an intriguing approach for portability due to their inherent lack of solvent

Received: May 2, 2013
Accepted: May 30, 2013
Published: May 30, 2013

   dx.doi.org/10.1021/ac4013286 | *Anal. Chem.* 2013, 85, 6545−6552

and generated waste, as well as the ability to change the discharge gas composition for improved desorption/ionization capabilities.[19,20] Plasma assisted desorption/ionization (PADI)[21] has been demonstrated as a potentially portable ambient ionization source without the need for a pressurized gas.[22] Another plasma-based approach that meets all of the requirements for portability is low-temperature plasma (LTP) ambient ionization, based on a room-temperature dielectric barrier discharge.[23] The LTP operates at gas flow rates below 100 mL/min with power of less than 1 W, requirements that can be met by a miniature helium tank and small batteries. No solvents or liquid/gas pumps are necessary. In addition, the ability to directly analyze solid, liquid, and gaseous samples with LTP-MS allows for a wide variety of applications.[23−25]

Here, we present the development and application of the first handheld and wireless LTP source for point-and-shoot analysis using both benchtop and miniature mass spectrometers. The entire source, including consumables such as helium and power, is enclosed in a handheld device weighing ∼0.9 kg. Various samples have been analyzed to compare the analytical performance of the handheld source to the LTP source described by Harper et al.,[23] as well as the effects of helium versus air as the discharge gas. A long-distance ion transport interface from the sampling region to the MS inlet has demonstrated analysis of samples at locations that are nonproximate to the mass spectrometer.

EXPERIMENTAL SECTION

Chemicals and Reagents. Pesticide analytical standards were purchased from Dr. Ehrenstorfer GmbH (Ausburg, Germany) and from Riedel de Haën, Pestanal quality (Seelze, Germany). Analytical standards of explosives were purchased from Cerilliant Corporation (Round Rock, Texas). Individual pesticide and explosive stock solutions (200−300 μg mL^{-1}) were prepared in methanol and stored at −20 °C. Working solutions were prepared by appropriate dilution with acetonitrile. A Milli-Q-Plus ultrapure water system from Millipore (Bedford, MA, USA) was used to obtain HPLC-grade water. HPLC-grade acetonitrile and methanol were obtained from Mallinckrodt Baker Inc. (Phillipsburg, NJ, USA).

Handheld Low-Temperature Plasma Ion Source. The handheld LTP source consisted of a battery-powered circuit, a glass tube for plasma formation, a miniature helium cylinder with a regulator (49615HeK, Leland Limited Inc., South Plainfield, NJ, USA), and a plastic housing (A9056208, OKW Enclosures, Inc., Bridgeville, PA, USA). The circuit, converting a low amplitude DC potential to a high amplitude AC potential, is discussed in greater detail in the Results and Discussion section. Parts used for the circuit consisted of an N-channel MOSFET (497-2758-5-ND, Digi-key, Thief River Falls, MN, USA), 555 timer (497-1963-5-ND, Digi-key, Thief River Falls, MN, USA), 6-V regulator (497-1444-5-ND, Digi-key, Thief River Falls, MN, USA), step-up transformer (28K077, Information Unlimited, Amherst, NJ, USA), and a 7.4-V, 900 mAh lithium polymer battery (Tenergy Corp., Fremont, CA, USA). The entire source cost less than $290 USD in parts, which included $198 USD for the gas regulator.

The actual LTP probe used was a smaller version of one reported previously.[23] A 1/16 in. Swagelok tee was used to connect a 1.6 mm o.d. PEEK gas line, a borosilicate capillary (1.6 mm o.d., 0.86 mm i.d.), and a grounded stainless-steel wire (32 AWG) that is coaxially positioned inside the glass capillary. The gas line contains an additional 1 cm long piece of PEEK capillary (100 μm i.d., 1.6 mm o.d.) to restrict He flow to the plasma to extend the lifetime of the miniature He cylinder; the flow rate could be controlled by adjusting the outlet pressure on the helium regulator. The high-voltage electrode on the outside of the glass tube consisted of a coiled and soldered wire (approximately 2 mm in width) positioned such that the internal grounded wire terminated in the center of the external electrode. The external electrode was connected to the high-voltage output from the secondary winding of the transformer. A mechanical trigger connected to the positive terminal of the battery completed the circuit and, along with the flow of either He or air as discharge gas, enabled plasma formation. It is important to note that, when air was used as the discharge gas, it was typically supplied by a large cylinder of compressed air. However, a small diaphragm pump (NMP015M, KNF Neuberger, Inc., Trenton, NJ, USA) can also be used to supply flowing air to the plasma region by supplying 6 V (regulated) from the battery; the pump greatly increased power consumption and was not used in these studies to conserve battery power. This small pump adds minimal weight (65 g) and size to the device while providing sufficient air flow to sustain the discharge.

Benchtop Mass Spectrometer. Initial experiments were performed using a benchtop Thermo LTQ linear ion trap mass spectrometer (Thermo Fisher Scientific, San José, CA) tuned for optimum detection of the precursor ion of interest via the Xcalibur software. LTP-MS analyses were performed in the positive- and negative-ionization mode, making no changes to the source including the applied voltage, and spectra were collected with automatic gain control enabled, a maximum ion-trap injection time of 200 ms, and 2 microscans per spectrum. The main experimental parameters were: capillary temperature: 200 °C; tube lens: −65 V; capillary voltage: −15 V. Tandem mass spectrometry experiments (MS/MS) were performed via collision-induced dissociation (CID) in order to confirm the presence of particular agrochemicals in the studied samples. These experiments were performed using an isolation window of 1.5 Th and 25−35% collision energy (manufacturer's scale). Long-distance ion transport was achieved with a direct connection of a one-meter-long Tygon tube (1/8 in. o.d. and 1/16 in. i.d.) to the LTQ inlet capillary, which pulled ions (and air) into the LTQ from a Tygon and Teflon sampling vessel that enclosed the LTP sampling region when placed flush with the sample.

Miniature Mass Spectrometer. Miniature mass spectrometer experiments were performed using a Mini 10.5 mass spectrometer as described by Gao et al.[5] Key features include the use of a rectilinear ion trap (RIT), TPD011 hybrid turbomolecular pump (Pfeiffer Vacuum Inc., Nashua, NH), a two-stage diaphragm roughing pump (KNF Neuberger Inc., Trenton, NJ), and a discontinuous atmospheric pressure interface (DAPI); all combined as a compact device weighing ∼10 kg and consuming less than 75 W. The DAPI consisted of a pinch valve (390NC24330, ASCO Valve Inc., Florham Park, NJ) surrounding conductive tubing (i.d. of 1.6 mm., an o.d. of 3.2 mm., and a length of 5.0 cm), which was connected to two capillaries. A transfer capillary (i.d. One mm, o.d. 1.6 mm, 5 cm length) was connected via Swagelok fittings to allow direct injection of ions into the RIT while the sampling capillary (i.d. 250 μm, o.d. 1.6 mm, 10 cm length) was filed to a point and exposed to the atmosphere. Upon application of a variable 5 V pulse from the Mini 10.5, the pinch valve would open for a short period of time, which allowed packets of air/ions from

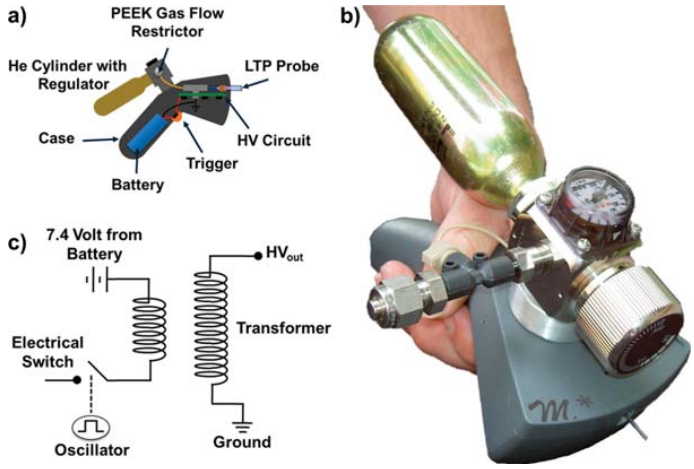

Figure 1. (a) Schematic, (b) photograph, and (c) circuit schematic of the handheld LTP ionization source.

atmosphere to enter the ion trap. Mini 10.5 operating conditions include: 15 ms DAPI open time, m/z 50−500 mass range, and grounded and nonheated inlet capillary. MS/MS was performed via notch broadband isolation and resonant excitation of the mass-selected ion.

Safety Considerations. Exposed, ac high voltages were present at the LTP source and mass spectrometer inlet. Electrically insulating gloves and extreme care were used to prevent electrical shock. Material safety data sheets for all chemicals used were consulted prior to performing experiments.

RESULTS AND DISCUSSION

Specifications for Handheld LTP. A diagram, photograph, and circuit schematic of the handheld LTP probe are shown in Figure 1. The overall weight of the source is 910 g, which reduces to ∼280 g when air is used as the discharge gas due to the replacement of the helium cylinder and regulator by a diaphragm pump. The parts for the source are easy to assemble and inexpensive, with most of the cost being that of the regulator. The incorporation of a PEEK flow restrictor reduced helium flow rates to 100 mL/min or less, depending on the back pressure supplied by the regulator. With this configuration and a back pressure of ∼70 kPa, there was sufficient helium in the cylinder to sustain the plasma for over 8 h. In addition, the simple, battery-operated power supply (Figure 1b) was able to power the plasma with ∼2 kV_{p-p} at 100 kHz for over 2 h continuously. It should be noted that the total time of operation of the source in the field is much longer, considering the power supply is only triggered as needed; the helium supply may be turned off while not in use for a prolonged lifetime as well, typically lasting 8−10 h before requiring a battery recharge or new helium cylinder. The circuit utilized a 7.4 V, 900 mAh Li-polymer battery, which was down-regulated to 6 V for circuit stability by a voltage regulator. The constant 6 V output was applied to one lead of the primary winding of a transformer as well as a 555 timer. The output of the 555 timer, which was wired in an astable configuration with a repetition rate of ∼100 kHz with 50% duty cycle, was connected to the gate of an N-channel MOSFET. The drain of the MOSFET was connected to the other lead on the primary winding of the transformer, while the source of the transistor was held at ground. One end of the secondary winding provided the high-voltage AC waveform for the LTP, while the other was grounded. Even though the input to the transformer was a square wave, the circuit behaves as a resonant LC circuit, so the output closely resembles a sine wave.

Handheld LTP Testing Using Benchtop MS. *Tablet Analysis.* The performance of the handheld LTP probe was characterized through various applications on a conventional benchtop ion-trap instrument. Pharmaceutical tablet analysis has been a targeted application for ambient MS analysis since the onset of the field,[22,26−29] acting as a demonstration of direct sample analysis with no preparation. The mass spectra recorded for the direct analysis of a headache relief tablet with the handheld LTP-MS (acquired with a Thermo LTQ) revealed the three active ingredients: caffeine, acetaminophen, and aspirin (Supporting Information, Figure S1). In the positive-ion mode, the ion $[M + H]^+$, where M indicates an intact molecule, was detected for all three compounds at 195 Th for caffeine, 152 Th for acetaminophen, and 181 Th for aspirin. Numerous adduct and fragment peaks were also evident, especially for aspirin. The same experiment was also done in the negative-ionization mode, without changing any of the ion-source settings. Analysis of the tablet in the negative-ion mode revealed a small peak for the proton-abstraction ion, $[M - H]^-$, of aspirin at m/z 179 as well as a fragment ion at m/z 137, $[M - H - C_2H_2O]^-$, as the most abundant peak (Figure S1b, Supporting Information). No negative ions were detected for acetaminophen or caffeine because of their high gas-phase basicities. The assignment of each of the detected species was verified with MS/MS.

Large-Scale vs Handheld LTP. One important metric of the handheld, portable version of the LTP probe is how well it compares with the large-scale LTP probe (Table 1). The conditions used for the large LTP were those used in the original optimization.[23] The large-scale LTP source was operated with a lower-frequency voltage waveform, increased voltage/power, increased helium flow rates, and within a larger diameter glass tube compared to the handheld LTP probe. Figure 2 displays MS/MS data recorded for a common agrochemical, atrazine (24 pg, absolute on surface), using the large-scale (Figure 2a) and handheld (Figure 2b) LTP with a

dx.doi.org/10.1021/ac4013286 | *Anal. Chem.* 2013, 85, 6545−6552

Table 1. Specifications of Handheld LTP versus Large-Scale LTP

	handheld LTP	large-scale LTP
frequency, kHz	100	2.8
voltage, kV	~2	5−15
gas flow, mL/min	<100	~400
weight, kg	0.910	~67[a]
probe O. D., mm	1.5	6.35
probe I. D., mm	0.86	3.75

[a]Weight includes LTP source, function generator, DC power supply, gas regulator, and a 6.9 kL helium gas cylinder.

Thermo LTQ. The fragmentation observed is due to propene loss from $[M + H]^+$.

Using optimized conditions for each probe on the same MS instruments, the absolute signal was slightly greater with the handheld LTP probe (S/N ~22) than for the handheld probe (S/N ~16). This trend was also true for most other analytes when comparing the two sources. Of eleven agrochemicals analyzed, LODs ranged from being essentially identical to about an order of magnitude better with the handheld LTP source (Table 2). While the small discrepancies in LODs between the large-scale and handheld LTP source could be attributed to various instrumental and operating parameters, including gas-flow profile, source-to-sample orientation, and detector efficiency, it is clear that reducing the power and helium flow for the handheld LTP did not negatively affect the analytical performance.

Effect of Discharge Gas: Air vs Helium. The handheld LTP probe can be operated using either helium or simply air as discharge gas. To remain consistent in comparing the use of an air and a helium discharge, similar voltages were used for each gas, which included the use of the same PEEK flow restrictor and a large cylinder with a back pressure of 140 kPa. It should be noted that, while the voltage was held constant for the helium and air plasmas, the current necessarily was not, resulting in different currents/powers for the two discharges. Figure 3 shows tandem mass spectra using a handheld LTP with a Thermo LTQ for the detection of 1.2 ng of the agrochemical isoproturon obtained with helium and air, respectively, and revealing fragment ions at 72 and 165 Th. Interestingly, the signal was approximately twice as high with helium compared to air. The LODs obtained for the analysis of other agrochemicals that readily undergo proton transfer (Table 2) were typically 1−2 orders of magnitude better with helium. Trinitrotoluene (TNT) was a unique example where no analyte ions were detected with air LTP, despite being able to readily detect analyte ions with helium LTP. This phenomenon is attributed to the fact that TNT ionizes by either deprotonation or electron attachment, while the eleven pesticides undergo protonation. The use of air enforces a difference in the LTP sampling region, so that neither ionization mechanism can take place for TNT. This point is

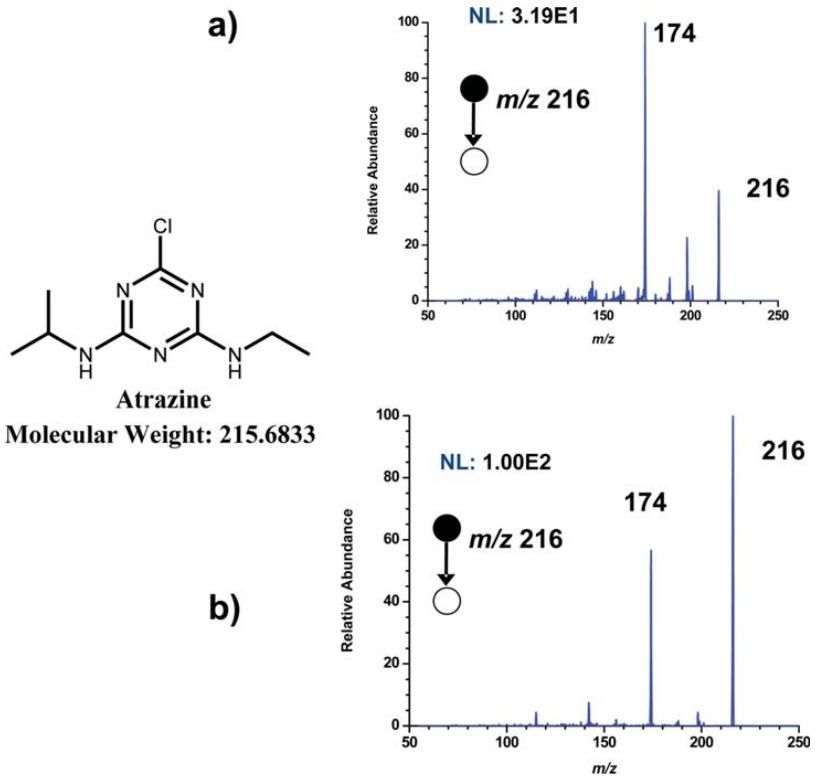

Figure 2. Atrazine (24 pg) MS/MS spectra recorded with (a) large-scale and (b) handheld LTP acquired using a Thermo LTQ and optimized conditions for each LTP probe.

Table 2. Limits of Detection for Various Analytes

		LODs[a] (ng)			
analyte category	analyte	air handheld LTP	He handheld LTP	He large-scale LTP	He handheld LTP/mini MS
pesticides	amitraz	0.3	0.05	0.8	50
	atrazine	0.01	0.003	0.005	0.1
	buprofezin	0.2	0.004	0.04	0.2
	DEET	0.2	0.04	0.003	0.6
	diphenylamine	0.6	0.04	0.07	0.2
	ethoxyquin	300	0.9	8	30
	isofenphos-methyl	6	0.09	1	10
	isoproturon	0.7	0.04	0.2	6
	malathion	5	0.2	0.7	1
	paration-ethyl	0.2	0.05	0.01	200
	terbuthylazine	0.004	0.001	0.006	0.3
explosives	RDX	0.02	0.02	n.m.	n.m.
	TNT	n.d.	0.02	n.m.	n.m.
	PETN	0.2	0.05	n.m.	n.m.
	Tetryl	2	2	n.m.	n.m.

[a]LODs were calculated on the basis of S/N = 3 from a calibration curve of at least 3 points using at least 3 repetitions for each point. The linear equation from the calibration curve was used to calculate the LOD between the lowest concentration detected and the highest concentration not detected (varying each concentration by ∼1 order of magnitude). n.d., not detected; n.m., not measured.

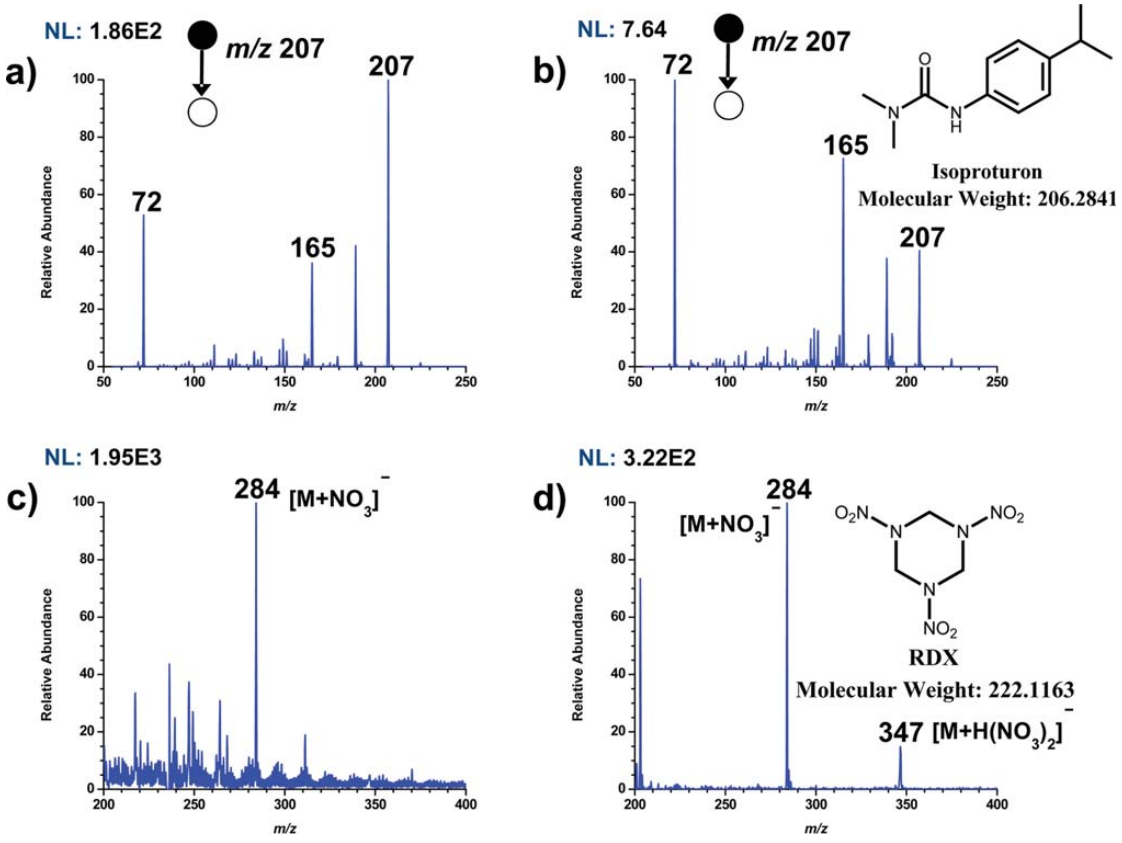

Figure 3. Positive ion tandem mass spectrum of 1.2 ng isoproturon with (a) helium- and (b) air-based handheld LTP. Negative-ion full-scan mass spectrum of 200 pg RDX with (c) helium and (d) air used as the discharge gas. All four spectra were acquired with a Thermo LTQ. Air was supplied by a large compressed air cylinder for air-based handheld LTP.

dx.doi.org/10.1021/ac4013286 | *Anal. Chem.* 2013, 85, 6545−6552

further evidenced in Figure 3c,d, where there is much less chemical noise in the negative ion mode when using air-based LTP.

It has been seen in other studies that the use of helium as a discharge gas for LTP often produces an abundance of background ions as compared to a nitrogen- or air-based LTP,[23] likely due to excited states of helium exceeding 19 eV capable of ionizing a greater range of species.

Examples of cases where the analytical performance was similar when either air or helium was used as the discharge gas includes the analysis of explosives that readily undergo nitrate adduction, as with RDX, PETN, and tetryl. In Figure 3, the analysis of 200 pg of RDX with both plasma gases for the handheld LTP revealed the $[M + NO_3]^-$ adduct at m/z 284 (cf. Figure 3c,d) using a Thermo LTQ. The signal for RDX was higher when helium was used, but the ratio of the signal to the surrounding chemical noise was much poorer. Overall, the detection limits (Table 2) are roughly the same for air and helium discharges for explosives which undergo nitrate addition. In general, helium is the appropriate choice for achieving better LODs for most samples, unless nitrate addition is favored. The ability of both helium and air plasmas to generate NO_3^- and higher-order nitrate clusters in large abundance in the ambient air from N_2 and O_2 allows sufficient adduct formation with appropriate analytes. However, the reason for reduced sensitivity with air versus helium for proton transfer ionization is unclear, but it is likely due to a difference in reagent ions formed with the different discharge gas compositions.

Handheld LTP on Mini 10.5 MS. Coupling a handheld LTP with a miniature mass spectrometer produces a completely field-portable instrument, capable of analyzing gaseous, liquid, and solid samples in their native, ambient environment. The process of minimizing helium and power in comparison to large-scale LTP has other benefits. The decreased voltage for operation of the source reduced the radiated AC noise which has adverse effects on the MS instrumentation as observed with previous versions of the LTP. In addition, lower helium flow rates also helped when coupling the source to a Mini MS which has limited pumping capacity because the performance of the small turbomolecular pumps degrades when helium is being pumped. This phenomenon has required the use of supplemental pumping in the past,[30] which was not needed for coupling of the handheld LTP with the Mini 10.5 MS.

An MS/MS spectrum for 1.2 ng of malathion on the Mini 10.5 (Figure S2 in Supporting Information) reveals the expected loss of ethanol. Tandem mass spectra for malathion and other pesticides were used in determining LODs for handheld LTP on the miniature instrument. Absolute quantities within an order of magnitude of a few nanograms could confidently be detected for all of the agrochemicals, and they produced adequate signals for the qualitative assessments often desired for in situ experiments. The Mini 10.5 instrument did not have the ability to detect negative ions, so explosives were not analyzed.

Drugs of abuse represent another potential compound class that might be detected using a portable instrument. This has been demonstrated with the large-scale LTP on a benchtop instrument,[24] LODs being in the pg to ng range, absolute. In the current study, the ability to detect a drug directly from an individual's finger after a few hours after exposure was tested. A small amount, 1 μg, of methamphetamine was deposited onto a human finger and analyzed 2 h after application by MS/MS using the handheld LTP-Mini 10.5 combination. The subject performed daily tasks as usual for the 2 h. It should be noted that the subject did not wash his hands between the time of spotting the drug and analysis. The spectrum in Figure 4 was

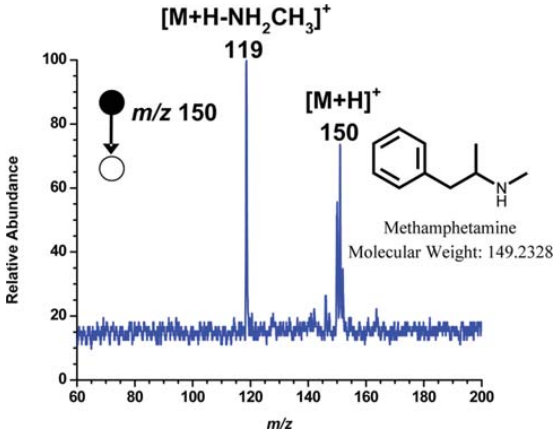

Figure 4. Analysis of 1 μg of methamphetamine on an individual's finger 2 h after deposition using the handheld LTP on a Mini 10.5.

obtained by direct finger analysis with the handheld LTP probe, revealing the presence of methamphetamine with the $[M + H]^+$ and characteristic fragment ions present at 150 and 119 Th, respectively. The nondestructive and room-temperature nature of the handheld LTP allows analysis of delicate samples, such as human skin, without damage or discomfort.

Long-Distance Ion Transfer. To demonstrate the most likely way a handheld ambient ionization source would be used in the field, a long-distance ion transfer system was implemented to help transport ions from a nonproximate sample to the MS inlet. Similar designs have been reported by Cotte-Rodriguez et al. for nonproximate detection with DESI[31] and by Garimella et al., where simulations and experimental results demonstrated that plastic tubing allows effective transfer of ions produced by DESI and LTP for distances over 1 m.[32] This simple system, diagrammatically shown in Figure 5a, consisted of a large Tygon and Teflon vessel, which can be placed flush with a sample surface, allowing interaction of excited species from the LTP with the sample at a fixed geometry. The ions/neutral species were transferred to the MS inlet via a flexible one-meter-long Tygon tube. Laminar flow is established 1 cm into the tube, so any reasonable bends in the tube had little effect on signal. The vacuum within the Thermo LTQ created the suction necessary to pull the ions/neutrals to the MS inlet. This arrangement was tested on the commercial benchtop Thermo LTQ. Figure 5b shows the resulting mass spectrum from the analysis of 10 μg of RDX on a glass microscope slide. Again, the $[M + NO_3]^-$ ion was present at m/z 284. Cocaine, prevalent on US banknotes,[33] was also detected on an untreated U.S. one dollar bill using tandem MS (Figure 5c). The expected loss of benzoic acid yields the base peak at 182 Th from the parent $[M + H]^+$ ion at 304 Th. Two orders of magnitude of signal loss was experienced, and this remains an area of future work as does the implementation of long-distance ion transport on miniature MS instruments.

dx.doi.org/10.1021/ac4013286 | *Anal. Chem.* 2013, 85, 6545−6552

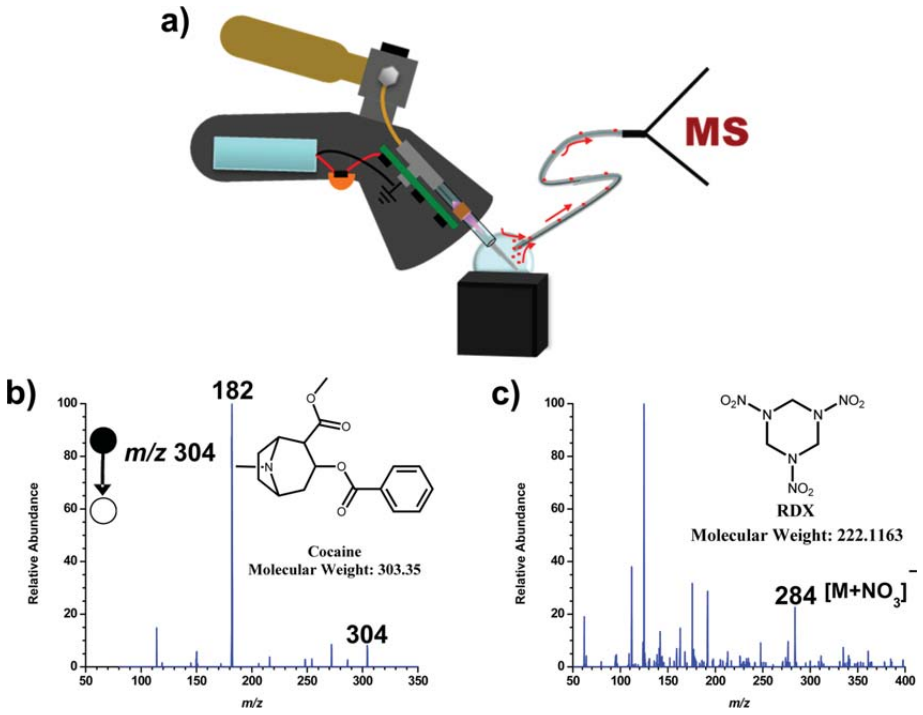

Figure 5. (a) Schematic of the handheld LTP with an interface used for long-distance ion transport to a Thermo LTQ. (b) Analysis of a U.S. one dollar bill using the same configuration as well as (c) 10 μg of RDX from a glass slide.

CONCLUSIONS

A handheld low-temperature plasma probe has been developed for both miniature and benchtop MS applications. Despite using lower power and helium flow rates in comparison to a conventional, large-scale LTP, there was no loss in analytical performance with the handheld LTP-MS. While helium was typically used as the discharge gas, due to typically yielding better LODs, air was also effective for many analytes. When using air, the weight of the handheld source was ~280 g, with electrical current from a 7.4 Li-polymer battery being the only consumable. When coupled with a Mini 10.5 MS, LODs at the nanogram level were achieved for various agrochemicals as well as the ability to directly detect methamphetamine from skin; however, the desorption capabilities of plasma sources inherently limit the methodologies to lower molecular weight analytes. The demonstration of long-distance ion transfer with the handheld LTP and a flexible transfer line has shown the potential for point-and-shoot analysis with a free range of motion about the MS instrument.

ASSOCIATED CONTENT

Supporting Information

Additional information as noted in text. This material is available free of charge via the Internet at http://pubs.acs.org.

AUTHOR INFORMATION

Corresponding Author

*E-mail: cooks@purdue.edu. Telephone: (765) 494-5262. Fax: (765) 494-9421.

Present Address

†Institute for Inorganic and Analytical Chemistry, University of Münster, Corrensstr. 28, Münster 48149, Germany.

Notes

The authors declare no competing financial interest.

ACKNOWLEDGMENTS

The authors thank Santosh Soparawalla and Robert Noll for advice and acknowledge support from the Center for Analytical Instrumentation Development (CAID). This research was also supported by an award from the US Department of Energy (DOE) Office of Science Graduate Fellowship Program (DOE SCGF). The DOE SCGF Program was made possible in part by the American Recovery and Reinvestment Act of 2009. The DOE SCGF program is administered by the Oak Ridge Institute for Science and Education for the DOE. ORISE is managed by Oak Ridge Associated Universities (ORAU) under DOE contract number DE-AC05-06OR23100. All opinions expressed in this paper are the authors' and do not necessarily reflect the policies and views of DOE, ORAU, or ORISE. Additional support was proved by the National Science Foundation Instrumentation Development for Biological Research (DBI 0852740).

REFERENCES

(1) Sutherland, W. S.; Alarie, J. P.; Stokes, D. L.; Vodinh, T. *Instrum. Sci. Technol.* **1994**, *22*, 231.
(2) Karttunen, J. O.; Evans, H. B.; Henderson, D. J.; Markovic, P. J.; Niemann, R. L. *Anal. Chem.* **1964**, *36*, 1277.
(3) Harrick, N. J. *J. Phys. Chem.* **1960**, *64*, 1110.

(4) Debrasguedon, J.; Liodec, N. *C.R. Hebd. Acad. Sci.* **1963**, *257*, 3336.
(5) Gao, L.; Cooks, R. G.; Ouyang, Z. *Anal. Chem.* **2008**, *80*, 4026.
(6) Sanders, N. L.; Kothari, S.; Huang, G.; Salazar, G.; Cooks, R. G. *Anal. Chem.* **2010**, *82*, 5313.
(7) Sokol, E.; Noll, R. J.; Cooks, R. G.; Beegle, L. W.; Kim, H. I.; Kanik, I. *Int. J. Mass Spetrom.* **2011**, *306*, 187.
(8) Takats, Z.; Wiseman, J. M.; Gologan, B.; Cooks, R. G. *Science* **2004**, *306*, 471.
(9) Brady, J. J.; Judge, E. J.; Levis, R. J. *Rapid Commun. Mass Spectrom.* **2009**, *23*, 3151.
(10) Nemes, P.; Vertes, A. *Anal. Chem.* **2007**, *79*, 8098.
(11) Shelley, J. T.; Ray, S. J.; Hieftje, G. M. *Anal. Chem.* **2008**, *80*, 8308.
(12) Peng, W. P.; Yang, Y. C.; Kang, M. W.; Tzeng, Y. K.; Nie, Z. X.; Chang, H. C.; Chang, W.; Chen, C. H. *Angew. Chem., Int. Ed.* **2006**, *45*, 1423.
(13) Rezenom, Y. H.; Dong, J.; Murray, K. K. *Analyst* **2008**, *133*, 226.
(14) Monge, M. E.; Harris, G. A.; Dwivedi, P.; Fernández, F. M. *Chem. Rev.* **2013**, *113*, 2269.
(15) Wang, H.; Liu, J.; Cooks, R. G.; Ouyang, Z. *Angew. Chem., Int. Ed.* **2010**, *49*, 877.
(16) Hu, B.; So, P. K.; Chen, H. W.; Yao, Z. P. *Anal. Chem.* **2011**, *83*, 8201.
(17) Santos, V. G.; Regiani, T.; Dias, F. F. G.; Romao, W.; Jara, J. L. P.; Klitzke, C. F.; Coelho, F.; Eberlin, M. N. *Anal. Chem.* **2011**, *83*, 1375.
(18) Schwab, N. V.; Porcari, A. M.; Coelho, M. B.; Schmidt, E. M.; Jara, J. L.; Visentainer, J. V.; Eberlin, M. N. *Analyst* **2012**, *137*, 2537.
(19) Heywood, M. S.; Taylor, N.; Farnsworth, P. B. *Anal. Chem.* **2011**, *83*, 6493.
(20) Wright, J. P.; Heywood, M. S.; Thurston, G. K.; Farnsworth, P. B. *J. Am. Soc. Mass. Spectrom.* **2013**, *24*, 335.
(21) Ratcliffe, L. V.; Rutten, F. J. M.; Barrett, D. A.; Whitmore, T.; Seymour, D.; Greenwood, C.; Aranda-Gonzalvo, Y.; Robinson, S.; McCoustra, M. *Anal. Chem.* **2007**, *79*, 6094.
(22) Bowfield, A.; Barrett, D. A.; Alexander, M. R.; Ortori, C. A.; Rutten, F. M.; Salter, T. L.; Gilmore, I. S.; Bradley, J. W. *Rev. Sci. Instrum.* **2012**, *83*, 063503.
(23) Harper, J. D.; Charipar, N. A.; Mulligan, C. C.; Zhang, X. R.; Cooks, R. G.; Ouyang, Z. *Anal. Chem.* **2008**, *80*, 9097.
(24) Jackson, A. U.; Garcia-Reyes, J. F.; Harper, J. D.; Wiley, J. S.; Molina-Diaz, A.; Ouyang, Z.; Cooks, R. G. *Analyst* **2010**, *135*, 927.
(25) Zhang, Y.; Ma, X.; Zhang, S.; Yang, C.; Ouyang, Z.; Zhang, X. *Analyst* **2009**, *134*, 176.
(26) Chen, H. W.; Talaty, N. N.; Takats, Z.; Cooks, R. G. *Anal. Chem.* **2005**, *77*, 6915.
(27) Green, F. M.; Salter, T. L.; Stokes, P.; Gilmore, I. S.; O'Connor, G. *Surf. Interface Anal.* **2010**, *42*, 347.
(28) Steeb, J.; Galhena, A. S.; Nyadong, L.; Facundo, J. J.; Fernandez, M. *Chem. Commun.* **2009**, 4699.
(29) Williams, J. P.; Scrivens, J. H. *Rapid Commun. Mass Spectrom.* **2005**, *19*, 3643.
(30) Huang, G.; Xu, W.; Visbal-Onufrak, M. A.; Ouyang, Z.; Cooks, R. G. *Analyst* **2010**, *135*, 705.
(31) Cotte-Rodriguez, I.; Mulligan, C. C.; Cooks, G. *Anal. Chem.* **2007**, *79*, 7069.
(32) Garimella, S.; Xu, W.; Huang, G.; Harper, J. D.; Cooks, R. G.; Ouyang, Z. *J. Mass Spectrom.* **2012**, *47*, 201.
(33) Armenta, S.; de la Guardia, M. *TrAC, Trends Anal. Chem.* **2008**, *27*, 344.